LANDSCAPE EVOLUTION IN WESTERN AMAZONIA: PALYNOSTRATIGRAPHY, PALAEOENVIRONMENTS AND DIVERSITY OF THE MIOCENE SOLIMÕES FORMATION, BRAZIL

By

Carlos D'Apolito

A thesis submitted to the University of Birmingham

for the degree of DOCTOR OF PHILOSOPHY

School of Geography, Earth and

Environmental Sciences

College of Life and Environmental Sciences

University of Birmingham

June 2016

ABSTRACT

During the Miocene (23.03 to 5.33 Ma), western Amazonia experienced major changes in its geography and biodiversity as a response to Andean uplift. To better understand these changes, the palynology of the Solimões Formation (NW Brazil) is presented with the objective of providing age control, and establishing palaeoenvironments and pollen richness within the framework of geological and climatic events. The ninety-five palynological samples yield 491 palynomorphs, of which 76 pollen and 25 spores are new. Correlation with a nearby calibrated biozonation resulted in ages from 18.7 to 10.7 Ma (late early to earliest-late Miocene). The pollen associations are typical of Amazonian humid forests, with abundant palms, Bombacoideae, trees and grasses, and lack diverse and abundant herbs or dry forest indicators. Spikes in algae and dinoflagellates show phases of lake development and two marine incursions – one between 18.4 and 17.8 Ma, and another between 14.1 and 13.7 Ma. Statistical analyses of the data show inundations had no effect in the vegetation composition. Estimates of diversity using different metrics clearly show a diversity increase and community change at ca. 16 Ma, independent of lithofacies. This change is driven by the Middle Miocene Climatic Optimum and not correlated with any of the marine incursions. Altogether, the results bring more detail to the environmental history of western Amazonia, establishing two inundation events and furthering the climate-diversification relationship in Neotropical biomes into the Miocene period.

To my family and teachers.

ACKNOWLEDGMENTS

Many thanks to:

-My supervisor Guy Harrington for his constant support, patience and source of ideas throughout these years.

-Carlos Jaramillo, with whom I initially formulated the PhD idea and who helped me with many aspects of my work.

-The Geological Survey of Brazil (CPRM), Fernando Burgos and Gert Woeltje (DNPM-Manaus) for access and sampling permits.

-Vladimir Zapata, who spent a very hard-working month describing and sampling sediment cores with me in the heat of Manaus.

-Frank Wesselingh and Stephen Louwye for help with identification of molluscs and dinoflagellates, respectively.

-Ingrid Romero, Silane Silva Caminha and Fátima Leite for their previous works, shared data and many discussions on the taxonomy of pollen and spores from the Amazon.

-Mario Vicente Caputo and Emílio Amaral, for sending papers/reports and for many discussions on aspects of the geology of the Amazon basin.

-Aruna and Gretchel (Earth Sciences, UoB) for their help with facilities and paperwork in the department.

-John Ortiz for his brilliant work producing stratigraphic logs using R codes!

-James Bendle, Frederike Wittkopp and Heiko Moossen for their help teaching me and providing ideas for geochemistry work.

-Jon Sadler for his role as second supervisor.

-Tom Dunkley-Jones and Alejandro Machado for trying to find nannofossils and foraminifera in my samples, unfortunately they didn't.

-All the staff and colleagues of Earth Sciences, for the nice environment created, coffee mornings, field trips, paper clubs, supervision groups, and also some pub time eventually – cheers!

-All my friends in Birmingham, life would have been much harder without them – thank you!

-My housemates Plamen, Simiao and Mayra for sharing a house and many great times together!

-Agno Acioli, Ronaldo Almeida, Miranda, Seu Nixon and the staff of Universidade Federal do Amazonas in Benjamin Constant for their support during field work.

-Suzette Flantua for sharing data from the Latin American Pollen Database.

I am grateful to the following for funding:

-CAPES (Coordenação de Aperfeiçoamento de Pessoal em Nível Superior) for the scholarship that allowed me to be abroad for my studies. And also thanks to Maria L. Absy who was my tutor for this scholarship application.

-ASSP (American Association of Stratigraphic Palynologists) for a small research grant and a travel grant that helped me having lab work finished and attending an international conference.

CONTENTS

CD (enclosed on inside back cover)

1. Excel sheet with raw pollen counts of core 1-AS-105-AM;

2. Excel sheet with all cores and depths used to build isopach map;

3. Text files (.txt) used for the age model (to accompany R codes for age model);

3. All R code as .rtf files;

4. Excel sheet with raw data organised for CCA analysis and for producing pollen diagrams.

Total word count: 43,026

(Excluding tables and figure captions)

LIST OF FIGURES

LIST OF TABLES

Chapter 1: Introduction

1.1 The Miocene World

The Miocene spans from 23.03 to 5.33 million years (Gradstein *et al*. 2012) (Fig. 1.1) and is characterised as an interval of global cooling that nevertheless still had predominantly warmer temperatures than present day (Zachos *et al*. 2001, 2008). This represented a continuation of a long-term cooling trend from the mid Eocene, but punctuated by a climatic optimum that took place at the middle Miocene, known as the Mid-Miocene Climatic Optimum (MMCO; ca. 17 to 15 Ma, Zachos *et al*. 2001). The estimated temperatures for this event are approximately 3° to 4 C° higher than today (You et al. 2009, Goldner *et al*. 2014) and therefore they could represent a close analogue to postulated climate scenarios for the next one or two centuries (IPCC 2014), making the event of particular interest for palaeoenvironmental studies. Following the MMCO, global conditions entered a progressively cooling phase referred to as the Middle Miocene Climatic Transition (MMCT). As with other periods of palaeoclimatic history, the temperature trend of the Miocene seems to be coupled with fall of atmospheric carbon dioxide levels (from 400-500 ppmv or more around the MMCO to 300 ppmv or less at the late stages of the Miocene; Fig. 1.1., Beerling and Royer 2011, Foster *et al*. 2012, Zhang *et al*. 2013). There is still considerable debate on the relation of CO^2 and temperature during the Miocene, a debate driven by studies that show a decoupling of these variables (e.g. alkenone derived SST, LaRiviere *et al*. 2012), and modelled warmth estimates requiring CO2 concentrations of ca. 800 ppmv (Goldner *et al*. 2014), which are significantly higher than most reconstructions. Nevertheless, the relationship seems to hold (Beerling and Royer 2011) as supported by newly available alkenone records (Zhang *et al*. 2013), boron isotope (Foster *et al*. 2012), and leaf stomatal reconstructions (Kürschner *et al*. 2008).

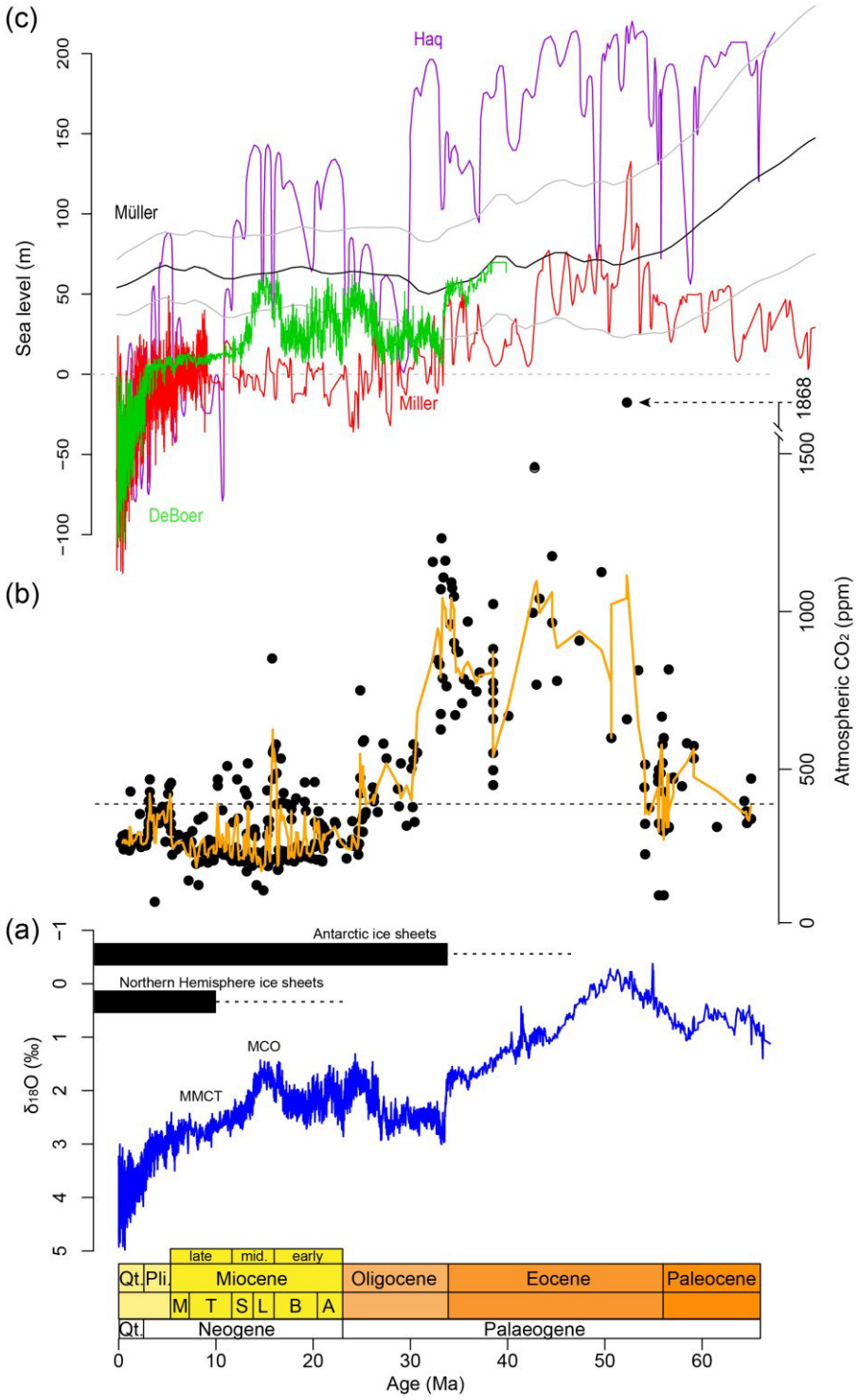

Figure 1.1. Palaeoclimatic proxies and sea level estimates for the Cenozoic. Panel a): $\delta^{18}O$ from benthic foraminifera (Zachos *et al*. 2001, 2008) used as a temperature proxy; Miocene stages, M: Messinian, T: Tortonian, S: Serravalian, L: Langhian, B: Burdigalian and A: Aquitanian. Panel b): Atmospheric CO_2 (ppm) estimates derived from stomate, phytoplankton, palaeosols, liverworts, Boron and B/CA (data compiled by Beerling and Royer 2001), dotted line is present-day CO_2 cc (390 ppm). Panel (c): global sea levels estimates (Haq *et al*. 1987, Miller *et al*. 2005, Müller *et al*. 2008 and DeBoer *et al*. 2010).

As a result of the temperature evolution and its direct influence on ice volume stored on land (Foster and Rohling 2013), sea levels also fluctuated (Fig. 1.1). Despite estimation uncertainties and inconsistencies among published records, most studies seem to agree that the sea level throughout or intermittently during the Miocene was higher than present (Haq *et al*. 1987, Miller *et al*. 2005, Müller *et al*. 2008, DeBoer *et al*. 2010) and somewhat mirrored benthic $\delta^{18}O$ data (Zachos *et al*. 2001) and temperature estimates (DeBoer *et al*. 2010, Beerling and Royer 2011). This implies that sea levels were at their highest levels during the MMCO (ca. 50-60 metres a.s.l., Fig. 1.1), and subsequently started to drop steadily in response to cooler climatic conditions. The climatic evolution also translated into changes in ice caps on both North and South poles. Antarctic has been glaciated since ca. 34 Ma ago, but it was during the middle Miocene that a permanent ice cover developed in east Antarctic (Shackelton and Kennett 1975). In the northern hemisphere ice sheets have existed at least since the late Miocene (but probably as early as the middle Miocene; Wright 1998, Zachos *et al*. 2008), and it was during the Miocene that bipolar glaciations started. All these climatic changes had a worldwide effect on the distribution of vegetation, following the long-term cooling trend forests were beginning to adapt to colder temperatures that have persisted since the early Miocene. Nonetheless, a warmer than present world meant current biomes could be present at higher latitudes, for instance following the MMCO cool-temperate forests existed in the high north, warm-temperate mixed forests in mid-latitudes and shrubby tundra in Antarctica (Pound *et al*. 2012). These vegetation types were gradually narrowing their distribution as the world got cooler, tundra disappeared from Antarctica by the late Miocene and taiga developed in the high north (Pound *et al*. 2012). In the equatorial Neotropics, broadleaf evergreen forests have existed since the early Miocene (Hoorn 1993, Hoorn *et al*. 2010, Silva-Caminha *et al*. 2010, Jaramillo *et al*. 2014), and by the late Miocene dry biomes

have appeared for example in the Patagonian steppe (Palazzesi *et al*. 2014), the cerrados of central Brazil (Simon *et al*. 2009), and savannahs/deserts worldwide (Pound *et al*. 2012).

Ocean currents during the Miocene underwent important shifts that made them nearly as they are today. From early to middle Miocene, plate rearrangements caused the closure of the Tethys ocean (Okay *et al*. 2010) and the Indonesian gateway (Kuhnt *et al*. 2004), and the rise of the Panama isthmus (Coates *et al*. 2004, Montes *et al*. 2015) resulting in the termination of the circum-equatorial current and its replacement by the subtropical Pacific and Atlantic ocean gyres as well as a strengthened Gulf stream (Potter and Szatmari 2009). Middle Miocene opening of the Greenland-Scotland ridge affected the North Atlantic by controlling the input of arctic cold waters (Wright and Miller 1996, Wright 1998). All these changes transformed the global oceans currents and had impacts on the climate and consequently on biome distributions on the planet as a whole. In terms of landscape, continental configurations underwent important transformations, and in the middle to late Miocene major mountain chains like the Himalayas (Powell and Conaghan 1973, Copeland and Harrison 1990) and the Andes (Hoorn *et al*. 2010) had accelerated rates of uplift. By late middle to late Miocene overall continental distribution was nearly that of the present-day (Potter and Szatmari 2009).

1.2 The Amazon Basin

The Amazon craton is one of the oldest pieces of continental crust on Earth, with basement rocks dating back to Precambrian times (Wanderley-Filho *et al*. 2010). The craton migrated west after the break-up of Gondwana to form the core of South America (Scotese 2009), which then drifted away from the African continent from the Triassic onwards, remaining an isolated landmass from middle Cretaceous (ca. 100 Ma) until the closure of the Panama isthmus in the Miocene ca. 13 to 15 Ma ago (sensu Montes *et al*. 2015).

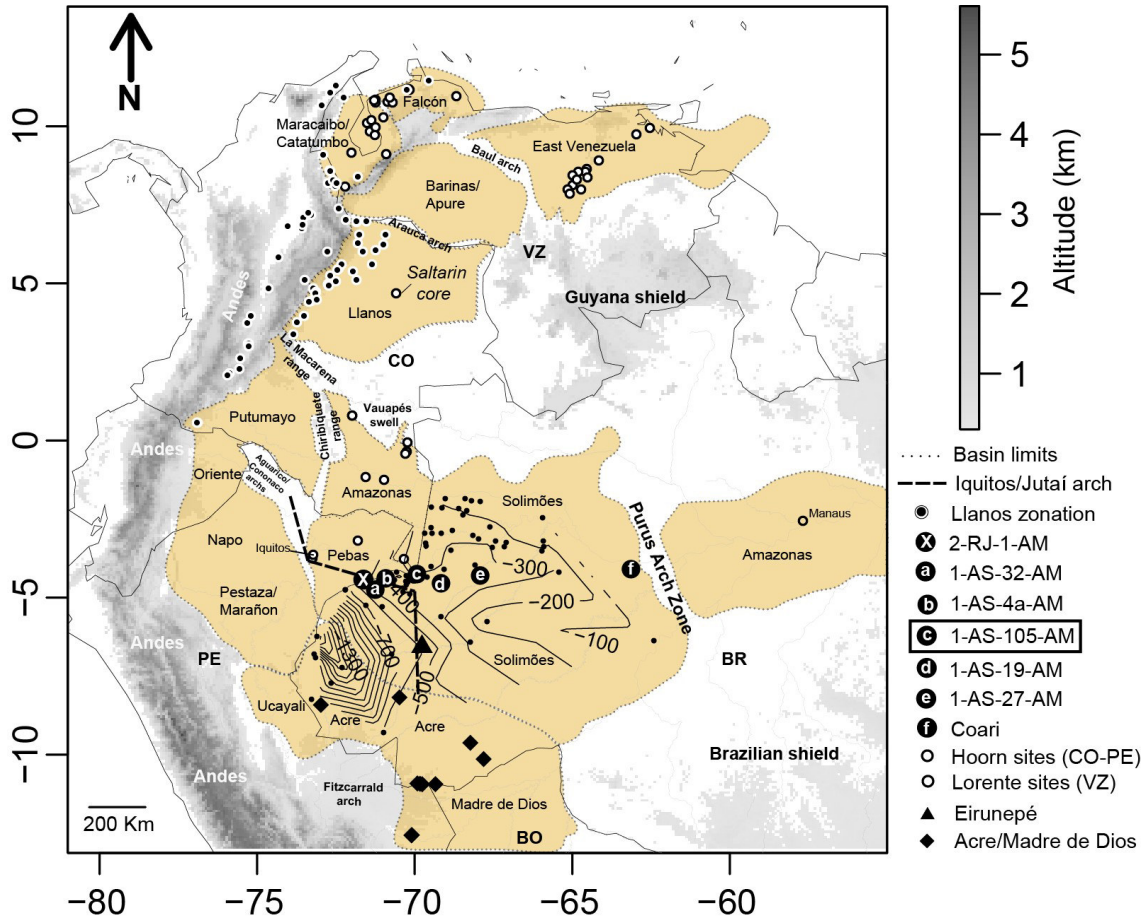

Figure 1.2. Map of NW South America with all sites cited in this thesis. Basin names are within the limits drawn with dotted lines. Sites in the Llanos basin and surroundings are part of the Llanos and Llanos foothills pollen zonation of Jaramillo *et al*. (2011); Sites in Venezuelan basins are part of the pollen zonation of Lorente (1986) and sites in Colombian and Peruvian Amazonas basin are from studies by Hoorn (1993, 1994a, 1994b). Letter X (2-RJ-1-AM) is Solimões type section (Eiras *et al*. 1994); Letters (a to f) in the Solimões basin are as follow: a) core 1-AS-32-AM (Latrubesse *et al*. 2010), b) core 1-AS-4a-AM (Hoorn 1993), **c) core 1-AS-105-AM (this work)**, d) and e) cores 1-AS-19-AM and 1-AS-27-AM, respectively (Silva-Caminha *et al*. 2010), f) outcrops around Coari city (Nogueira *et al*. 2013). Solid triangle is outcrops close to Eirunepé city (Gross *et al*. 2011); solid diamonds are Acre/Madre de Dios sites of Latrubesse *et al*. (2010). Isopach lines were plotted using formation thickness measured in 107 boreholes (small solid circles scattered around Solimões basin including sites X, a, b, c, d and e) from the Brazilian Geological Survey (CPRM) and Petrobrás, data was linearly interpolated using R package Akima. Positions of basins and arches after Hoorn (1993), White *et al*. 1995, Roddaz *et al*. (2005), Mora *et al*. 2010, Montenegro and Barragán (2011), Sarmiento (2011) and Kroonenberg and Reeves (2011). DEM plotted is ≥300 m derived from ETOPO 1 (Amante and Eakins 2009). BR: Brazil, BO: Bolivia, PE: Peru, CO: Colombia, VZ: Venezuela.

The Amazon hydrographic basin is an intracratonic feature that extends from the Andes in the west to the Atlantic coast in the east. It is bounded by the Guyana shield to the north, and the Guaporés, or Central Brazil, shield to the south (Fig.1.2). Basin infill has developed since early Palaeozoic times, including phases of glacial and marine sedimentation in the Ordovician–Upper Cambrian, and marine to continental in the Meso-Cenozoic (Eiras *et al*. 1994). From the Late Cretaceous sedimentation was influenced by mountain building in the west associated with the Andean chain. The basin is divided by structural arches along its E-W axis (Fig.1.2). The western basins harbour sequences of sediments that accumulated in continental and marginal marine environments with clastic supply from the Precambrian shields, and increasingly from the Andes as it uplifted. The Andean orogeny resulted in the cessation of river flow to the west, which drained the area to the Pacific Ocean in the Palaeogene, and in the gradual development of a low energy system of meandering rivers, lakes and swamps, which had its maximum development during the Neogene (Miocene plus Pliocene, i.e. 23.03 to 2.59 Ma), when a vast wetland covered the western Amazon (Wesselingh *et al*. 2002, Hoorn *et al*. 2010). It was also during the Neogene that the Andes had its last major uplift, an event that drastically changed the drainage system and culminated in the formation of the Amazon River that began flowing east from late Miocene (Figueiredo *et al*. 2009, Sacek 2014).

Today Amazonia extends over ca. seven million km^2 in nine different countries and it is the largest tropical forest on the planet, with a key role in influencing the global climate (Goulding 2003). The region is a major component of the global carbon cycle, producing ~20 Pg C/year by photosynthesis, accounting for ~20% of global terrestrial carbon cycling (ca. double annual fossil fuel emissions) and holding ~25% of terrestrial biomass (Grace *et al*. 2001), a number that is ca. 86 Pg C (Saatchi *et al*. 2007). It is also a principle component of the global hydrological cycle — the Amazon River accounts for ~20% of all the freshwater

discharged into the world's oceans (Franzinelli and Potter 1984). Along its course from the Andes to the Atlantic Ocean, it runs ca. 6.700 km and connects to tributaries that are amongst the largest rivers on the planet (e.g. the Madeira and Purus Rivers) (Goulding 2003). Precipitation is high almost across the entire basin and is primarily controlled by the Intertropical Convergence Zone, which brings moisture to the hinterland from the tropical Atlantic. Rainfall is higher in the western Amazonia, where months with precipitation <100 mm does not exist in vast areas that are thus non-seasonal (Sombroek 2001). A huge amount of water is recycled in the basin through the precipitation/evaporation cycle (up to 50%) (Salati and Vose 1984, van der Ent *et al*. 2010); the associated evapotranspiration vents latent heat into the atmosphere, contributing to the largest land-based atmospheric convection centre on Earth with connections to extra-tropical hydrology and circulation (Barry and Chorley 1995).

In terms of biodiversity, Amazonia has always called the attention of scientists for its high and partially unexplored diversity. After decades of collection, even large mammals are found in recent times like the newly described titi monkey (Dalponte *et al*. 2014), as well as several bird species (Miranda *et al*. 2013), not to mention the more often new plant species (e.g. Campacci *et al*. 2010, Koch *et al*. 2013). Diversity estimates of plant species richness have been ongoing for many decades and usually involve the counting of trees in forest plots (Black *et al*. 1950, Pires *et al*. 1953), and because of the high number or rare species these estimates rely on statistical modelling. Numbers vary from over 11,000 to 16,000 trees >10 cm DBH (diameter at breast height) (Hubbell *et al*. 2008, Steege *et al*. 2013), to overall plant diversity between 30,000 and 80,000 (numbers are quite variable due to sampling gaps and herbaria misidentification or lack of identification, Hopkins 2007). A general pattern has been found and shows a gradient of increasing diversity from east to west (Morales and Vinicius 2003, Steege *et al*. 2006), that seems to follow rainfall, soil fertility and ecosystem

productivity. The diversity of Amazon plants is spread along a vast area of lowland that, contrary to long held views, is highly heterogeneous. Various types of habitats exist (Fig. 1.3): the *terra firme* forest is the upland type, covering up to 90% of the land, not prone to flooding, the most diverse, with a higher canopy and relatively clear understory (Pires 1974, Schubart 2000). This forest also has specific vegetal formations like those dominated by lianas, palms, bamboo and in ecotone regions it can acquire a dryer than normal appearance (Pires and Prance 1985). The second most important type of vegetation is the seasonally flooded forests, divided in whitewater (*várzea*) and blackwater (*igapó*) forests. *Várzeas* are flooded by rivers originating in the Andes that carry a heavy sediment load and therefore are rich in nutrients. *Igapós* are flooded by low nutrient waters washed from inside forests and rich in humic acids from leaf decomposition, like those of the Negro River (Prance 1978, Pires and Prance 1985, Wittmann *et al*. 2002, Junk *et al*. 2011). Scattered around and in lower proportion there are savannah and *campina* forests – savannahs are restricted to bordering areas where dryer climates prevail like in the northern Brazilian state of Roraima. Campinas are heath forests, present all over the basin and having an edaphic constraint in their development, poor soils composed largely of white sand and sometimes waterlogged (Adeney *et al*. 2016). Contrary to *terra firme* and flooded forests, savannahs and *campinas* have a low stature in their physiognomies, they differ from each other in that savannahs can have a dense grass cover but campinas do not (Pires and Prance 1985, Ferreira 2009). This diversity in habitat types increases the number of endemic species and in turn the overall plant diversity in Amazonia.

A matter of constant debate is the origin of diversity in Amazonia. When and how did so many species originate? What is the relation of climate, ecology, geography and other variables in triggering speciation? Hypotheses have existed for over a century, and started as old as in 1878 when Alfred R. Wallace postulated that the long term stability of the

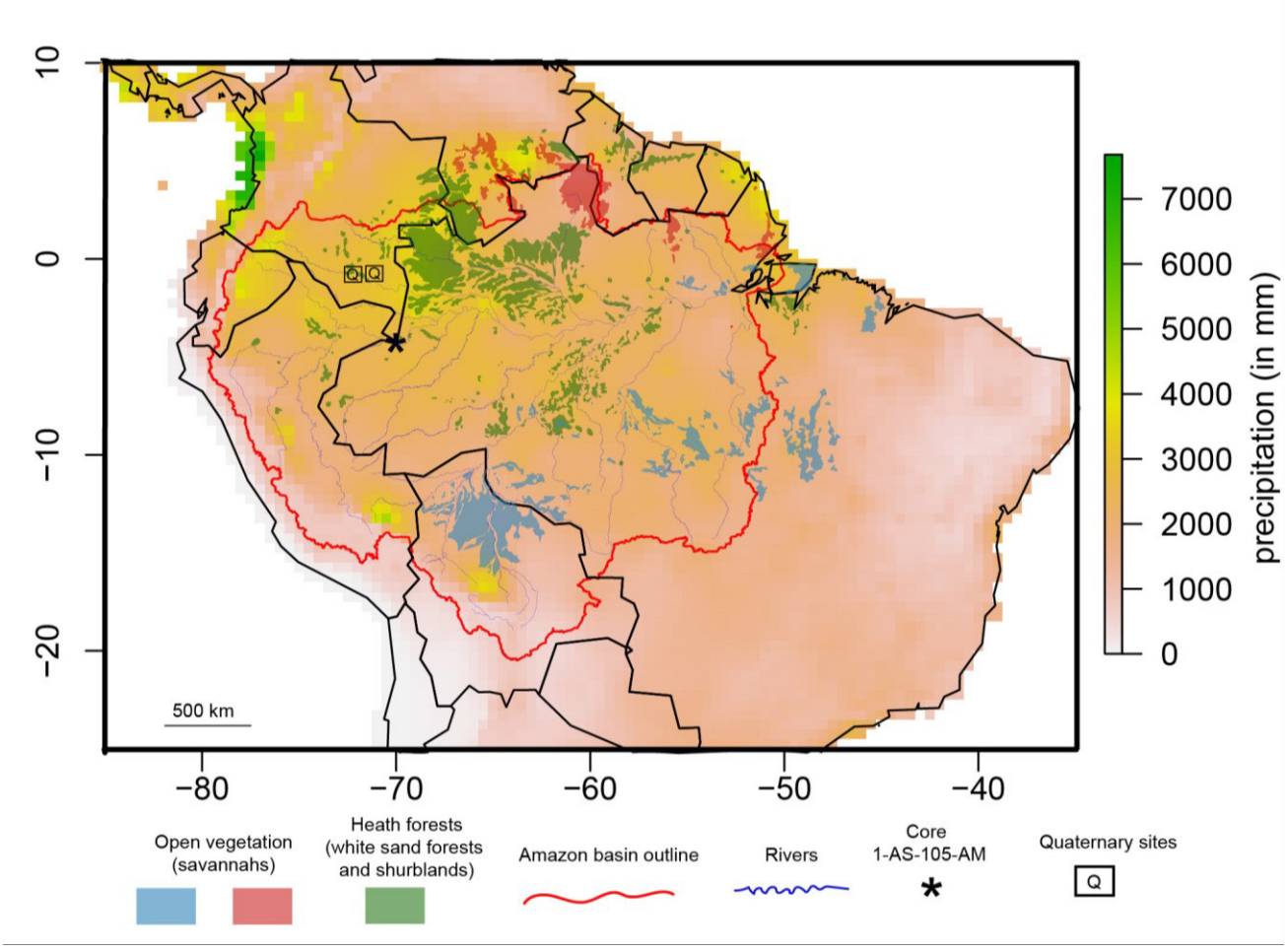

Figure 1.3. Map of NW South America with mean annual precipitation (coloured background) and limit of the Amazon hydrographic basin (red line). Vegetation types are shown for the area within the red line and close surroundings only. Dense evergreen forest (*terra firma*) covers the majority of the area (not shown in any colour, for clarity) and small patches of other main vegetation types are shown in blue (savannahs), red (savannahs including highland open ares of the Guyana mountains) and green (white-sand formations); see texts for details. Flooded forests (*várzea* and *igapó*) are associated with the main rivers (thin blue lines). Background map procuded using R package '`dismo`' (Hijmans *et al*. 2013) and vegetation adapted from Adeney *et al*. (2016).

ecosystem would create appropriate conditions for the gradual accumulation of species. In that regard, tropical areas are museums, where low extinction rates (Stebbins 1974) lead to increments to the species pool as time passes by. Not only are tropical areas museums, but also cradles where animals and plants originate and subsequently spread to and adapt in extratropical areas (Davis *et al*. 2002, Jablonski *et al*. 2006, 2013; Antonelli *et al*. 2015). The birth of tropical diversity posits two main types of questions, the first about mechanisms and the second about timing of species originations. Mechanisms leading to diversity in the tropics can be associated with a variety of factors like (i) biotic relationships (Dobzhansky 1950, Vermeij 2005, Schemske *et al*. 2009) and to (ii) expansion of the available area that species occupy (Rosenzweig 1995, Fine *et al*. 2008). Timing of diversification is a more tractable topic that can be studied using the fossil record as well as genetics. Using dated phylogenies and fossil calibration of typical understory plants from the Neotropics, Davis *et al*. (2005) postulated a mid-Cretaceous origin for the tropical forest structure. Perhaps with more certainty, a modern-like plant association started existing in the Paleogene ca. 58 Ma, as revealed by the Cerrejón Coal deposits of Colombia, where many affinities were established between extant plant families and Paleogene macrofossils (Wing *et al*. 2009). Following this first record of a tropical forest, no fundamental changes to the structure and composition of plant diversity have been recorded, and dominant families seem to have since then been the same all around the tropics (Ricklefs and Renner 2012). Irrespective of a relatively stable tropical forest during the past ca. 60 Ma, diversity oscillates constantly and this oscillation does not seem to occur randomly. Temperature is thought to be a key player in driving plant diversity - plant communities responded to warming periods of the Tertiary by promoting diversification (Jaramillo *et al*. 2006, Jaramillo *et al*. 2010b). Overall neotropical plant diversity seems to mirror global temperature records, with peaks of diversification during peaks in temperature, e.g. the PETM (Paleocene-Eocene Thermal Maximum) and decreases

during cooling periods like the Oligocene. Direct and important conclusions of this story are that (i) there is a directionality in plant diversity over time closely related to climate and (ii) tropical forests already experienced much higher temperatures without collapsing (e.g. Dick *et al*. 2013).

1.3. The Miocene of western Amazonia

During the Miocene, the Amazon basin largely acquired a modern geography. The basin's dimensions were similar to present, except in early to middle times of the Miocene when west Amazonia was connected to the Orinoco, Magdalena and north Paraná drainages (Lundberg *et al*. 1998). These Pan-Amazonia connections were possible because Andean deformation was not yet developed enough to generate the water-shed divides that later isolated basins (Mora *et al*. 2010). As a result of lower topographic ranges in the Andean chain during the early to earliest middle Miocene, drainage developed in cratonic areas (e.g. Guyana shield) with a westward flow into western Amazonia, and sediment accumulation developed along the Andean south-north stretching basins and east-west intracratonic basins (Hoorn *et al*. 2010). This drainage system was also flowing north into the Orinoco and subsequently into the Caribbean Sea, from which marine incursions advanced against the continent at times (Vonhof *et al*. 1998, Hovikoski *et al*. 2007, 2010, Linhares *et al*. 2011, Boonstra *et al*. 2014, Jaramillo *et al*. in prep (this thesis chapter 6 and appendix)). This vast area had a very low topographic gradient, rivers flowed slowly and because of that vast lakes (a.k.a. 'Pebas system') were formed and persisted for thousands to millions of years (Hoorn 1993, 1994a, 1994b, 2010, Wesselingh 2002, 2006, Wesselingh *et al*. 2006c) during the early and middle Miocene. During the late Miocene, a peak in Andean orogeny at ca. 12 Ma intensified sediment infilling of the Andean foreland basins (Uba *et al*. 2007) that eventually

became overfilled and therefore the wetlands had their demise (Wesselingh *et al*. 2002, Hoorn *et al*. 2010).

The late Miocene in western Amazonia is characterised by more river dominated environments (Westaway 2006, Latrubesse *et al*. 2007, 2010, Silva-Caminha *et al*. 2010, Gross *et al*. 2011). With accelerated basin infill generated by continued uplift of the Andes, large-scale accretion processes advanced eastward until the central Amazonia Purus arch was breached (Sacek 2014). Expression of this evolution is recorded at the Amazon Fan, with replacement of the carbonate platform with more terrigenous sediments from ca. 11.8 Ma (Figueiredo *et al*. 2009), suggesting the onset of the reversed drainage at this point of time. By the latest late Miocene and Pliocene, important rivers disconnected from the Andes as a result of local uplifts (Latrubesse *et al*. 2010), like the Fitzcarrald and Vaupés highs (Fig. 1.2) (Mora *et al*. 2010). This lead to the final reorganisation of the transcontinental Amazon drainage system.

Biodiversity

The evolution of the Amazon biota follows the story narrated above. The Pebasian wetland was inhabited by a diverse molluscan fauna that included an outstanding number of endemics (Nuttall 1990, Wesselingh 2006). Lakes and rivers also witnessed the diversification of a rich fish fauna (Monsch 1998, Lundberg *et al*. 2010), part of which invaded western Amazonia from the Caribbean during marine connections (Lovejoy *et al*. 1998, 2006, Cooke *et al*. 2011). This invasion includes the river dolphin (Hamilton *et al*. 2001). Large mammals and reptilians also lived in and around the Miocene wetlands, like crocodilians and rodents (Kay *et al*. 1997, Cozzuol 2006, Latrubesse *et al*. 2010), among others. One of the most extraordinary megafaunal records has been the apex predator *Purussaurus brasiliensis* that reached over 12 metres long and had a bite force comparable to

that of a *Tyrannosaurus rex* (Aureliano *et al*. 2015). The great majority of this fauna went extinct by the Late Miocene and Pliocene, when the wetlands drained. At ca. 10 Ma, the intensification of the Great American Biotic Interchange (GABI) brought completely new elements to the faunal diversity of western Amazonia from central and north America (Carrillo *et al*. 2015).

Knowledge of Miocene plant diversity in western Amazonia greatly depends on palynology. To date, known botanical affinities of Miocene pollen and spores is scarce, but nevertheless allow us to have a picture of palaeovegetation. Tropical evergreen forest has existed over the entire Miocene with no change in biome type (Hoorn *et al*. 1993, 1994a, 1994b, Silva-Caminha *et al*. 2010). What is more, the continuous and frequent presence of abundant palms, Bombacoideae, grass and aquatic plants pollen in sedimentary sequences attest to the presence of flood plains (*várzeas*) and swamps. Some authors (Hooghiemstra and Van der Hammen 1998, Van der Hammen and Hooghiemstra 2000, Jaramillo *et al*. 2006) have used pollen counts from west Amazonia sites to tentatively compare them to similar modern sites and suggested that plant diversity may have been higher in the Miocene. Other attempts found no significant difference between Miocene and extant pollen diversity (Jaramillo *et al*. 2010a). Most importantly there is a complete lack of a comprehensive Miocene pollen diversity analysis that details how diversity changed over time and the relationship to other extrinsic variables.

1.4 Objectives of the present thesis

1.4.1 To improve the Neogene biostratigraphy of western Amazonia by means of performing palynological analyses of borehole samples. Regional palynostratigraphy is entirely dependent on correlation with pollen zonations in Venezuela and Colombian Llanos (Lorente 1986, Jaramillo *et al*. 2011). A need for more robust biostratigraphical frameworks

exists. Hence detailed palynological work must seek to improve the number of correlative points (key species) used basinwide. This is done by means of dating one core (Chapter 5) and fully describing its palynology, including new species (Chapter 4).

1.4.2. To identify marine incursions during the time of deposition studied (Chapter 6). Due to the fairly low-angle deposition and dense vegetation cover, studied outcrops are short sections over long geographic distances. This in turn significantly hampers correlation of strata and as a result mapping and timing of marine incursions has been very contentious (e.g. Hovikoski *et al*. 2010 and Latrubesse *et al*. 2010). How many times did brackish or marine water reach western Amazonia? What was the duration of such incursions? The null hypothesis of non-existence of such marine incursions is ruled out due to well-known episodic incursions (Hoorn 1993, Linhares *et al*. 2011).

1.4.3. Marine incursions potentially were major disturbances to the environment in a large basin-wide scale, yet little is known about vegetation responses to these disturbances. Are there differences in the floristic composition before and after marine incursions? Did they cause origination or extinction? (Chapter 6 and 7).

1.4.4. Does plant diversity correlate with global temperature? (Chapter 7). Following existing patterns shown by Jaramillo *et al*. (2006, 2010b), species diversity correlates positively with temperature change, thus showing increase in biodiversity during warm periods. Conversely, temperature change could promote extinction, or diversity is steady over time. The Neogene has a well-known temperature trend, with a thermal maximum during the mid Miocene, and then a decreasing pattern towards the Quaternary (see Fig. 1.1).

Chapter 2: Study site

2.1 Introduction

Miocene deposits in Amazonia can be found covering a wide geographical area. In central parts of Amazonia, the Novo Remanso Formation (Dino *et al*. 2012) (Amazonas basin in Fig. 1.2) harbours unknown thicknesses of Miocene sediments that accumulated in fluvial settings most likely in isolation from western Amazonian areas (Dino *et al*. 2012, Nogueira *et al*. 2013). Sediments of the Novo Remanso lack a good mapping of their extension and morphology and also facies suitable for pollen analysis are rather rare. In western Amazonia, on the other hand, the Solimões Formation harbous a thick package of early to late Miocene deposits (see chapter 5) accumulated in paralic settings like those of the Pebas System of lakes and megalakes (Wesselingh *et al*. 2006, Hoorn *et al*. 2010), and its morphology is much better understood (e.g. Maia *et al*. 1977, Latrubesse *et al*. 2010). Many studies have shown thick and flat sequences of pollen rich sediments with a wealth of diversity and possible marine connections with the Caribbean area as indicagted by marine palynomorphs and other structure and fossil forms (Hoorn 1993, Silva-Caminha *et al*. 2010, see chater 6 for a more detailed account).

2.2 Solimões Formation

The Solimões Formation in Brazil is located within the Solimões and Acre basins (Fig.1.2). It extends laterally to neighbouring countries with different names: to the northwest in Colombia (Amazonas Formation), to the west in Peru (Pebas Formation), and to the southwest and south in Peru and Bolivia (Ucayali and Madre de Dios, respectively). This entire system is bounded north and south by high topographic domains, namely the Guyana and Brazilian shields formed of Precambrian basement rocks. To the east, a structural high called the Purus Arch is the boundary, although doubts remain towards the real tectonic

activity of this structure during deposition of the Solimões Formation (Caputo 2011). To the west, the Iquitos Arch is a divide that separated the Solimões/Pebas system from other Andean foreland basins (Fig.1.2), and that at least partially affected regional deposition - the position and activity of this arch are still debated (e.g. Latrubesse *et al*. 2010). Other smaller structures also play a role in the spatial configuration detailed above, their locations can be seen in Fig.1.2. The Formation overlies the Paleocene-Miocene Alter do Chão Formation in the east and the (possibly) Paleocene Ramón Formation in the west, and is overlain throughout the basins by the Pleistocene Içá Formation, modern fluvial sediments or it crops out (Caputo 1973, Maia *et al*. 1977). The Solimões type locality was proposed by Eiras *et al*. (1994) from core 2-RJ-1-AM (Fig.1.2). Sediments accumulated predominantly in fluvio-lacustrine environments and the lithology found is that of grey to green muds and clays, silts, sands and, less abundantly, layers of lignite and rarely limestone. Age relies most heavily on biostratigraphy (mammals, reptilians, molluscs and palynology) due to the lack of other dating means. Early Miocene to Pliocene ages have been established, however, there is some degree of uncertainty especially regarding spatial variability of these ages.

Borehole data from the Brazilian Geological Survey (CPRM) and Petrobras were used to create an isopach map (Maia *et al*. 1977, Latrubesse *et al*. 2010, and Fig.1.2). It shows the depocentre of the Formation is located in the Acre region, westward the Arch of Iquitos, with depths of up to 2,000 metres. This configuration has been used to suggest that sedimentation was spatially influenced by the Iquitos arch (Latrubesse *et al*. 2010). The Brazilian geological service and a series of researchers worked in the Solimões and Içá Formations with the aims of detailing age, modes of deposition, paleoenvironments and paleogeography of this vast area (Maia *et al*. 1977, Couto 1981, Frailey, 1986, Hoorn 1993, Hoorn *et al*. 2010, Latrubesse *et al*. 1997, 2007, 2010, Nuttall 1990, Räsänen *et al*. 1995, Monsch, 1998, Vonhof *et al*.

2003, Hovikoski *et al*. 2005, 2007, 2008,2010, Westaway, 2006, Wesselingh, 2006 Cozzuol, 2006, Silva-Caminha *et al*. 2010, Linhares *et al*. 2011, Gross *et al*. 2011).

2.3 The 'Carvão no Alto Solimões' project

Along the upper reaches of the Solimões River, thin layers of coaly sediments like lignite can be found in outcrops. A coal prospection project in the mid-seventies, the 'Carvão no Alto Solimões' (*Upper Solimões Coal*) was performed by the Brazilian Geological Survey (Maia *et al*. 1977). Eighty-four cores were retrieved using rotatory diamond drilling with H diameter (top 20 metres), N diameter (up to 200 metres) and B diameter (deeper than 200 metres). The cores are stored in Manaus, Brazil, at the facilities of DNPM (Departamento Nacional de Pesquisa Mineral, 'National Department for Mineral Production') and CPRM (Compainha de Pesquisas em Recursos Minerais, 'Mineral Resources Research Company').

2.3.1. Core 1-AS-105-AM

Many of the cores from the Solimões project were damaged because of poor storage conditions, but some remain in good state of preservation. Among those, core 1-AS-105-AM was not only well preserved but also in a strategic position: it is between cores 1-AS-4a-AM (Hoorn 1993) and 1-AS-27-AM (Silva-Caminha *et al*. 2010), which are of early to early-middle Miocene and late Miocene ages, respectively, and therefore a good coverage of the middle Miocene could be advanced, which was essential to answer the research questions here proposed. Core 1-AS-105-AM is located in the vicinity of Tabatinga, Brazil (-4.5, -69.933), it reached 405.2 m and had a total recovery of 271.14 m. The top 26.2 m were discarded at the drilling site, as they were composed of recent fluvial sandy deposits of no interest at the time. The core is composed almost entirely of the Solimões Formation, from 26.2 to 332.7 m, and the remaining 72.5 m are described as Ramón Formation. A summary

core log is presented here (Fig. 2.1) and a detailed log is attached to the appendix material of this thesis (Fig 9.4). Overall, sediments of the Solimões Formation in this borehole are poorly consolidated, mostly massive, with few preserved structures or bioturbation. Fossil content is seen as fragmented carbonized plant remains of millimetric scale, fragmented shell bits but also some layers with rich, very well preserved shells in life position. Beds sit conformably on each other and there is no evidence for discontinuities. Lithologies do not vary much and are mostly composed of alternating clays, silts and muds of grey, green and dark colours, and sand of yellowish, cream and greyish colours. Black peats and lignites are sporadically found, never exceeding one meter in thickness, mostly of a few centimetres. Very thin (ca. 10 cm) reddish paleosoils and (ca. 20-40 cm) dark green biomicrite are also seen; the latter could be thicker (up to 3 metres) as most of them are recorded below and above coring gaps. The bottom parts of the core associated with the Ramón Formation are similar in composition, but thicker beds of white/cream sand seem to prevail towards the base of the section.

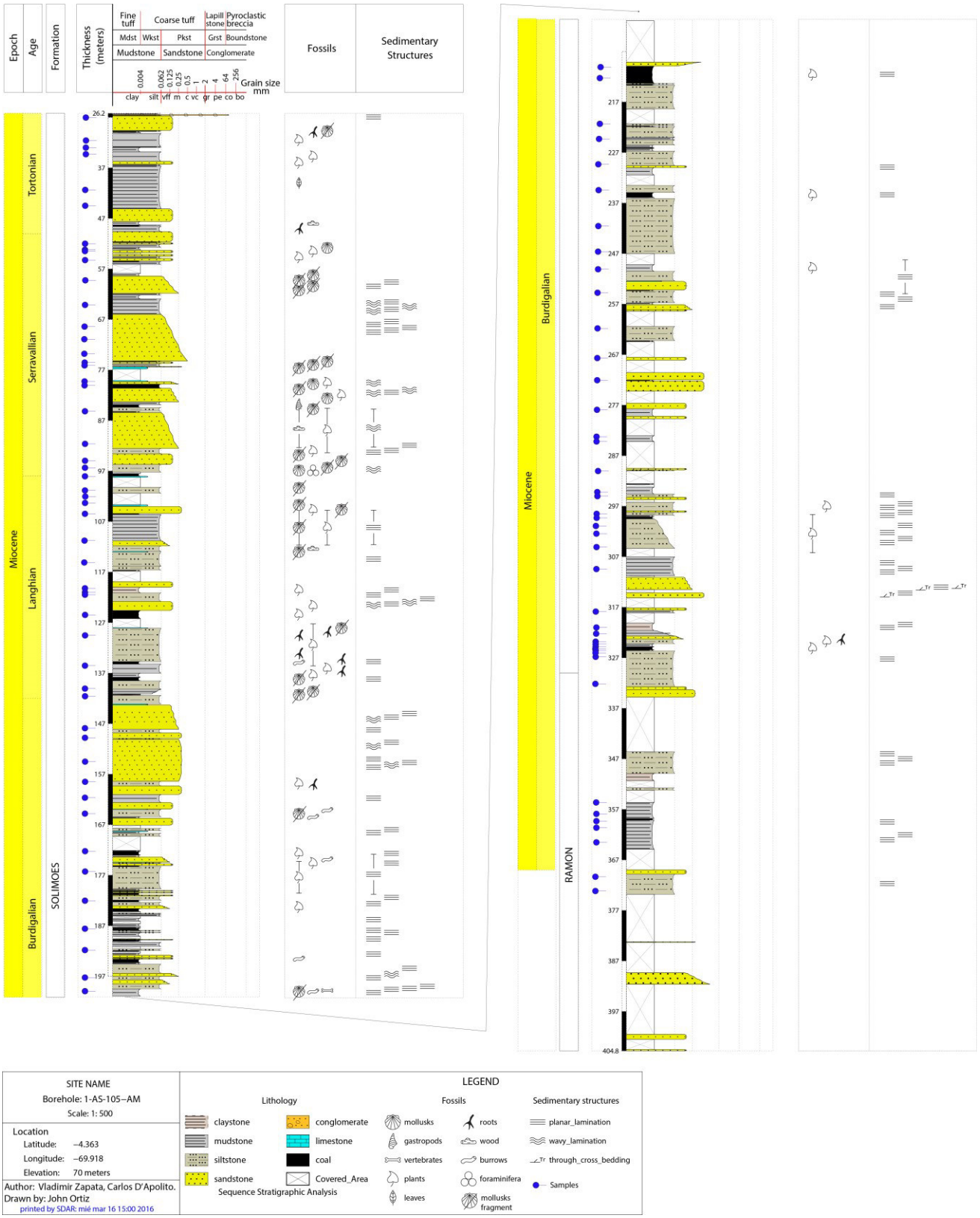

Figure 2.1. Summary stratigraphic log of well 1-AS-105-AM (for a more detailed version see Appendix Fig. 9.4). Age/Stages are from current thesis (Chapter 5).

Chapter 3: General Methods

3.1 Introduction

This section presents all methods used in each of the following chapters, from sample collection and lab techniques to analytical/statistical approaches. Details on the sequence stratigraphy analysis are not included here as this was not performed by me, but it can be found in the appendix material at the end of this thesis.

3.2 Sampling

In March and April 2012 I visited the facilities of CPRM in Manaus together with a sedimentologist for core descriptions and sample collection. We were granted a permit to collect a quarter of the circumference (ca. 1 to 2 cm^3) of the core and selected fine and organic rich sediments that were appropriate for palynological study. Sampling was undertaken throughout the entire core 1-AS 105-AM. The sampling strategy collected one sample at every meter, unless there was a lithological change, in which case sampling resolution was increased to guarantee all lithologies were sampled, especially at lithological boundaries. This in turn meant collecting sometimes many samples per meter. This strategy follows from previous studies of colleagues who found weak signals of marine incursions in other cores of the area (e.g. rare dinoflagellate cysts or foraminiferal linings), we assumed a priori that the incursions were rather rapid and hence even a small sampling gap could mean we would completely miss a marine incursion. Samples were given individual field collection numbers and later they were incorporated into the Smithsonian Tropical Research Institute online geological database at http://biogeodb.stri.si.edu/jaramillo2/fossildb/ that generates labels and numbers that were used for laboratory analytical purposes. Well preserved gastropod and bivalve shells were collected as well.

3.3 Laboratory processing

Pollen samples were processed following conventional methods (Wood *et al.* 1996). They consist of digestion of ca. 10 grams of sediment in hydrochloridric acid for 12 hours (for carbonate extraction), then digestion in hydrofluoric acid for at least 24 hours (for silicate extraction). Neutralisation with water and decanting were used after each acid digestion step. The dissolved mineral portion was later sieved in 250 µm and 10 µm meshes for elimination of coarser portions. The fraction <10 µm was then disaggregated in ultrasonic bath and the less dense organic matter portion recovered. This residue was cleaned in ultrasonic bath for a few seconds and concentrated in a centrifuge. Slides were then mounted with polyvinyl alcohol and sealed with Canada balsam. Analyses were done on an optical microscope Zeiss Axioskop 40 and photomicrographs taken in 1000 x magnification with a Canon EOS-500D. Multiple pictures were made in different focus for each species. Afterwars, when possible, pictures were stacked up together using Adobe Photoshop in order to include as much focus as possivle to individual pictures. Laboratory processing was done by Paleoflora Ltda., Colombia, and pollen analyses performed by me at the University of Birmingham, UK.

Pollen counts were taken on every slide aiming for a minimum of 300 individual specimens of pollen plus spores. Reworked pollen and spores and other structures were also counted (dinocysts, algae cells, foraminiferal linings), but kept outside the 300 count. This results in the total count varying from sample to sample. Identification of pollen and spores followed local and regional publications that describe and illustrate the palynology of upper Tertiary deposits (Germeraad *et al*. 1968, Lorente 1986, Muller *et al*. 1987, Hoorn 1993, Silva-Caminha *et al*. 2010) and the online electronic morphological database of Jaramillo and Rueda (2013) accessible at http://biogeodb.stri.si.edu/jaramillo/palynomorph/pollen that hosts updated taxonomic information of northern south America pollen and spores publications of

Cretaceous and Cenozoic ages. Dinoflagellate cyst identifications were supported by the help of Neogene specialist Stephen Louwye (University of Ghent, Belgium).

3.4. Palynostratigraphy

The age of core 105-AM was determined almost entirely by means of palynology using the method of Graphic Correlation (Shaw 1964, Edwards 1984, 1989). Events of first (FAD) and last (LAD) appearance of the studied section were imported to the software GraphCor (Hood 1998) where the analyses were run. Topmost and bottommost samples were ignored in order to minimize the edge effect (Foote 2000) that artificially increases the numbers of FADs at the bottom and LADs at the top of sections. Next, a correlation was performed between the composite standard section of Jaramillo *et al*. (2011) and core 105-AM. The composite section of Jaramillo *et al*. (2011) was created from 70 sections of late Cretaceous to Recent ages in the Colombian Llanos, Andean foothills and western Venezuela, this zonation was erected using Graphic Correlation and Constrained Optimization (Kemple *et al*. 1995) and calibrated against the geological timescale (Gradstein *et al*. 2012) using data on foraminifera, magnetostratigraphy and bulk carbon isotopes ($\delta^{13}C_{TOM}$). The zonation is currently the most updated one in northern South America and has very good correlation with older zonations from Venezuela (Germeraad *et al*. 1968, Muller *et al*. 1987). Because the composite units are calibrated, ages can be derived for all events of FAD and LAD and therefore ages for individual samples can be interpolated. Recently, some new sections have been added to the composite, which increased the number of taxa used for correlation. One section in particular was key for the correlations made in this thesis: the borehole Saltarin in the Colombian Llanos (Fig. 1.1) is a ca. 700 m Miocene section with very good pollen recovery and displayed a better correlation to the initial composite section than did 105-AM. After addition of Saltarin to the composite, more events could be used to

correlate the resulting composite to 105-AM. These events are marine surfaces (dinocysts acmes) and Sequence Stratigraphical points from the correlation between 105-AM and Saltarin, and altogether they refine the age model. Sequence Stratigraphy was performed by German Bayona (Jaramillo *et al.* in prep). A direct correlation between Saltarin and 105-AM was also performed aiming for similar results. After a careful investigation of suitable taxa to be used, the line of correlation (LOC) was traced manually in every round of correlation. The taxa used were chosen because they fall in the criteria of (i) having a frequent occurrence after their FAD, (ii) having a distinguished morphology that does not allow misidentification and (iii) having a well-known coverage and distribution in the previous zonations, what actually characterizes them as key taxa (see chapter 5 and Fig. 5.1). Correlation equations were then used to derive composite units, which in turn were transformed into ages. All lists of FAD and LAD events, equations for LOCs and R functions used to derive composite units and ages are shown in the Appendix (9.1.a-f).

Molluscan biostratigraphy was also explored as a dating tool. This could only be used for a short part of the section (from 52.9 to 83 m), where well preserved shells were found. Mollusc identification was supported by Frank Wesselingh, Naturalis Institute, Leiden, The Netherlands, and the results compared to the Amazon Molluscan zonation (Wesselingh *et al*. 2006a).

3.5. Palaeoecology

In order to reconstruct the environmental settings in which the Solimões Formation was deposited, palynomorphs were grouped according to their environmental affinities: land pollen (pollen + spores), fresh water algae (*Botryococcus* spp + *Pediastrum* spp) and marine (dinocysts + foraminiferal linings). Among land pollen, subgroups were also adopted, like for instance the mangrove *Rhizophora* spp. (fossil type *Zonocostites* spp) and *Pelliciera* spp.

(fossil type *Lanagiopollis crassa*), palm trees, herbs, aquatic plants and others. A list with all known botanical affinities can be found in Appendix Table 9.2. These groups and subgroups were transformed into relative abundances of the total counts. Pollen diagrams were plotted with R package 'rioja' (Juggins 2015).

Floristic patterns were assessed in different manners. First, pollen diversity (here used as the total number of species) was estimated within-samples using rarefaction (Sanders 1968). This technique standardizes the sample size to a count number lower than the actual sample size. Such a procedure is necessary because the total number of species in a given sample is controlled by the numbers of specimens counted, which in turn vary from sample to sample. A cut-off number (n=226) was chosen in order to maximize the number of samples to be included in the analysis, so samples with less than this value were not included in the diversity analysis. The diversity described above is a within-sample estimate, but groups of samples (among-sample) were also analysed once they were detected, i.e. when a set of samples has similar diversity estimates to another set of samples above or below. This was done with bootstrapped species accumulation curves (Gilinsky 1991). All analyses were performed in R package 'vegan' (Oksanen *et al*. 2015). A comparison with late Holocene pollen diversity was also attempted. Data from four Holocene cores in western Amazonia was sourced from the Latin American Pollen Database (Flantua *et al*. 2015). These sites were: Monica 1 (7,260 yrs Before Present (BP)), Monica 2 (4,010 yrs BP) and Monica 3 (3,200 yrs BP) (Behling *et al*. 1999), which are located at the low terraces of the Caquetá River, approximately 460 km from core 1-AS-105-AM; and Quebrada del Amor (ca. 300 yrs) (Berrio *et al*. 2003), also located at the terraces of the Caquetá River, approximately 490 km from core 1-AS-105-AM. They were chosen because they are lowland sites in western Amazonia, other lowland sites in other areas or upland (montane) sites were not included as they could represent a particular vegetation type only (e.g. montane or submontane biomes),

or be too far away from the study site and therefore suffer influences of different biomes/plant diversity trends. Samples of these cores were combined into one dataset and subjected to the same analysis as Miocene samples.

Second, a multivariate approach was taken to explore the existence of palynofloristic gradients over time. If the abundance data of one species is one variable to be looked at among all samples, then there are as many variables as there are species, which in pollen studies tallies to the hundreds and makes it impractical for single species analysis. Instead, multivariate statistics compress all variables into a few axes of variation. These axes represent similarity showing how samples relate to each other (Legendre and Legendre 1998, Borcard *et al*. 2011) and can be used to explore patterns of the entire plant community on a given gradient that in this case is time. Two ordinations were used: Detrended Correspondence Analysis (DCA) and Canonincal Correspondence Analysis (CCA). Both techniques are rather similar, but CCA allows the addition of environmental variables (Ter Braak 1986), which in the present study was presence or absence of a given paleoenvironmental type (fresh or marine water). This was done to explore how much floristic change can be associated with particular environmental characteristic, i.e. inundations. DCA and CCA were performed in R package 'vegan' (Oksanen *et al*. 2015).

Third, standing diversity, originations and extinctions were calculated. These were used to show if diversity and community behaviours relate to times of specific high/low originations and extinctions. Originations and extinctions are simply the total number of species appearing for the first time or disappearing from the data set. Standing diversity is a more realistic estimate as it assumes a range-through approach of the data (Boltovsky 1998). However, we cannot rely entirely on the standing diversity measures as it is heavily influenced by the edge effect (Foote 2000). A tentative method for estimating the edge effect was introduced by Jaramillo (2002, 2008). It consists of performing a piecewise regression on

both LAD and FAD data separately. Piecewise regressions fit two segmented regression lines to the data, choosing the lines with lowest residual. The breakpoint is the intersection between both lines, and can be interpreted as the stratigraphical point where the edge effect is minimal. Analyses of origination, extinction and standing diversity were run in R package 'stratigraph' (Green 2015). An R code for the piecewise regression was written by Jaramillo (2008) and is shown in the Appendix, adapted to the present data.

Finally, evolutionary models were used to test if there is a preferential direction in diversity change through time (Hunt 2006, 2008, Hunt and Carrano 2010). These models were originally created to fit models of body-size and other morphometric data, but they have been successfully used for diversity metrics (e.g. Sessa *et al*. 2012). The models tested were generalized random walk (GRW), unbiased random walk (URW) and stasis, and they were fitted to diversity estimates and ecological ordination scores. GRW assumes variation of the mean with a trended direction over time. URW and stasis are models that express no trend in the data, the difference is that in stasis there is no accumulation of change over time, and hence time is not significant, whereas in the URW there is variation over time but still no directionality is assumed. Bins of 0.5 Ma were used and model fit was compared using the corrected Akaike information criterion (AICc). Analyses were run in R package 'paleoTS' (Hunt 2015).

Chapter 4. Systematic palynology

4.1. Introduction

In this section the palynology of core 1-AS-105-AM is described and illustrated. Descriptions are given to new forms of particular interest (either common and frequent stratigraphically or, if rare, with a characteristic morphology). Formal established species from the literature are illustrated but not described. A number of new combinations are proposed for species placed in invalid genera. Descriptions of new species were ordered by major morphological groups (e.g. Monoletes, Triletes, Monocolpate, etc), then alphabetical within section. New species and genera were erected and compared to exisiting species in the literature using the online morphological database of Jaramillo and Rueda (2013), which hosts updated taxonomic information on pollen and spores of Cretaceous-Cenozoic ages in northern South America, including key Amazon sites where a high number of species have been described and identified in this study. In total, 491 different palynomorph types were recognized, of which 320 are pollen and 82 are spores species. Newly described species are 76 pollen (38 genera, of which two are proposed as new) and 25 spores (17 genera); fourteen pollen species are new combinations. The terminology used in descriptions follows Punt *et al.* (2007), with some modifications from Jaramillo and Dilcher (2001). All grains are located using the England Finder coordinate system (EF).

For spores the following terminology is used:

1) TLI refers to the Trilete index, which is ‘radius length/ (spore diameter/2)’;

2) MLI refers to the Monolete index, which is ‘laesura length/spore length’.

For pollen the terms used are:

1) CPi is calculated in equatorial view, being ‘colpi length/polar diameter’;

2) CEi was calculated in polar view, being ‘colpi length/equatorial diameter’.

4.2. Pteridophyte and bryophyte spores (alphabetical order)

Monolete spores

Genus *Echinosporis* Krutzsch 1967

Type species. *Echinosporis echinatus* Krutzsch 1967

Echinosporis densiechinatus sp. nov.

Plate 1, figures 1-4

Holotype. Plate 1, figures 1-2, sample 22140, EF P-40-1/2

Paratype. Plate 1, figures 3-4, sample 22326, EF V-37

Type locality: Well 1-AS-105-AM, Solimões Formation, Amazonas, Brazil.

Description. Spores single, symmetry radial, oval; monolete, curvature absent, laesura mid-sized, 15 µm, MLI 0.6, margo absent, commissure indistinct, intexine 1-2 µm, echinate. Echinae densely and evenly distributed over the entire surface of the spore, conical shaped, 2-3 µm tall, 1-1.5 µm wide at base and 1-2 µm spaced.

Dimensions. Equatorial diameter 15-(17.6)-18 µm; polar diameter 26-(25.3)-25 µm; polar/equatorial 1.43. nm=3, no=14.

Remarks. *Echinosporis* sp. Raine 1981 has shorter and sparser echinae. *Polypodiisporites echinatus* Jaramillo and Dilcher 2001 has much longer and wider conical spines and is less dense.

Derivation of name. After the dense echinate pattern.

Genus *Laevigatosporites* Raine 1981

Type species. *Laevigatosporites vulgaris* Ibrahim, 1933

Laevigatosporites caoticus sp. nov.

Plate 1, figures 5-6

Holotype. Plate 1, figures 5, sample 22287, EF H-5-1/2

Paratype. Plate 1, figures 6, sample 22272, EF J-11

Type locality: Well 1-AS-105-AM, Solimões Formation, Amazonas, Brazil.

Description. Spores single, symmetry radial, reniform; monolete, curvature absent, laesura mid-sized, 20 µm, MLI 0.5, margo indistinct, commissure indistinct, intexine 1 µm, scabrate. Scabrae densely and evenly distributed over the entire surface of the spore, short < 0.5 µm, and sometimes anastomosing creating small rugulae.

Dimensions. Equatorial diameter 27 µm; polar diameter 40 µm; polar/equatorial 1.48 µm; nm=2, no=55.

Remarks. *Punctatosporites* sp. A Brenner and Bickoff 1992 is smaller and scabration is almost indistinct meanwhile in *L. caoticus* sp. nov. it is dense and readily recognizable. *P. scabratus* (Couper 1958) Singh 1971 is granulate-scabrate.

Derivation of name. After the irregular (chaotic) scabrate surface.

Laevigatosporites cultellus sp. nov.

Plate 1, figures 7-8

Holotype. Plate 1, figures 7, sample 22279, EF K-24

Paratype. Plate 1, figures 8, sample 22158, EF K-6-1

Type locality: Well 1-AS-105-AM, Solimões Formation, Amazonas, Brazil.

Description. Spores single, symmetry radial, reniform; monolete, curvature absent, laesura long, 58 µm, MLI 0.78, margo raised as a blade along the entire laesura, 6-4 µm wide, commissure straight, intexine 1-1.5 µm, laevigate.

Dimensions. Equatorial diameter 46 µm; polar diameter 74-(65)-56 µm; polar/equatorial 1.41; nm=2, no=2.

Remarks. *Laevigatosporites belfordii* Burger 1976 differs from *L. cultellus* sp. nov. in having a depression in the laesura area.

Derivation of name. After the blade-like margo, the Latin word 'cultellus' means dagger.

Genus *Microfoveolatosporis* Krutzsch 1959

Type species. *Microfoveolatosporis pseudodentatus* Krutzsch 1959

Microfoveolatosporis simplex sp. nov.

Plate 1, figures 11

Microfoveolatosporis sp.1 Silva-Caminha *et al.* 2010

Holotype. Plate 1, figures 11, sample 22354, EF Q-26-4

Type locality: Well 1-AS-105-AM, Solimões Formation, Amazonas, Brazil.

Description. Spores single, symmetry radial, reniform; monolete, curvature absent, laesura distinct, middle small, 15 µm, MLI 0.36, margo distinct, 2 µm wide, segmented to granulate, commissure distinct, straight, intexine 1 µm. Foveolate. Foveolae circular to elongate, 0.7-1.5 µm wide, 1.2 µm apart. Homobrochate, uniformly distributed over the entire surface of the spore.

Dimensions. Equatorial diameter 26 µm; polar diameter 41 µm; equatorial/polar diameter 1.57; nm=1, no=1.

Remarks. *M. skottsbergii* (Selling, 1946) Srivastava, 1971 is larger and has larger foveolae.

Derivation of name. After the rather simple morphology.

Genus *Polypodiisporites* Potonié 1956

Type species. *Polypodiisporites favus* Potonié 1956

Polypodiisporites densus sp. nov.

Plate 1, figures 13-14

Holotype. Plate 1, figures 13, sample 22277, EF D-45-4

Holotype. Plate 1, figures 14, sample 22158, EF W-9-2

Type locality: Well 1-AS-105-AM, Solimões Formation, Amazonas, Brazil.

Description. Spores single, symmetry radial, oval; monolete, curvature absent, laesura mid-sized, 20 µm, MLI 0.47, margo indistinct, commissure indistinct, intexine 2 µm, verrucate. Verrucae densely and evenly distributed over the entire surface of the spore, closely spaced and of constant hight, 1 µm tall, 1-4 µm wide and 1 µm spaced.

Dimensions. Equatorial diameter 35-(29.5)-24 µm; polar diameter 42-(46)-50 µm; polar/equatorial 1.55; nm=2, no=8.

Remarks. *Polypodiisporites* aff. *specious* Sah 1967 is laevigate on the proximal face and has larger irregular verrucae with bases that sometimes connect. This is not a feature in *P. densus*. A thicker sporoderm and laevigate proximal side is a feature of *P. pachyexinatus*. Conversely *P. usmensis* (Van der Hammen, 1956a) Khan and Martin 1972 is gemmate while *P.*? *planus* Silva-Caminha *et al.* 2010 has flat verrucae. The uniform size and distribution of verrucae is characteristic of *P. densus* sp. nov.

Derivation of name. After the dense verrucate pattern.

Polypodiisporites discretus sp. nov.

Plate 2, figures 1-2

Holotype. Plate 2, figures 1, sample 22140, EF N-5-2/4

Paratype. Plate 2, figures 2, sample 22140, EF G-23-4

Type locality: Well 1-AS-105-AM, Solimões Formation, Amazonas, Brazil.

Description. Spores single, symmetry radial, reniform; monolete, curvature absent, laesura mid-sized, 20µm, MLI 0.52, margo indistinct, commissure indistinct, intexine 1 µm,

verrucate. Verrucae sparsely distributed over the entire surface of the spore, very short, <0.5 µm tall, 2 µm wide and 3-5 µm apart.

Dimensions. Equatorial diameter 25-(25.5)-26 µm; polar diameter 38 µm; polar/equatorial 1.49 µm; nm=2, no=68.

Remarks. *Polypodiisporites* aff. *specious* Sah 1967 is laevigate on the proximal face and has larger irregular verrucae. *P. scabraproximatus* Silva-Caminha *et al.* 2010 has a scabrate proximal face.

Derivation of name. After the discrete verrucate pattern.

Polypodiisporites fossulatus sp. nov.

Plate 2, figures 3-4

Holotype. Plate 2, figures 3-4, sample 22418, EF V-43-1/3

Type locality: Well 1-AS-105-AM, Solimões Formation, Amazonas, Brazil.

Description. Spores single, symmetry radial, reniform; monolete, curvature absent, laesura mid-sized, 13 µm, MLI 0.54, margo absent, commissure indistinct, intexine 1.5 µm, foveo-fossulate. Foveolae and fossulae irregularly distributed over the surface of the spore, foveolae appearing isolated less often than anastomosed, in which case they create fossulae. Fossulae of variable size and distribution, sometimes seen as long ridges, very short, <0.5 µm tall, 0.5-1 µm wide and 1-1.5 µm apart. Where fossulae are wider, small verrucae or granulae can be present.

Dimensions. Equatorial diameter 15 µm; polar diameter 24 µm; polar/equatorial 1.6 µm. nm=1, no=5.

Remarks. No fossulate monoletes have been recordered yet. *Microfoveolatosporis* Krutzsch 1959 species are foveolate.

Derivation of name. After the fossulate pattern.

Genus *Puncatosporites* Ibrahim 1933

Type species. *Punctatosporites minutus* Ibrahim 1933

Punctatosporites? latrubessei sp. nov.

Plate 2, figures 9-12

Holotype. Plate 2, figures 9-10, sample 22354, EF J-19

Paratype. Plate 2, figures 11-12, sample 22402, EF E-11-3/4

Type locality: Well 1-AS-105-AM, Solimões Formation, Amazonas, Brazil.

Description. Spores single, symmetry radial; monolete, reniform, curvature absent, laesura mid-sized, 18 µm, MLI 0.58, simple, commissure distinct, invaginated, ends pointed; intexine 1 µm. Scabrate. Scabrae very densely and evenly distributed over the entire surface of the spore, forming a mat-like layer, 1.5-2 µm tall.

Dimensions. Equatorial diameter 18-(18.5)-19 µm; polar diameter 31-(31.5)-32 µm; polar/equatorial 1.7 µm. nm=2, no=4.

Remarks. *Puncatosporites minutus* Ibrahim 1933, *P. scabratus* (Couper 1958) Singh 1971, *P. walkomii* de Jersey 1962 and *Laevigatosporites granulatus* Jaramillo *et al.* 2007 have considerably less dense scabrae and thinner intexine.

Derivation of name. After the geologist Edgardo Latrubesse.

Genus *Reticulosporis* Krtuzsch 1959

Type species. *Reticulosporis miocenicus* (Selling) Krutzsch 1959

Reticulosporis diversus sp. nov.

Plate 2, figures 13-16

Holotype. Plate 2, figures 13-14, sample 22354, EF G-7

Paratype. Plate 2, figures 15-16, sample 22354, EF T-13

Type locality: Well 1-AS-105-AM, Solimões Formation, Amazonas, Brazil.

Description. Spores single, symmetry radial, reniform; monolete, curvature absent, laesura distinct, straight, 20 µm long, tapering, margo distinct, 1.5 µm wide, also tapering, commissure distinct, intexine 1-2 µm. Reticulate. Very few lumina, very broad and of irregular shape, curvy and sometimes lobed. Lumina 10-20 µm wide, muri 1 µm thick, lumina 2 µm apart. Occasionally, luminae are thin, having a canaliculated appearance. Intrareticulate surface laevigate to sparsely granulose, with circular granules, 1-2 µm wide.

Dimensions. Equatorial diameter 21-(23)-25 µm; polar diameter 36-(38)-40 µm; polar/equatorial 1.65; nm=2, no=2.

Remarks. All other monolete-reticulate spores have more regular reticulate patterns.

Derivation of name. After its different (from the Latin "diversus") morphology.

Trilete spores

Genus *Camarozonosporites* Pant ex Potonié 1956, emend. Klaus 1960

Type species. *Camarozonosporites cretaceous* (Weyland and Krieger 1953) Potonié 1956

Camarozonosporites fossulatus sp. nov

Plate 3, figures 4-5

Holotype. Plate 3, figures 4-5, sample 22277, EF S-39

Type locality: Well 1-AS-105-AM, Solimões Formation, Amazonas, Brazil.

Description. Spores single, symmetry radial, circular to subcircular; trilete, curvatura absent, laesura distinct, straight, radii middle sized, 8 µm, TLI 0.61, margo distinct, very thin, 0.5-1 µm wide, commissure distinct, straight, ends pointed; interradial crassitude, intexine 3 µm at the interradial area and 1 µm at corners. Fossulate over the entire surface of the spore. Fossulae long, curvey and irregular, 1 µm wide, 2-3 µm apart, sometimes bifurcating.

Dimensions. Equatorial diameter length 26 µm; equatorial diameter width 25 µm, length/width 1.04; nm=1, no=1.

Remarks. *Camarozonosporites* Pant ex Potonié 1956, emend. Klaus 1960 accommodates verrucate spores with interradial crassitude. *C. crassus* Silva-Caminha *et al.* 2010 is verrucate. *Camarozonosporites* sp. 1 Jaramillo and Dilcher 2001 has thinner interradial crassitude, is laevigate proximally and fossulae is smaller.

Derivation of name. After lobate appearance of the interradial crassitude.

Genus *Camarozonosporites* Pant ex Potonié 1956, emend. Klaus 1960

Type species. *Camarozonosporites cretaceous* (Weyland and Krieger 1953) Potonié 1956

Camarozonosporites trilobatus sp. nov

Plate 3, figures 6-9

Holotype. Plate 3, figures 6-7, sample 22277, EF U-35-4

Holotype. Plate 3, figures 8-9, sample 22278, EF H-37-1

Type locality: Well 1-AS-105-AM, Solimões Formation, Amazonas, Brazil.

Description. Spores single, symmetry radial, triangular-obtuse-convex; trilete, curvatura absent, laesura distinct, straight, radii middle sized, 10 µm, TLI 0.83, margo distinct, very thin, 0.5-1 µm wide, commissure distinct, straight, intexine 5-6 µm at interradial area and 1 µm at corners. Verrucate. Verrucae distributed on the entire surface of the spore. Verrucae larger and irregular on the distal face, and smaller and circular on the proximal face. Verrucae distally can be very large and irregular. Around the equator, verrucae merge and form interradial crassitude that can sometimes resemble lobes. Verrucae 2-7 µm wide, 2-5 µm tall, 1-4 µm apart.

Dimensions. Equatorial diameter length 24-(24.5)-25 µm; equatorial diameter width 20-(20.5)-22 µm, length/width 1.19, nm=2, no=2.

Remarks. *Camarozonosporites* Pant ex Potonié 1956, emend. Klaus 1960 accommodates verrucate spores with interradial crassitude. *C. crassus* Silva-Caminha *et al.* 2010 has smaller and more regular verrucae and thinner interradial crassitude.

Derivation of name. After lobate appearance of the interradial crassitude.

Genus *Cicatricosisporites* Potonié and Gelletich, 1933 emend. Potonié, 1966

Type species. *Cicatricosisporites dorogensis* Potonié and Gelletich, 1933

Cicatricosisporites pseusograndiosus sp. nov.

Plate 3, figures 12-13

Holotype. Plate 3, figures 12-13, sample 22278, EF H-8-3

Type locality: Well 1-AS-105-AM, Solimões Formation, Amazonas, Brazil.

Description. Spores single, symmetry radial, triangular-obtuse-convex; trilete, curvatura absent, laesura distinct, straight, radii long reaching equator, 40µm, TLI 1, margo indistinct, commissure distinct, straight; intexine 0.7 µm. Cicatricose over the entire surface of the spore. Distal ribs 5-7 µm wide, flat, straight, separated by thin grooves 1 µm wide. Ribs arranged in one set on the distal face, running parallel to the equator, sometimes bifurcating, ribs extremities pinch out gently toward the equator and coalesce in the apices. On the proximal face, ribs are similar to the distal face but run in three set, one in each interradial area.

Dimensions. Equatorial diameter length 51-(63)-75 µm; equatorial diameter width 45-(52.5)-60 µm, length/width 1.2; nm=2, no=4.

Remarks. *Cicatricosisporites subrotundus* Brenner 1963 has ribs arranged parallel to the equator in the distal face. *C. pseudograndiosus* sp. nov. differs from *M. grandiosus* (Kedves and Sole de Porta, 1963) Dueñas, 1980 and other species of *Cicatricosisporites* in having much larger ribs and a much higher ribs-groove width ratio.

Derivation of name. After resemblance with *Magnastriatites grandiosus* (Kedves and Sole de Porta, 1963) Dueñas, 1980.

Genus Cingulatisporites Thomson in Thomson and Pflug, 1953

Type species. *Cingulatisporites levispeciosus* Pflug, 1953, in Thomson and Pflug, 1953

Cingulatisporites cristatus sp. nov.

Plate 3, figures 14

Holotype. Plate 3, figures 14, sample 22279, EF U-43

Type locality: Well 1-AS-105-AM, Solimões Formation, Amazonas, Brazil.

Description. Spores single, symmetry radial, circular to triangular-obtuse-convex; trilete, curvatura absent, laesura distinct, curvey, radii long, 10 µm, reaching equator, TLI 0.9, margo distinct, very thin <0.5 µm wide, commissure indistinct, intexine 1 µm. Laevigate with sporadic small verrucae on the surface of the spore. Cingulum is cristate, 2-5 µm thick. Cingulum sculptural elements 1 µm wide, 1 µm tall.

Dimensions. Equatorial diameter length 22-(22.5)-23 µm; equatorial diameter width 20-(20.5)-21 µm, length/width 1.09; nm=2, no=2.

Remarks. Thickness of the cingulum can vary but there is not a clear interradial crassitude. Other species of *Cingulatisporites* do not present a cristate cingulum.

Derivation of name. After cristate cingulum.

Cingulatisporites matisiense sp. nov.

Plate 3, figures 15-18

Holotype. Plate 3, figures 15-16, sample 22278, EF S-19

Paratype. Plate 3, figures 17-18, sample 22278, EF E-12-4

Type locality: Well 1-AS-105-AM, Solimões Formation, Amazonas, Brazil.

Description. Spores single, symmetry radial, circular, cingulate; trilete, curvatura imperfecta, laesura distinct, straight, radii long, reaching equator, 12 µm long, TLI 0.8, margo distinct, 2 µm wide, serrulate border, commissure distinct, straight, cingulum 2-3 µm. Verrucate-rugulate. Verrucae sparse and tend to be clustered in the proximal face, circular, 1-2 µm wide. Distal face has sparse and irregular rugulae, 4-6 µm wide, 2-3 µm thick.

Dimensions. Equatorial diameter length 30-(32.5)-35 µm; equatorial diameter width 30 µm; length/width 1.08; nm=2, no=2.

Remarks. *Cingulatisporites verrucatus* Regali *et al.* 1974 has a much wider cingulum and laevigate proximal face. *Polypodiaceoisporites pseudopsilatus* Lorente 1986 has a triangular prominence on the distal face. *Pteridaceoisporis gemmatus* Silva-Caminha *et al.* 2010 has thicker cingulum, shorter radii and denser and more diverse verruca-rugulae. *Cingulatisporites rugulatus* Silva-Caminha *et al.* 2010 has waving commissure, thinner margo, proximal rugulae and distal scabrae.

Derivation of name. After the amazon indigenous tribe Matis.

Genus *Echinatisporis* Krutzsch 1959

Type species. *Echinatisporis longechinus* Krutzsch 1959

Echinatisporis connectus sp. nov.

Plate 4, figures 7-10

Holotype. Plate 4, figures 7-8, sample 22278, EF P-24

Paratype. Plate 4, figures 9-10, sample 22140, EF L-13

Type locality: Well 1-AS-105-AM, Solimões Formation, Amazonas, Brazil.

Description. Spores single, symmetry radial, circular; trilete, curvatura absent, laesura distinct, irregular, radii reaches the equator, 20 µm long, TLI 0.8, marginate, margo 1 µm wide, commissure irregular; intexine 2-3 µm. Echinate. Spines present on the entire surface,

but more densely distributed on the distal face; 2 µm wide at base, 2 µm tall, conical shapes, closely spaced, 1-2 µm apart. Spines tend to connect to another spine and sometimes create rugulae.

Dimensions. Equatorial diameter length 50-(51)-52 µm; equatorial diameter width 46-(48)-50 µm, length/width 1.06 µm; nm=2, no=2.

Remarks. *E. brevispinosus* Jaramillo, Dilcher 2001 and *E. muelleri* (Regali *et al*., 1974) Silva-Caminha *et al*. 2010 and *E. circularis* Silva-Caminha *et al.* 2010 are much smaller and differ in spine morphology.

Derivation of name. After connection between spines.

Echinatisporis infantus sp. nov.

Plate 4, figures 11-13

Holotype. Plate 4, figures 11-12, sample 22140, EF S-51-2

Paratype. Plate 4, figures 13, sample 22170, EF F-32-2/4

Type locality: Well 1-AS-105-AM, Solimões Formation, Amazonas, Brazil.

Description. Spores single, symmetry radial, circular; trilete, curvatura absent, laesura distinct, straight, radii middle-sized, 10 µm long, TLI 0.66, marginate, margo very thin, 0.7 µm wide, commissure straight; intexine 0.5 µm. Echinate. Spines present on the entire surface; 0.5 µm wide at base, 1 µm tall, 2-3 µm apart. Spines small, conical, evenly distributed.

Dimensions. Equatorial diameter length 30 µm; equatorial diameter width 26 µm, length/width 1.15; nm=1, no=2.

Remarks. *Planisporites* sp. 2 Jaramillo and Dilcher has larger spines and margo is raised. *Acantotriletes levidensis* Balme 1957 has larger spines and radii that reaches equator, E. circularis Silva-Caminha *et al.* 2010 is thicker and has larger spines.

Derivation of name. After the reduced size of spines.

Genus Hamulatisporis Krutzsch 1959

Type species. *Hamulatisporis caperatus* (van Hoeken-Klinkenberg, 1964) Schrank 1994

Hamulatisporis bare sp. nov.

Plate 5, figures 4-5

Holotype. Plate 5, figures 4-5, sample 22140, EF V-9-1

Type locality: Well 1-AS-105-AM, Solimões Formation, Amazonas, Brazil.

Description. Spores single, symmetry radial, circular to triangular-obtuse-convex; trilete, curvatura absent, laesura distinct, straight, radii middle sized, 15 µm long, TLI 0.75, margo thin, 1 µm wide, commissure distinct, straight; intexine 1-2 µm. Hamulate over the entire surface of the spore, slightly coarser distally. Rugula 1 µm wide, curvey, mostly connected and sometimes forming isolated foveolae. Fossula 1.5 µm wide.

Dimensions. Equatorial diameter length 36-(38)-40 µm; equatorial diameter width 33-(35)-37 µm, length/width 1.08 µm, nm=2, no=2.

Remarks. *H. caperatus* (Van Hoeken-Klinkenberg 1964) Schrank 1994 has a finer hamulate pattern. *H. insignis* (Norris 1967) Kedves 1995 has interradial crassitude, rugulae have a radial arrangement and amb is more circular.

Derivation of name. After the Amazon indigenous group Baré.

Genus Ischyosporites Balme 1957

Type species. *Ischyosporites crateris* Balme 1957

Ischyosporites dubius sp. nov.

Plate 5, figures 8-11

Holotype. Plate 5, figures 8-9, sample 22140, EF Q-6-1

Paratype. Plate 5, figures 10-11, sample 22293, EF U-11

Type locality: Well 1-AS-105-AM, Solimões Formation, Amazonas, Brazil.

Description. Spores single, symmetry radial, triangular-obtuse-convex; trilete, curvatura absent, laesura distinct, straight, radii mid-sized, 12 µm long, TLI 0.52, marginate, margo 2-3 µm wide, undulating to straight, thining outwards, commissure distinct, straight; intexine 1.5 µm. Verrucate. Verrucae present over the entire surface of the grain. Most verrucae anastomose to form a rugulate pattern; verrucae very variable, 5 µm wide, 0.5-1 µm tall, with fossulae separating them, of irregular shape.

Dimensions. Equatorial diameter length 27-(36.5)-46 µm; equatorial diameter width 21-(33)-45 µm, length/width 1.1; nm=2, no=7.

Remarks. *I. problematicus* Jaramillo and Dilcher 2001 is fossulate, with higher proportion of fossula in comparison to sculptural elements (verrucae, rugulae). *I. variegatus* (Couper 1958) Jansonius and Hills 1990 is distally foveo-reticulate and proximally granulose to verrucose. *I. badagriensis* Jan du Chene *et al.* 1978 has broad reticulum. *I. crateris* Balme 1957 is thicker and foveolate. *I. dubius* sp. nov. has also a resemblance with *Verrucatotriletes* spp., the difference being the anastomosing character of verrucae and the present of fossula.

Derivation of name. After the large variation of sculptural elements.

Ischyosporites granulatus sp. nov.

Plate 5, figures 12-13

Holotype. Plate 5, figures 12-13, sample 22293, EF D-5-1/2

Type locality: Well 1-AS-105-AM, Solimões Formation, Amazonas, Brazil.

Description. Spores single, symmetry radial, triangular to triangular-obtuse-convex; trilete, curvatura absent, laesura distinct, straight, radii long, almost reaching the equator, 14µm long, TLI 0.73, marginate, margo thick, 3-2 µm, with an irregular outter border, commissure

distinct, straight; intexine 3-2 µm. Rugulate distally and granular to verrucate proximally. Rugulae irregular, long and bifurcating, connecting to each other, sometimes forming sporadic luminae, and of constant width; 4-5 µm wide and of variable length. Granules on the proximal face are sparse, circular and 1-3 µm wide.

Dimensions. Equatorial diameter length 29-(33.5)-38 µm, equatorial diameter width 26-(31)-36 µm, length/width 1.08; nm=2, no=2.

Remarks. Other species of *Ischyosporites* are fossulate and reticulate. Rugulae in *I. granulatus* sp. nov. do not form regular luminae.

Derivation of name. After granulate ornamentation.

Genus Lycopodiumsporites Thiergart 1938

Type species. *Lycopodiumsporites agathoecus* (Potonié) Thiergart 1938

Lycopodiumsporites clavatoides sp. nov.

Plate 5, figures 15-16

Holotype. Plate 5, figures 15-16, sample 22279, EF T-16

Type locality: Well 1-AS-105-AM, Solimões Formation, Amazonas, Brazil.

Description. Spores single, symmetry radial, triangular-obtuse-convex; trilete, curvatura absent, laesura distinct, straight, radii middle sized, 12µm long, TLI 0.8, margo indistinct, commissure indistinct; intexine 3-4 µm. Reticulate over the entire surface of the spore. Lumina circular, 2-3 µm wide, thin muri, 0.7 µm wide. Muri very tall, 3 µm tall.

Dimensions. Equatorial diameter length 30-(34.5)-39 µm; equatorial diameter width 29-(34)-36 µm, length/width 1.01; nm=2, no=2.

Remarks. *L. novomexicanum* Drugg 1967 and *Retitriletes austraclavatoides* (Cookson 1953) Döring *et al*. in Krutzsch 1963 have shorter muri and larger luminae. *Retitriletes altimuratus* Silva-Caminha *et al.* 2010 has shorter muri and indistinct laesura. *Retitriletes baqueroense*

Archangelsky and Villar de Seoane 1998 and *L. fastigioides* (Couper 1953) Boltenhagen 1967 are laevigate on the proximal face.

Derivation of name. After the resemblance with spores of the modern species *Lycopodium clavatum*.

Genus *Neoraistrickia* (Cookson 1953) Potonié 1956

Type species. *Neoraistrickia truncata* (Cookson 1953) Potonié 1956

Neoraistrickia dubiosa sp. nov.

Plate 6, figures 2-5

Holotype. Plate 6, figures 2-3, sample 22293, EF K-50-1/2

Paratype. Plate 6, figures 4-5, sample 22326, EF J-14

Type locality: Well 1-AS-105-AM, Solimões Formation, Amazonas, Brazil.

Description. Spores single, symmetry radial, circular; trilete, curvatura absent, laesura distinct, irregular to straight, radii short, 8 µm long, TLI 0.66, marginate, margo very thin < 1 µm wide, commissure distinct; intexine 1-1.5 µm. Baculate. Bacula present on the entire surface of the spore; 1-1.5 µm wide at base, 1.5-3 µm tall, 1 µm apart, densely distributed and most are constricted at the base.

Dimensions. Equatorial diameter length 24-(24.5)-25 µm; equatorial diameter width 22-(23)-24 µm, length/width 1.06; nm=2, no=3.

Remarks. *N. truncata* (Cookson 1953) Potonié 1956 has larger, less dense bacula and shape is more triangular.

Derivation of name. After the dubious variation of the ornamentation elements, constricted and non-constricted.

Genus *Psilatriletes* Van der Hammen 1954 ex Potonié 1956

Type species. *Psilatriletes detortus* (Weyland and Krieger 1953) Potonié 1956

Psilatriletes delicatus sp. nov.

Plate 6, figures 10-11

Holotype. Plate 6, figures 10, sample 22257, EF P-39-2

Paratype. Plate 6, figures 11, sample 22148, EF M-6-3/4

Type locality: Well 1-AS-105-AM, Solimões Formation, Amazonas, Brazil.

Description. Spores single, symmetry radial, circular; trilete, curvatura absent, laesura distinct, radii long almost reaching the equator, 10 µm long, TLI 0.69, slightly marginate, margo 0.5 µm wide, commissure straight, ends pointed; intexine 0.7 µm. Laevigate. Spore very easily folded, especially around the equator, often creating a false cingunlate appearance.

Dimensions. Equatorial diameter length 22-(25.5)-29 µm, equatorial diameter width 19-(22)-25 µm, length/width 1.15; nm=2, no=8.

Remarks. *Cyathidites minor* Couper 1953 and *C. australis* Couper 1953 are triangular-subtriangular and with thicker intexine. *Biretisporites potoniaei* Delacourt and Sprumont 1955 has radii reaching the equator and thicker intexine and margo. *Hydrosporis minor* Silva-Caminha *et al.* 2010 is smaller and thicker (1.5 µm).

Derivation of name. After the thin and foldable intexine.

Psilatriletes marginata sp. nov.

Plate 6, figures 13-15

Holotype. Plate 6, figures 13-14, sample 22277, EF D-50-2

Paratype. Plate 6, figures 15, sample 22277, EF H-25-3/4

Type locality: Well 1-AS-105-AM, Solimões Formation, Amazonas, Brazil.

Description. Spores single, symmetry radial, triangular-obtuse-straight to slightly convex; trilete, curvatura absent, laesura distinct, straight, radii medium-sized, 10µm long, TLI 0.76, marginate, margo 3-4 µm wide, wider toward the centre the Y-mark, commissure straight, ends pointed; intexine 1.5-2 µm. Laevigate to micropitted. Sporoderm is very often densely perforated but laevigate specimens have been seen. Margo is characteristic, it can be straight or deflected at the central area of the spore, forming two segments.

Dimensions. Equatorial diameter length 26-(31.5)-37 µm; equatorial diameter width 25-(28.5)-32 µm; length/width 1.1; nm=2, no=12.

Remarks. *Dictyophyllidites impensus* (Heldlund 1966) Singh 1983 is circular and has thinner margo. *Hydrosporis minor* Silva-Caminha *et al.* 2010 is smaller, more circular and has thinner margo with granulae.

Derivation of name. After the presence of a margo.

Genus *Rotverrusporites* Döring 1964

Type species. *Rotverrusporites obscurilaesuratus* (Pocock 1962) Doring 1964

Rotverrusporites amazonicus sp. nov.

Plate 7, figures 5-8

Holotype. Plate 7, figures 5-6, sample 22277, EF E-49-1

Paratype. Plate 7, figures 7-8, sample 22279, EF G-8-4

Type locality: Well 1-AS-105-AM, Solimões Formation, Amazonas, Brazil.

Description. Spores single, symmetry radial, circular to subcircular; trilete, curvatura absent, laesura distinct, straight, radii long, 12µm long, almost reaching equator, TLI 0.80, margo distinct, 1 µm wide, straight, commissure distinct, straight; intexine 2 µm thick. Verrucate over the entire surface of the spore. Verrucae 0.5-2 µm wide, 1 µm tall, circular, 0.5 µm apart. Wider verrucae (2 µm wide) are more predominant than smaller ones.

Dimensions. Equatorial diameter length 30-(33)-36 µm; equatorial diameter width 30-(33)-36 µm, length/width 1; nm=2, no=2.

Remarks. *Rotverrusporites rupununiensis* van der Hammen and Burger 1966 is larger, much thicker and has larger verrucae. *Rotverrusporites obscurilaesuratus* (Pocock 1962) Doring 1964 does not have distinct laesura.

Derivation of name. After the Amazon.

Verrucatotriletes pseudoviruleoides sp. nov.

Plate 7, figures 11-12

Holotype. Plate 7, figures 11-12, sample 22278, EF O-9-3/4

Type locality: Well 1-AS-105-AM, Solimões Formation, Amazonas, Brazil.

Description. Spores single, symmetry radial, circular to subcircular; trilete, curvatura absent, laesura distinct, radii middle sized, 17 µm long, TLI 0.73, margo absent, commissure distinct, straight, intexine 2 µm. Verrucate. Verrucate sparse, veru short, over the entire spore. Verrucae 1 µm wide, < 0.5 µm tall, circular, irregularly distributed over entire grain, 2 µm apart.

Dimensions. Equatorial diameter length 46 µm; equatorial diameter width 44 µm, length/width 1.04; nm=1, no=2.

Remarks. *V. viruleoides* Jaramillo *et al.* 2007 has smaller and denser verrucae and thinner intexine.

Derivation of name. After similarity to *V. viruleoides* Jaramillo *et al.* 2007.

4.3. Anteturma Pollenites (ordered by morphological groups, then alphabetical)

Inaperturate

Genus *Inaperturopollenites* (Pflug) Potonié 1958

Type species *Inaperturopollenites dubius* (Potonié & Venitz) Thomson & Pflug 1953

Inapertuporpollenites tectatus sp. nov.

Plate 8, figures 4

Holotype. Plate 8, figures 4, sample 22278, EF T-50

Type locality: Well 1-AS-105-AM, Solimões Formation, Amazonas, Brazil.

Description. Monad, radial, isopolar, amb circular, inaperturate. Tectate, exine 1 μm, nexine 0.3 μm, columellae distinct, 0.3 μm, tectum 0.3 μm thick, micropitted, pits < 0.5 μm, circular, homobrochate.

Dimensions. Polar diameter 24 μm, nm=1, no=21.

Remarks. Usually appears folded. *Inaperturopollenites cursis* Sarmiento, 1992 and *I. curvimuratus* Regali 1974 are reticulate; *I. dubius* (Potonié and Venitz) Pflug and Thomson 1953 in Thomson and Pflug 1953 and *I. simplex* Regali 1974 are atectate-psilate;

Derivation of name. After tectate exine.

Monosulcate

Genus *Arecipites* Wodehouse 1933 emend. Nichols *et al*. 1973

Type species *Arecipites punctatus* Wodehouse, 1933 ex Potonié, 1958

Arecipites membranosus sp. nov.

Plate 8, figures 10

Holotype. Plate 8, figures 10, sample 22460, EF P-20-4

Type locality: Well 1-AS-105-AM, Solimões Formation, Amazonas, Brazil.

Description. Monad, bilateral, heteropolar, prolate to perprolate. Monocolpate, colpi long, reaching poles, ends rounded, borders straight, slightly tapered, colpi 36 µm long, CPi 0.92. Colpi marginate, margo 1 µm wide with a membranous extension reaching halfway through the equatorial diameter in each side of the colpus, membrane very thin, <0.5 µm thick, irregular border and tapering; tectate, exine 1.5 µm, nexine 0.5 µm, columellae 0.5 µm, distinct and packed, tectum 0.5 µm, thick; micropitted, pits <0.5 µm, circular, homobrochate, densely distributed.

Dimensions. Polar diameter 35-(37)-39 µm, equatorial diameter 18-(18.5)-19 µm, polar/equatorial 2; nm=2, no=2.

Remarks. Monocolpate pollen with this type of margo have not been described in Tertiary deposits of northern South America. *Arecipites regio* (Van der Hammen and Garcia, 1966) Jaramillo and Dilcher, 2001 is similar but has a different, often indistinct margo.

Derivation of name. After the membranous appearance of the margo.

Genus *Longapertites* van Hoeken-Klinkenberg 1964

Type species *Longapertites marginatus* van Hoeken-Klinkenberg 1964

Longapertites lisus sp. nov.

Plate 8, figures 15-16

Holotype. Plate 8, figures 15, sample 22279, EF T-9-1/3

Paratype. Plate 8, figures 16, sample 22418, EF G-20-1/2

Type locality: Well 1-AS-105-AM, Solimões Formation, Amazonas, Brazil.

Description. Monad, bilateral, isopolar, prolate. Zonosulcate, grain nearly split in two halves; tectate, exine 1 µm, nexine 0.4 µm, columellae 0.3 µm, distinct and packed, tectum 0.4 µm, thick; psilate to very finely micrpitted. Columellae tips can be seen through tectum.

Dimensions. Polar diameter 42-(44)-46 µm, equatorial diameter 26-(27)-28 µm, polar/equatorial 1.62; nm=2, nm=2.

Remarks. Other *Longapertites* species are micropitted and reticulate.

Derivation of name. After the smooth surface of the grain.

Longapertites sutilis sp. nov.

Plate 9, figures 1-2

Holotype. Plate 9, figures 1-2, sample 22272, EF K-6-3

Type locality: Well 1-AS-105-AM, Solimões Formation, Amazonas, Brazil.

Description. Monad, bilateral, isopolar, perprolate. Monocolpate, colpi longer than the length of grain, almost splitting the grain in two and thus one polar area is open, ends open, borders straight, colpi 34 µm long (on each side), CPi 0.94. Colpi marginate, margo 1 µm wide; tectate, exine 1 µm, nexine 0.4 µm, columellae 0.2 µm, indistinct, tectum 0.4 µm, thick; micropitted, lumina <0.5 µm, elongate, homobrochate, densely distributed, very shallow, lumina sometimes anastomosing and forming fossulae..

Dimensions. Polar diameter 36 µm, equatorial diameter 18 µm, polar/equatorial 2; nm=1, no=2.

Remarks. *Longapertites fossuloides* Gonzalez 1967 has much wider and deeper fossulae and is bigger. *L. marginatus* van Joeken-Klinkenberg 1964 is larger and has heterobrochate micropitted ornamentation. *L. microfoveolatus* Adegoke and Jan du Chene 1978 has a different outline shape (elliptical) and shorter colpus. *L. vaneendenburgi* Germeraad *et al*. 1968 is much larger and evenly micropitted.

Derivation of name. After its subtle appearance.

Genus *Retimonocolpites* Pierce 1961

Type species *Retimonocolpites dividuus Pierce* 1961

Retimonocolpites normalis sp. nov.

Plate 9, figures 11-12

Holotype. Plate 9, figures 11-12, sample 22402, EF U-37-3

Type locality: Well 1-AS-105-AM, Solimões Formation, Amazonas, Brazil.

Description. Monad, bilateral, isopolar, prolate spheroidal. Monocolpate, colpus long, reaching poles, ends open, borders straight, colpi 26 µm long, 3-4 µm wide, simple, CPi 1. Semitectate, exine 1.5 µm, nexine 0.5 µm, columellae 0.5 µm, distinct, ca. 0.5 µm apart, tectum 0.5 µm thick; reticulate, lumina <0.5 µm, circular to slightly elongate, homobrochate, muri 0.5 µm wide

Dimensions. Polar diameter 26 µm, equatorial diameter 24 µm, polar/equatorial 1.08; nm=1, no=1.

Remarks. Similar to *R. claris* Sarmiento 1992 but *R. normalis* nov. sp. differs in having cearly distinct columellae and homobrochate reticulum meanwhile *R. claris* has indistinct columellae, is sometimes intectate, and has quite variable lumina size. *R. longicolpatus* Lorente 1986 is micropitted to finely reticulate. *R. absyae* Hoorn 1993 is heteropolar and has a shorter colpus.

Derivation of name. After the rather generalised morphology.

Zonosulcate

Genus *Proxapertites* Van der Hammen 1956

Type species *Proxapertites operculatus* Van der Hammen 1956

Proxapertites finus sp. nov.

Plate 9, figures 13-14

Holotype. Plate 9, figures 13-14, sample 22326, EF M-21-1/3

Type locality: Well 1-AS-105-AM, Solimões Formation, Amazonas, Brazil.

Description. Monad, radial, heteropolar, oval shaped. Zonosulcate, colpus long, splitting grain in two uneven halves (smaller=54 x 91 µm, larger=65 x 91 µm), borders straight, marginate, margo thin, 1 µm long. Atectate, exine 2 µm thick, covered by a thin and almost translucent perine, <0.5 µm thick, that forms a very coarse reticulum, lumina ca. 10 µm wide, very irregular, muri 1.5 µm wide, somewhat curvimurate.

Dimensions. Wider diameter 84-(91)-98 µm, smaller diameter 58-(65)-72 µm, nm=2, no=8.

Remarks. Halves usually found isolated; reticulum variable in size, sometimes not seen.

Derivation of name. After the fine perine layer.

Trichotomosulcate

Genus *Trichotomosulcites* Couper 1953

Type species *Trichotomosulcites subgranulatus* Couper 1953

Trichotomosulcites amazonicus sp. nov.

Plate 9, figures 17

Holotype. Plate 9, figures 17, sample 22140, EF D-32-3

Type locality: Well 1-AS-105-AM, Solimões Formation, Amazonas, Brazil.

Description. Monad, radial, heteropolar, triangular-obtuse-straight to slighlty concave. Trichotomosulcate, colpus long, radii 19 µm, reaching equator, ends usually open to rounded, marginate, margo 1 µm wide. Semitectate, exine 1.5 µm, exine 0.5 µm, columellae 0.5 µm, distinct, < 0.5 µmapart, tectum 0.5 µm thick. Microreticulate, homobrochate, lumina <0.5 µm wide, circular, muri ca. 0.5 µm wide.

Dimensions. Equatorial diameter length 26-(32)-38 μm, equatorial diameter width 26-(32)-38, length/width 1; nm=2, no=10.

Remarks. *Trichotomosulcites ornatus* Boltenhagen 1976 has much wider reticulum; *T. laevigatus* Boltenhagen 1976 is psilate.

Derivation of name. After the Amazon.

Trichotomosulcites normalis sp. nov.

Plate 9, figures 18

Holotype. Plate 9, figures 18, sample 22405, EF Q-42-1

Type locality: Well 1-AS-105-AM, Solimões Formation, Amazonas, Brazil.

Description. Monad, radial, heteropolar, triangular-obtuse-convex. Trichotomosulcate, colpus long, radii 14 μm long, 3-4 μm wide, almost reaching equator, ends rounded, marginate, margo restricterd to middle section of the sulcus, ca. 1 μm wide and pinching out towards colpi ends. Tectate, exine 2.1 μm, exine 0.7 μm, columellae 0.7 μm, distinct, dense (but not packed) and very thin, tectum 0.7 μm thick. Psilate, columellae tips seen through tectum, giving a micropitted appearance.

Dimensions. Equatorial diameter length 37-(38)-39 μm, equatorial diameter width 35-(36.5)-38, length/width 1.04; nm=2, no=3.

Remarks. *Trichotomosulcites laevigatus* Boltenhagen 1976 has a narrower colpus with wide margo and seems to be atectate.

Derivation of name. After the rather simple morphology.

Monoporate

Genus *Monoporopollenites* (Meyer 1956) Potonié 1960

Type species *Monoporopollenites gramineoides* Meyer

Monoporopollenites annuloides sp. nov.

Plate 10, figures 2-3

Holotype. Plate 10, figures 1-2, sample 22140, EF F-36

Type locality: Well 1-AS-105-AM, Solimões Formation, Amazonas, Brazil.

Description. Monad, bilateral, isopolar, circular. Monoporate, pore 3.5-5 µm wide, annulate, annulus 1.5-2 µm. Tectate, exine 1 µm, nexine 0.4 µm, columellae 0.2 µm, indistinct, tectum 0.3 µm. Psilate to finely micropitted, pits < 0.5 µm wide, circular, scattered over entire grain.

Dimensions. 22-(22.5)-23 µm across; nm=2, no=49.

Remarks. Differs from *Monoporopollenites annulatus* (Van der Hammen, 1954) Jaramillo and Dilcher, 2001 in being thicker, having pitted ornamentation and wider pore and annulus.

Derivation of name. After its resemblance with *M. annulatus*.

Dicolpate

Genus *Dicolpopollis* Pflanzl 1956, emend Potonié

Type species *Dicolpopollis kockeli* Pflanzl 1965

Dicolpopollis? costatus sp. nov.

Plate 10, figures 4-5

Holotype. Plate 10, figures 3-4, sample 22460, EF D-48-2

Type locality: Well 1-AS-105-AM, Solimões Formation, Amazonas, Brazil.

Description. Monad, radial, isopolar, amb sub-circular. Dicolporate, ectocolpi short, ends rounded, 12 µm long, costate, costa produced by a thickening of the whole exine around colpi, 2 µm thick, 8 µm wide, endopores, pore characteristics not visible. Atectate, exine 1-2 µm thick, psilate.

Dimensions. Equatorial diameter length 22-(24.6)-26 µm, equatorial diameter width 21-(22.6)-25 µm, length/width 1.08; nm=3, no=2.

Remarks. The genus *Dicolporites* van der Hammen 1956 is *nomen nudum*. *Dicolpopollis* Pflanzl 1956 accommodates dicolpate grains; I place the present fossil type provisionally in the genus *Dicolpopollis*. *D.? costatus* could be related to the modern genus *Macoubea* (Apocynaceae) which is tricolporate and dicolporate (Colinvaux *et al.* 1999).

Derivation of name. After costate aperture.

Botanical affinity. *Macoubea* (Apocynaceae).

Tricolpate

Genus *Foveotricolpites* Pierce 1961

Type species *Foveotricolpites sphaeroides* Pierce 1961

Foveotricolpites colpiconstrictus Hoorn 1994 nov. comb.

Basionym. *Retitricolpites colpiconstrictus* Hoorn 1994, page 38, plate 4, fig. 2.

Specimens. Plate 10, figures 17-18, sample 22140, EF T-9-1

Description. Monad, radial, isopolar, prolate; tricolpate, endo and ectocolpi coinciding, long, 22 µm long, CPi 0.73, marginate, margo 1 µm thick, ends pointed, constriction present at mesocolpia area of colpi; polar area small, 10 µm wide; tectate, exine 2 µm thick, slightly thicker at apocolpia, nexine 0.5 µm thick, columellae 0.5 µm thick, packed, tectum 1 µm thick; micropitted, pits 0.5 µm, 0.5 µm apart, evenly and densely distributed over the entire grain.

Dimensions.Polar diameter 30 µm, equatorial diameter 22 µm, polar/equatorial 1.36; nm=1, no=10.

Remarks. *Psilatricolporites* van der Hammen 1956b ex Pierce 1961 is an obligate later synonym of *Tricolporites* van der Hammen 1954 (non Erdtman 1949) because they have the same type species; as *Tricolpites* is not validly published and a later synonym of *Clethra*, so is *Psilatricolporites* (Jansonius and Hills 1976, card 2234). *Foveotricolpites* Pierce 1961 accommodates subprolate tricolpate pollen with foveolate ornamentation.

Foveotricolpites simplex Gonzalez 1967 nov. comb.

Basionym. *Retitricolpites simplex* Gonzalez 1967, page 31, plate 2, fig. 1.

Specimens. Plate 11, figures 1-2, sample 22418, EF X-17

Specimens. Plate 11, figures 3, sample 22436, EF L-10-1/2

Description. Monad, radial, isopolar, prolate; tricolp(or)ate, endo and ectocolpi coinciding, 32 µm long, very slightly marginate, margo 0.5 µm wide, CEi 0.68, CPi 0.78, borders straight, ends pointed, polar area very small, 6 µm wide; endopores circular, simple, 10 µm wide; tectate, exine 2.5 µm thick, nexine 0.7 µm thick, columellae 1 µm thick, 0.5 µm wide, 0.5 µm apart, tectum 0.7 µm thick, perforated; foveolate to microreticulate appearance, lumina 0.5 µm wide, muri 0.5 µm thick, densely and evenly distributed over the entire grain.

Dimensions. Equatorial view: polar diameter 36-(38.5)-41 µm, equatorial diameter 20-(24)-28, polar/equatorial 1.60. Polar view: polar diameter length 41 µm, polar diameter width 41 µm, length/width 1; nm=3, no=216.

Remarks. *Retitricolpites* Van der Hammen 1956 ex Pierce 1961 is invalid and a later synonym of *Neea* (Jansonius and Hills 1976, card 2401). *Foveotricolpites* Pierce 1961 accommodates subprolate tricolpate pollen with foveolate ornamentation.

Genus *Ladakhipollenites* Mathur and Jain 1980

Type species *Ladakhipollenites levis* (Sah and Dutta 1966) Mathur and Jain 1980

Ladakhipollenites baitacolumellatus sp. nov.

Holotype. Plate 11, figures 4-5, sample 22257, EF K-45-3

Paratype. Plate 11, figures 6, sample 22140, EF D-16-1/2

Type locality: Well 1-AS-105-AM, Solimões Formation, Amazonas, Brazil.

Description. Monad, radial, isopolar, prolate to subprolate, amb circular; tricolpate, colpi 16 µm long, CEi 0.47, CPi 0.58, long, borders very slightly invaginating, ends rounded, ectocolpi marginate, margo 5 µm wide and 1 µm thick, formed by the decrease of columellae thickness towards colpi, also slightly costate, costa 1 µm wide; polar area small, 6 µm wide; tectate, exine 2 µm thick, nexine 0.5 µm thick, columellae 1 µm thick, columellae thin, 0.5 µm wide, 0.5 µm apart, tectum 0.5 µm thick; tips of columellae seen through tectum, giving a foveolate appearance. Psilate.

Dimensions. Equatorial view: Polar diameter 34 µm, equatorial diameter 25-(27)-29 µm, polar/equatorial 1.25. Polar view: equatorial diameter length 32 µm, equatorial diameter width 32, length/width 1; nm=3, no=7.

Remarks. *Psilatricolpites acerbus* Gonzalez 1967 has packed columellae. *P. anconis* Hoorn 1993 has indistinct columellae and is smaller. *P. clarissimus* (van der Hammen, 1954) van der Hammen and Wymstra 1964 has a different type of margin. *P. colpiconstrictus* van Hoeken-Klinkenberg 1966 has constriction of the colpi. *P. polaroides* Gonzalez 1967 has thicker exine at poles. *P. hammenii* Boltenhagen 1976 is atectate.

Derivation of name. After the Portuguese word ‘baita’, meaning big, many or good in reference to the columellae that are very clearly visible.

Ladakhipollenites colpiconstrictus van Hoeken-Klinkenberg 1966 nov. comb.

Basionym: *Psilatricolpites colpiconstrictus* van Hoeken-Klinkenberg 1966, page 41, plate 1, fig. 13.

Specimens. Plate 11, figures 7-8, sample 22445, EF U-35

Description. Monad, radial, isopolar, prolate-spheroidal; tricolpate, endo and ectocolpi coinciding, 18 µm long, CPi 0.66, borders straight, ends rounded, polar area small, 5 µm wide, costate, costa 1 µm wide; constriction present at mesocolpia area of colpi; tectate, exine 2 µm thick, nexine 0.5 µm thick, columellae 1 µm thick, distincth, 0.3 µm wide, 0.2 µm apart, tectum 0.5 µm thick; tips of columellae seen through tectum. Psilate.

Dimensions. Polar diameter 27 µm, equatorial diameter 25 µm, polar/equatorial 1.08; nm=1, no=10.

Remarks. *Psilatricolporites* van der Hammen 1956b ex Pierce 1961 is an obligate later synonym of *Tricolporites* van der Hammen 1954 (non Erdtman 1949) because they have the same type species; as *Tricolpites* is not validly published and a later synonym of *Clethra*, so is *Psilatricolporites* (Jansonius and Hills 1976, card 2234). *Ladakhipollenites* Mathur and Jain 1980 accommodates tricolpate psilate pollen grains.

Ladakhipollenites nanus sp. nov.

Plate 11, figures 9-10

Holotype. Plate 11, figures 9-10, sample 22148, EF G-12

Type locality: Well 1-AS-105-AM, Solimões Formation, Amazonas, Brazil.

Description. Monad, radial, isopolar, prolate to perprolate; tricolpate, colpi 18-15 µm long, CPi 0.81-0.78, borders straight, ends pointed, simple, polar area small, 5 µm wide; tectate, exine 1 µm thick, nexine 0.3 µm thick, columellae 0.5 µm thick, indistinct, tectum 0.3 µm thick. Psilate.

Dimensions. Polar diameter 19-(19.5)-20 µm, equatorial diameter 9-(10.5)-12 µm, polar/equatorial 1.85; nm=2, no=7.

Remarks. *Psilatricolpites minutus* Gonzalez 1967 has constriction in the mesocolpi, appearing tricolporate.

Derivation of name. After the small size.

Ladakhipollenites simplissimus sp. nov.

Plate 11, figures 11-12

Holotype. Plate 11, figures 11-12, sample 22282, EF R-11-1

Type locality: Well 1-AS-105-AM, Solimões Formation, Amazonas, Brazil.

Description. Monad, radial, isopolar, amb circular; tricolpate, endo and ectocolpi coinciding, 20 µm long, CEi 0.8, long, borders slightly invaginated, ends pointed, margo 3 µm wide x 1 µm thick, formed by the decrease of columellae thickness towards colpi, polar area small, 6 µm wide; tectate, exine 1.8 µm thick, nexine 0.6 µm thick, columellae 0.6 µm thick, distinct, tectum 0.6 µm thick. Psilate. Columellae tips can be seen through tectum and sometimes are indistinct.

Dimensions. Equatorial diameter length 21-(24)-26 µm, equatorial diameter width 18-(22)-25 µm, length/width 1.09; nm=3, no=4.

Remarks. Similar to *L. baitacolumellatus* sp. nov., but differs in the fact that exine is thinner and columella are much thinner and appearing more discrete. *P. clarissimus* (van der Hammen, 1954) van der Hammen and Wymstra, 1964 has a different type of margin.

Derivation of name. Afer its rather simple morphology.

Genus *Retibrevitricolpites* Hoeken-Klinkenberg 1966

Type species *Retibrevitricolpites triangulatus* Hoeken-Klinkenberg 1966

Retibrevitricolpites pseudoretibolus sp. nov.

Plate 12, figures 1-2

Synonymy. *Retibrevitricolpites sp. 1* Silva-Caminha *et al.* 2010 (?)

Holotype. Plate 12, figures 1, sample 22140, EF W-13-2

Paratype. Plate 12, figures 2, sample 22287, EF H-8-1/2

Type locality: Well 1-AS-105-AM, Solimões Formation, Amazonas, Brazil.

Description. Monad, radial, isopolar, amb circular; tricolpate, colpi simple, 4 µm long, CEi 0.18, short, borders straight, ends pointed, polar area large, 14µm wide; tectate, exine 1.8-2 µm thick, nexine 0.6 µm thick, columellae 0.6 µm thick, distinct, tectum 0.6 µm thick. Microreticulate. Lumina 0.5-1 µm, circular, muri 0.5-1 µm wide, homobrochate. Nexine endocracks can be seen in different degrees of intensity.

Dimensions. Equatorial diameter length 22-(25)-28 µm, equatorial diameter width 22-(24.75)-27.5 µm, length/width 1.01; nm=2, no=36.

Remarks. *Retibrevitricolpites retibolus* Leidelmeyer 1966 is tricolp(or)ate and has shorter colpi. *R. distinctus* van Hoeken-Klinkenberg 1966 has much larger heterobrochate reticulum. *R. triangulatus* van Hoeken-Klinkenberg 1966 and *R. deltoides* Dueñas 1986 have strong triangular amb.

Derivation of name. After its similarity with *R. retibolus*.

Genus *Retitrescolpites* Sah 1967

Type species *Retitrescolpites typicus* Sah 1967

Retitrescolpites brevicolpatus sp. nov.

Plate 12, figure 3

Holotype. Plate 12, figure 3, sample 22506, EF R-5-2

Type locality: Well 1-AS-105-AM, Solimões Formation, Amazonas, Brazil.

Description. Monad, radial, isopolar, circular amb; tricolpate, colpi 14 µm long, CEi 0.4, short, costate, borders straight, ends pointed, polar area 20µm wide, costa 2 µm wide, 2 µm

thick; semitectate, exine 2.5 µm thick, nexine 0.5 µm thick, columellae distinct, 1.5 µm thick, 1 µm wide, 1 µmapart, tectum very thin, 0.5 µm thick, almost not visible, giving the wall a retipilate appearance on cross section. Reticulate, lumina 3-4 µm wide, curvimurate to irregular, muri 1 µm wide, simplicolumellate, homobrochate.

Dimensions. Polar diameter length 35-(37.3)-41 µm, polar diameter width 27-(30)-33 µm, length/width 1.24; nm=3, no=13.

Remarks. *Retitrescolpites* Sah 1967 accommodates retitricolp(or)ate with coarse retipilate or reticulate exine. Its type species, *R. typicus* Sah 1967 is described as having "muri usually sinuous", in other words curvimurate. *R.*? *irregularis* (Van der Hammen and Wymstra, 1964) Jaramillo and Dilcher, 2001 is colporate and nexine is thicker than the sexine, the opposite of *R. brevicolpatus* sp. nov. *R. magnus* (Gonzalez, 1967) Jaramillo and Dilcher 2001 and *R. saturum* Jaramillo and Dilcher 2001 are longicolpate.

Derivation of name. After the short colpi.

Genus *Rhoipites* Wodehouse 1933

Type species *Rhoipites bradleyi* Wodehouse 1933

Rhoipites? colpiverrucosus sp. nov.

Plate 12, figures 5-6

Holotype. Plate 12, figures 5-6, sample 22522, EF H-10-2

Type locality: Well 1-AS-105-AM, Solimões Formation, Amazonas, Brazil.

Description. Monad, radial, isopolar, amb circular; tricolpate, colpi 28µm long, CEi 0.7, mid sized, borders straight, ends pointed, marginate, margo produced by a very slight decrease in columellae thickness towards colpi, 2 µm wide, 1 µm thick, costate, costa formed by small and irregular verrucae distributed along colpi, 1-2 µm wide, polar 12 µm wide; semitectate, exine 1 µm thick, nexine 0.4 µm thick, columellae 0.2 µm thick, barely distinct, tectum 0.4

μm thick; stratification is not very clear, and the wall sometimes appears intectate. Microreticulate, lumina 0.5 μm, circular to slightly elongate, 0.5 μm wide, muri 0.5 μm wide, homobrochate.

Dimensions. Equatorial diameter length 35-(37.5)-40 μm, equatorial diameter width 31-(32)-33 μm, Polar/equatorial diameter 1.17; nm=2, no=3.

Remarks. *Retitricolpites scabratus* Herngreen 1975 is thicker with margines that decrease in the size of pits towards the colpi and with a scabrate pattern along the colpi that decreases towards the polar area.

Derivation of name. After scabrae-verrucae along colpi.

Rhoipites? pluricolumellatus nov. sp.

Plate 12, figures 7-8

Holotype. Plate 12, figures 7-8, sample 22158, EF R-12-3

Type locality: Well 1-AS-105-AM, Solimões Formation, Amazonas, Brazil.

Description. Monad, radial, isopolar, suboblate; tricolpate, colpi 11μm long, CPi 0.39, CEi 0.41 , mid-sized, borders straight, ends pointed, polar area 10 μm wide; semitectate, exine 1 μm thick, nexine 0.4 μm thick, columellae 0.2 μm thick, barely distinct, appears to be very thin and can often be seen through muri, tectum 0.4 μm thick. Reticulate, lumina 1-2 μm, circular to polygonal, muri 1 μm wide, pluricolumellate, homobrochate. A few lumina can be smaller, 1 μm wide, but these are not confined to any specific part of the grain's surface. In cross section, the tectum can be seen as an undulating feature, making the reticulum look more salient.

Dimensions. Equatorial view: polar diameter 28 μm, equatorial diameter 32 μm, polar/equatorial 0.87. Polar view: Equatorial diameter length 34 μm, equatorial diameter width 34 μm, length/width 1; nm=2, no=4.

Remarks. *Retitricolpites wijningae* Hoorn 1994 has much longer colpi and is prolate.

Derivation of name. After pluricolumellate pattern.

Genus *Bombacacidites* Couper 1960

Type species *Bombacacidites bombaxoides* Couper 1960

Bombacacidites germeraadi sp. nov.

Plate 13, figures 1-2

Holotype. Plate 13, figures 1-2, sample 22522, EF S-41-4

Type locality: Well 1-AS-105-AM, Solimões Formation, Amazonas, Brazil.

Description. Monad, radial, isopolar, triangular-obtuse-straight grains. Tricolpate, planaperturate with colpi short, 18µm long and straight with pointed ends, CEi 0.45, costae 1.5 µm wide, 2 µm thick, costae surrounding the entire margin of the colpi, having a horse-shoe appearance, and slightly protruding, polar area large, 16 µm wide; semitectate, exine 2 µm thick, nexine 0.7 µm thick, columellae 0.6 µm thick, distinct, 0.5 µm wide, 0.5 µm apart, regularly distributed, tectum 0.7 µm thick. Microreticulate, lumina circular to slightly elongate, 0.5 µm wide, muri 0.5 µm wide, homobrochate.

Dimensions. Polar diameter length 40 µm, polar diameter width 33-(36.5)-40 µm, length/width 1.09; nm=2, no=16.

Remarks. *Bombacacidites soleaformis* Muller *et al.* 1987 is micropitted and has concave sides. *B. brevis* (Dueñas 1980) Muller *et al.* 1987 is smaller, has a circular to triangular-convex amb, thinner wall and costae (sometimes missing), and lacks bulging costae.

Derivation of name. After the palynologist J. H. Germeraad.

Bombacacidites lorenteae Hoorn 1993 nov. comb.

Basionym: *Retitricolpites lorenteae* Hoorn 1993, page 301, plate 1, fig. 27.

Plate 13, figures 3

Specimens. Plate 13, figures 3, sample 22140, EF P-11-3

Description. Monad, radial, isopolar, triangular-obtuse-concave; tricolporate, planaperturate, colpi medium, 18µm long, CEi 0.39, borders straight, rounded pointed, costae thin, 1 µm wide, 1 µm thick, polar area medium, 15 µm wide; semitectate, exine 2 µm thick, nexine 0.7 µm thick, columellae 0.7 µm thick, distinct, 0.7 µm apart, regularly distributed, tectum 0.7 µm thick. Reticulate, lumina circular to elongate, 1-0.5 µm wide, muri 1 µm wide, heterobrochate, lumina increases in size slightly (0.5 to 1 µm) towards polar ares, simplicolumellate.

Dimensions. Polar diameter length 46-(49)-52 µm, polar diameter width 43-(46)-49 µm, length/width 1.06; nm=2, no=9.

Remarks. *Retitricolpites* Van der Hammen 1956 ex Pierce 1961 is invalid and a later synonym of *Neea* (Jansonius and Hills 1976, card 2401). *Bombacacidites* Couper 1960 accommodates planaperturate pollen grains with affinity to genera of the Bombacoideae subfamily.

Tricolporate

Genus *Echitricolporites* Van der Hammen 1956 ex Germeraad *et al.* 1968

Type species *Echitricolporites spinosus* Van der Hammen 1956 ex Germeraad *et al.* 1968

Echitricolporites magnificus sp. nov.

Plate 13, figures 7-10

Malvacipolloides? sp. 3 Silva-Caminha *et al.* 2010

Holotype. Plate 13, figures 7-8, sample 22365, EF S-9-2

Paratype. Plate 13, figures 9-10, sample 22279, EF D-10-2

Type locality: Well 1-AS-105-AM, Solimões Formation, Amazonas, Brazil.

Description. Monad, radial, isopolar, subprolate, circular amb; tricolporate, colpi mid-sized, 20 µm long, borders slightly invaginated, ends pointed, CEi 0.57, costate, costa 1 µm wide, 1 µm thick, costae sometimes only in the central part of the colpi or completely absent, polar area 8 µm; endopores simple, characteristics not seen, sometimes not visible; tectate, exine 1.5 µm thick, nexine 0.5 µm thick, columellae 0.5 µm thick, distinct, closely spaced, regularly distributed, tectum 0.5 µm thick. Supratectal ornamentation echinate, echinae very small, < 0.5 µm tall, 0.5 µm wide at base, well-spaced and homogeneously distributed, 2 µm apart. Intraechinae surface psilate to finely micropitted.

Dimensions. Polar diameter length 25-(30)-35 µm, polar diameter width 25-(30)-35 µm, length/width 1; nm=2, no=15.

Remarks. *Brevitricolpites microechinatus* Jaramillo and Dilcher 2001 is brevicolpate and intectate. *Echitricolpites communis* Regali *et al.* 1974 is colpate.

Derivation of name. After large size and clear morphology.

Genus *Foveotricolporites* Pierce 1961

Type species *Foveotricolporites rhombohedralis* Pierce 1961

Foveotricolporites lolongatis sp. nov.

Plate 14, figures 2-3

Holotype. Plate 14, figures 2-3, sample 22290, EF R-37

Type locality: Well 1-AS-105-AM, Solimões Formation, Amazonas, Brazil.

Description. Monad, radial, isopolar, prolate-spheroidal; tricolporate, endocolpi long, 16 µm long, very thin, almost inconspicuous, invaginating, ends pointed, CPi 0.84, simple; endopores simple, lolongate, 3 x 2 µm; tectate, exine 1 µm thick, nexine 0.3 µm thick, columellae 0.3 µm thick, sometimes indistinct, tectum 0.3 µm thick, overall stratification not

particularly clear. Ornamentation micropitted to psilate, pits circular, < 0.5 µm wide, 0.5 µm apart. The endocolpi borders create a shadow in the pores that may look like an operculum.

Dimensions. Polar diameter 19-(19.6)-21 µm, equatorial diameter 18-(18.6)-19 µm, polar/equatorial 1.05; nm=3, no=102.

Remarks. Lolongate tricolporate pollen grains are not often described in northern South America. *Foveotricolporites rugulatus* and *F.* sp. 3 Jaramillo and Dilcher 2001 are larger and coarsely ornamented. *Rhoipites guianensis* (Van der Hammen and Wymstra, 1964) Jaramillo and Dilcher, 2001 and *Retitricolporites ogowensis* Boltenhagen 1976 are reticulate.

Derivation of name. After lolongate pores.

Genus *Ladakhipollenites* Mathur and Jain 1980

Type species *Ladakhipollenites levis* (Sah and Dutta 1966) Mathur and Jain 1980

Ladakhipollenites? *cassioides* sp. nov.

Plate 14, figures 8-10

Holotype. Plate 14, figures 8, sample 22140, EF L-9

Paratype. Plate 14, figures 9-10, sample 22518, EF N-6-3

Type locality: Well 1-AS-105-AM, Solimões Formation, Amazonas, Brazil.

Description. Monad, radial, isopolar, prolate spheroidal; tricolporate, endo and ectocolpi coinciding, long, 19µm long, CPi 0.79, strongly constricted at equator, ends rounded, polar area 8 µm wide, colpi costate, costae thin, 1 µm wide, sometimes indistinct, pores characteristic not visible; tectate, exine 1.5 µm thick, nexine 0.6 µm thick, columellae 0.4 µm long, sometimes indistinct, tectum 0.6 µm thick; psilate. Sometimes wall structure can not be seen and seems to be atectate.

Dimensions. **Dimensions**. Polar diameter 24 µm, equatorial diameter 21-(22.5)-24 µm, polar/equatorial 1.06; nm=2, no=19.

Remarks. *Psilatricolporites costatus* Dueñas 1980 has much thicker costa. *P. vanus* Gonzalez 1967 is spherical, has nexine = sexine and colpi are simple (?). *L. constrictus* (van Hoeken-Klinkenberg 1966) nov. comb. is colpate, has thicker exine with columellae tips clearly visible through tectum.

Derivation of name. After resemblance with modern genus *Cassia* (Fabceae).

Ladakhipollenites? *corvattatus* sp. nov.

Plate 14, figures 11-12

Holotype. Plate 14, figures 11-12, sample 22278, EF H-11-3

Type locality: Well 1-AS-105-AM, Solimões Formation, Amazonas, Brazil.

Description. Monad, radial, isopolar, prolate spheroidal; tricolporate, ectocolpi mid-sized, 13 µm long, CPi 0.72, ends pointed, constricted at equator, costate, costae 1 µm wide, not extending until the end of colpi and gently fading away, giving the colpi the appearance of a bow tie, endopores very small and narrow, simple, lalongate, 2 x 0.5 µm wide. Polar area 7 µm wide; tectate, exine 1.5 µm thick, nexine 0.5 µm thick, columellae indistinct, 0.5 µm thick, tectum 0.5 µm thick; psilate.

Dimensions. Polar diameter 18-(19)-20 µm, equatorial diameter 16-(17)-18 µm, polar/equatorial 1.11; nm=2, no=2.

Remarks. *Psilatricolporites costatus* Dueñas 1980 has much thicker costa and longer colpi. *P. cassioides* nov. sp. has clear colpi constriction and costa along entire colpi. *Psilatricolpites constrictus* van Hoeken-Klinkenberg 1966 is colpate and has thicker exine.

Derivation of name. After the word *corvatta* meaning tie, for the appearance of the costa endocolpi.

Ladakhipollenites? *endoporatus* sp. nov.

Plate 14, figures 13-14

Holotype. Plate 14, figures 13-14, sample 22522, EF P-13-1

Type locality: Well 1-AS-105-AM, Solimões Formation, Amazonas, Brazil.

Description. Monad, radial, isopolar, prolate; tricolporate, ectocolpi long and very thin, 33µm long, CP1 0.86, ends pointed, costate, costae 2 µm wide throughout entire extension, 1.5 µm thick near mesocolpia and decreasing to 1 µm thick towards apocolpia, borders straight, polar area small, 10 µm, endopores slightly lalongate, simple, 5 x 4 µm wide; tectate, exine 1.8 µm thick, nexine 0.5 µm thick, columellae packed, indistinct, 0.8 µm thick, tectum 0.5 µm thick; psilate.

Dimensions. Polar diameter 35-(36.5)-38 µm, equatorial diameter 22-(23.5)-25 µm, polar/equatorial 1.55; nm=2, no=11.

Remarks. *Ladakhipollenites? caribbiensis* (Muller *et al*., 1987) Silva-Caminha *et al.* 2010 has simple colpi, much larger pores and thick, distinct columellae. *Psilatricolporites costatus* Dueñas 1980 has thicker costa and equatorial constriction. *P. atalayensis* Hoorn 1993 has perforated exine, equatorial constriction and larger pore. *P. crassoexinatus* Hoorn 1993 has thicker exine, with short columella and lalongate pores. *L.? magniporatus* (Hoorn 1993) nov. comb. has much wider pores and thicker tectum.

Derivation of name. After clear endopores.

Ladakhipollenites? *garzonii* Hoorn 1993 nov. comb.

Basionym. *Psilatricolporites garzonii* Hoorn 1993, page 304, plate 2, fig. 7-8.

Plate 14, figures 15-17

Specimens. Plate 14, figures 15-16, sample 22140, EF M-11-3/4

Specimens. Plate 14, figures 17 sample 22140, EF U-12

Description. Monad, radial, isopolar, pblate spheroidal, subtriangular amb; tricolporate, endocolpi short, 10 µm long, costate, costae 1.5 µm wide, 1.5 µm thick, ectocolpi simple, very thin, borders slightly invaginated, ends pointed, polar area small, 7 µm, CPi 0.71, CEi 0.71, endopores lalongate, simple, 2 x 1 µm wide; tectate, exine 1.5 µm thick, nexine 1 µm thick, columellae distinct, 0.5 µm thick, tectum 0.5 µm thick; psilate to very finely micropitted. Thick exine in relation to small grain size.

Dimensions. Polar view: Equatorial diameter length 14 µm, equatorial diameter width 14 µm, length/width 1; Equatorial view: Polar diameter 14 µm, equatorial diameter 15 µm, polar/equatorial 0.93; nm=2, no=7.

Remarks. *Psilatricolporites* van der Hammen 1956b ex Pierce 1961 is an obligate later synonym of *Tricolporites* van der Hammen 1954 (non Erdtman 1949) because they have the same type species; as *Tricolpites* is not validly published and a later synonym of *Clethra*, so is *Psilatricolporites* (Jansonius and Hills 1976, card 2234). *Ladakhipollenites* Mathur and Jain 1980 accommodates tricolpate psilate pollen grains. The grain is provisionally placed in *Ladakhipollenites* as it cannot be satisfactorily placed in any other genus.

Ladakhipollenites? *labiatus* Hoorn 1993 nov. comb.

Basionym. *Psilatricolporites labiatus* Hoorn 1993, page 304, plate 2, fig. 14.

Plate 14, figures 18

Specimens. Plate 14, figures 18, sample 22140, EF L-16-4

Description. Monad, radial, isopolar, prolate; tricolporate, endo and ectocolpi coinciding, short and very thin, almost imperceptible, 12 µm long, CPi 0.44, borders straight, ends pointed, costate, costae 5 µm wide, restricted to area on top and bottom of pores, polar area broad, 12 µm, endopores lalongate, simple, 5 x 2.5 µm wide, pores areas protruding; atectate, exine 1 µm thick; psilate.

Dimensions. Polar diameter 27 µm, equatorial diameter 20 µm, polar/equatorial 1.35; nm=1, no=1.

Remarks. *Psilatricolporites* van der Hammen 1956b ex Pierce 1961 is an obligate later synonym of *Tricolporites* van der Hammen 1954 (non Erdtman 1949) because they have the same type species; as *Tricolpites* is not validly published and a later synonym of *Clethra*, so is *Psilatricolporites* (Jansonius and Hills 1976, card 2234). *Ladakhipollenites* Mathur and Jain 1980 encompasses tricolpate psilate pollen grains. This pollen grain is placed provisionally in *Ladakhipollenites* as it cannot be satisfactorily placed in any other genus.

Ladakhipollenites? *magniporatus* Hoorn 1993 nov. comb.

Basionym. *Psilatricolporites magniporatus* Hoorn 1993, page 304, plate 2, fig. 24.

Plate 14, figures 19-20

Specimen. Plate 14, figures 19-20, sample 22336, EF E-43-4

Description. Monad, radial, isopolar, prolate; tricolporate, colpi long, 31µm long, CPi 0.88, endo and ectocolpi coinciding, simple, borders straight, costate, costae 2 µm wide, 2 µm thick, polar area 10 µm wide, rounded, endopores simple, large, circular, 8 x 8 µm wide, almost anastomosing each adjacent pores; tectate, thick exine, exine 2 µm thick, nexine 1 µm thick, columellae distinct, 0.5 µm thick, tectum 0.5 µm thick; psilate to microreticulate.

Dimensions. Polar diameter 35 µm, equatorial diameter 20-(22)-24 µm, polar/equatorial 1.59; nm=2, no=2.

Remarks. *Psilatricolporites* van der Hammen 1956b ex Pierce 1961 is an obligate later synonym of *Tricolporites* van der Hammen 1954 (non Erdtman 1949) because they have the same type species; as *Tricolpites* is not validly published and a later synonym of *Clethra*, so is *Psilatricolporites* (Jansonius and Hills 1976, card 2234). *Ladakhipollenites* Mathur and Jain 1980 embraces tricolpate psilate pollen grains. We place this pollen grain provisionally

in *Ladakhipollenites* as it cannot be satisfactorily placed in any other genus. The original description says this fossil type is psilate-microreticulate. The specimen seen here is more microreticulate than psilate although otherwise the overall characteristics are similar.

Ladakhipollenites? *nanus* sp. nov.

Plate 14, figures 21

Holotype. Plate 14, figures 21, sample 22320, EF D-48

Type locality: Well 1-AS-105-AM, Solimões Formation, Amazonas, Brazil.

Description. Monad, radial, isopolar, subprolate to prolate; tricolporate, ecto and endocolpi coinciding, 8 µm long, CPi 0.61, borders straight, ends pointed, slightly costate, costae 0.5 µm wide, polar area small, 6 µm wide, endopores circular, simple, rather large in relation to total size of the grain, 2-1 x 2-1 µm wide; walls tructure not visible, probably atectate, exine 0.7 µm thick; psilate.

Dimensions. Polar diameter 12-(12.5)-13 µm, equatorial diameter 9-(9.5)-10 µm, polar/equatorial 1.31; nm=2, no=19.

Remarks. *Psilatricolporites vanus* Dueñas 1983 is bigger (19-29 µm) and has much smaller pores in relation to the grain size.

Derivation of name. After its diminute size.

Ladakhipollenites? *obesus* Hoorn 1993 nov. comb.

Basionym. *Psilatricolporites obesus* Hoorn 1993, page 304, plate 2, fig. 20.

Plate 14, figures 22-23

Holotype. Plate 14, figures 22-23, sample 22140, EF V-22-2

Description. Monad, radial, isopolar, prolate spheroidal; tricolporate, ecto and endocolpi coinciding, short, 8 µm long, CPi 0.47, very thin and almost not visible, borders straight, ends

pointed, costate, costae 1 µm wide, 1 µm thick, restricted to the area on top and bottom of the pores, polar area large, 9 µm, pores quite lalongate, simple, 6 x 1 µm wide; tectate, exine 1 µm thick, nexine 0.3 µm thick, columellae indistinct, 0.3 µm thick, tectum 0.3 µm thick; psilate.

Dimensions. Polar diameter 17µm, equatorial diameter 16 µm, polar/equatorial 1.06; nm=2, no=3.

Remarks. *Psilatricolporites* van der Hammen 1956b ex Pierce 1961 is an obligate later synonym of *Tricolporites* van der Hammen 1954 (non Erdtman 1949) because they have the same type species. However, *Tricolpites* is not validly published and a later synonym of *Clethra* as is *Psilatricolporites* (Jansonius and Hills 1976, card 2234). *Ladakhipollenites* Mathur and Jain 1980 accommodates tricolpate psilate pollen grains. This pollen grain is placed provisionally in *Ladakhipollenites* as it cannot be satisfactorily placed in any other genus.

Ladakhipollenites? *pseudonanus* sp. nov.

Plate 14, figures 24

Holotype. Plate 14, figures 24, sample 22412, EF D-8-1

Type locality: Well 1-AS-105-AM, Solimões Formation, Amazonas, Brazil.

Description. Monad, radial, isopolar, prolate to perprolate; tricolporate, colpi long, 14 µm long, CPi 0.77, costate, costae 1 µm wide, 1 µm thick, polar area small, 6 µm wide, endopores lalongate, simple, fairly small in relation to total size of the grain, 1 x 0.5 µm wide; tectate, exine 1.5 µm, sexine 0.4 µm thick, columellae 0.4 µm thick, indistinct, tectum 0.7 µm thick; psilate.

Dimensions. **Dimensions**. Polar diameter 18 µm, equatorial diameter 9 µm, polar/equatorial 2; nm=1, no=1.

Remarks. *Psilatricolporites nanus* sp. nov. has very thin exine and larger circular pores. *Psilatricolporites vanus* Dueñas 1983 is more oblate, has very thin exine and smaller pores in relation to grain size.

Derivation of name. After resemblance with *Psilatricolporites nanus* sp. nov.

Ladakhipollenites? *pseudosilvaticus* sp. nov.

Plate 14, figures 25-26

Holotype. Plate 14, figures 25-26, sample 22320, EF R-13

Type locality: Well 1-AS-105-AM, Solimões Formation, Amazonas, Brazil.

Description. Monad, radial, isopolar, prolate spheroidal; tricolporate, ecto and endocolpi coinciding, hardly seen, mid-sized, 6 µm long, CPi 0.4, costate, costae 1 µm thick and encircling the whole mesocolpium area, tapering polewards, mesocolpium area is darker due to thicker nexine (costa), polar area large, 8 µm, endopores narrow, lalongate, simple, 5 x 1.5 µm wide; tectate, exine 1 µm, sexine 0.3 µm thick, columellae 0.3 µm thick, indistinct, tectum 0.3 µm thick; psilate to micropitted.

Dimensions. Polar diameter 15-(16.5)-18 µm, equatorial diameter 14-(15)-16 µm, polar/equatorial 1.1; nm=2, no=4.

Remarks. *L.? silvaticus* (Hoorn 1993) nov. comb. has costate endopores with constriction making them salient on cross section, and polar are is much more rounded than *L.? pseudosilvaticus* sp. nov.

Derivation of name. After its resemblance with *L.? silvaticus* (Hoorn 1993) nov. comb.

Ladakhipollenites? *silvaticus* Hoorn 1993 nov. comb.

Basionym. *Psilatricolporites silvaticus* Hoorn 1993, page 304, plate 2, fig. 21.

Plate 14, figures 27-28

Specimens. Plate 14, figures 27-28, sample 22140, EF S-42

Description. Monad, radial, isopolar, subprolate; tricolporate, colpi short, 8 µm long, CPi 0.5, costate, costae 1 µm wide and encircling the whole mesocolpium area, tapering polewards, mesocolpium area is darker due to thicker nexine (costa), pores area slightly protruding; polar area broad, 8 µm, endopores lalongate, simple, 5 x 2 µm wide; tectate, exine 1 µm thick, nexine 0.3 µm thick, columellae 0.3 µm thick, tectum 0.3 µm thick; psilate.

Dimensions. Polar diameter 16-(19)-22 µm, equatorial diameter 14-(16.5)-19 µm, polar/equatorial 1.15; nm=2, no=19.

Remarks. *Psilatricolporites* van der Hammen 1956b ex Pierce 1961 is an obligate later synonym of *Tricolporites* van der Hammen 1954 (non Erdtman 1949) because they have the same type species; as *Tricolpites* is not validly published and a later synonym of *Clethra*, so is *Psilatricolporites* (Jansonius and Hills 1976, card 2234). *Ladakhipollenites* Mathur and Jain 1980 accommodates tricolpate psilate pollen grains. We place this pollen grain provisionally in *Ladakhipollenites* as it cannot be satisfactorily placed in any other genus.

Ladakhipollenites? *sphericus* sp. nov.

Plate 14, figures 29-30

Holotype. Plate 14, figures 29-30, sample 22140, EF X-7-1

Type locality: Well 1-AS-105-AM, Solimões Formation, Amazonas, Brazil.

Description. Monad, radial, isopolar, spheroidal; tricolporate, ectocolpi long, 14µm long, CPi 0.73, simple, endocolpi slightly costate, costae 0.5 µm wide, 0.5 µm thick, ends pointed, polar area small, 5 µm, rounded, ectopores circular, simple, large in relation to grain's total size, 5 x 5 µm wide; tectate, exine 1 µm, sexine 0.3 µm thick, columellae 0.3 µm thick, barely distinct, tectum 0.3 µm thick; psilate to micropitted.

Dimensions. Polar diameter 16-(17.5)-19 µm, equatorial diameter 16-(17.5)-19 µm, polar/equatorial 1; nm=2, no=2.

Remarks. *Psilatricolporites vanus* Gonzalez 1967 has mid-sized colpi and small pores. *P. atalayensis* Hoorn 1993 jas much thicker costa and lalongate pores. *P. crassoexinatus* Hoorn 1993 has thicker exine and lalongate pores. *P. magniporatus* Hoorn 1993 has much thicker exine and is more prolate.

Derivation of name. After circular pores.

Ladakhipollenites? *xatanawensis* sp. nov.

Plate 15, figures 1-3

Holotype. Plate 15, figures 1-3, sample 22140, EF W-35-1

Paratype. Plate 15, figures 4, sample 22256, EF O-40-3/4

Type locality: Well 1-AS-105-AM, Solimões Formation, Amazonas, Brazil.

Description. Monad, radial, isopolar, prolate; tricolporate, ecto and endocolpi coinciding, mid-sized, 25µm long, CPi 0.67, ends rounded, costate, costae 1 µm wide, 1 µm thick, thinning out towards apocolpia, polar area large, 14 µm, rounded, endopores lalongate, oval to lense-shaped, simple, 8-5 x 4-3 µm wide; tectate, exine 1.5 µm, nexine 0.5 µm, columellae 0.5 µm, indistinct, tectum 0.5 µm, stratification not very clear; psilate. Some grains appear to have atectate psilate apocolpia whereas the mesocolpia is slightly micropitted.

Dimensions. Polar diameter 36.5-(36.75)-37 µm, equatorial diameter 20-(20.5)-21 µm, polar/equatorial 1.79; nm=2, no=3.

Remarks. *Psilatricolporites cyamus* van der Hammen and Wymstra, 1964 is smaller and thicker and has an equatorial constriction. *P. atalayensis* Hoorn 1993 is thicker, apocolium is acute and pores have a different shape. *P. magniporatus* Hoorn 1993 is thicker, has distinct

columellae and larger pore. *Retitricolporites poriconspectus* Hoorn 1993 is micropitted, of different shape, smaller and has circular pores.

Derivation of name. After the indigenous tribe Xatanawa of western Amazonia.

Genus *Malvacipolloides* Anzótegui & Garalla 1986

Type species *Malvacipolloides densiechinata* Anzótegui & Garalla 1986

Malvacipolloides dubiosus sp. nov.

Plate 15, figures 9-10

Malvacipolloides sp. 1 Silva-Caminha *et al.* 2010

Holotype. Plate 15, figures 9-10, sample 22287, EF L-8

Type locality: Well 1-AS-105-AM, Solimões Formation, Amazonas, Brazil.

Description. Monad, radial, isopolar, circular; tricolporate, colpi very short, 6 µm long, CEi 0.16, simple, almost indistinguishable from pores, pores circular 10 µm wide, simple; tectate, exine 1.5-2 µm thick, nexine 0.6 µm thick, columellae 0.3 µm thick, distinct, tectum 0.6 µm thick; sculpture echinate, spines 4-4 µm tall, 3-3 µm wide at base, 4-6 µm apart, solid and strongly conical, of homogeneous size, spines slightly sunken into tectum, interspines surface micropitted, pits small, circular <0.5 µm wide and distributed evenly over surface of the grain.

Dimensions. Polar diameter length 37-(38)-39 µm, polar diameter width 36-(37)-38 µm, length/width 1.02; nm=2, no=9.

Remarks. This grain is very similar to *Malvacipolloides maristellae* (Muller *et al.* 1987) Silva-Caminha *et al.* 2010 but differs in spine morphology - *M. maristellae* has raised columellae beneath the spines whereas *M. dubiosus* nov. sp. has a constant columellae thickness. In addition *M. maristellae* has longer spines around the apertures and the spines are bottle shaped, with a rounded base.

Derivation of name. After its superficial resemblance to *M. maristellae*.

Genus *Margocolporites* Ramanajuan 1966

Type species *Margocolporites tsukadai* Ramanajuan 1966

Margocolporites bilinearis sp. nov.

Plate 15, figures 13-15

Holotype. Plate 15, figures 13-15, sample 22290, EF L-45-2

Type locality: Well 1-AS-105-AM, Solimões Formation, Amazonas, Brazil.

Description. Monad, radial, isopolar, subprolate to prolate; tricolporate, ectocolpi long, 18 µm long, CPi 0.75, ends pointed, marginate, margo produce by fading of the sexine along colpi, margo 2 µm wide, endocolpi costate, costa 1.5-1 µm wide and 1 µm thick, thinning out towards apocolpia; endopores circular 3 x 3 µm, simple; tectate, exine 2 µm thick, nexine 0.5 µm thick, columellae 0.5 µm thick, distinct, tectum 0.5 µm thick; sculpture reticulate, lumina 0.5-1.5 µm wide, circular, homobrochate, muri 0.5 µm wide.

Dimensions. Polar diameter 24-(25)-26 µm, equatorial diameter 16-(19)-22 µm, polar/equatorial 1.31; nm=2, no=5.

Remarks. *Margocolporites vanwijhei* Germeraad *et al*. 1968 has much wider margo and is baculate near colpi. *Siltaria hammenii* Silva-Caminha *et al.* 2010 has indistinct columellae and is micropitted.

Derivation of name. After margo running along colpi, resembling two lines.

Margocolporites carinae sp. nov.

Plate 15, figures 16-17

Holotype. Plate 15, figures 16-17, sample 22140, EF Q-20-4

Type locality: Well 1-AS-105-AM, Solimões Formation, Amazonas, Brazil.

Description. Monad, radial, isopolar, triangular-obtuse-straight to slightly convex; tricolporate, colpi short, 12 µm long, CEi 0.34, ends pointed, ectocolpi simple, endocolpi costate, with complex costa: part produced by an outward thickening of nexine around colpi (4 µm wide and 3 µm thick), part produced by absence of the nexine around colpi (3 µm wide), and part immediately along colpi by nexine thickening (3 µm wide). Pores circular 4 µm wide, pore characteristics not clear; tectate, exine 1-1.5 µm thick, nexine 0.5 µm thick, columellae 0.5 µm thick, distinct, tectum 0.5 µm thick; psilate to finely and irregularly pitted. Mid part of the mesocolpia has a slight depression of the exine. Rare tetracolporate forms have been seen.

Dimensions. Polar diameter length 29-(32)-35 µm, polar diameter width 27-(30)-33 µm, length/width 1.06; nm=2, no=4.

Remarks. *Margocolporites* sp. 1 Jaramillo and Dilcher 2001 has dense columellae easily seen through tectum. *M. fastigiatus* Silva-Caminha *et al.* 2010 has margo produced by absence of sexine, not nexine and is fastigiate.

Derivation of name. After palynologist Carina Hoorn.

Botanical affinity. Aspidosperma (Apocynaceae).

Margocolporites "incertus"

Plate 15, figures 18-19

Holotype. Plate 15, figures 18-19, sample 22434, EF N-53-3/4

Type locality: Well 1-AS-105-AM, Solimões Formation, Amazonas, Brazil.

Description. Monad, radial, isopolar, circular; tricolporate, ectocolpi long, 20 µm long, CEi 0.83, ends rounded, marginate, margo produced by absence of the sexine around colpi, 2 µm wide, endocolpi not very clear, costate, costa 1 µm wide. Pores circular 2 x 2 µm wide,

simple; tectate, exine 1.5 µm thick, nexine 0.5 µm thick, columellae 0.5 µm thick, barely distinct, very thin, regularly distributed, tectum 0.5 µm thick; psilate.

Dimensions. Polar diameter length 24 µm, polar diameter width 23 µm, length/width 1; nm=1, no=3.

Remarks. Left under open nomenclature until more specimens are found to elucidate its morphology.

Genus *Paleosantalaceaepites* Biswas 1962 ex Dutta & Sah 1970

Type species *Paleosantalaceaepites dinoflagellatus* Biswas 1962 ex Dutta & Sah 1970

Paleosantalaceaepites invaginatus sp. nov.

Plate 16, figures 5-6

Paleosantalaceaepites sp. 1 Silva-Caminha *et al.* 2010

Holotype. Plate 16, figures 5-6, sample 22278, EF S-20

Type locality: Well 1-AS-105-AM, Solimões Formation, Amazonas, Brazil.

Description. Monad, radial, isopolar, prolate; tricolporate, ecto and endocolpi coinciding, long and very thin, 21 µm long, CPi 0.84, costate, costae 1 µm wide, 1 µm thick, borders highly ingavinated, ends pointed, polar area small, 4 µm wide, endocingulate, endocingulum simple, 2.5 µm wide, formed by endopores connecting to each other; tectate, exine 2 µm thick, nexine 0.7 µm thick, columellae 0.7 µm long, distinct, < 0.5 µm apart, tectum 0.7 µm thick; sculpture foveolate, lumina 0.5 µm wide, circular, distributed over the entire surface of the grain, muri 1 µm wide, homobrochate.

Dimensions. Polar diameter 25-(27)-30 µm, equatorial diameter 17-(17.6)-18 µm, polar/equatorial 1.53; nm=3, no=10.

Remarks. *Paleosantalaceaepites distinctus* Jaramillo & Dilcher 2001 has shortcolpi and costate endocingulum. *P. cingulatus* Jaramillo *et al.* 2010 is larger and has a much wider operculate ectocolpi and costate endocingulum.

Derivation of name. After invaginating colpi.

Paleosantalaceaepites kaarsii Hoorn 1993 nov. comb.

Basyonim. *Retitricolporites kaarsii* Hoorn 1993, page 305, plate 1, fig. 11-12.

Plate 16, figures 7-8

Specimens. Plate 16, figures 7-8, sample 22434, EF E-40

Description. Monad, radial, isopolar, spheroidal; tricolporate, ectocolpi and endocolpi coinciding, very thin, almost imperceptible, and short, 12µm long, CPi 0.27, colpi ends pointed, polar area rounded and quite broad, 38 µm wide, marginate, margo produced by a descrease in lumina size around colpi; pores anastomose and form an endoncingulum, 2.5 µm wide, costate, costa 5 µm thick, thining out towards apocolpia; semitectate, exine 3.5 µm thick, nexine 1.5 µm thick, columellae 1.5 µm thick, distinct, 1 µm wide, 1 µm apart, tectum 0.5 µm thick. Reticulate, lumina circular to curvy, 1-5 µm wide, muri 1-1.5 µm wide, simplicolumellate, often smaller lumina ca. 1 µm wide are present on the corners of larger ones.

Dimensions. Polar diameter 30-(36.5)-43 µm, equatorial diameter 30-(36)-42 µm, polar/equatorial 1.01; nm=2, no=11.

Remarks. *Retitricolporites* (Van der Hammen 1956) Van der Hammen and Wymstra 1964 is invalid and a later synonym of *Viburnum* (Jansonius and Hills 1976, card 2402). *Paleosantalaceaepites* Biswas 1962 ex Dutta and Sah 1970 accommodates tricolporate pollen grainds with long or short colpi and endocingulum. The original description of the holotype

shows a lumina variation from micro (0.5 µm) to mesoreticulate (2.5 µm), we have observed more often larger lumina individuals but microreticulation has also been seen.

Genus *Ranunculacidites* Sah 1967

Type species *Ranunculacidites communis Sah 1967*

Ranunculacidites reticulatus sp. nov.

Plate 16, figures 15-17

Holotype. Plate 16, figures 15-16, sample 22518, EF L-16-1

Paratype. Plate 16, figures 17, sample 22518, EF L-9-3

Type locality: Well 1-AS-105-AM, Solimões Formation, Amazonas, Brazil.

Description. Monad, radial, isopolar, subprolate to prolate shperoidal; tricolporate, ecto and endocolpi coinciding, long and wide, 6-7 µm wide, 17 µm long, CPi 0.56, simple, polar area 7 µm, operculate, operculum as long as colpi, 4 µm wide; pores indistinct; semitectate, exine 2 µm, nexine 1 µm, notably thicker then sexine, columellae 0.5 µm, distinct, 0.5 µm wide, 0.5 µm apart, tectum 0.5 µm; reticulate, lumina circular, elongate to slightly polygonal, 1 µm wide, muri 0.5 µm thick, homobrochate. Operculum coalesces with grain at colpi extremeties in such a way that reticulum of colpi and grain is continuous and has no differentiation of lumina size or shape. Operculum often remains well preserved.

Dimensions. Polar diameter 29-(29.5)-30 µm, equatorial diameter 26-(27)-28 µm, polar/equatorial 1.09; nm=2, no=18.

Remarks. *Ranunculacidites* Sah 1967 accommodates small, tricolp(or)ate, with variable exine ornamentation and operculum covering colpi entirely or partially. *Ranunculacidites operculatus* (Van der Hammen and Wymstra, 1964) Jaramillo and Dilcher 2001 is psilate-micropitted. *Retitricolpites operculatus* Herngreen 1973 is smaller, has larger lumina in comparison to grain size and operculum is psilate.

Derivation of name. After reticulate ornamentation.

Genus *Retibrevitricolporites* Legoux 1978

Type species. *Retibrevitricolporites obodoensis* Legoux 1978 (?)

Retibrevitricolporites solimoensis Hoorn 1993 nov. comb.

Basyonim. *Retitricolporites solimoensis* Hoorn 1993, page 305, plate 2, fig. 12.

Plate 16, figures 20-23

Specimens. Plate 16, figures 20-21, sample 22140, EF H-25

Specimens. Plate 16, figures 22-23, sample 22140, EF D-10-1/3

Description. Monad, radial, isopolar, spheroidal, amb circular; tricolporate, endo and ectocolpi coinciding, very short, 4 µm long, CEi 0.28, simple, borders straight, colpi ends rounded, polar area broad, 11 µm wide; endopores lalongate, 3 x 1.5 µm wide, costate, costa 1 µm wide, restricted to the bottom and top; tectate, exine 1 µm thick, nexine 0.3 µm thick, columellae 0.3 µm thick, distinct, tectum 0.3 µm thick. Microreticulate, lumina circular, < 0.5 µm wide, muri < 0.5 µm wide, homobrochate.

Dimensions. Equatorial diameter length 14-(14.6)-15 µm, equatorial diameter width 14-(14.6)-15 µm; length/width 1; nm=3, no=5.

Remarks. *Retitricolporites* (Van der Hammen 1956) Van der Hammen and Wymstra 1964 is invalid and a later synonym of *Viburnum* (Jansonius and Hills 1976, card 2402). *Retibrevitricolporites* Legoux 1978 accommodates retibrevitricolporate pollen grains.

Genus *Retitrescolpites* Sah 1967

Type species *Retitrescolpites typicus* Sah 1967

Retitrescolpites benjaminense sp. nov.

Plate 17, figures 1-4

Holotype. Plate 17, figures 1-2, sample 22506, EF H-14

Holotype. Plate 17, figures 3-4, sample 22522, EF G-12-4

Type locality: Well 1-AS-105-AM, Solimões Formation, Amazonas, Brazil.

Description. Monad, radial, isopolar, oblate-spheroidal; tricolporate, ectocolpi simple, 16 µm long, CPi 0.55, CEi 0.87, borders straight, ends rounded, endocolpi costate, costa 2 µm wide and 2 µm thick, polar area 8 µm wide; endopores simple, slightly lolongate, 2 x 3 µm wide; semitectate, exine 3 µm thick, nexine < 1 µm thick, columellae 2 µm thick, distinct, 0.5 µm wide, 0.5 µm apart, and double the normal size at the poles, 4 µm thick, tectum very thin, ca. 0.5 µm thick, almost not visible, giving the wall a retipilate appearance on cross section. Microreticulate, lumina 0.5 µm, elongate to curvimurate, muri 0.5 µm wide, homobrochate.

Dimensions. Equatorial view: Polar diameter 29 µm, equatorial diameter 29 µm, Polar/equatorial 1.

Polar view: Polar diameter length 32 µm, polar diameter width 32 µm, length/width 1; nm=2, no=44.

Remarks. *Retitrescolpites* Sah 1967 accommodates retitricolp(or)ate with coarse retipilate or reticulate exine. Its type species, *R. typicus* Sah 1967 is described as having "muri usually sinuous", in other words curvimurate. *R. baculatus* Jaramillo and Dilcher 2001 is much larger and thicker and tricolpate. *R.*? *irregularis* (Van der Hammen and Wymstra, 1964) Jaramillo and Dilcher, 2001, *R. magnus* (Gonzalez, 1967) Jaramillo and Dilcher, 2001, *R. peculiaris* and *R. saturum* Jaramillo and Dilcher 2001 have much coarser reticulum. *R. definidus* Jaramillo *et al.* 2007 has a well-defined costa around colpi.

Derivation of name. After the town Benjamin Constant in Amazonas state, Brazil.

Retitrescolpites grossus sp. nov.

Plate 17, figures 5-6

Holotype. Plate 17, figures 5-6, sample 22503, EF U-8-1

Type locality: Well 1-AS-105-AM, Solimões Formation, Amazonas, Brazil.

Description. Monad, radial, isopolar, subspheroidal, circular amb; tricolporate, ecto and endocolpi coinciding, 30µm long, CPi 0.83, borders invaginated, ends pointed, marginate, margo 2 µm wide, produced by a decrease in columellae thickness and lumina size towards colpi, also costate, costa 2 µm wide and µm thick, thining out towards apocolpia, polar area small; ecto and endopores coinciding, lolongate, 6 µm x 3 µm wide, costate, costa 1.5 µm wide; semitectate, exine 2.5 µm thick, nexine 1 µm thick, columellae 0.5 µm thick, distinct, 1 µm wide, 1 µm apart, tectum 1 µm thick. Reticulate, lumina 1.5-3 µm, elongate to curvimurate, muri 1 µm wide, simplicolumellate, homobrochate.

Dimensions. Equatorial view: Polar diameter 36 µm, equatorial diameter 35 µm, Polar/equatorial 1.02. Polar view: Polar diameter length 25-(32)-39 µm, polar diameter width 24-(31)-38 µm length/width 1.03; nm=3, no=32.

Remarks. *Retitrescolpites baculatus* Jaramillo and Dilcher 2001 is colpate and larger. *R.*? *irregularis* (Van der Hammen and Wymstra, 1964) Jaramillo and Dilcher, 2001 has wider lumina and costate colpi. *R. magnus* (Gonzalez, 1967) Jaramillo and Dilcher 2001 and *R. saturum* (Gonzalez, 1967) Jaramillo and Dilcher 2001 are colpate.

Derivation of name. After its thick wall.

Retitrescolpites marginatus sp. nov.

Plate 17, figures 7-9

Holotype. Plate 17, figures 7-9, sample 22518, EF N-25-2

Type locality: Well 1-AS-105-AM, Solimões Formation, Amazonas, Brazil.

Description. Monad, radial, isopolar, subprolate; tricolporate, ectocolpi marginate and costate, 22 µm long, CPi 0.70, thin, borders straight, ends rounded, polar area small, 16 µm

wide, margo ca. 2 µm wide, produced by a decrease in lumina size immediately along colpi, costa 2 µm wide, 1 µm thick, interrupted around pores; endopores lalongate, 5 µm x 2 µm wide; tectate, exine 0.5 µm thick, nexine 1 µm thick, columellae 0.5 µm thick, distinct, tectum 0.5 µm thick, hardly visible. Suprareticulate, lumina 2-5 µm, highly curvimurate, muri 1 µm wide and 0.5 µm tall, heterobrochate. Reticulum is created by raised muri on top of tectum, meaning muri is not sustained by columellae, but solid.

Dimensions. Polar diameter 31 µm, equatorial diameter 27 µm. Porlar/equatorial 1.14; nm=1, no=5.

Remarks. The combination of suprareticulum with curvimuri has not been described. *R. marginatus* sp. nov. bears some resemblance with *Rohipites guianensis* (Van der Hammen and Wymstra, 1964) Jaramillo and Dilcher, 2001 but the later has lolongate indistinct pores and wall and reticulate structure are also different (elongated).

Derivation of name. After margine of the colpi.

Genus *Rhoipites* Wodehouse 1933

Type species *Rhoipites bradleyi* Wodehouse 1933

Rhoipites caputoi Hoorn 1993 nov. comb.

Basyonim. *Retitricolporites caputoi* Hoorn 1993, page 305, plate 3, fig. 1-2.

Plate 17, figures 18-19

Specimens. Plate 17, figures 18-19, sample 22412, EF P-12-4

Description. Monad, radial, isopolar, prolate; tricolporate, ectocolpi coinciding, mid-sized, 21 µm, CPi 0.66, very thin, borders slightly straight, colpi ends rounded, polar area medium, 13 µm wide, endocolpi costate, costa 1 µm thick and 2 µm wide; pores slightly lalongate, 5 µm x 4 µm wide, simple; tectate, exine 2 µm thick, nexine 0.6 µm thick, columellae 0.8 µm thick, distinct and packed, tectum 0.6 µm thick. Reticulate, lumina circular to slightly

elongate, 1 µm wide, muri 1 µm wide, heterobrochate, lumina decreases slightly towards mesocolpium.

Dimensions. Polar diameter 29-(30.8)-32 µm, equatorial diameter 18-(20.3)-22 µm, polar/equatorial 1.51; nm=3, no=44.

Remarks. *Retitricolporites* (Van der Hammen 1956) Van der Hammen and Wymstra 1964 is invalid and a later synonym of *Viburnum* (Jansonius and Hills 1976, card 2402). *Rhoipites* Wodehouse 1933 accommodates tricolporate pollen grains that are reticulate-pitted, prolate, with marginate/costate colpi (Jansonius and Hills 1976, card 2421, Pocknall & Crosbie 1982, Frederiksen 1983).

Rhoipites caricatus sp. nov.

Plate 17, figures 20-23

Holotype. Plate 17, figures 20-21, sample 22164, EF P-7

Paratype. Plate 17, figures 22-23, sample 22272, EF S-39

Type locality: Well 1-AS-105-AM, Solimões Formation, Amazonas, Brazil.

Description. Monad, radial, isopolar, prolate spheroidal, amb circular; tricolporate, ectocolpi long, 14 µm long, CEi 0.77, CPi 0.68, marginate, margo produced by thining of columellae thickness towards colpi, margo 2 µm wide and 1 µm thick, borders slightly invaginated, colpi ends rounded, polar area small, 3 µm wide, endocolpi costate, costa 1 µm thick and 1 µm wide, all along colpi; pores circular to slightly lalongate, 2.5 µm x 2 µm wide, slightly costate, costa 0.5 µm thick; tectate, exine 2 µm thick nexine 0.7 µm thick, columellae 0.7 µm thick, distinct, tectum 0.7 µm thick. Microreticulate, lumina circular to elongate, 0.5-1 µm wide, muri 0.5-1 µm wide, homobrochate.

Dimensions. Equatorial view: Polar diameter 16-(17.5)-19 µm, equatorial diameter 15-(15.5)-16 µm. Polar/equatorial 1.12. Polar view: Equatorial diameter length 18 µm, equatorial diameter width 16 µm, length/width 1.12; nm=3, no=9.

Remarks. *Retitricolporites milnei* Hoorn 1993 has short colpi, flat, lalongate pores and smaller reticulum. *Siltaria dilcheri* Silva-Caminha *et al.* 2010 is micropitted, has pores with well developed costa and slightly protruding. *Rhoipites crassicostatus* Van der Hammen and Wymstra 1964 nov. comb. Differs in being heterobrochate, foveolate in mesocolpia and in having a much thicker costa endocolpi and simple pores

Derivation of name. After 'caricature', a drawing which has simplified aspects of an object, in reference to the fact that *R. caricatus* sp. nov. has a very common tricolporate morphology.

Rhoipites crassicostatus Van der Hammen and Wymstra 1964 nov. comb.

Basyonim. *Retitricolporites crassicostatus* Van der Hammen and Wymstra 1964, page 236, plate 1, fig. 7-8.

Plate 17, figures 24-25

Specimens. Plate 17, figures 24-25, sample 22140, EF T-17-3

Description. Monad, radial, isopolar, prolate spheroidal; tricolporate, ectocolpi mid-sized, 11 µm, CPi 0.68, simple, borders straight, colpi ends pointed, polar area 7 µm wide, endocolpi costate, costa 2 µm wide and 1 µm thick, nexine around costa is decreased in thickness creating a clear contour; pores lalongate, 3 µm x 1.5 µm wide, simple; tectate, exine 1.5 µm thick, nexine 0.5 µm thick, columellae 0.5 µm thick, distinct, tectum 0.5 µm thick. Foveo-reticulate, lumina circular, < 0.5-0.5 µm wide, muri 1-1.5 µm wide, being denser in the apocolpia where it is microreticulate, and less dense in the mesocolpium where it is foveolate, heterobrochate.

Dimensions. Polar diameter 16 µm, equatorial diameter 14 µm, polar/equatorial 1.14; nm=1, no=2.

Remarks. *Retitricolporites* (Van der Hammen 1956) Van der Hammen and Wymstra 1964 is invalid and a later synonym of *Viburnum* (Jansonius and Hills 1976, card 2402). *Rhoipites* Wodehouse 1933 accommodates tricolporate pollen grains that are reticulate-pitted, prolate, with marginate/costate colpi (Jansonius and Hills 1976, card 2421, Pocknall & Crosbie 1982, Frederiksen 1983).

Rhoipites crassitectatus sp. nov.

Plate 17, figures 26-27

Holotype. Plate 17, figures 26-27, sample 22290, EF M-17

Type locality: Well 1-AS-105-AM, Solimões Formation, Amazonas, Brazil.

Description. Monad, radial, isopolar, subprolate; tricolporate, endo and ectocolpi coinciding, 25 µm long, CPi 0.86, borders straight, colpi ends rounded, polar area small, 4 µm wide, costate, costa 2 µm wide and 1.5 µm thick, along entire colpi; ectoopores circular, 4 x 4 µm wide, simple; tectate, exine 3 µm thick, nexine 0.7 µm thick, columellae 0.7 µm thick, distinct, well spaced, tectum 1.5 µm thick. Micropitted, pits circular, <0.5 µm wide, muri ca. 0.5 µm wide, homobrochate.

Dimensions. Polar diameter 29 µm, equatorial diameter 24 µm, polar/equatorial 1.2; nm=1, no=1.

Remarks. *Retitricolporites crassopolaris* Hoorn 1994 has thicker exine in polare areas and is thinner. *R. poriconspectus* Hoorn 1994 has indistinct columellae and broader apocolpium. Foveotricolporites crassiexinus van Hoeken-Klinkenberg 1966 is foveolate, has much wider lumina.

Derivation of name. After its thick tectum.

Rhoipites crassnexinicus sp. nov.

Plate 18, figures 1-4

Holotype. Plate 18, figures 1-3, sample 22158, EF P-46-4

Paratype. Plate 18, figures 4, sample 22158, EF N-38-3/4

Type locality: Well 1-AS-105-AM, Solimões Formation, Amazonas, Brazil.

Description. Monad, radial, isopolar, prolate spheroidal; tricolporate, endo and ectocolpi coinciding, 18 µm long, CPi 0.81, ectocolpi simple, borders straight, colpi ends rounded, polar area small, 8 µm wide, endocolpi costate, costa 2 µm wide and 1.5 µm thick, along entire colpi and very gently thining out towards apocolpia; ectocolpi has a slight constriction at the equator that is mirrored by the costa endocolpi shape that is absent in the pores area; endopores lalongate, simple, 4 µm x 1.5 µm wide; tectate, exine 1.5 µm thick at apocolpia and 3 µm thick at mesocolpia, nexine 1 µm thick at apocolpia and 2 µm thick at mesocolpia, columellae 0.5-0.3 µm thick, distinct, tectum 0.5-0.3 µm thick. Microreticulate, lumina circular to elongate, 0.5 µm wide, muri 0.5 µm wide, homobrochate.

Dimensions. Polar diameter 22-(23)-24 µm, equatorial diameter 20 µm. Polar/equatorial 1.15; nm=2, no=2.

Remarks. *Retitricolpites colpiconstrictus* Hoorn 1994 is tricolpate and has different exine.

Derivation of name. After thick nexine.

Rhoipites guttus sp. nov.

Plate 18, figures 7-8

Holotype. Plate 18, figures 7-8, sample 22277, EF H-39-1

Type locality: Well 1-AS-105-AM, Solimões Formation, Amazonas, Brazil.

Description. Monad, radial, isopolar, spheroidal; tricolporate, ectocolpi medium-sized, 12 µm, CPi 0.54, simple, borders straight, colpi ends rounded, very thin, polar area broad, 10 µm wide, endocolpi costate, costa 1.5 µm wide and 2.5 µm thick, turned inwards, restricted to the bottom and top side of pore, endopores large, lalongate, 6 x 3.5 µm wide, simple; tectate, exine 1.6 µm thick, nexine 1 µm, columellae 0.3 µm thick, distinct, well spaced, tectum 0.3 µm thick. Reticulate, lumina circular to elongate, 1-2 µm wide, muri < 1 µm wide, homobrochate.

Dimensions. Polar diameter 22-(24)-26 µm, equatorial diameter 22-(24)-26 µm, polar/equatorial 1; nm=2, no=2.

Remarks. *Retitricolporites oblatus* Hoorn 1994 is micropitted and has narrow pores. *Retibrevitricolporites solimoensis* Hoorn 1993 nov. comb. Is much smaller.

Derivation of name. From the Latin ‘gutta’ meaning drop, after the costa shape in lateral view.

Retitricolporites nanus sp. nov.

Plate 18, figures 9-10

Holotype. Plate 18, figures 9-10, sample 22287, EF T-17-3

Type locality: Well 1-AS-105-AM, Solimões Formation, Amazonas, Brazil.

Description. Monad, radial, isopolar, prolate, very small; tricolporate, endo and ectocolpi coinciding, long, 12 µm long, CPi 0.75, ectocolpi simple, borders straight, colpi ends pointed, polar area small, 2 µm wide, endocolpi costate, costa 0.5-1 µm wide and 0.5-1 µm thick; pores very large in relation to grain size, slightly lalongate, simple, 3 µm x 2.5 µm wide; tectate, exine 1 µm thick, nexine 0.4 µm, columellae 0.2 µm thick, indistinct, tectum 0.4 µm thick. Reticulate, lumina circular to elongate, 1 µm wide, muri 1 µm wide, homobrochate. Often, but not always, seen in clumps.

Dimensions. Polar diameter 16-(17)-18 µm, equatorial diameter 10-(11)-12 µm, polar/equatorial 1.54; nm=2, no=4.

Derivation of name. After its very small size.

Rhoipites oblatus Hoorn 1994 nov. comb.

Plate 18, figures 11-12

Basyonim. *Retitricolporites oblatus* Hoorn 1994, page 39, plate 3, fig. 11-12.

Specimens. Plate 18, figures 11-12, sample 22290, EF S-45

Description. Monad, radial, isopolar, oblate to oblate spheroidal; tricolporate, endo and ectocolpi coinciding, mid-sized, 12 µm long, CPi 0.63, ectocolpi simple, borders slightly invaginated, colpi ends pointed, polar area broad, 6 µm wide, endocolpi costate, costa 2-0.5 µm wide and 2.5-1 µm thick, much thicker around equator, turned inwards and gradually thining out towards apocolpia, almost conical shaped and partially extending around pores; endopores lalongate, 4.5 µm x 2 µm wide, simple; tectate, exine1.5 µm thick, nexine 0.6 µm thick, columellae 0.3 µm thick, distinct, tectum 0.6 µm thick. Microreticulate, lumina circular, 0.5 µm wide, muri 0.5 µm wide, homobrochate.

Dimensions. Polar diameter 18-(19.5)-21.5 µm, equatorial diameter 16-(17.5)-18.5 µm, polar/equatorial 1.11; nm=3, no=17.

Remarks. *Retitricolporites* (Van der Hammen 1956) Van der Hammen and Wymstra 1964 is invalid and a later synonym of *Viburnum* (Jansonius and Hills 1976, card 2402). *Rhoipites* Wodehouse 1933 accommodates tricolporate pollen grains that are reticulate-pitted, prolate, with marginate/costate colpi (Jansonius and Hills 1976, card 2421, Pocknall & Crosbie 1982, Frederiksen 1983).

Rhoipites poropartitus sp. nov.

Plate 18, figures 13-14

Holotype. Plate 18, figures 13-14, sample 22386, EF T-10-2

Type locality: Well 1-AS-105-AM, Solimões Formation, Amazonas, Brazil.

Description. Monad, radial, isopolar, prolate; tricolporate, ecto and endocolpi coinciding, long, 32 µm, CPi 0.76, ectocolpi simple, borders straight, colpi ends rounded, polar area small, 4 µm wide, endocolpi costate, costa 1 µm wide and 1 µm thick; endopores discrete, circular, simple, 4 µm x 3 wide, part of the costa endocolpi runs trhough pores giving the impression that pores are split in two; semitectate, exine 2 µm thick, nexine 1 µm, columellae 0.7 µm thick, distinct, tectum 0.3 µm thick, not very clear. Reticulate, lumina circular to polygonal, 1 µm wide, muri 1 µm wide, homobrochate.

Dimensions. Polar diameter 42 µm, equatorial diameter 30 µm, polar/equatorial 1.4; nm=1, no=1.

Remarks. *Retitricolporites wijmstrae* Hoorn, 1994 has large, lalongate pores and is thicker.

Derivation of name. After pores appearing split.

Rhoipites protoguttus sp. nov.

Plate 18, figures 15-17

Holotype. Plate 18, figures 15, sample 22518, EF M-17-3

Paratype. Plate 18, figures 16-17, sample 22522, EF O-13-2

Type locality: Well 1-AS-105-AM, Solimões Formation, Amazonas, Brazil.

Description. Monad, radial, isopolar, oblate spheroidal to prolate spheroidal, amb circular; tricolporate, endo and ectocolpi coinciding, mid-sized, 20µm long, CPi 0.64, CEi 0.66, very thin, ectocolpi marginate, margo discrete, only seen in porlar view, created by a thickening of columellae around colpi, from 0.3 to 0.5 µm thick, borders very slightly invaginating, ends rounded, polar area broad, 15-13 µm wide, endocolpi simple; endopores very large, lalongate,

lense shapes with beak-like extremeties, 10 µm x 6 µm wide, costate, costa restricted to bottom and top of pores, 1 µm wide and 2 µm thick, turned inwards; tectate, exine 2 µm thick, nexine 0.3 µm, columellae 0.3 µm thick, distinct, tectum 0.3 µm thick. Microreticulate to micropitted, lumina circular, 0.5 µm wide, muri 0.5-1 µm wide, homobrochate.

Dimensions. Equatorial view: polar diameter 31-(33)-35 µm, equatorial diameter 32-(32.5)-33 µm, polar/equatorial 1.01. Polar view: equatorial diameter length 36, equatorial diameter width 36, length/width 1; nm=3, no=6.

Remarks. *Retitricolporites wijmstrae* Hoorn 1994 has long costate colpi and wall structure is different. *R. crassopolaris* Hoorn 19994 has thicker wall at apocolpia.

Derivation of name. After resemblance to *R. guttus* sp. nov.

Rhoipites pseudocrassopolaris sp. nov.

Plate 18, figures 18-19

Holotype. Plate 18, figures 18-19, sample 22140, EF W-10-4

Type locality: Well 1-AS-105-AM, Solimões Formation, Amazonas, Brazil.

Description. Monad, radial, isopolar, prolate; tricolporate, endo and ectocolpi coinciding, long, 17 µm, CPi 0.7, ectocolpi simple, colpi borders straight, ends rounded, polar area small, 3 µm wide, endocolpi costate, costa 1.5 µm wide and 1.5 µm thick, thining out towards apocolpia; endopores lalongate, 4 µm x 2 µm wide, simple, abruptly protruding; tectate, polar are is thicker due to a gradual thickening of the columellae from mesocolpium to apocolpium, exine 1.5 µm thick at mesocolpia and 2.5 µm thick at apocolpia, nexine 0.5 µm, columellae 0.5 µm thick at mesocolpia and 1.5 µm thick at apocolpia, distinct, very thin, < 0.5 µm wide, tectum 0.5 µm thick. Micropitted, lumina circular, 0.5 µm wide, muri 0.5-1 µm wide, homobrochate.

Dimensions. Polar diameter 24 μm, equatorial diameter 16 μm. Polar/equatorial 1.5; nm=1, no=1.

Remarks. *Retitricolporites crassopolaris* Hoorn 1994 has a different wall structure, lacks protruding pores and nexine rather than columellae is what makes polar areas thicker.

Derivation of name. After false resemblance to *Retitricolporites crassopolaris* Hoorn 1994.

Rhoipites pseudopilatus sp. nov.

Plate 18, figures 20-21

Holotype. Plate 18, figures 20-21, sample 22320, EF L-44-3/4

Type locality: Well 1-AS-105-AM, Solimões Formation, Amazonas, Brazil.

Description. Monad, radial, isopolar, prolate; tricolporate, ecto and endocolpi coinciding, long, 16 μm, CPi 0.69, ectocolpi simple, colpi borders invaginated, ends rounded, polar area small, 4 μm wide, ectocolpi costate, costa 2 μm wide and 2 μm thick; ecto and endopores coinciding, large, lolongate, 9 μm x 4 μm wide, simple; tectate, exine 1 μm thick, nexine 0.3 μm, columellae 0.4 μm thick, distinct, regularly distributed, 0.3 μm wide, 0.3 μm apart, tectum 0.3 μm thick. In cross section, wall appears to be pilate, but true tectum forms. Microreticulate, lumina circular, 0.5-1 μm wide, muri 0.5-1 μm wide, homobrochate.

Dimensions. Polar diameter 21-(22)-23 μm, equatorial diameter 16-(17)-18 μm, polar/equatorial 1.43-1.29; nm=2, no=2.

Remarks. Very few retitricolporate grains are described as lolongate. *Foveotricolporites lolongatis* sp. nov. is psilate-micropitted with different wall structure.

Derivation of name. After false pilate appearance.

Rhoipites ticunaensis sp. nov.

Plate 18, figures 22-25

Holotype. Plate 18, figures 22-23, sample 22349, EF D-40-2

Paratype. Plate 18, figures 24-25, sample 22456, EF Q-7-2

Type locality: Well 1-AS-105-AM, Solimões Formation, Amazonas, Brazil.

Description. Monad, radial, isopolar, spheroidal, amb triangular-obtuse-straight. Grains are mostly found in oblique view, where shape is somewhat pentagonal; tricolporate, ecto and endocolpi coinciding, colpi mid-sized, 12 µm long, CPi 0.76, CEi 0.57, ectocolpi simple, colpi borders invaginated, ends rounded, polar area 6 µm wide, endocolpi costate, costa 1.5 µm wide and 1.5 µm thick; endopores circular, 3 µm x 3 µm wide, atriate, atrium circular and simple, 6 x 6 µm wide; tectate, exine 2 µm thick, nexine 1 µm, columellae 0.5 µm thick, distinct, tectum 0.5 µm thick. Reticulate, lumina circular to polygonal, with two size modes: in the apocolpia there are larger lumina (1-2 µm wide) usually surrounded by smaller lumina (0.5 µm wide) what does not seem to happen in the mesocolpia, homobrochate, muri 0.5-1 µm thick. When seen in equatorial view (rarely), each mesocolpium has a markedly trapezoidal shape.

Dimensions. Equatorial view: polar diameter 21 µm, equatorial diameter 21 µm, polar/equatorial 1.

Polar view: equatorial diameter length 20-(20.5)-21 µm, equatorial diameter width 18-(18.5)-19 µm, length/width 1.10; nm=3, no=18.

Remarks. Botanical affinity: *Schefflera*/*Didymopanax* (Araliaceae). *Byttneripollis rudeae* Silva-Camina *et al.* 2010 and *B. rugulata* sp. nov. are also atriate, but are triporate and overall morphology differs significantly.

Derivation of name. After the western Amazonia indigenous tribe Ticuna.

Rhoipites toigoi sp. nov.

Plate 19, figures 1-4

Holotype. Plate 19, figures 1-3, sample 22422, EF Q-21-2

Paratype. Plate 19, figures 4, sample 22386, EF L-43-2

Type locality: Well 1-AS-105-AM, Solimões Formation, Amazonas, Brazil.

Description. Monad, radial, isopolar, prolate spheroidal to spheroidal; tricolporate, ectocolpi med-sized, 15 µm long, CPi 0.5, simple, very thin and sometimes not visible; colpi borders straight, ends rounded, polar area large, 10 µm wide; endopores lalongate, 9 µm x 2 µm wide, costate, costa restricted to bottom and top of pores, 3 µm wide and 2 µm wide thick; tectate, exine 2.5 µm thick, nexine 1 µm, columellae 1 thick, distinct, very thin and regularly distributed, tectum 0.5 µm thick. Suprareticulate, coarse reticulation, lumina large, circular, 2-3 µm wide, muri thick, 1.5 µm wide, homobrochate, smaller lumina (ca. 1 µm wide) appear within the muri, usually at lumina corners. Reticulum short, formed by raised tectum, which has an undulating appearance in cross section, intraluminal surface psilate.

Dimensions. Polar diameter 30-(36)-42 µm, equatorial diameter 30-(33.5)-37 µm, polar/equatorial 1-1.07; nm=2, no=5.

Remarks. This grain bears resemblance to *R.? pluricolumellatus* sp. nov., but it is tricolporate and has much shorter and less conspicuous colpi. *Retitricolporites wijmstrae* Hoorn 1994 has long costate colpi and wall structure is different.

Derivation of name. After Brazilian palynologist Marleni Toigo.

Genus *Striatopollis* Krutzsch 1959

Type species *Striatopollis sarstedtensis* Krutzsch 1959

Striatopollis macrolobium sp. nov.

Plate 20, figures 3-5

Holotype. Plate 20, figures 3-4, sample 22140, EF Q-7-3

Holotype. Plate 20, figures 5, sample 22282, EF H-11-4

Type locality: Well 1-AS-105-AM, Solimões Formation, Amazonas, Brazil.

Description. Monad, radial, isopolar, prolate; tricolporate, ecto and encocolpi coinciding, very long and wide, 30µm long, CPi 0.9, simple, colpi borders invaginated, ends open, polar area very small to absent; endopores circular, 3-4 µm x 3-4 µm wide, simple, not easily visible; tectate, exine 2.5 µm thick, nexine 0.3 µm, columellae 0.3 µm thick, distinct, very short in relation to tectum, dense and regularly distributed, tectum 2 µm thick. Striate, striae solid, running parallel to the polar axis, 1.5 µm wide, 0.5 µm apart, interstriae surface psilate. Some striae can be shorter near the colpi, hence not connecting pole to pole as most striae.

Dimensions. Polar diameter 29.5-(31.25)-33 µm, equatorial diameter 17-(19)-21 µm, polar/equatorial 1.64; nm=2, no=13.

Remarks. Similar to *Striatopollis catatumbus* (Gonzalez, 1967) Takahashi and Jux, 1989 but with distinctive thicker tectum/striae and a clearly different relation of columellae-tectum thicknesses.

Derivation of name. After the extant Fabaceae genus *Macrolobium*, to which the fossil type bears resemblance.

Genus *Verrutricolporites* van der Hammen & Wijmstra 1964

Type species *Verrutricolporites rotundiporus* van der Hammen & Wijmstra 1964

Verrutricolporites pequenus sp. nov.

Plate 20, figures 10-11

Holotype. Plate 20, figures 10-11, sample 22140, EF N-37

Type locality: Well 1-AS-105-AM, Solimões Formation, Amazonas, Brazil.

Description. Monad, radial, isopolar, subprolate; tricolporate, ectocolpi mid-sized, 10 µm long, CPI 0.64, thin, simple, colpi borders straight, ends pointed, polar area broad and rounded, 4 µm wide; endopores lalongate, relatively large, 4 µm x 2.5 µm wide, simple;

tectate, exine relatively thick, 2.1 µm thick, nexine 1.5 µm, columellae 0.3 thick, barely distinct, tectum 0.3 µm thick. Verrucate, verrucae very short and of irregular shape, ca. 1 µm wide, < 0.5 µm tall, 0.5-1 µm apart. A few larger verrucae are spread over the grain's surface.

Dimensions. Polar diameter 15.5-(15.75)-16 µm, equatorial diameter 13-(13.5)-14 µm, polar/equatorial 1.16; nm=2, no=2.

Remarks. *Verrutricolporites rotundiporus* Van der Hammen and Wymstrae 1964 has smaller and circular pore, and a smaller ration of verruca and grain sizes.

Derivation of name. From the Portuguese word 'pequeno', meaning small.

Verrutricolporites simplex sp. nov.

Plate 20, figures 14-17

Holotype. Plate 20, figures 14-15, sample 22482, EF F-10

Paratype. Plate 20, figures 16-17, sample 22481, EF F-48

Type locality: Well 1-AS-105-AM, Solimões Formation, Amazonas, Brazil.

Description. Monad, radial, isopolar, prolate spheroidal, amb subtriangular; tricolporate, colpi long, 14 µm long, CPi 0.77, colpi borders slightly invaginated, ends rounded, simple; pores lolongate, 4 x 3 µm long, slightly costate, costa ca. 1 µm wide; intectate, exine 2-3 µm thick, nexine 1 µm, sexine 2 µm thick. Verrucate, verrucae rounded, 2 µm wide, 2 µm tall, ca. 1 µm apart. Verrucae of constant size and shape.

Dimensions. Polar diameter 18 µm, equatorial diameter 17, polar/equatorial 1.05.

Polar diameter length 16 µm, equatorial diameter width 20 µm, length/diameter 0.8; nm= 2, no=3.

Remarks. *Verrutricolporites haplites* Gonzalez 1967 is larger has costate colpi and irregular verrucae. *V. rotundiporus* Van der Hammen and Wymstra, 1964 is tectate, with clearly

distinct columellae, has shorter verrucae, indistinct colpi and circular pore. *V. pequenus* sp. nov. is tectate and has larger lalongate pore.

Derivation of name. After the rather simple morphology.

Triporate

Genus *Byttneripollis* Konzalová 1976

Type species *Byttneripollis coronarius* Konzalová 1976

Byttneripollis rugulata sp. nov.

Plate 20, figures 22-25

Holotype. Plate 20, figures 22-23, sample 22277, EF L-13-3

Paratype. Plate 20, figures 24-25, sample 22158, EF G-20-1

Type locality: Well 1-AS-105-AM, Solimões Formation, Amazonas, Brazil.

Description. Monad, radial, isopolar, circular amb; triporate, ectopores circular, 4-5 µm wide, aspidate, aspis 2 µm tall, endopores simple; tectate, exine 1.8 µm thick, nexine 0.6 µm thick, columellae 0.6 µm thick, indistinct , tectum 0.6 µm thick, undulating, which creates a fine rugulate ornamentation; micropits also seen with irregular distribution. Rugulae ca. 0.5 µm wide, very short and of irregular length.

Dimensions. Polar diameter length 26-(27)-28 µm, polar diameter width 25-(25.5)-26 µm; length/width 1.05; nm=2, no=3.

Remarks. *Byttneripollis* Konzalová 1976 accommodates 3-6 porate grains with a fringe-like aspis (thickening around pores). *B. ruedae* Silva-Caminha *et al.* 2010 is triangular-obtuse in shape, reticulate endopores costate and has higher aspis around pores than *B. rugulata* sp. nov.

Derivation of name. After rugulate pattern.

Genus *Foveotriporites* Gonzales-Guzman 1967

Type species *Foveotriporites hammenii* Gonzales-Guzman 1967

Foveotriporites? nodus sp. nov.

Plate 21, figures 5-6

Holotype. Plate 21, figures 5-6, sample 22253, EF F-38-1

Type locality: Well 1-AS-105-AM, Solimões Formation, Amazonas, Brazil.

Description. Monad, radial, isopolar, triangular amb, apices are folded forming small nodular structures; triporate, pores indistinct. Tectate, exine 1 μm thick, nexine 0.4 μm thick, columellae 0.2 μm thick, indistinct, tectum 0.4 μm thick, perforated, micropitted; micropits circular, <0.5 μm wide, 0.5 μm apart, homobrochate.

Dimensions. Polar diameter length 26 μm, polar diameter width 23 μm, length/width 1.13; nm=1, no=1.

Remarks. *Proteacidites triangulatus* Lorente 1986 has large, clear pores and is thicker. *Byttneripollis* species are atriate.

Derivation of name. After node-like, or nodular apertures area.

Genus *Proteacidites* Cookson 1950 ex Couper 1953 emend.

Type species *Proteacidites adenanthoides* Cookson 1950

Proteacidites poriscabratus sp. nov.

Plate 21, figures 7-9

Holotype. Plate 21, figures 7-8, sample 22330, EF G-41-1

Paratype. Plate 21, figures 9, sample 22326, EF C-20-3

Type locality: Well 1-AS-105-AM, Solimões Formation, Amazonas, Brazil.

Description. Monad, radial, isopolar, triangular amb; triporate, pores distinct, circular, 3 μm wide, annulate, annulus produced by a dense scabrate cover around pores, 2 μm wide, 1 μm

thick; intectate, exine 0.8 µm thick, nexine 0.5, scabrate, scabrae circular, 0.3 µm tall, <0.5 µm wide, densely and evenly distributed.

Dimensions. Polar diameter length 30-(32.5)-35 µm, polar diameter width 24-(27.5)-31 µm, length/width 1.18; nm=2, no=2.

Remarks. *Proteacidites triangulatus* Lorente 1986 has large, clear pores and is thicker. *P. dehaani* Germeraad *et al.* 1968 is reticulate. *P. miniporatus* van Hoeken-Klinkenberg, 1966 has very slight scabration and simple, smaller pores.

Derivation of name. After scabrae around apertures.

Proteacidites pseudodehaani sp. nov.

Plate 21, figures 10

Holotype. Plate 21, figures 10, sample 22412, EF L-9-1/3

Type locality: Well 1-AS-105-AM, Solimões Formation, Amazonas, Brazil.

Description. Monad, radial, isopolar, triangular amb; triporate, pores distinct, circular, 7 µm wide, annulate, annulus produced by a thickening of the endexine, 3 µm wide, 1 µm thick, and then by a thinning of the endexine 2 µm wide; tectate, exine 1.5 µm thick, nexine 1 µm thick, columellae 0.3 µm thick, barely distinct, tectum 0.3 µm thick; microreticulate, lumina circular, 0.5-1 µm wide, muri 0.5-1 µm wide, homobrochate.

Dimensions. Polar diameter length 31-(34.5)-38 µm, polar diameter width 28-(31)-34 µm, length/width 1.11; nm=2, no=3.

Remarks. *P. dehaani* Germeraad *et al.* 1968 has smaller pores, relative thicker annulus and is heterobrochate. *Proteacidites miniporatus* van Hoeken-Klinkenberg 1966 is scabrate and has smaller pores. *P. triangulatus* Lorente 1986 is thicker and micropitted.

Derivation of name. After close similarity to *P. dehaani* Germeraad *et al.* 1968.

Genus *Psilatriporites* (van der Hammen) Mathur 1966

Type species *Psilatriporites inornatus* (van der Hammen) Mathur 1966

Psilatriporites minimum sp. nov.

Plate 21, figures 13-14

Holotype. Plate 21, figures 13, sample 22506, EF S-4-3

Paratype. Plate 21, figures 14-15, sample 22303, EF U-22-2

Type locality: Well 1-AS-105-AM, Solimões Formation, Amazonas, Brazil.

Description. Monad, radial, isopolar, spheroidal, circular amb; triporate, pores distinct, circular, 3 μm wide, slightly sunken, slightly costate, costa <1 μm; atectate, exine 1 μm thick, psilate.

Dimensions. Equatorial view: polar diameter 14 μm, equatorial diameter 13 μm, polar/equatorial 1.07,

Polar view: polar diameter length 19 μm, polar diameter width 15 μm, length/width 1.26; nm=2, no=3.

Remarks. *Momipites* spp. and *Triporopollenites* spp. have triangular amb and slightly protruding pores. *Psilatriporites sarmientoi* Hoorn 1993 have much larger pores in relation to the grains size. *P. corstanjei* Hoorn 1993 have larger pores with thick annulus.

Derivation of name. After diminute size.

Botanical affinity. Moraceae/Urticaceae (?).

Psilatriporites salafrarius sp. nov.

Plate 21, figures 16-17

Holotype. Plate 21, figures 16-17, sample 22460, EF X-8-3

Paratype. Plate 21, figures 18, sample 22460, EF V-7-3

Type locality: Well 1-AS-105-AM, Solimões Formation, Amazonas, Brazil.

Description. Monad, radial, isopolar, subprolate, triangular amb; triporate, endo and ectopores coinciding, 2.5 x 2.5 µm wide, circular, simple, slightly protruding In equatorial view, there seems to be colpi as well, with invaginated mesocolpia; tectate, exine 1.5 µm thick, nexine 0.5 µm thick, columellae distinct, 0.5 µm thick, tectum 0.5 µm thick, psilate to finely micropitted.

Dimensions. Polar diameter 20-(20.5)-21 µm, equatorial diameter 17 µm, polar/equatorial 1.20; nm=2, no=51.

Remarks. *Florschuetzia trilobata* Germeraad *et al.* 1968 is strongly lobate, i.e., each mesocolpium is highly invaginated, which does not happen in *P. salafrarius* sp. nov. *P. sarimentoi* and *P. costanjei* Hoorn 1993 are circular. *P. desilvae* Hoorn 1993 has pseudocolpi along with pores.

Derivation of name. From the Brazilian word 'salafrário' meaning 'deceiver', as the grain makes one think it is tricolporate but there are no colpi.

Genus *Retitriporites* Ramanujam 1966

Type species *Retitriporites curvimurati* Ramanujam 1966

Retitriporites discretus sp. nov.

Plate 21, figures 19-22

Holotype. Plate 21, figures 19-20, sample 22518, EF V-17

Paratype. Plate 21, figures 21-22, sample 22522, EF S-47-1/2

Type locality: Well 1-AS-105-AM, Solimões Formation, Amazonas, Brazil.

Description. Monad, radial, isopolar, circular to subtriangular amb; triporate, endo and ectopores coinciding, 2 µm wide, circular, slightly protruding, annulate, annulus produced by thickening of the endexine, 3 µm wide, 2 µm tick; tectate, exine 2 µm thick, nexine 1 µm thick, columellae distinct, 0.5 µm thick, tectum 0.5 µm thick, fossu-reticulate. Some lumina

are circular, 0.5-1 μm wide, but most form fossulae, variable in size, muri 0.5-1 μm wide. Homobrochate.

Dimensions. Polar diameter length 23.5 μm, equatorial diameter width 18-(19.5)-21 μm, length/width 1.2; nm=2, no=2.

Remarks. *Retitriporites dubiosus* Gonzalez 1967, *R. poricostatus* Jaramillo and Dilcher 2001, *R. typicus* Gonzalez 1967 and *R. simplex* van der Kaars 1983 all reticulate and have much larger lumina. *R. acostai* Dueñas 1986 is heterobrochate and has larger pores.

Derivation of name. After simple morphology.

Retitriporites tuberosum sp. nov.

Plate 22, figures 1-2

Holotype. Plate 22, figures 1-2, sample 22290, EF F-42-2

Type locality: Well 1-AS-105-AM, Solimões Formation, Amazonas, Brazil.

Description. Monad, radial, isopolar, subtriangular amb; triporate, endo and ectopores coinciding, 5-6 μm wide, circular, simple, pore outline irregular, highly protruding almost like tubular appendages. Tectate, exine 1.5 μm thick, nexine 0.6 μm thick, columellae indistinct, 0.3 μm thick, tectum 0.6 μm thick; reticulate, lumina of irregular shape and size, circular to elongate, 1-3 μm wide, muri 1.5 μm wide, smaller and circular lumina at apocolpia and larger, more elongate lumina at mesocolpia, heterobrochate.

Dimensions. Polar diameter length 35-(36.5)-38 μm, equatorial diameter width 30-(34)-38 μm, length/width 1.07; nm=2, no=2.

Remarks. *Byttneripollis* spp have atrium, different from the simple protusions in *R. tuberosum* sp. nov.

Derivation of name. After highly protruding apertures, like tubes.

Pantocolpate

Genus *Lymingtonia* Erdtman 1960

Type species *Lymingtonia rhetor* Erdtman 1960

Lymingtonia amazonica sp nov.

Plate 22, figures 5-6

Holotype. Plate 22, figures 5-6, sample 22278, EF O-32

Type locality: Well 1-AS-105-AM, Solimões Formation, Amazonas, Brazil.

Description. Monad, radial, isopolar, circular to slightly quadrangular; pantocolpate, ecto and endocolpi coinciding, 6-colpate (4 colpi around equator and 1 in each apocolpium), 8 µm long, 2 µm wide, slightly sunken, CEi 0.36, ends rounded, colpi costate, costae thin, 0.5 µm thick, 0.5 µm wide; tectate, exine 2 µm thick, endexine 0.7 µm thick, columellae 0.7 µm thick, very thin and regularly distributed, tectum 0.7 µm thick; sculpture psilate, columellae tips seen through tectum.

Dimensions. Equatorial diameter length 22-(23)-24 µm, equatorial diameter width 21-(22)-23 µm, length/width 1.04; nm=2, no=2.

Remarks. *Lyminthgonia* Erdtman 1960 accommodates pantocolpate pollen. So far the only pantocolpate form described in northern southamerica is *Lymingtonia*? sp. 1 Jaramillo and Dilcher 2001, it is intectate-echinate.

Derivation of name. After Amazonia.

Lymingtonia splendens sp nov.

Plate 22, figures 7-8

Holotype. Plate 22, figures 7-8, sample 22506, EF O-48-3/4

Type locality: Well 1-AS-105-AM, Solimões Formation, Amazonas, Brazil.

Description. Monad, radial, isopolar, circular; pantocolpate, ecto and endocolpi coinciding, 16-colpate (8 colpi around equator and 4 on each apocolpium), small, 11 µm long, , CEi 0.29, ends rounded, colpi marginate, margo produced by a gradual thinning of the columellae until they completely disappear and hence colpi are slightly sunken; tectate, exine 3 µm thick, endexine 1 µm thick, columellae 1 µm thick, 1 µm wide and 1 µm apart, tectum 1 µm thick; sculpture psilate to microechinate, microechinae only perceptible on cross section, very short 0.1-0.2 µm tall; columellae tips seen through tectum giving the impression of a negative reticulum.

Dimensions. Equatorial diameter length 54-(56)-60 µm, equatorial diameter width 50-(52)-54 µm, length/width 1.07; nm=2, no=2.

Remarks. *Lymingtonia amazonica* sp. nov. is smaller and has 6 colpi. *Lymingtonia*? sp. 1 Jaramillo and Dilcher 2001 is intectate-echinate.

Derivation of name. After the latin word 'splendens' meaning shining or brilliant, for the pollen's large size and exquisite morphology.

Botanical affinity. Convolvulaceae (*Evolvulus* spp., *Jacquemontia* spp.).

Stephanocolpate

Genus *Retistephanocolpites* Leidelmeyer 1966

Type species *Retistephanocolpites angeli* Leidelmeyer 1966

Retistephanocolpites curvimuratus sp. nov.

Plate 23, figures 1-3

Holotype. Plate 23, figures 1-2, sample 22386, EF L-46-2

Paratype. Plate 23, figures 3, sample 22422, EF E-30

Type locality: Well 1-AS-105-AM, Solimões Formation, Amazonas, Brazil.

Description. Monad, radial, isopolar, circular to quadrangular; stephanocolpate, 4 short colpi, 10 µm long, CEi 0.27, CPi 0.25, borders slightly invaginated, ends pointed, costate, costa 3 µm wide, µm thick; semitectate, exine 4 µm thick, nexine 1 µm thick, columellae 2 µm long, distinct, 1 µm thick, 0.5 µm apart, tectum 1 µm thick; reticulate, lumina 1.5-2 µm wide, curvimurate, muri 1 µm wide, homobrochate.

Dimensions. Polar view: equatorial diameter length 42-(42.5)-43 µm, equatorial diameter width 40-(41)-42 µm, length/width 1.03. Equatorial view: polar diameter 40, equatorial diameter 44, polar/equatorial 0.9; nm=3, no=3.

Remarks. Curvimurate stephanocolpate pollen have not been described yet. Similar to *Retistephanocolpites* sp. 2 Jaramillo and Dilcher 2001, but curvimurate.

Derivation of name. After curvimurate reticulum.

Retistephanocolpites liberalis sp. nov.

Plate 23, figures 4-6

Holotype. Plate 23, figures 4-5, sample 22282, EF L-14-2

Paratype. Plate 23, figures 6, sample 22287, EF S-17-1

Type locality: Well 1-AS-105-AM, Solimões Formation, Amazonas, Brazil.

Description. Monad, radial, isopolar, circular to quadrangular; stephanocolpate, endo and ectocolpi coinciding, 4 colpi, simple, mid-sized, colpi 20 µm long, CEi 0.54, borders slightly invaginated, ends pointed, colpi often wide open; tectate, exine 2 µm thick, nexine 0.7 µm thick, sometimes with endocracks, columellae 0.6 µm long, distinct, ca. 0.5 µm thick, 0.5 µm apart, tectum 0.7 µm thick; reticulate, lumina 1 µm wide, rounded, elongate to angular, muri 1 µm wide, homobrochate.

Dimensions. Equatorial diameter length 37-(37.5)-38 µm, equatorial diameter width 33-(35)-37 µm, length/width 1.07; nm=2, no=7.

Remarks. *Retistephanocolpites angeli* Leidelmeyer 1966 and *R. finalis* Gonzalez 1967 have 5 very short colpi. *R. regularis* van Hoeken-Klinkenberg 1966 has 5 longer colpi and smaller luminae. *R. tropicalis* Dueñas 1980 has minute lumina (< 0.5 μm) and much more invaginated colpi. *R. circularis* Silva-Caminha *et al.* 2010 has 5 very short marginate colpi.

Derivation of name. After simple and open ('liberate') character of colpi.

Retistephanocolpites passionis sp. nov.

Plate 23, figures 7-9

Holotype. Plate 23, figures 7-8, sample 22261, EF H-38-3/4

Paratype. Plate 23, figures 9, sample 22272, EF G-6-4

Type locality: Well 1-AS-105-AM, Solimões Formation, Amazonas, Brazil.

Description. Monad, radial, isopolar, spheroidal, circular amb; stephanocolpate, ecto and endocolpi coinciding, 6 colpi, simple, mid-sized, colpi 14 μm long, CPi 0.46, CEi 0.55, borders straight, ends rounded, polar area 8 μm wide; tectate, exine 2.5 μm thick, nexine 1 μm thick, columellae 1 μm long, distinct, 1 μm thick, 2 μm apart, tectum 0.5 μm thick; reticulate, lumina large, 1-5 μm wide, rounded to angular, homobrochate, muri 1 μm wide. Sporadic smaller luminae of ca. 0.5 μm at the vertices of wider luminae; reticulum simplicolumellate, and exine within lumina is micropitted.

Dimensions. Equatorial view: polar diameter 30 μm, equatorial diameter 32 μm, polar/equatorial 0.93. Polar view: equatorial length 36 μm, equatorial width 30 μm, polar/equatorial 1.2; nm=2, no=4.

Remarks. *Retistephanocolpites angeli* Leidelmeyer 1966 and *R. finalis* Gonzalez 1967 have 5 very short colpi and have smaller luminae. *R. regularis* van Hoeken-Klinkenberg 1966 has 5 colpi and much smaller luminae. *R. tropicalis* Dueñas 1980 has minute lumina (< 0.5 μm) and 4 colpi. *R. circularis* Silva-Caminha *et al.* 2010 has 5 very short marginate colpi.

Derivation of name. After affinity with *Passiflora* pollen.

Botanical affinity. *Passiflora* and Bignoniaceae (?).

Stephanocolporate

Loxocolporites foveolatus gen. et sp. nov.

Plate 24, figures 1-3

Holotype. Plate 24, figures 1-1, sample 22140, EF J-40-4

Type locality: Well 1-AS-105-AM, Solimões Formation, Amazonas, Brazil.

Description. Monad, radial, isopolar, subprolate; stephanocolporate, loxocolporate, endo and ectocolpi coinciding, 4 colpori, colpi mid-sized, 12 µm long, CPi 0.63, borders straight, ends pointed, polar area 8 µm wide, ectocolpi simple, endocolpi costate, costa discrete, 1.5 µm wide, 1.5 µm thick; ectopores simple, lalongate, 4 x 3 µm wide; tectate, exine 1.5 µm thick, nexine 1 µm thick, columellae 0.3 µm thick, distinct, regularly distributed, very thin tectum, 0.2 µm thick. Ornamentation foveolate to micropitted foveolae circular, 0.5-1 µm wide, 0.5-1 µm apart, homobrochate.

Dimensions. Polar diameter 19 µm, equatorial diameter 16.5 µm, polar/equatorial 1.15; nm=1, no=1.

Remarks. This morphology had not yet been described in northern South America.

Derivation of name. Genus named from the term ‘loxocolporate’, and species after foveolate ornamentation.

Genus *Psilastephanocolporites* Leidelmeyer 1966

Type species *Psilastephanocolporites fissilis* Leidelmeyer 1966

Psilastephanocolporites meliosus sp. nov.

Plate 24, figures 7-8

Holotype. Plate 24, figures 7-8, sample 22140, EF L-22-1/3

Paratype. Plate 24, figures 9, sample 22140, EF X-32

Type locality: Well 1-AS-105-AM, Solimões Formation, Amazonas, Brazil.

Description. Monad, radial, isopolar, subprolate to prolate; stephanocolporate, 5 colpori, endocolpi, mid-sized, colpi 16 µm long, CPi 0.64, ends pointed, polar area rounded, 7 µm wide, endocolpi costate, costa 1 µm wide, 1.5 µm thick; ectopores simple, circular, 5 x 5 µm; tectate, exine 2 µm thick, nexine 1 µm thick, sexine 1µm thick, columella absent, psilate.

Dimensions. Polar diameter 25-(28.16)-31.5 µm, equatorial diameter 20-(21)-22 µm, polar/equatorial 1.34; nm=2, no=74.

Remarks. *Psilastephanocolporites globulus* van Hoeken-Klinkenberg 1966 has 4 colpori, costate pores and is thicker. *P. marinamensis* Hoorn 1994 has 4 very short and indistinct colpi and lalongate pores. *P. matapiorum* Hoorn 1994 has 4 long colpori and lalongate pores. *P. schneideri* Hoorn 1993 has 4 colpori, large lalongate pores and is psilate-microreticulate. *Meliapollis* sp. 1 Silva-Caminha *et al.* 2010 has costate pores and simple colpi.

Derivation of name. After similarity with pollen from family Meliaceae (e.g. *Cedrela*).

Botanical affinity. Meliaceae (?).

Psilastephanocolporites pseudomarinamensis sp. nov.

Plate 24, figures 10-11

Holotype. Plate 24, figures 10-11, sample 22282, EF T-16-1

Type locality: Well 1-AS-105-AM, Solimões Formation, Amazonas, Brazil.

Description. Monad, radial, isopolar, prolate spheroidal to subprolate, stephanocolporate, 5 colpori, endo and ectocolpi coinciding, mid-sized, colpi 16 µm long, CPi 0.51, endocolpi costate, costa 2 µm wide, 1.5 µm thick, ends pointed, polar area rounded, 18 µm wide;

ectopores simple, lalongate, 5 x 2 µm wide, displaying a slight constriction, which makes them appear as 8-shaped; tectate, exine 2 µm thick, nexine 0.7 µm thick, columellae 0.6 µm thick, indistinct, tectum 0.7 µm thick. Psilate to micropitted, micropits < 0.5 µm, evenly distributed and very short.

Dimensions. Polar diameter 23-(27)-31 µm, equatorial diameter 22-(24)-26 µm, polar/equatorial 1.12; nm=2, no=4.

Remarks. *Psilastephanocolporites marinamensis* Hoorn 1994 has shorter colpi, is psilate and pores are perfectly lalongate. *P. schneideri* Hoorn 1993 has much larger pores and is smaller.

Derivation of name. After an apparent similarity with *Psilastephanocolporites marinamensis* Hoorn 1994.

Periporate

Crotoperiporites pulcher gen. et sp. nov.

Plate 24, figures 12-13

Holotype. Plate 24, figures 12-13, sample 22506, EF P-17

Type locality: Well 1-AS-105-AM, Solimões Formation, Amazonas, Brazil.

Description. Monad, radial, isopolar, circular; pantoporate, ecto/endopores coinciding, 12 pores, 2 x 2 µm wide, circular, slightly costate, costa ca. 1 µm wide; intectate, exine 2 µm thick, nexine 0.5 µm thick, sexine 1.5 µm thick, composed of clavae; sculpture croton type, rosette formed of 6-7 triangular ornaments (clavae tips), total rosette width 3-4 µm wide, circular to oval, adjonining the adjacent ones, with a circular centre of ca. 1 µm wide, each triangular ornament is 1-1.5 µm wide. Some grains display a reticulate pattern underneath clavae tips, probably formed by anastomosing clavae bases.

Dimensions. Equatorial diameter length 30-(32)-34 µm; equatorial diameter width 26-(27)-28 µm, length/width 1.18; nm=2, no=3.

Remarks. The combination of periporate pollen with croton ornamentation had not been described before.

Derivation of name. The generic name *Crotoperiporites* derives from the ornamentation plus the apertures type, the specific name from the latin word 'pulcher' meaning beautiful.

Genus *Multiporopollenites* Thomson & Pflug 1953

Type species *Multiporopollenites maculosus* (Potonié 1931) Thomson & Pflug 1953

Multiporopollenites intermedius sp. nov.

Plate 25, figures 2-3

Holotype. Plate 25, figures 2-3, sample 22164, EF J-10-1

Type locality: Well 1-AS-105-AM, Solimões Formation, Amazonas, Brazil.

Description. Monad, radial, isopolar, circular; pantoporate, ecto/endopores coinciding, 14-16 pores, pores 3 x 3 µm wide, simple, circular; semitectate, exine 2 µm thick, nexine 1 µm thick, columellae 0.5 µm thick, distinct, < 0.5 µm wide, 0.5 µm apart, tectum 0.5 µm thick; reticulate, lumina 1 µm wide, elongate, muri 0.5-1 µm thick, homobrochate.

Dimensions. Equatorial diameter length 28 µm; equatorial diameter width 22-(23)-24 µm, length/width 1.21; nm=2, no=3.

Remarks. *Multiporopollenites crassinexinatus* Silva-Caminha *et al.* 2010 has 24 pores and a thicker nexine than sexine. *M. pauciporatus* Jaramillo and Dilcher 2001 has 18-23 pores and is micropitted.

Derivation of name. After its generalist/intermediate morphology.

Genus *Parsonsidites* Couper 1960

Type species *Parsonsidites psilatus* Couper 1960

Parsonsidites? minibrenacii sp. nov.

Plate 25, figures 5-6

Holotype. Plate 25, figures 5, sample 22518, EF E-43-4

Paratype. Plate 25, figures 6, sample 22506, EF R-6-1/2

Type locality: Well 1-AS-105-AM, Solimões Formation, Amazonas, Brazil.

Description. Monad, radial, isopolar, circular; pantoporate, ecto/endopores coinciding, 12-14 pores, pores 2 x 2 µm wide, circular; tectate, exine 1 µm thick, nexine 0.4 µm thick, columellae 0.2 µm thick, indistinct, tectum 0.4 µm thick; psilate.

Dimensions. Equatorial diameter length 12-(12.6)-13 µm; equatorial diameter width 11-(11.6)-12 µm, length/width 1.08; nm=3, no=85.

Remarks. *Parsonsidites? brenacii* Silva-Caminha *et al.* 2010 is bigger and has relative thicker exine. *Multiporopollenites pauciporatus* Jaramillo and Dilcher 2001 is bigger, microppited and has 18-23 pores.

Derivation of name. After resemblance with *P.*? *brenacii* Silva-Caminha *et al.* 2010, but much smaller size and thickness.

Genus *Perisyncolporites* Germeraad *et al.* 1968

Type species *Perisyncolporites pokornyi* Germeraad *et al.* 1968

Perisyncolporites grossus nov. sp.

Plate 25, figures 7-8

Holotype. Plate 25, figures 7-8, sample 22282, EF O-10

Type locality: Well 1-AS-105-AM, Solimões Formation, Amazonas, Brazil.

Description. Monad, radial, isopolar, circular; syncolporate, 8 pores (4 around equator and 1 in each pole), pores widen towards inner exine, from 3 to 4 µm wide, circular, simple; endocolpi faintly developed and connecting one pore to the next adjacent pore, colpi 1.5 µm

wide; atectate, exine 4 μm thick, psilate. Inner part of the exine at the poles can be thinner, creating an irregular circular mark.

Dimensions. Equatorial diameter length 32-(32.5)-33 μm; equatorial diameter width 30-(31.5)-33 μm; length/width 1.03; nm=2, no=2.

Remarks. *Perisyncolporites pokornyi* Germeraad *et al.* 1968 is thinner and tectate.

Derivation of name. After thick exine.

Genus *Psilaperiporites* Regali 1974

Type species *Psilaperiporites robustus* Regali 1974

Psilaperiporites pauciporatus nov. sp.

Plate 25, figures 12-13

Holotype. Plate 25, figures 12-13, sample 22287, EF S-17-4

Type locality: Well 1-AS-105-AM, Solimões Formation, Amazonas, Brazil.

Description. Monad, radial, isopolar, circular; pantoporate, endo and ectopores coinciding, pores 4 x 4 μm wide, circular, simple, 5-6 pores; atectate, nexine 1 μm thick, sexine 1.5 μm thick, columellae absent; psilate.

Dimensions. Equatorial length 24 μm; equatorial width 22-(24)-26 μm; length/width 1; nm=2, no=6.

Remarks. *Psilaperiporites multiporatus* Hoorn 1994 is bigger and has 9-16 annulate pores. *P. suarezi* Vajda-Santivanez 1999 has 16-34 pores. *P. brenacii* Silva-Caminha *et al.* 2010 is tectate and has 10 pores. *Parsonsidites*? sp. 1 Jaramillo and Dilcher 2001 has 9 pores arranged differently (3 in equator and 6 opposite to each other half-way equator-pole). *Parsonsidites*? sp. 2 Jaramillo and Dilcher 2001 has 12 pores and is tectate. *Multiporopollenites pauciporatus* Jaramillo and Dilcher 2001 is tectate and has 18-23 pores.

Derivation of name. After the low number of pores.

Psilaperiporites redondus nov. sp.

Plate 25, figures 14-15

Holotype. Plate 25, figures 14-15, sample 22349, EF J-11-1

Type locality: Well 1-AS-105-AM, Solimões Formation, Amazonas, Brazil.

Description. Monad, radial, isopolar, circular; pantoporate, ecto/endopores coinciding, pores 4 x 4 µm wide, circular, simple, 19-20 pores; tectate, exine 1 µm thick, nexine very thin, nearly absent, 0.2 µm thick, columella 0.4 µm thick, distinct, < 0.5 µm wide and < 0.5 µm apart, tectum 0.4 µm thick; psilate. Columellae tips clearly seen through tectum.

Dimensions. Equatorial diameter length 43 µm; equatorial diameter width 33 µm; equatorial diameter length/width 1.3; nm=1, no=2.

Remarks. *Psilaperiporites multiporatus* Hoorn 1994 and *P. suarezi* Vajda-Santibanez 1999 are atectate. *Parsonsidites? brenacii* Silva-Caminha *et al.* 2010, *P.*? sp. 1 Jaramillo and Dilcher 2001 and

Parsonsidites? sp. 2 Jaramillo and Dilcher 2001 have fewer spores. *Multiporopollenites pauciporatus* Jaramillo and Dilcher 2001 is micropitted and pores are relatively smaller in comparison to overall grain size.

Derivation of name. After rounded shape of pollen and pores.

Stephanoporate

Genus *Verrustephanoporites* Leidelmeyer 1966

Type species *Verrustephanoporites simplex* Leidelmeyer 1966

Verrustephanoporites dubius sp. nov.

Plate 25, figures 18-19

Holotype. Plate 25, figures 18-19, sample 22412, EF M-13-2/4

Type locality: Well 1-AS-105-AM, Solimões Formation, Amazonas, Brazil.

Description. Monad, radial, isopolar, circular; stephanoporate, 6 pores, pores 2.5 x 2.5 µm wide, circular, costate, costa 1 µm wide and 1 µm thick; intectate, exine 2 µm thick, nexine 0.5 µm thick, sexine 1.5 µm thick; verrucate, verrucae circular to elongate, 2-4 µm wide, 0.5 µm apart, densely distributed over the entire surface.

Dimensions. Equatorial diameter length 26 µm; equatorial diameter width 24 µm; length/width 1.08; nm=1, no=3.

Remarks. *Verrustephanoporites intraverrucatus* sp. nov. has smooth sexine. *Ulmoideipites krempii* (Anderson, 1960) Elsik 1968 is tectate, has 3-5 pores and smaller verrucae.

Derivation of name. After false similarity with *Verrustephanoporites intraverrucatus* sp. nov. and *Ulmoideipites krempii* (Anderson, 1960) Elsik 1968

Verrustephanoporites intraverrucosus nov. sp.

Plate 25, figures 20-21

Holotype. Plate 25, figures 20-21, sample 22381, EF S-37-3

Type locality: Well 1-AS-105-AM, Solimões Formation, Amazonas, Brazil.

Description. Monad, radial, isopolar, circular; stephanoporate, 5 pores, pores 2 x 2 µm wide, circular, costate, costa 2 µm wide, formed of agglomeration of verrucae around pores, pores slightly protuding; atectate, exine 1.5 µm thick; infraverrucate, i.e. nexine is fragmented into verrucae, of circular shape, irregular size and distribution, 0.5-1 µm wide; verrucae of costae are larger.

Dimensions. Equatorial diameter length 30-(33.5)-37 µm, equatorial diameter width 28 µm; length/width 1.19; nm=2, no=3.

Remarks. *Ulmoideipites krempii* (Anderson, 1960) Elsik 1968 has external verrucae and is tectate.

Derivation of name. After internal verrucae.

Botanical affinity. *Forsteronia*/*Prestonia*/*Odontadenia* (Apocynaceae), but has even more resemblance with the African genus *Funtumia* (Apocynaceae).

Plate 1

1-2. *Echinosporis densiechinatus* sp. nov. (Holotype)

3-4. *Echinosporis densiechinatus* sp. nov. (Paratype)

5. *Laevigatosporites caoticus* sp. nov. (Holotype)

6. *Laevigatosporites caoticus* sp. nov. (Holotype)

7. *Laevigatosporites cultellus* sp. nov. (Holotype)

7. *Laevigatosporites cultellus* sp. nov. (Paratype)

9. *Laevigatosporites granulatus* Jaramillo *et al*. 2007

10. *Laevigatosporites tibuiensis* (Van der Hammen 1956a) Jaramillo and Dilcher 2001

11. *Microfoveolatosporis simplex* sp. nov.

12. Polypodiisporites aff. speciosus

13. *Polypodiisporites densus* sp. nov. (Holotype)

14. *Polypodiisporites densus* sp. nov. (Paratype)

PLATE 1

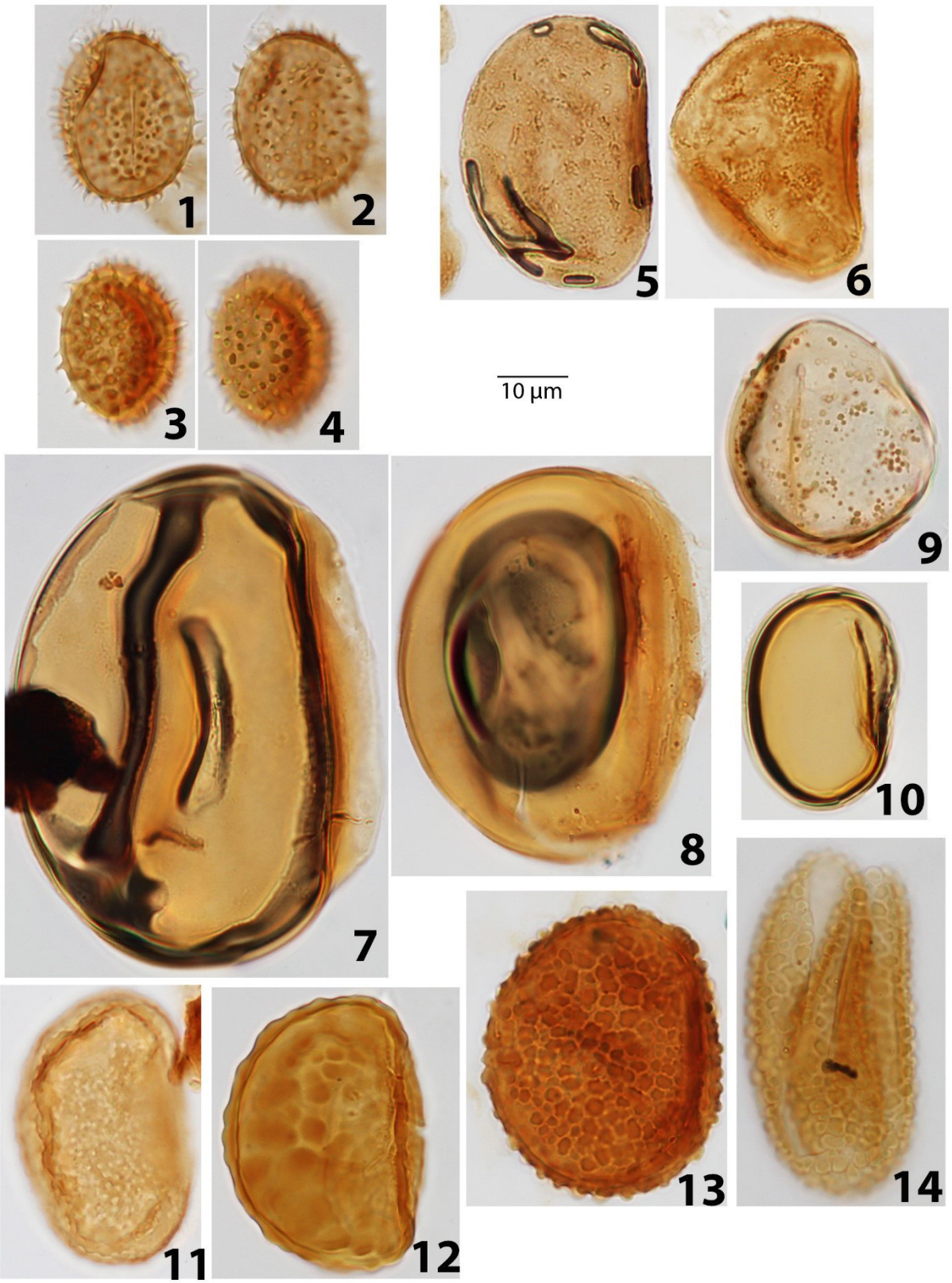

Plate 2

1. *Polypodiisporites discretus* sp. nov. (Holotype)

2. *Polypodiisporites discretus* sp. nov. (Paratype)

3-4. *Polypodiisporites fossulatus* sp. nov.

5. *Polypodiisporites scabraproximatus* Silva-Caminha *et al*. 2010

6-7. *Polypodiisporites usmensis* (Van der Hammen, 1956a) Khan and Martin 1972

8. *Polypodiisporites? planus* Silva-Caminha *et al*. 2010

9-10. *Punctatosporites? latrubessei* sp. nov. (Holotype)

11-12. *Punctatosporites? latrubessei* sp. nov. (Paratype)

13-14. *Reticulosporis diversus* sp. nov. (Holotype)

15-16. *Reticulosporis diversus* sp. nov. (Paratype)

Plate 2

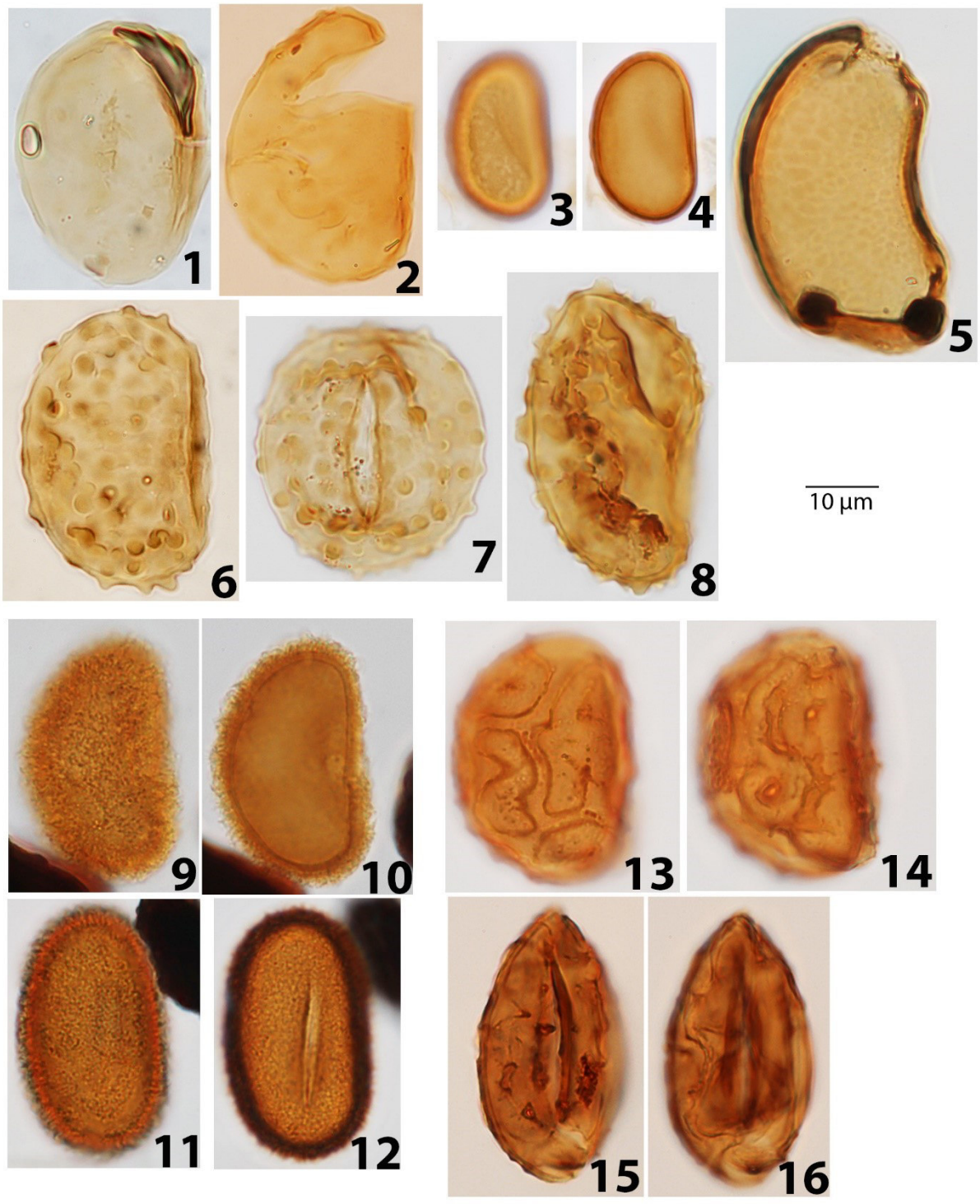

Plate 3

1*. *Azolla sp.*

2-3. *Camarozonosporites crassus* Silva-Caminha *et al*. 2010

4-5. *Camarozonosporites fossulatus* sp. nov.

6-7. *Camarozonosporites trilobatus* sp. nov. (Holotype)

8-9. *Camarozonosporites trilobatus* sp. nov. (Holotype)

10-11. *Cicatricosisporites baculatus* Regali *et al.* 1974

12-13*. *Cicatricosisporites pseudograndiosus* sp. nov.

14. *Cingulatisporites cristatus* sp. nov.

15-16. *Cingulatisporites matisiense* sp. nov. (Holotype)

17-18. *Cingulatisporites matisiense* sp. nov. (Paratype)

*picture is half sized

Plate 3

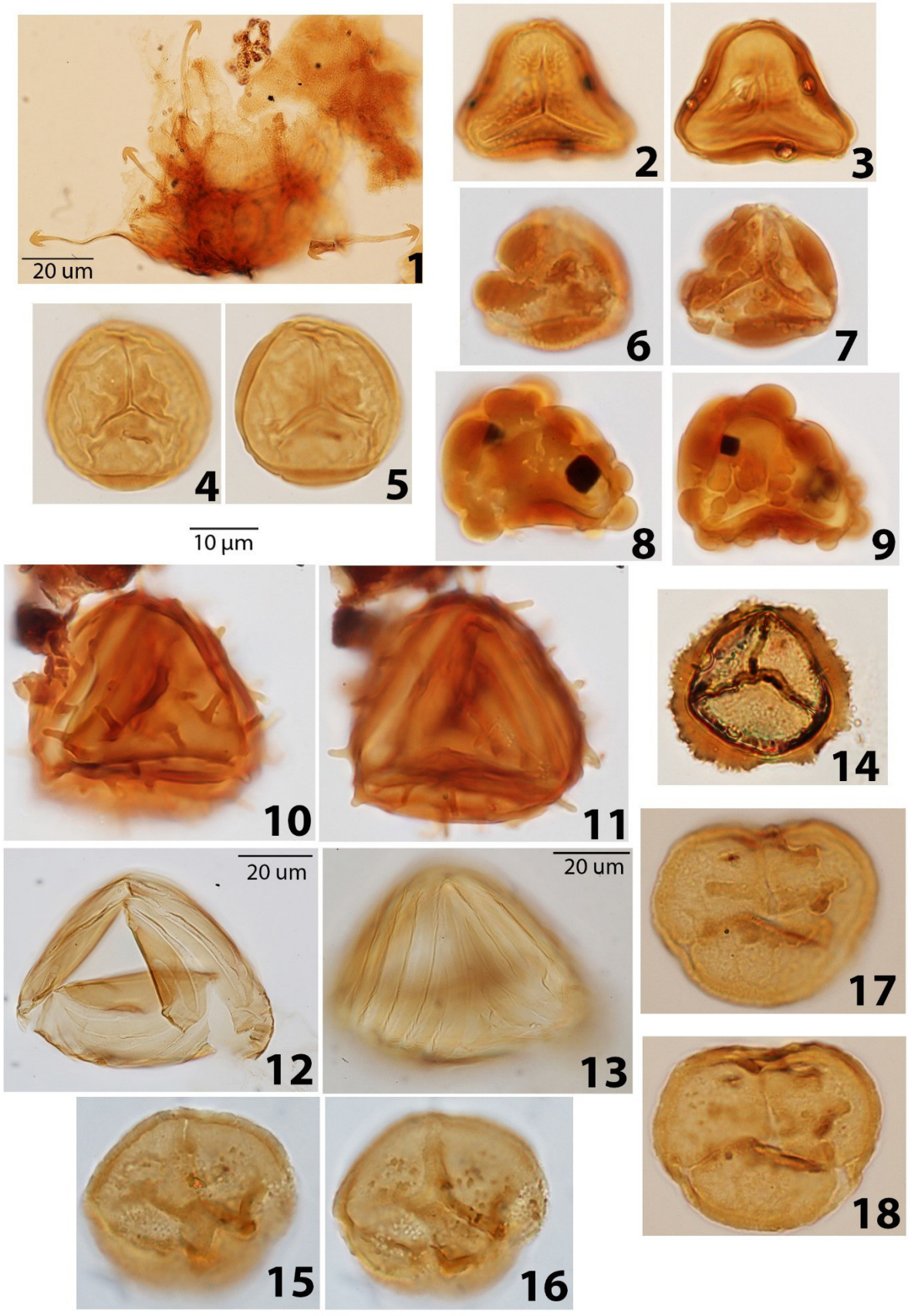

Plate 4

1-2*. *Crassoretitriletes vanraadshoovenii* Germeraad *et al*. 1968

3*. *Deltaidospora adriennis* (Potonié and Gelletich 1933) Frederiksen 1983

4-5. *Distaverrusporites margaritatusi* Muller 1968

6. *Echinatisporis circularis* Silva-Caminha *et al*. 2010

7-8. *Echinatisporis connectus* sp. nov. (Holotype)

9-10. *Echinatisporis connectus* sp. nov. (Paratype)

11-12. *Echinatisporis infantus* sp. nov. (Holotype)

13. *Echinatisporis infantus* sp. nov. (Paratype)

*picture is half sized

Plate 4

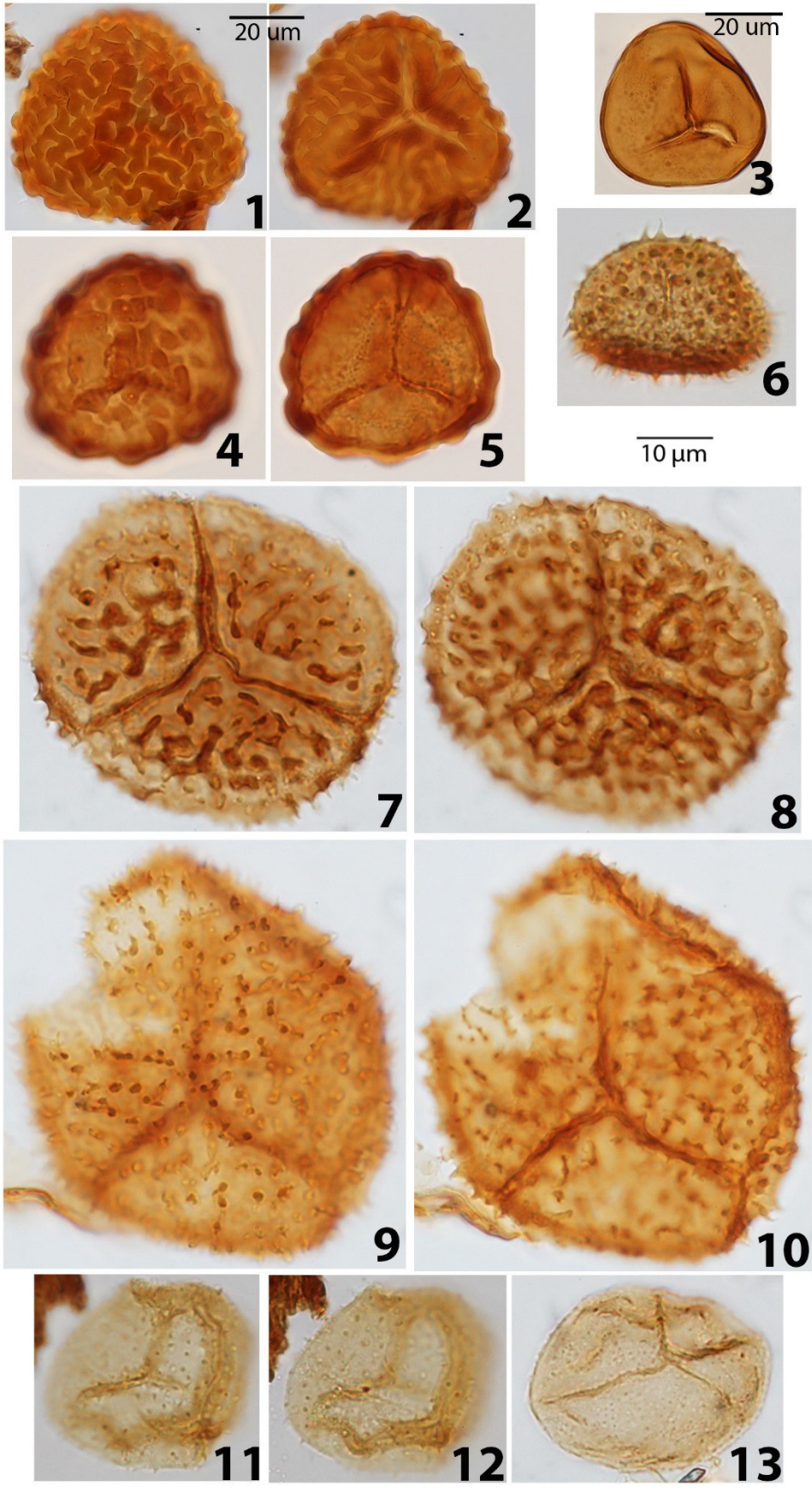

Plate 5

1. *Echinatisporis muelleri* (Regali *et al*. 1974) Silva-Caminha *et al*. 2010

2-3. *Foveotriletes ornatus* Regali *et al*. 1974

4-5. *Hamulatisporis bare* sp. nov.

6-7. *Hydrosporis minor* Silva-Caminha *et al*. 2010

8-9. *Ischyosporites dubius* sp. nov. (Holotype)

10-11. *Ischyosporites dubius* sp. nov. (Paratype)

12-13. *Ischyosporites granulatus* sp. nov.

14. *Kuylisporites waterbolkii* Potonié 1956

15-16. *Lycopodiumsporites clavatoides* sp. nov.

Plate 5

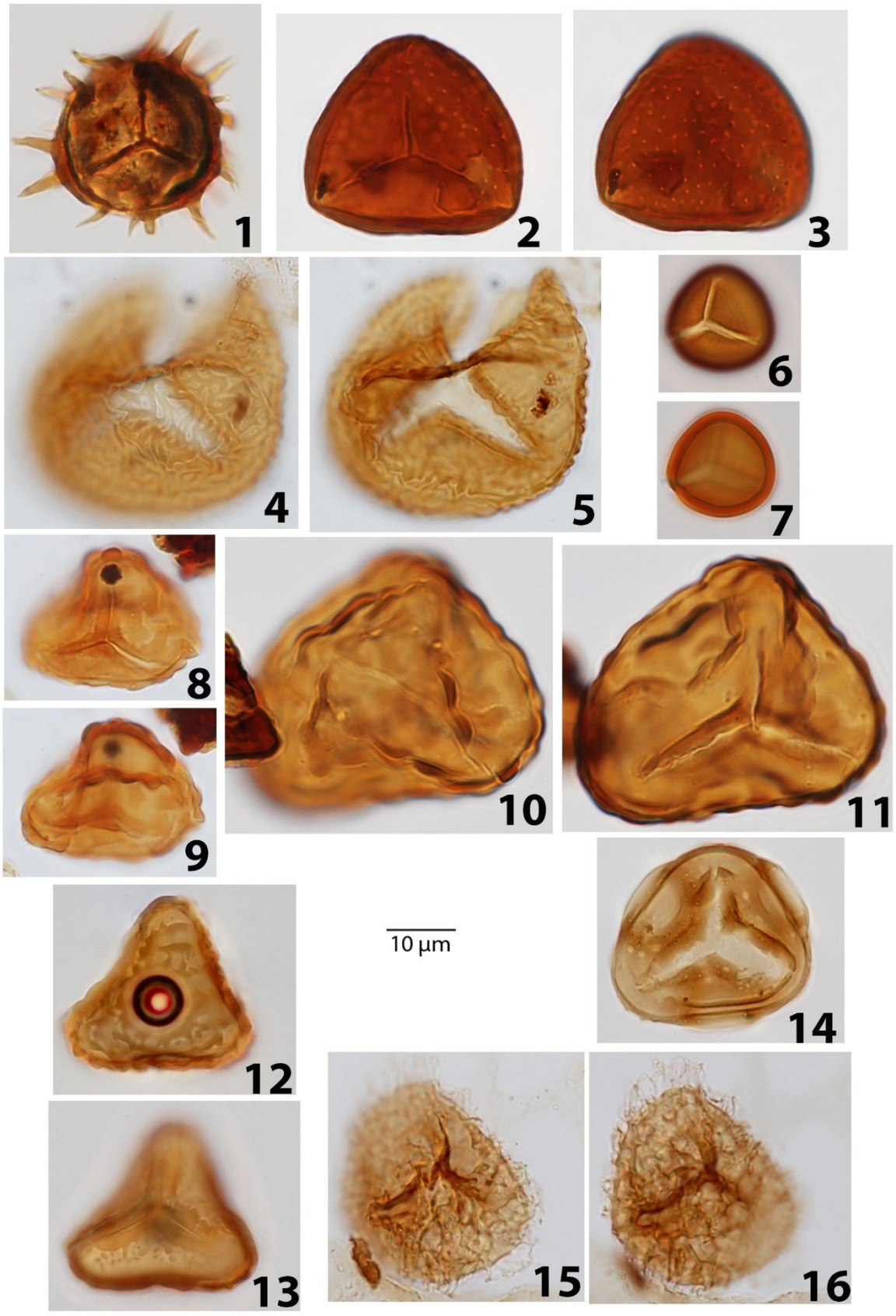

Plate 6

1. *Magnastriatites grandiosus* (Kedves and Sole de Porta 1963) Dueñas 1980

2-3. *Neoraistrickia dubiosa* sp. nov. (Holotype)

4-5. *Neoraistrickia dubiosa* sp. nov. (Paratype)

6-7. *Nijssenosporites fossulatus* Lorente 1986

8-9. *Polypodiaceoisporites pseudopsilatus* Lorente 1986

10. *Psilatriletes delicatus* sp. nov. (Holotype)

11. *Psilatriletes delicatus* sp. nov. (Paratype)

12. *Psilatriletes lobatus* Hoorn 1994

13-14. *Psilatriletes marginata* (Holotype)

15. *Psilatriletes marginata* (Paratype)

Plate 6

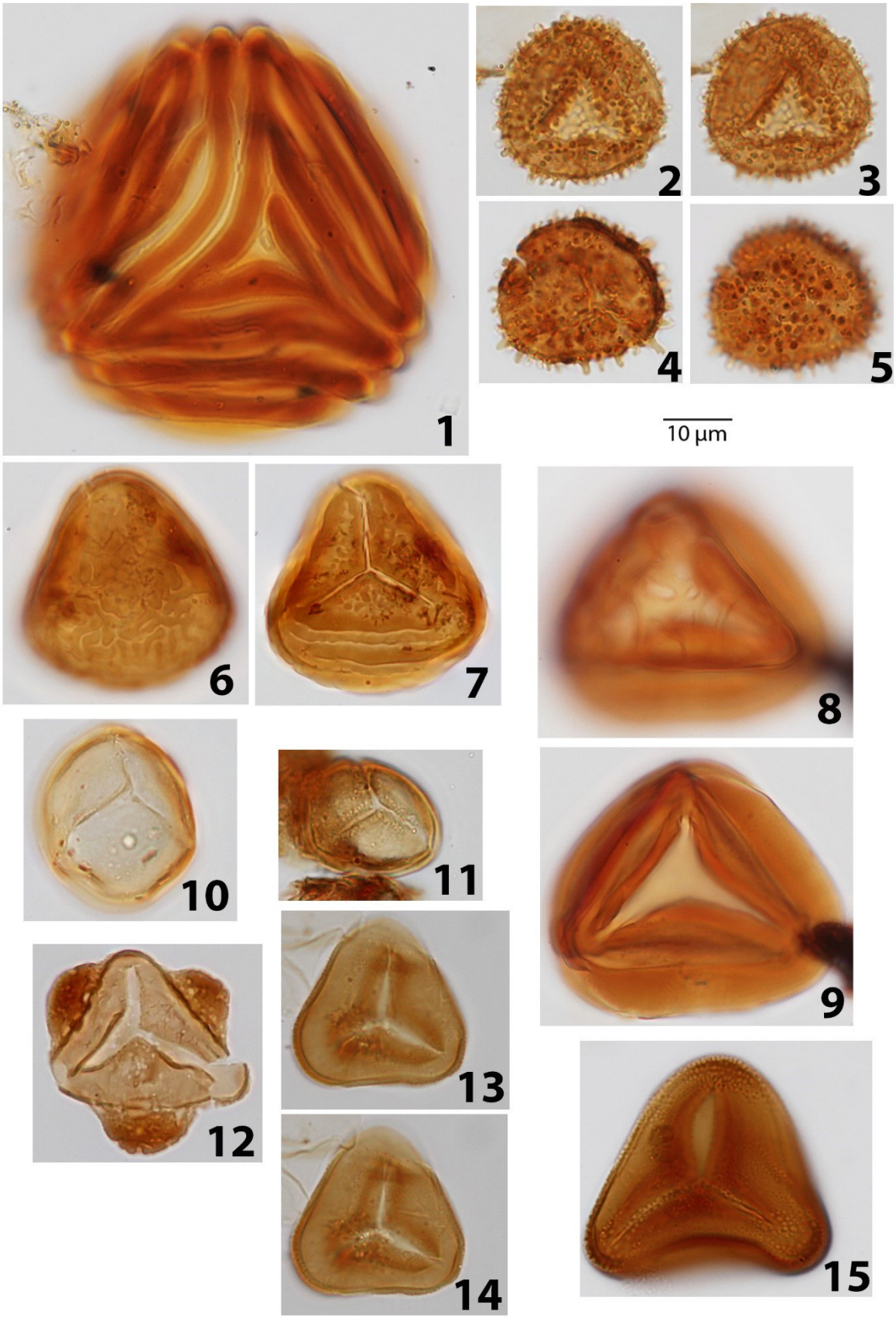

Plate 7

1-2. *Pteridaceoisporis gemmatus* Silva-Caminha *et al*. 2010

3-4. *Retitriletes altimuratus* Silva-Caminha *et al*. 2010

5-6. *Rotverrusporites amazonicus* sp. nov. (Holotype)

7-8. *Rotverrusporites amazonicus* sp. nov. (Paratype)

9-10. *Striatriletes saccolomoides* Jaramillo *et al*. 2010

11-12. *Verrucatotriletes pseusoviruleoides* sp. nov.

Plate 7

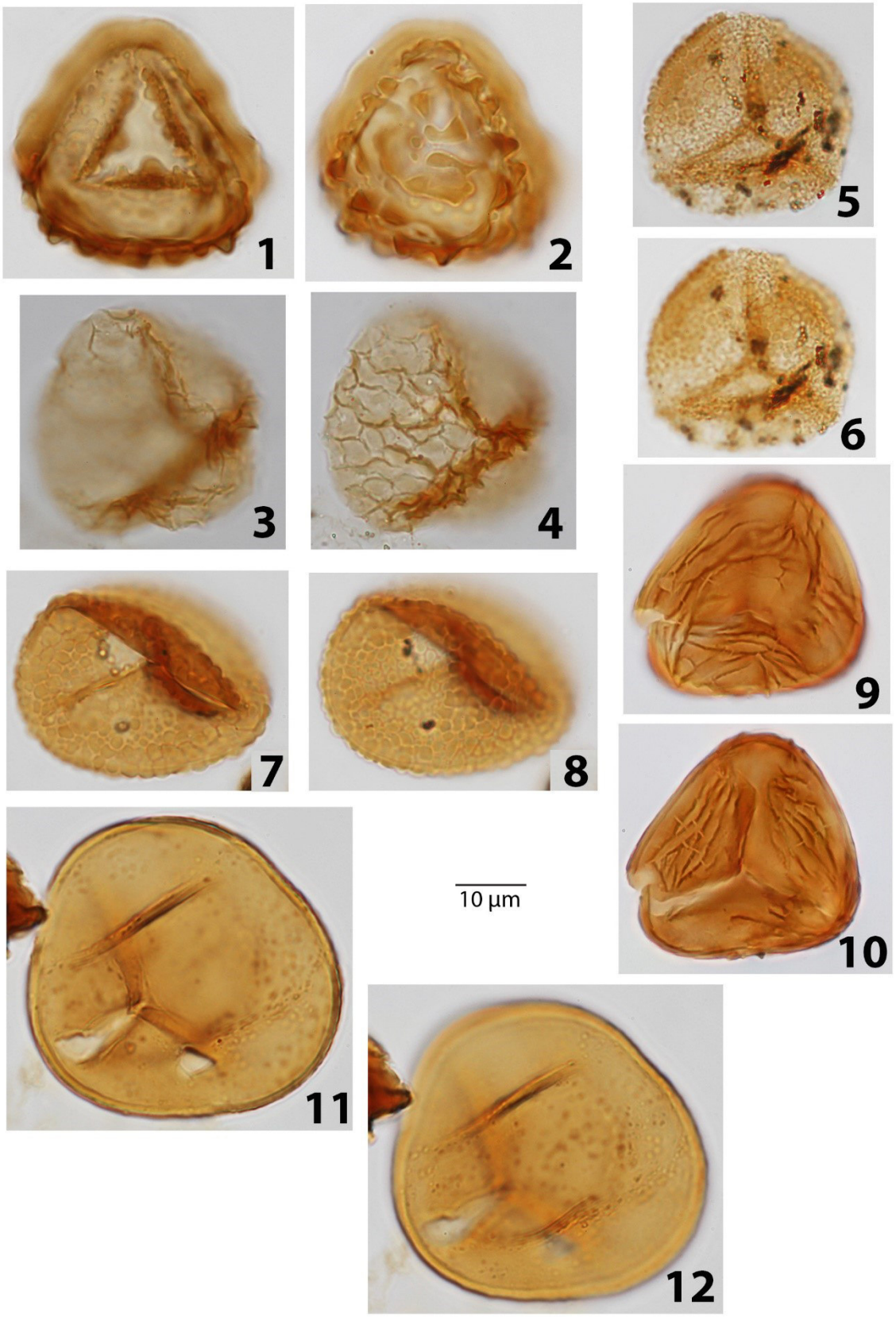

Plate 8

1. *Clavainaperturites microclavatus* Hoorn 1994

2-3*. *Crotonoidaepollenites reticulatus* Silva-Caminha *et al*. 2010

4. *Inapertuporpollenites tectatus* sp. nov.

5-8. *Polyadopollenites macroreticulatus* Salard-Cheboldaeff 1974

9. *Polyadopollenites mariae* Dueñas 1980

10. *Arecipites membranosus* sp. nov.

11. *Arecipites perfectus* Silva-Caminha *et al*. 2010

12. *Arecipites regio* (Van der Hammen and Garcia, 1966) Jaramillo and Dilcher, 2001

13-14. *Clavamonocolpites lorentei* Muller *et al*. 1987

15. *Longapertites lisus* sp. nov. (Holotype)

16. *Longapertites lisus* sp. nov. (Paratype)

17. *Longapertites microfoveolatus* Adegoke and Jan du Chene 1975

*picture 3 was taken with phase contrast

Plate 8

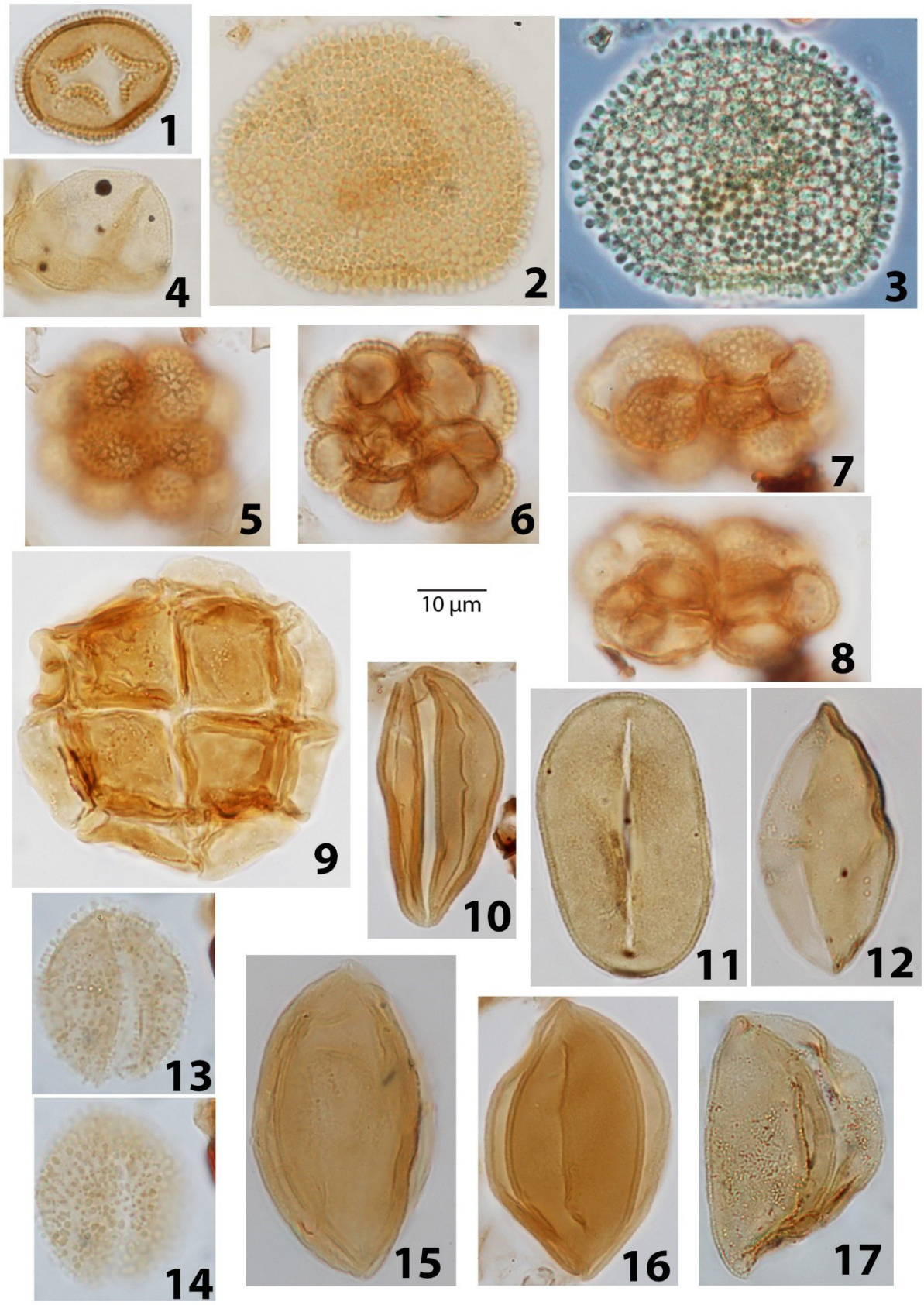

Plate 9

1-2. *Longapertites sutilis sp. nov.*

3-4. *Mauritiidites franciscoi* var. *franciscoi* (Van der Hammen, 1956) Van Hoeken Klinkenberg 1964

5. *Mauritiidites franciscoi* var. *minutus* Van der Hammen and Garcia 1966

6. *Mauritiidites franciscoi* var. *pachyexinatus* Van der Hammen and Garcia 1966

7. *Psilamonocolpites amazonicus* Hoorn 1993

8. *Psilamonocolpites medius* (Van der Hammen, 1956) Van der Hammen and Garcia, 1966

9. *Psilamonocolpites nanus* Hoorn 1993

10. *Retimonocolpites absyae* Hoorn 1993

11-12. *Retimonocolpites normalis* sp. nov.

13-14*. *Proxapertites finus* sp. nov.

15. *Proxapertites psilatus* Sarmiento 1992

16*. *Proxapertites tertiaria* Van der Hammen and Garcia 1966

17. *Trichotomosulcites amazonicus* sp. nov.

18. *Trichotomosulcites normalis* sp. nov.

*picture is half sized

Plate 9

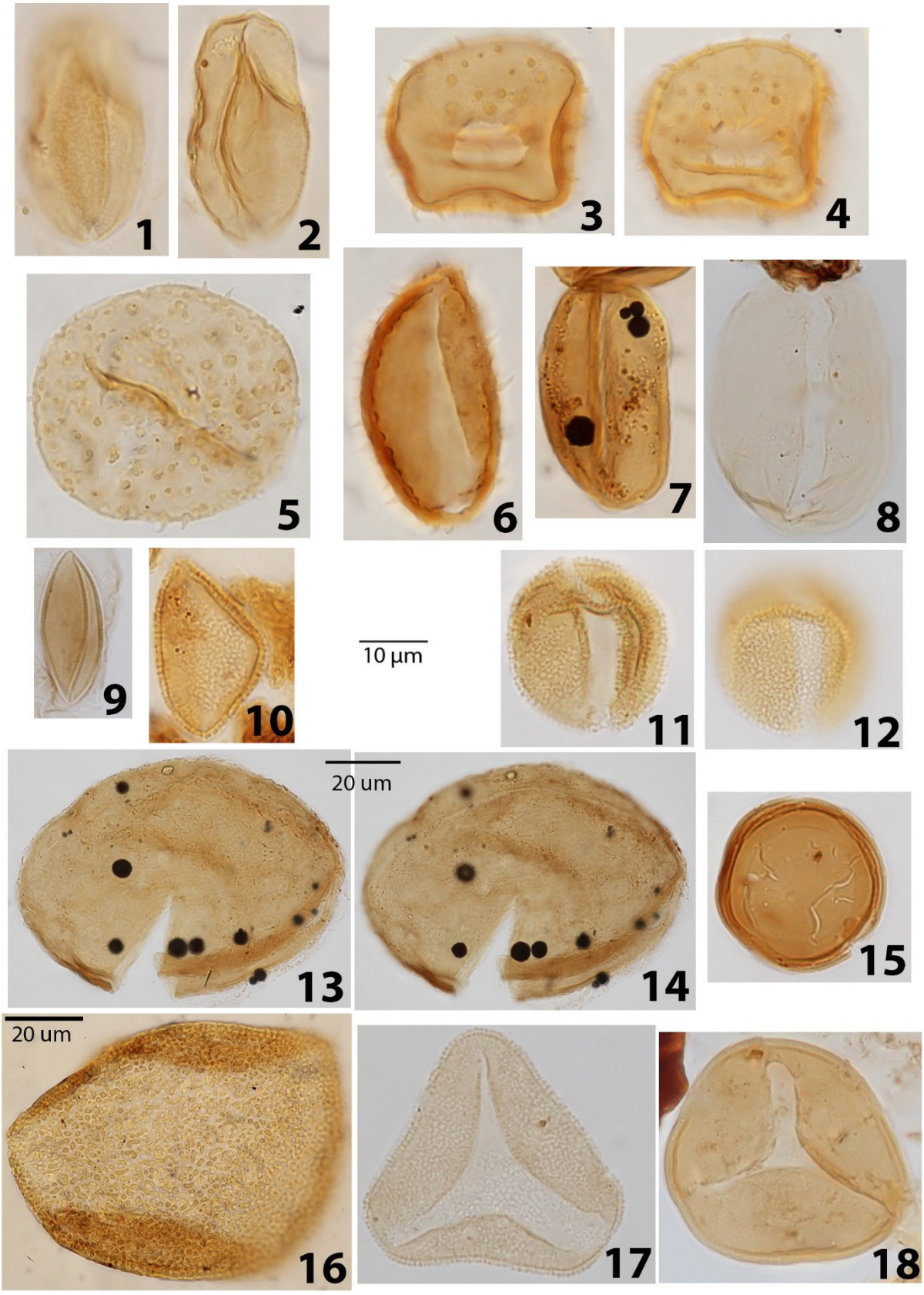

Plate 10

1. *Monoporopollenites annulatus* (Van der Hammen, 1954) Jaramillo and Dilcher 2001

2-3. *Monoporopollenites annuloides* sp. nov.

4-5. *Dicolpopollis? costatus* sp. nov.

6. *Multimarginites vanderhammenii* Germeraad *et al*. 1968

7. *Cyclusphaera scabrata* Jaramillo and Dilcher 2001

8-10. *Echidiporites barbeitoensis* Muller *et al*. 1987

11. *Psiladiporites minimus* Van der Hammen and Wymstra 1964

12. *Psiladiporites redundantis* Gonzalez 1967

13-14. *Crassiectoapertites columbianus* (Dueñas 1980) Lorente 1986

15. *Crototricolpites annemaria* Leidelmeyer 1966

16. *Crototricolpites finitus* Silva-Caminha *et al*. 2010

17-18. *Foveotricolpites colpiconstrictus* Hoorn 1994 nov. comb.

Plate 10

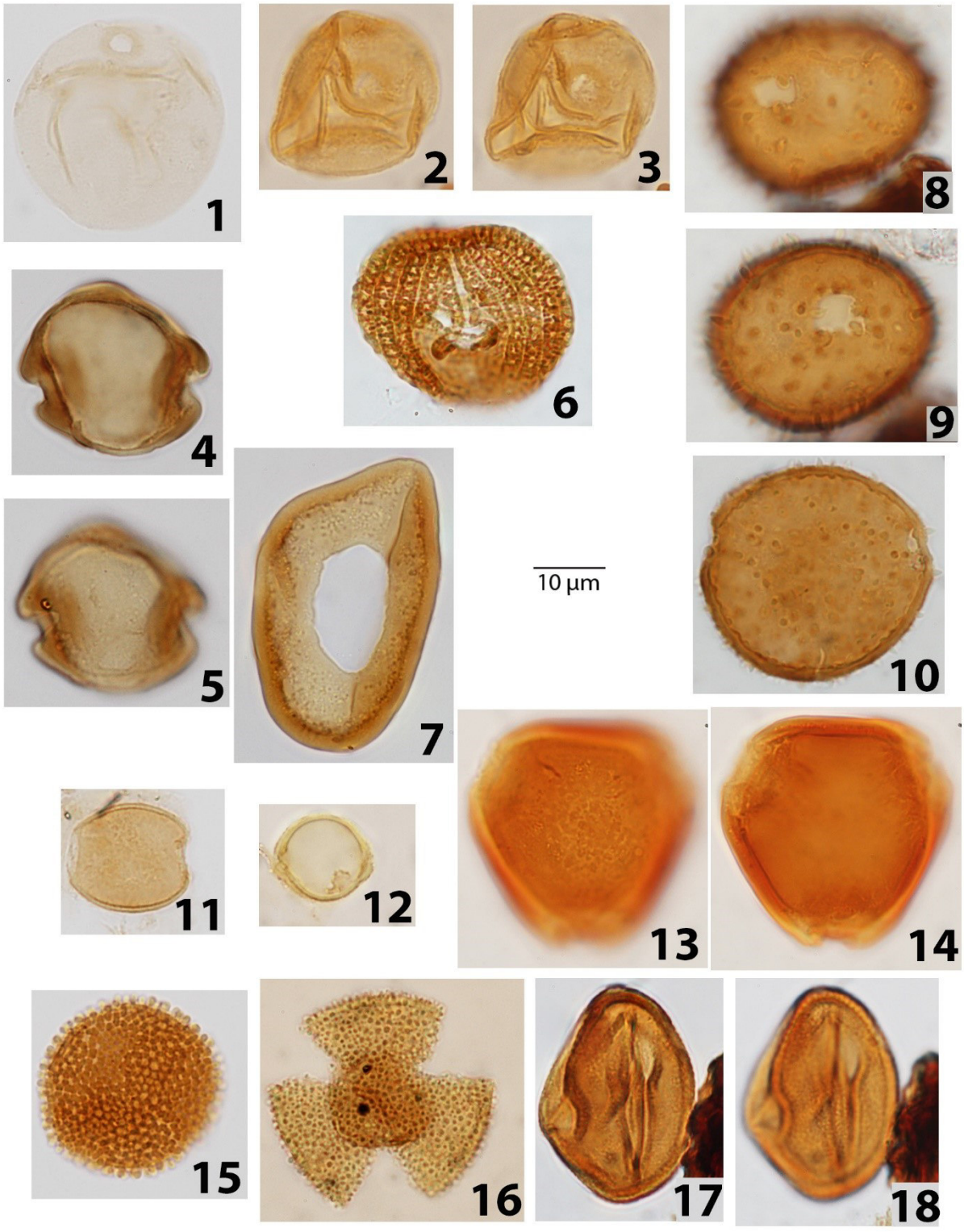

Plate 11

1-3. *Foveotricolpites simplex* Gonzalez 1967 nov. comb.

4-5. *Ladakhipollenites baitacolumellatus* sp. nov. (Holotype)

6. *Ladakhipollenites baitacolumellatus* sp. nov. (Paratype)

7-8. *Ladakhipollenites colpiconstrictus* van Hoeken-Klinkenberg 1966 nov. comb.

9-10. *Ladakhipollenites nanus* sp. nov.

11-12. *Ladakhipollenites simplissimus* sp. nov.

13-14. *Perfotricolpites digitatus* Gonzalez 1967

Plate 11

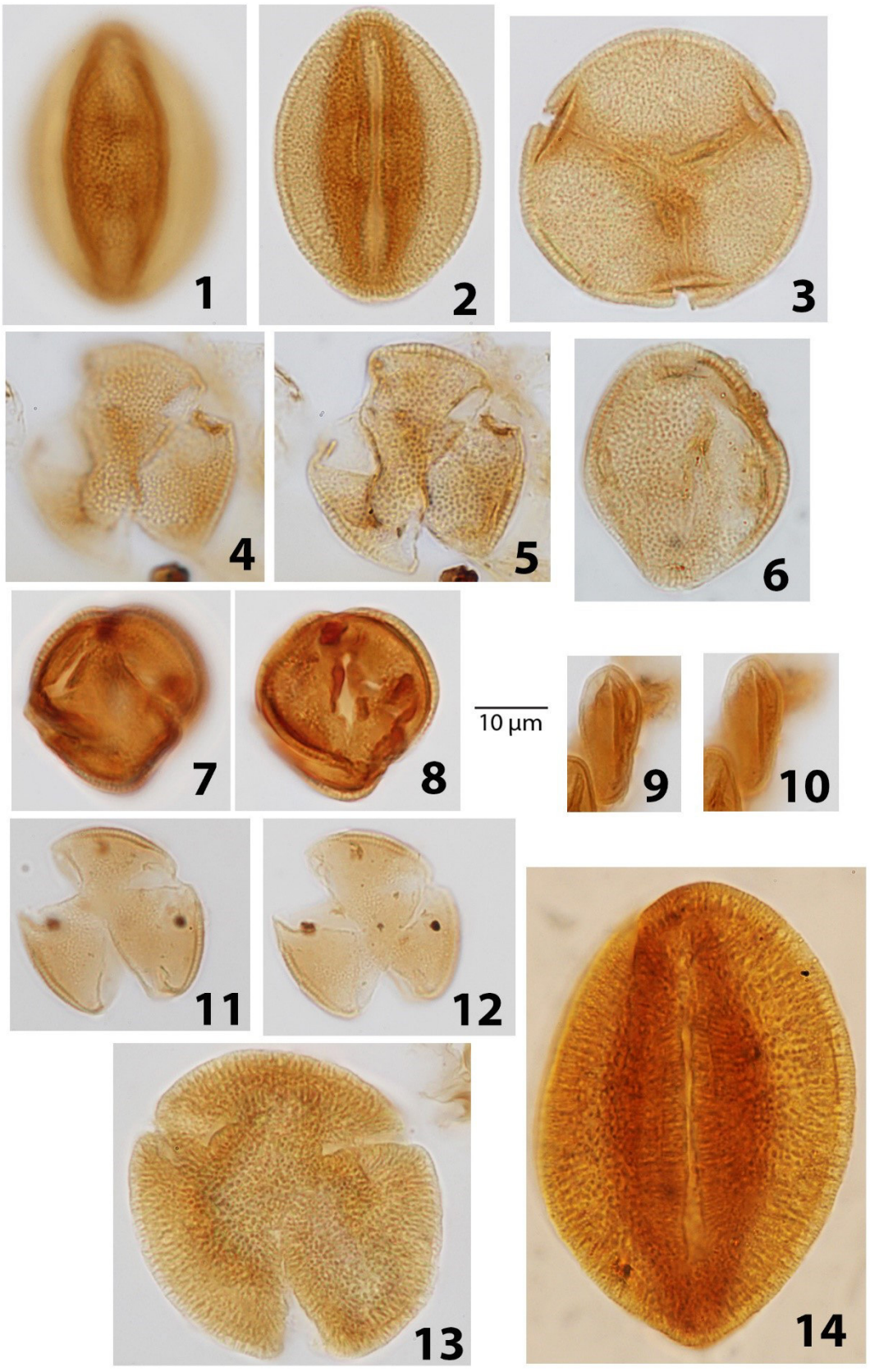

Plate 12

1. *Retibrevitricolpites pseudoretibolus* sp. nov. (Holotype)

2. *Retibrevitricolpites pseudoretibolus* sp. nov. (Paratype)

3. *Retitrescolpites brevicolpatus* sp. nov.

4. *Retitrescolpites magnus* (Gonzalez 1967) Jaramillo and Dilcher 2001

5-6. *Rhoipites? colpiverrucosus* sp. nov.

7-8. *Rhoipites? pluricolumellatus* nov. sp.

9-10. *Spirosyncolpites spiralis* Gonzalez 1967

11. *Tricolpites? pseudoclarensis* Silva-Caminha *et al*. 2010

12. *Bombacacidites araracuarensis* Hoorn 1994

13. *Bombacacidites baculatus* Muller *et al*. 1987

14. *Bombacacidites brevis* (Dueñas 1980) Muller *et al*. 1987

Plate 12

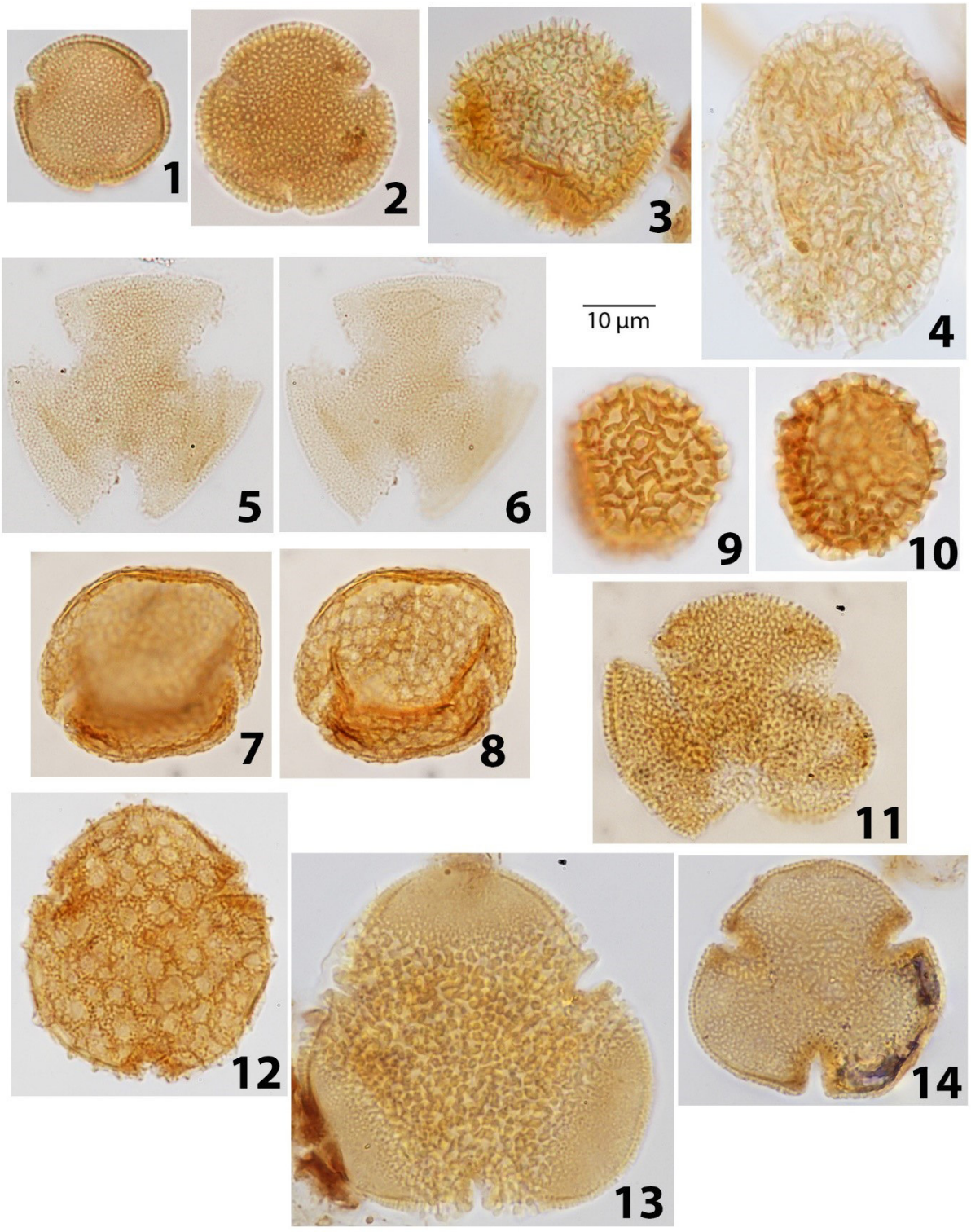

Plate 13

1-2. *Bombacacidites germeraadi* sp. nov.

3. *Bombacacidites lorenteae* Hoorn 1993 nov. comb.

4. *Bombacacidites muinaneorum* Hoorn 1993

5. *Bombacacidites nacimientoensis* (Anderson 1960) Elsik 1968

6. *Cichoreacidites longispinosus* (Lorente 1986) Silva-Caminha *et al*. 2010

7-8. *Echitricolporites magnificus* sp. nov. (Holotype)

9-10. *Echitricolporites magnificus* sp. nov. (Paratype)

11-12. *Echitricolporites mcneillyi* Germeraad *et al*. 1968

13-14. *Echitricolporites spinosus* Van der Hammen 1956

15-16. *Ericipites annulatus* Gonzalez 1967

Plate 13

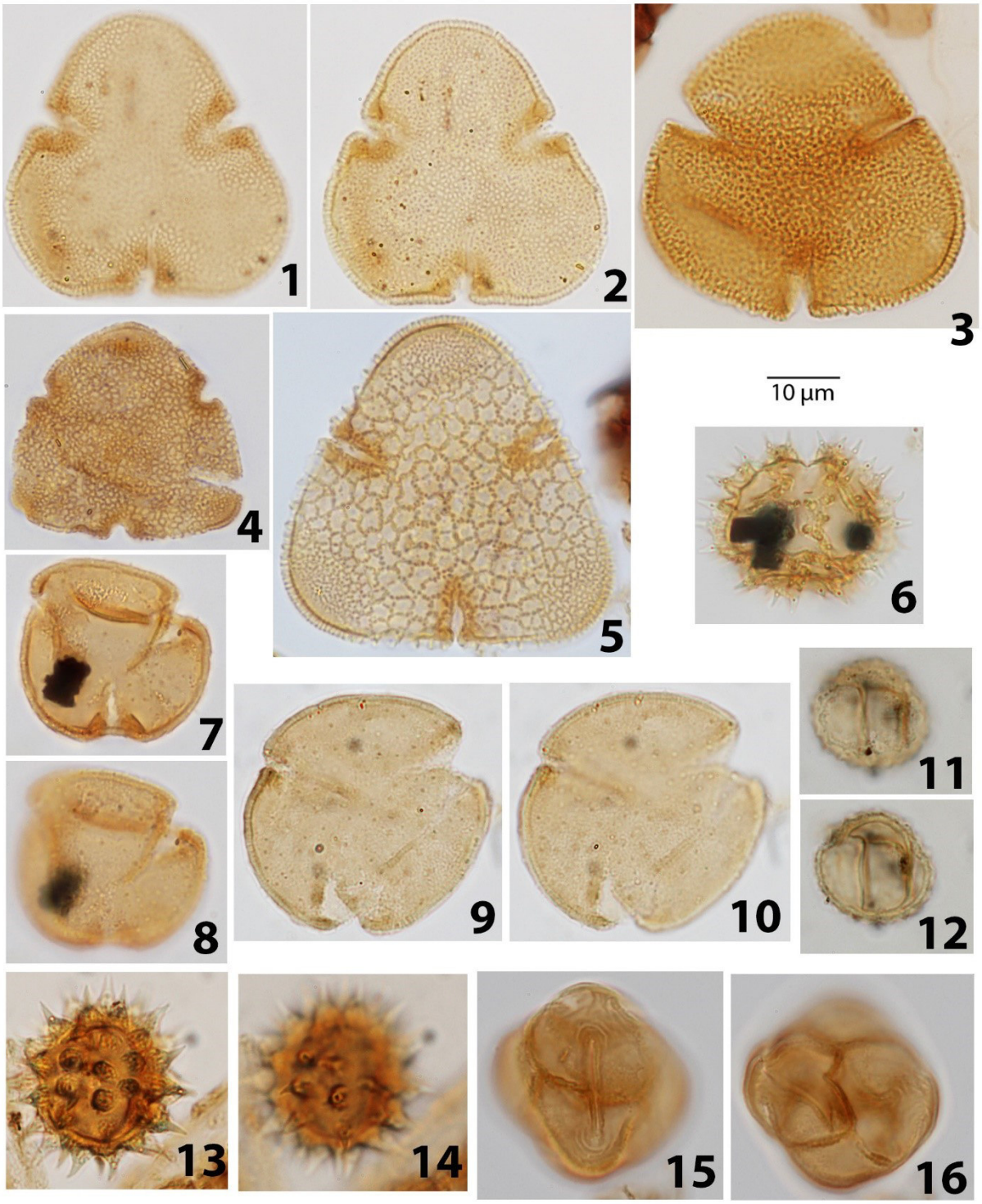

Plate 14

1. *Fenestrites spinosus* Van der Hammen 1956

2-3. *Foveotricolporites lolongatis* sp. nov.

4. *Foveotricolporites pseudodubiosus* Silva-Caminha *et al*. 2010

5-6. *Ilexipollenites tropicallis* Silva-Caminha *et al*. 2010

7. *Ladakhipollenites? Caribbiensis* (Muller et al 1987) Silva-Caminha *et al*. 2010

8. *Ladakhipollenites?cassioides* (Holotype)

9-10. *Ladakhipollenites?cassioides* (Paratype)

11-12. *Ladakhipollenites?corvattatus sp. nov.*

13-14. *Ladakhipollenites?endoporatus sp. nov*

15-17. *Ladakhipollenites?garzonni* Hoorn 1993 nov. comb.

18. *Ladakhipollenites*? *labiatus* Hoorn 1993 nov. comb.

19-20. *Ladakhipollenites*? *magniporatus* Hoorn 1993 nov. comb.

21. *Ladakhipollenites*? *nanus* sp. nov.

22-23. *Ladakhipollenites*? *obesus* Hoorn 1993 nov. comb.

24. *Ladakhipollenites*? *pseudonanus* sp. nov.

25-26. *Ladakhipollenites*? *pseudosilvaticus* sp. nov.

27-28. *Ladakhipollenites*? *silvaticus* Hoorn 1993 nov. comb.

29-30. *Ladakhipollenites*? *sphericus* sp. nov.

Plate 14

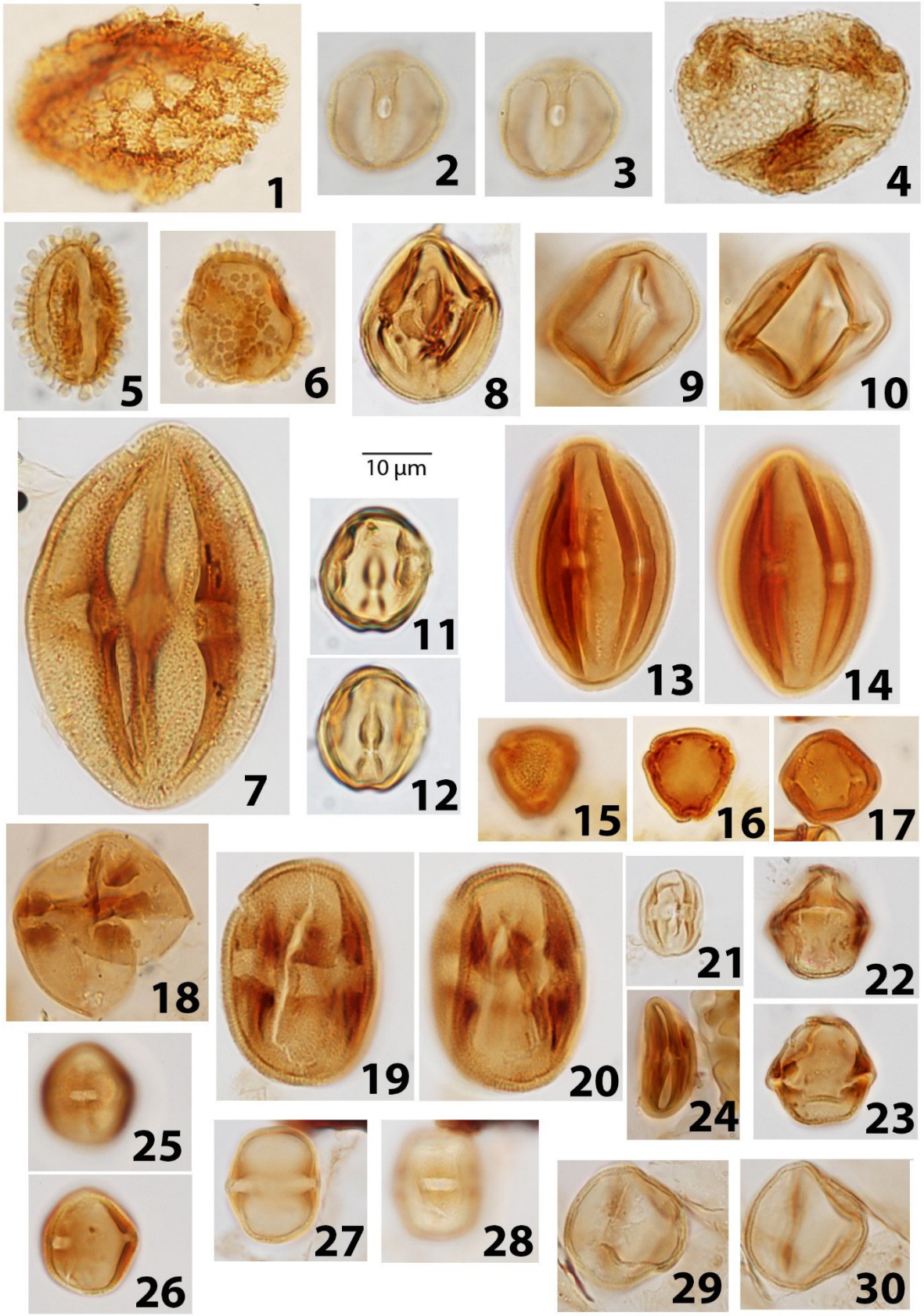
1
2
3
4
5
6
8
9
10
10 µm
11
12
13
14
7
15
16
17
18
19
20
21
22
24
23
25
26
27
28
29
30

Plate 15

1-3. *Ladakhipollenites*? *xatanawensis* sp. nov. (Holotype)

4. *Ladakhipollenites*? *xatanawensis* sp. nov. (Paratype)

5-6. *Lakhiapollis costatus* Silva-Caminha *et al*. 2010

7-8. *Lanagiopollis crassa* (Van der Hammen and Wymstra 1964) Frederiksen 1988

9-10. *Malvacipolloides dubiosus* sp. nov.

11-12. *Malvacipolloides maristellae* (Muller et al 1987) Silva-Caminha *et al*. 2010

13-15. *Margocolporites bilinearis* sp. nov.

16-17. *Margocolporites carinae* sp. nov.

18-19. *Margocolporites "incertus*"

Plate 15

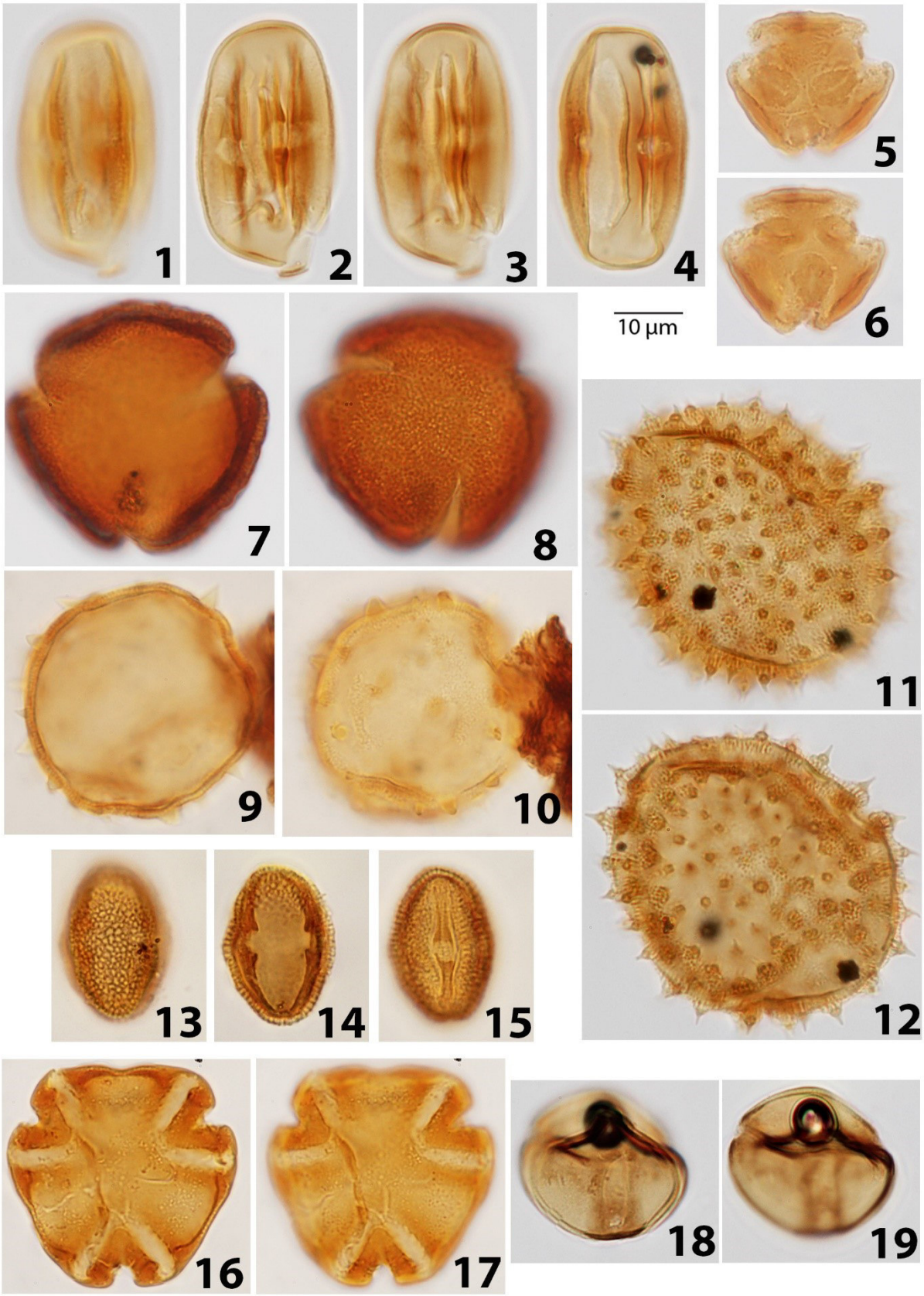

Plate 16

1-2. *Margocolporites vanwijhei* Germeraad *et al*. 1968

3-4. *Paleosantaceaepites* cf. *cingulatus*

5-6. *Paleosantaceaepites invaginatus* sp. nov.

7-8. *Paleosantalaceaepites kaarsii* Hoorn 1993 nov. comb.

9-11. *Psilabrevitricolporites devriesii* (Lorente 1986) Silva-Caminha *et al*. 2010

12-13. *Psilabrevitricolporites triangularis* (Van der Hammen and Wymstra 1964) Jaramillo and Dilcher 2001

14. *Ranunculacidites operculatus* (Van der Hammen and Wymstra 1964) Jaramillo and Dilcher 2001

15-16. *Ranunculacidites reticulatus* sp. nov. (Holotype)

17. *Ranunculacidites reticulatus* sp. nov. (Paratype)

18-19. *Retibrevitricolporites retibolus* Leidelmeyer 1966

20-23. *Retibrevitricolporites solimoensis* Hoorn 1993 nov. comb.

24-25. *Retibrevitricolporites yavarensis* (Hoorn 1993) Silva-Caminha *et al*. 2010

Plate 16

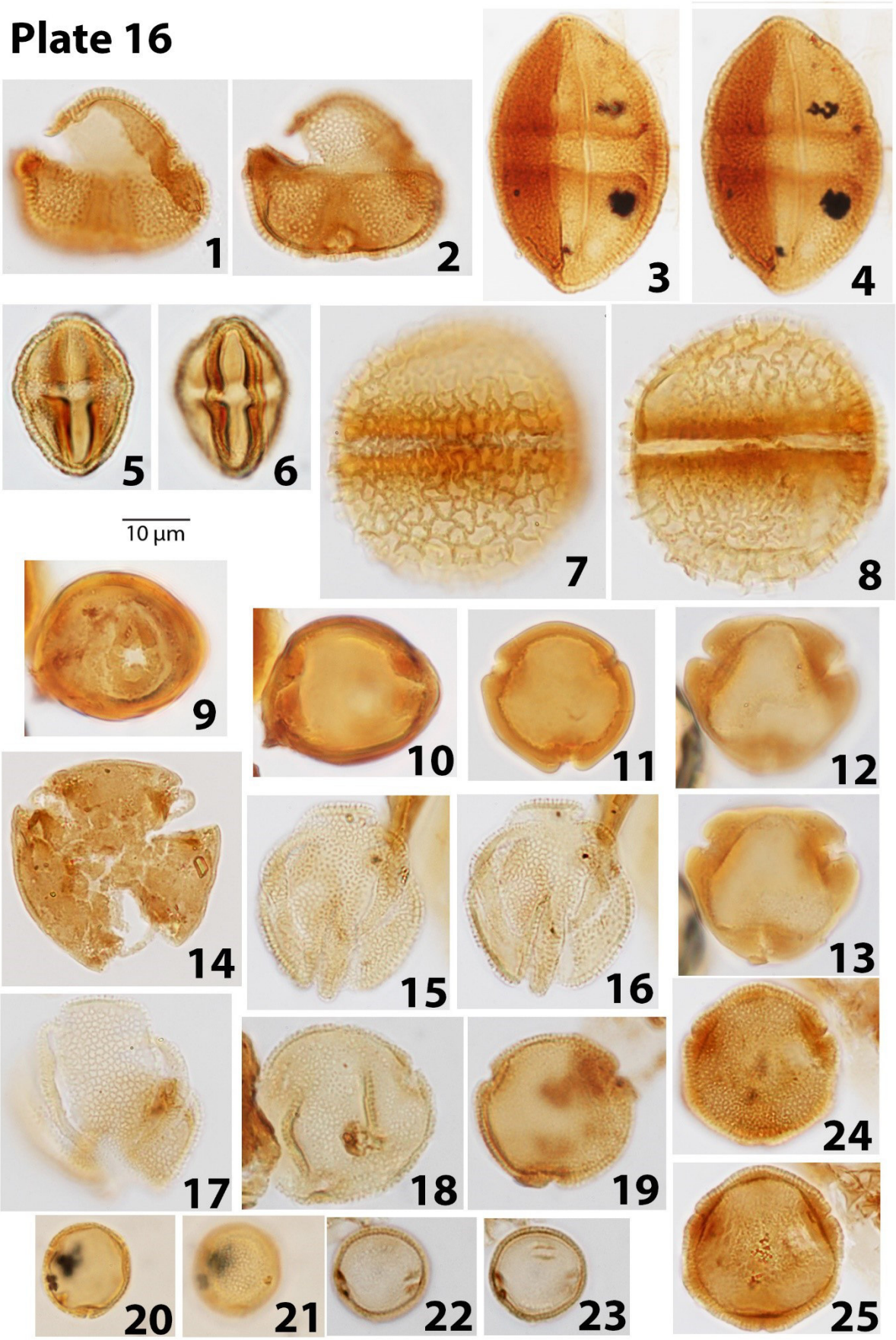

Plate 17

1-2. *Retitrescolpites benjaminense* sp. nov. (Holotype)

3-4. *Retitrescolpites benjaminense* sp. nov. (Paratype)

5-6. *Retitrescolpites grossus* sp. nov.

7-9. *Retitrescolpites marginatus* sp. nov.

10-11. *Retitrescolpites? Irregularis* (Van der Hammen and Wymstra 1964) Jaramillo and Dilcher 2001

12-13. *Retitrescolpites? Traversei* Silva-Caminha *et al*. 2010

14-15. *Retitricolporites milnei* Hoorn 1993

16-17. *Retitricolporites ticoneorum* Hoorn 1993

18-19. *Rhoipites caputoi* Hoorn 1993 nov. comb.

20-21. *Rhoipites caricatus* sp. nov. (Holotype)

22-23. *Rhoipites caricatus* sp. nov. (Paratype)

24-25. *Rhoipites crassicostatus* Van der Hammen and Wymstra 1964 nov. comb.

26-27. *Rhoipites crassitectatus* sp. nov.

Plate 17

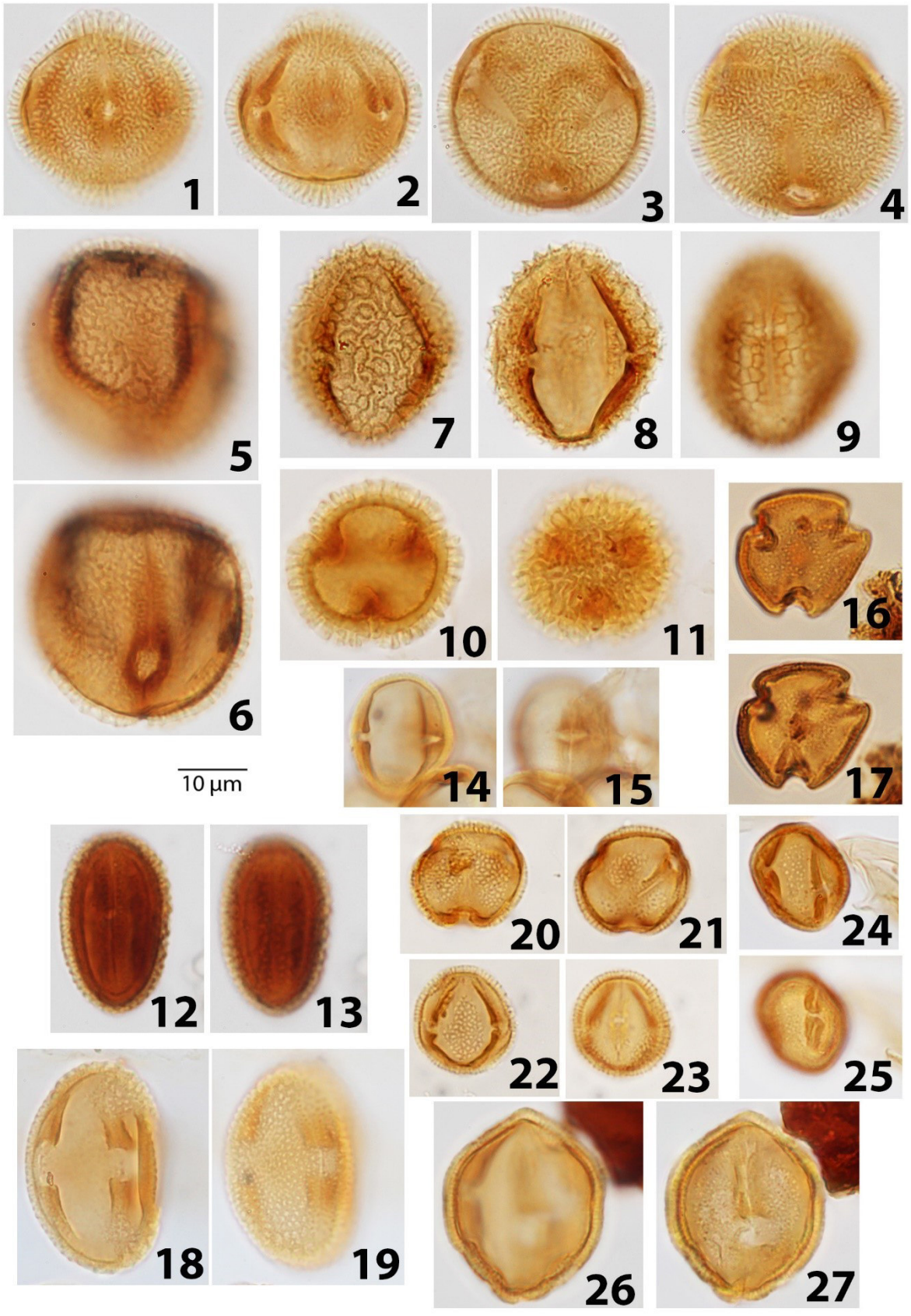

Plate 18

1-3. *Rhoipites crassnexinicus* sp. nov. (Holotype)

4. *Rhoipites crassnexinicus* sp. nov. (Paratype)

5-6. *Rhoipites guianensis* (Van der Hammen and Wymstra 1964) Jaramillo and Dilcher 2001

7-8. *Rhoipites guttus* sp. nov.

9-10. *Retitricolporites nanus* sp. nov.

11-12. *Rhoipites oblatus* Hoorn 1994 nov. comb.

13-14. *Rhoipites poropartitus* sp. nov.

15. *Rhoipites protoguttus* sp. nov. (Holotype)

16-17. *Rhoipites protoguttus* sp. nov. (Paratype)

18-19. *Rhoipites pseudocrassopolaris* sp. nov.

20-21. *Rhoipites pseudopilatus* sp. nov.

22-23. *Rhoipites ticunaensis* sp. nov. (Holotype)

24-25. *Rhoipites ticunaensis* sp. nov. (Paratype)

Plate 18

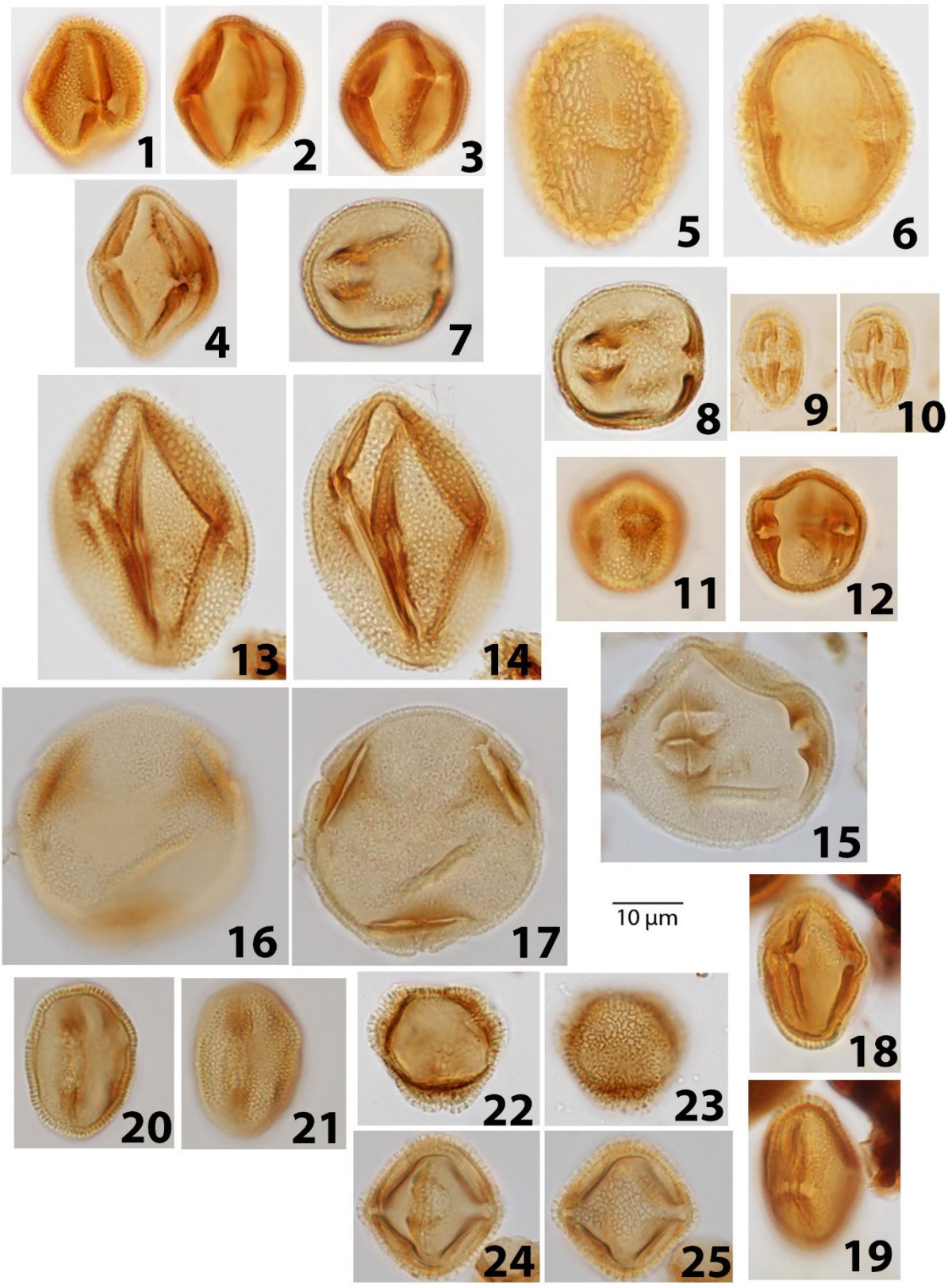

Plate 19

1-3. *Rhoipites toigoi* sp. nov. (Holotype)

4. *Rhoipites toigoi* sp. nov. (Paratype)

5-6. *Rugutricolporites arcus* Hoorn 1993

7-10. *Rugutricolporites felix* Gonzalez 1967

11-12. *Siltaria dilcheri* Silva-Caminha *et al*. 2010

13-14. *Siltaria santaisabelensis* (Hoorn 1994) Silva-Caminha *et al*. 2010

15-17. *Striasyncolpites anastomosatus* Silva-Caminha *et al*. 2010

Plate 19

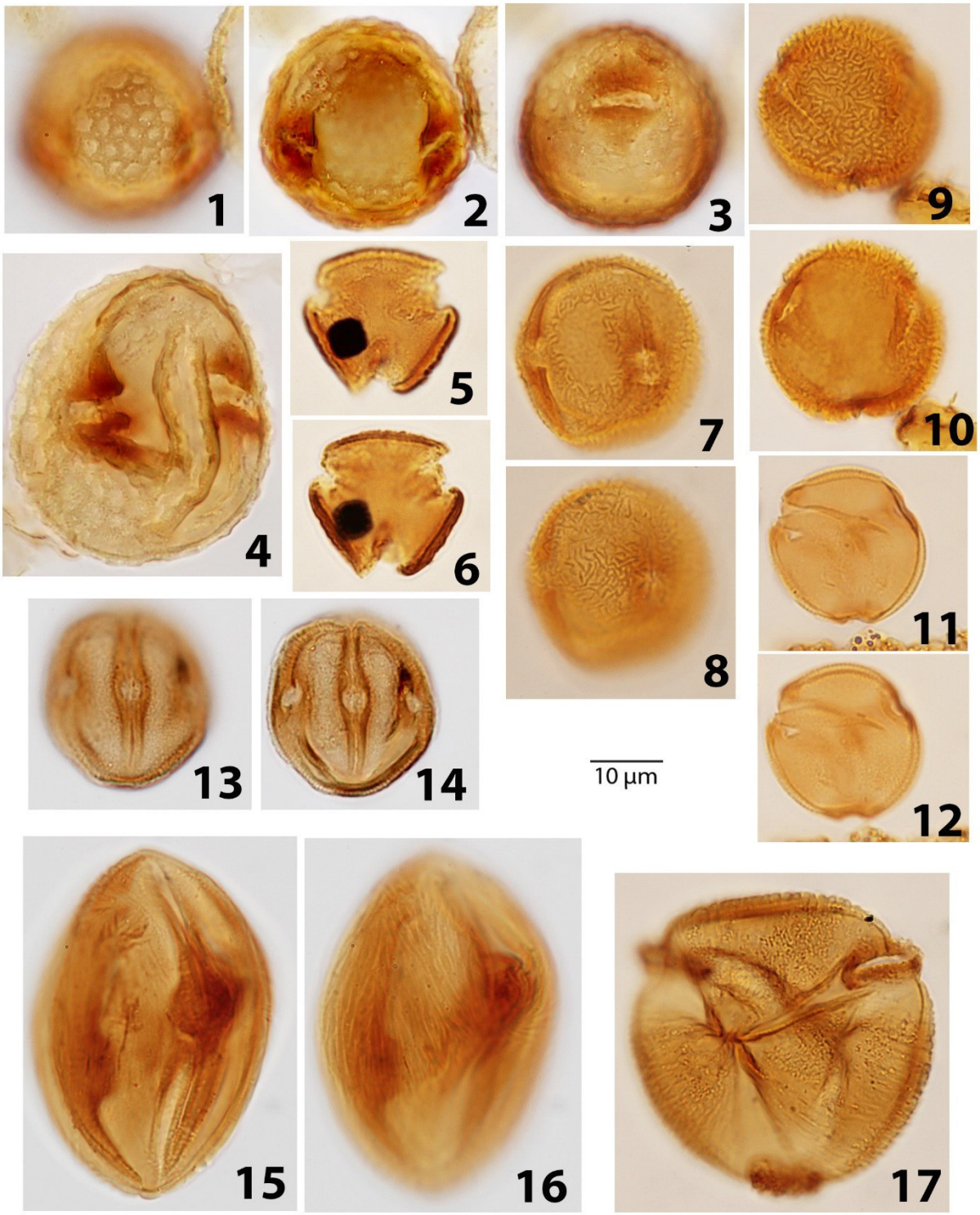

Plate 20

1-2. *Striatopollis catatumbus* (Gonzalez 1967) Takahashi and Jux 1989

3-4. *Striatopollis macrolobium* sp. nov. (Holotype)

5. *Striatopollis macrolobium* sp. nov. (Paratype)

6-7. *Striatopollis poloreticulatus* Silva-Caminha *et al*. 2010

8-9. *Syncolporites triangularis* Regali *et al*. 1974

10-11. *Verrutricolporites pequenus* sp. nov.

12-13. *Verrutricolporites rotundiporus* Van der Hammen and Wymstra 1964

14-15. *Verrutricolporites simplex* (Holotype)

16-17. *Verrutricolporites simplex* (Paratype)

18-19. *Zonocostites ramonae* Germeraad *et al*. 1968

20-21. *Byttneripollis ruedae* Silva-Caminha *et al*. 2010

22-23. *Byttneripollis rugulata* nov. sp. (Holotype)

24-25. *Byttneripollis rugulata* nov. sp. (Paratype)

Plate 20

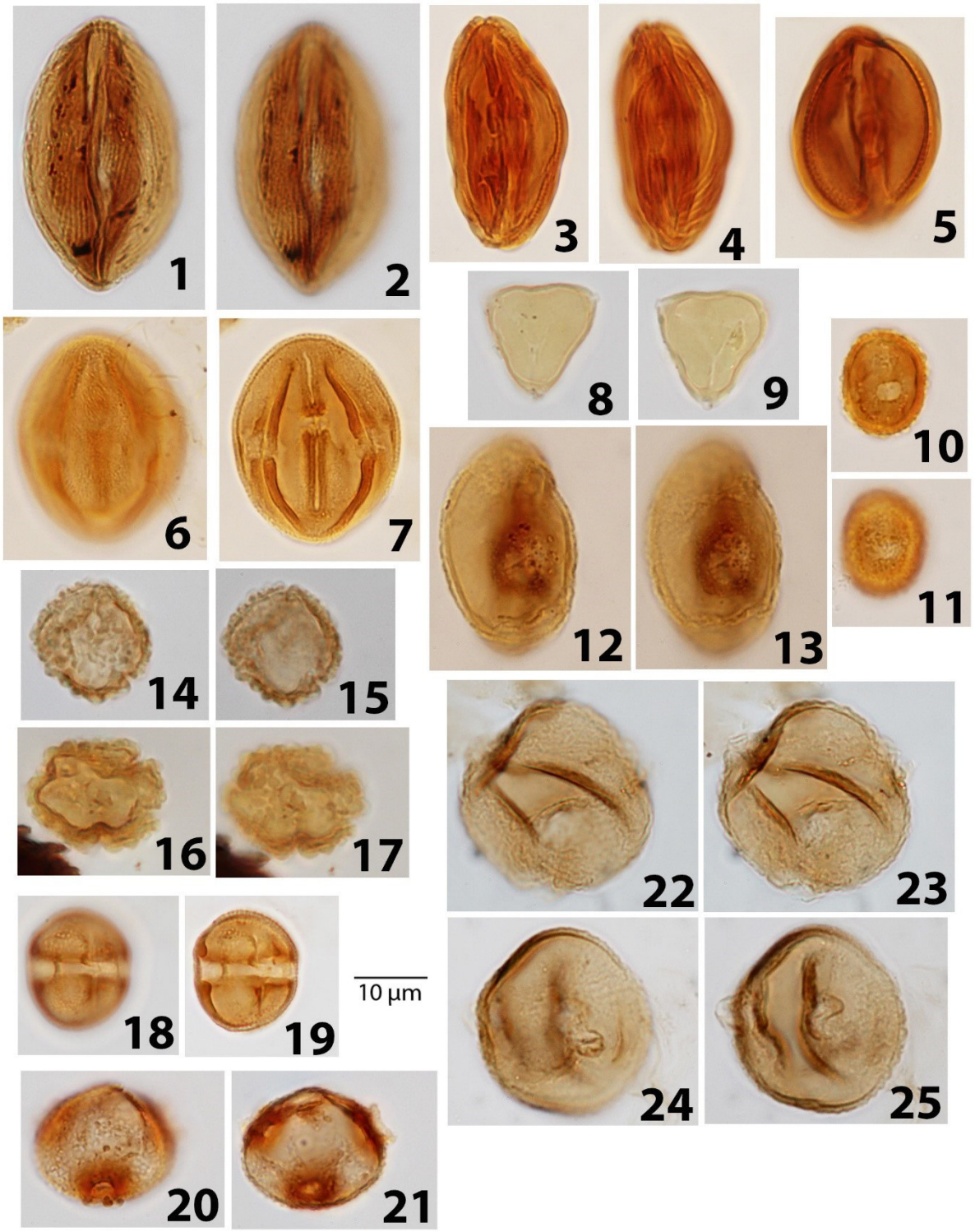

Plate 21

1. *Corsinipollenites collaris* Silva-Caminha *et al*. 2010

2-3. *Corsinipollenites oculusnoctis* (Thiergart 1940) Nakoman 1965

4. *Corsinipollenites scabratus* Silva-Caminha *et al*. 2010

5-6. *Foveotriporites? nodus* sp. nov.

7-8. *Proteacidites poriscabratus* sp. nov. (Holotype)

9. *Proteacidites poriscabratus* sp. nov. (Paratype)

10. *Proteacidites pseudodehaani* sp. nov.

11. *Proteacidites triangulates* Lorente 1986

12. *Psilatriporites desilvae* Hoorn 1993

13. *Psilatriporites minimum* sp. nov. (Holotype)

14-15. *Psilatriporites minimum* sp. nov. (Paratype)

16-17. *Psilatriporites salafrarius* sp. nov. (Holotype)

18. *Psilatriporites salafrarius* sp. nov. (Paratype)

19-20. *Retitriporites discretus* sp. nov. (Holotype)

21-22. *Retitriporites discretus* sp. nov. (Paratype)

Plate 21

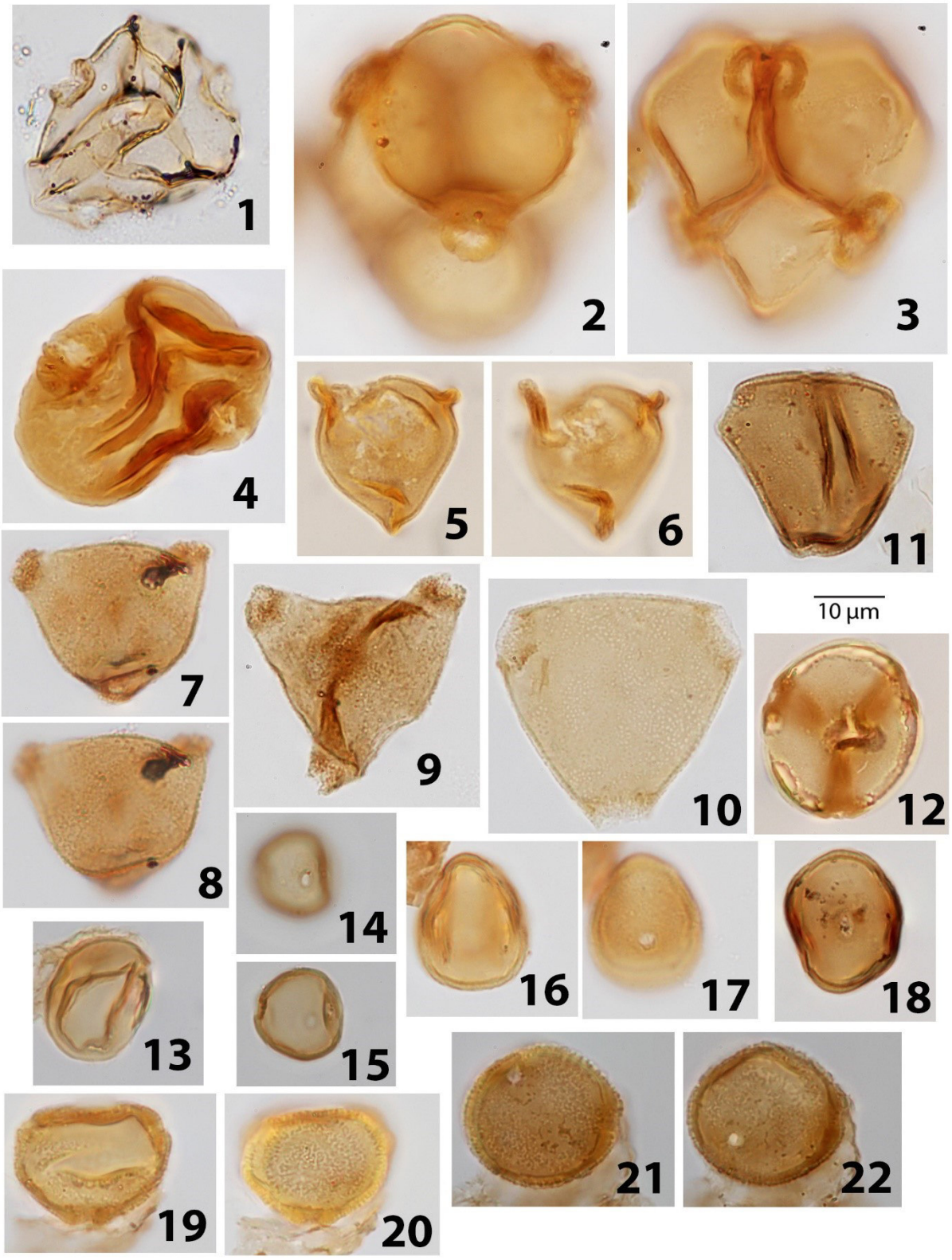

Plate 22

1-2. *Retitriporites tuberosum* sp. nov.

3-4. *Retitriporites typicus* Gonzalez 1967

5-6. *Lymingtonia amazonica* sp nov.

7-8. *Lymingtonia splendens* sp nov.

9-11. *Ctenolophinidites suigeneris* Silva-Caminha *et al*. 2010

Plate 22

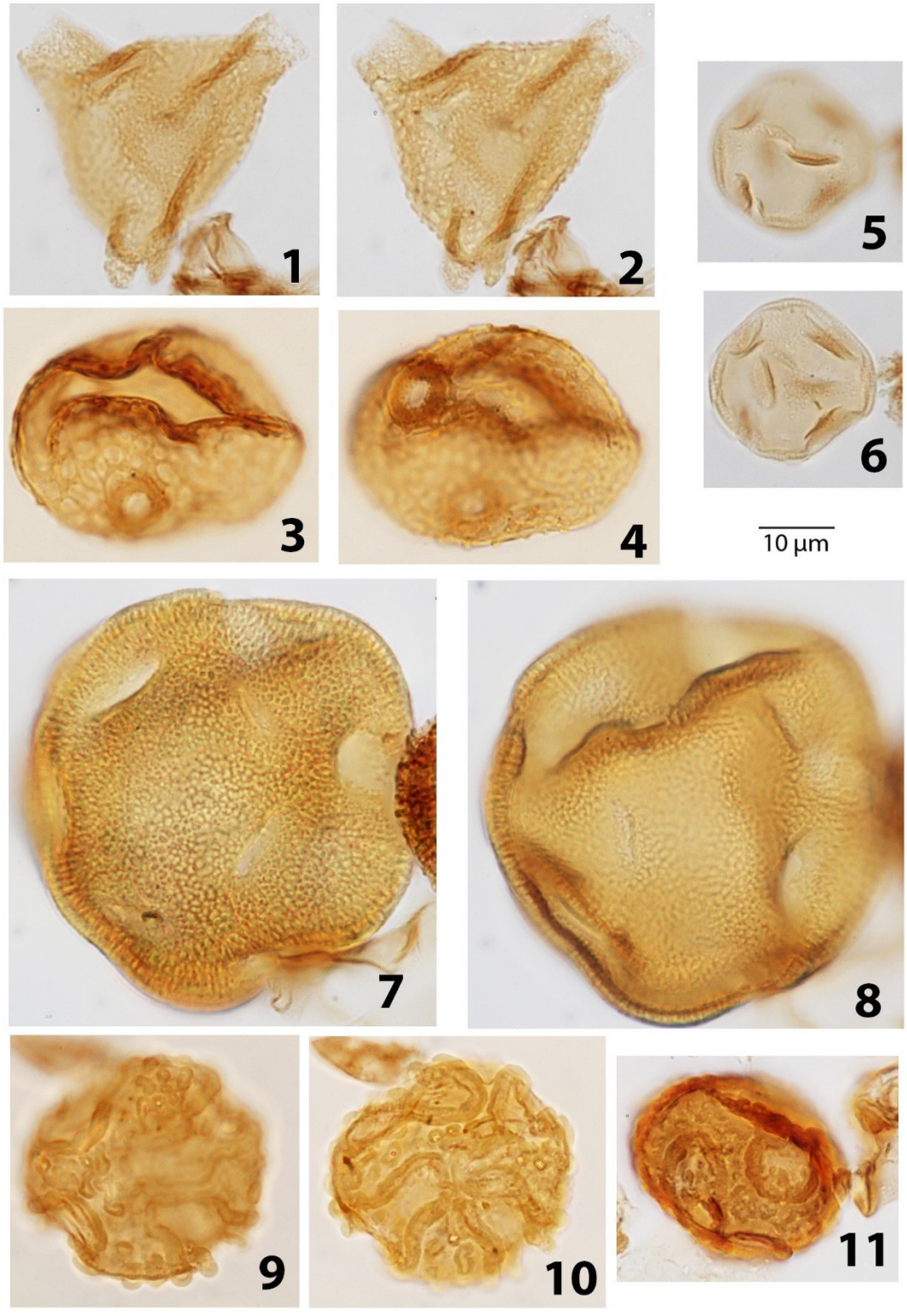

Plate 23

1-2. *Retistephanocolpites curvimuratus* sp. nov. (Holotype)

3. *Retistephanocolpites curvimuratus* sp. nov. (Paratype)

4-5. *Retistephanocolpites liberalis* sp. nov. (Holotype)

6. *Retistephanocolpites liberalis* sp. nov. (Paratype)

7-8. *Retistephanocolpites passionis* sp. nov. (Holotype)

9. *Retistephanocolpites passionis* sp. nov. (Paratype)

10-11. *Heterocolpites incomptus* Hoorn 1993

12. *Heterocolpites rotundus* Hoorn 1993

13-14. *Heterocolpites verrucosus* Hoorn 1993

15-16. *Heterocolpites brevicolpatus* Silva-Caminha *et al*. 2010

17. *Jandufouria minor* Jaramillo and Dilcher 2001

18-19*. *Jandufouria seamrogiformis* Jaramillo and Dilcher 2001

*picture is half sized

Plate 23

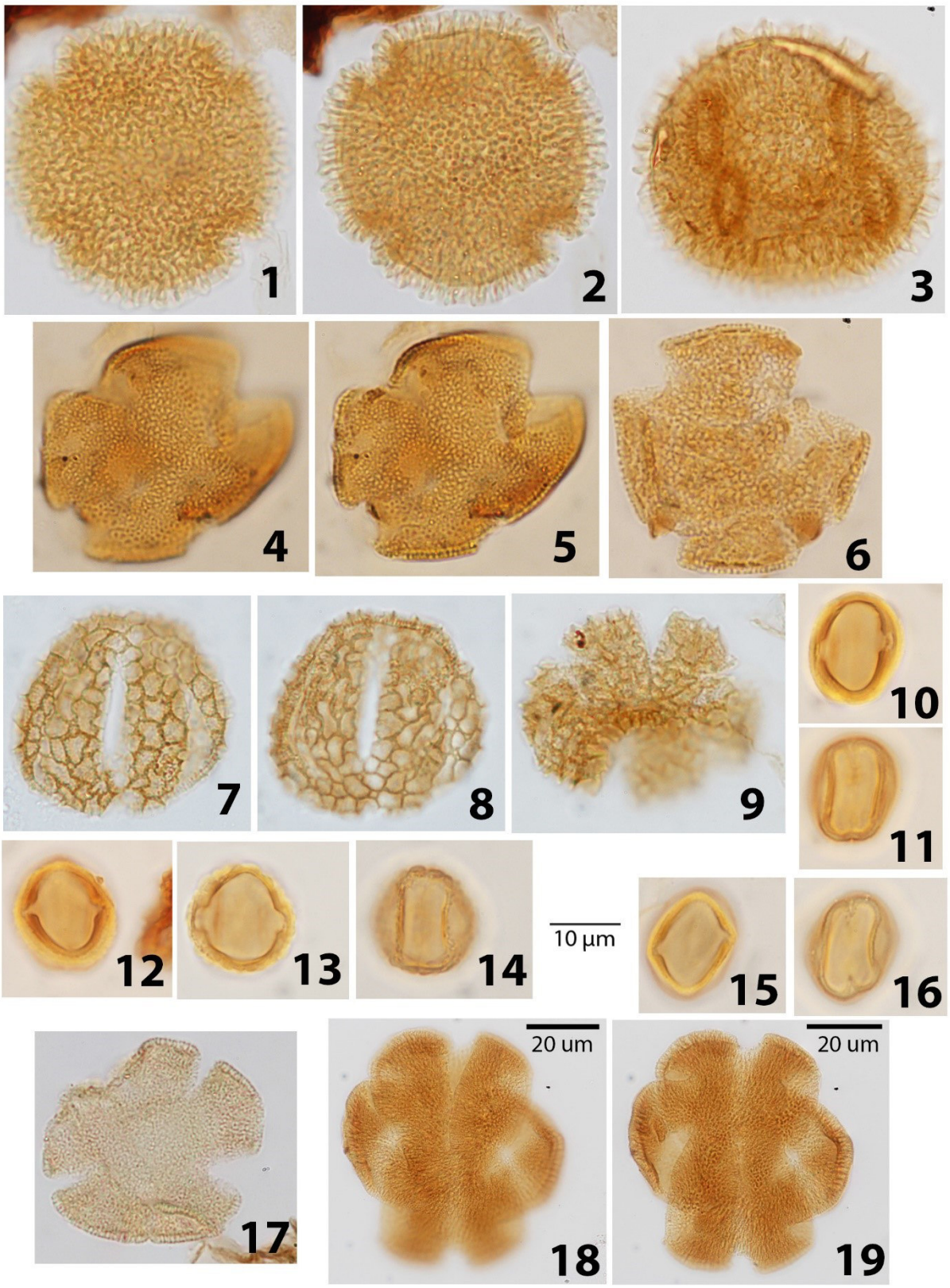

Plate 24

1-3.*Loxocolporites foveolatus* gen. et sp. nov.

4. *Psilastephanocolporites fissilis* Leidelmeyer 1966

5-6. *Psilastephanocolporites marinamensis* Hoorn 1994

7-8. *Psilastephanocolporites meliosus* sp. nov. (Holotype)

9. *Psilastephanocolporites meliosus* sp. nov. (Paratype)

10-11. *Psilastephanocolporites pseudomarinamensis* sp. nov.

12-13. *Crotoperiporites pulcher* gen. et sp. nov.

14-16. *Cyperaceaepollenites cf neogenicus* Krutzsch 1970

17-18. *Echiperiporites akanthos* Van der Hammen and Wymstra 1964

19*. *Echiperiporites estelae* Germeraad *et al*. 1968

20. *Echiperiporites intectatus* Silva-Caminha *et al*. 2010

21. *Echiperiporites jutaiensis* Silva-Caminha *et al*. 2010

22-23*. *Echiperiporites lophatus* Silva-Caminha *et al*. 2010

*picture is half sized

Plate 24

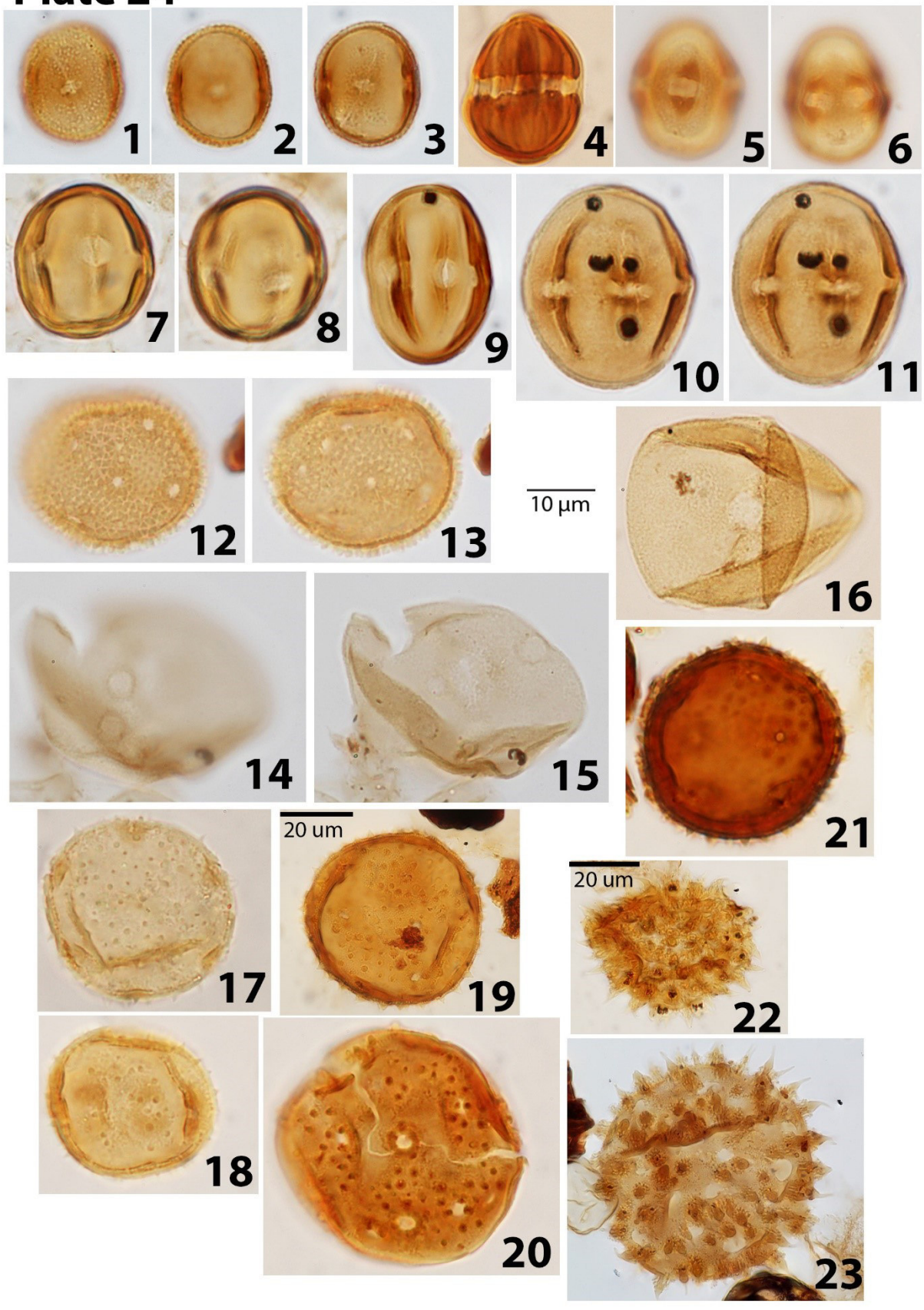

Plate 25

1. *Multiporopollenites crassinexinatus* Silva-Caminha *et al*. 2010

2-3. *Multiporopollenites intermedius* sp. nov.

4. *Parsonsidites? brenacii* Silva-Caminha *et al*. 2010

5. *Parsonsidites? minibrenacii* sp. nov. (Holotype)

6. *Parsonsidites? minibrenacii* sp. nov. (Paratype)

7-8. *Perisyncolporites grossus* nov. sp. (Holotype)

9-10. *Perisyncolporites pokornyi* Germeraad *et al*. 1968

11. *Psilaperiporites multiporatus* Hoorn 1994

12-13. *Psilaperiporites pauciporatus* nov. sp.

14-15. *Psilaperiporites redondus* nov. sp.

16. *Psilastephanoporites herngreenii* Hoorn 1993

17. *Retistephanoporites crassiannulatus* Lorente 1986

18-19. *Verrustephanoporites dubius* sp. nov.

20-21. *Verrustephanoporites intraverrucosus* nov. sp.

Plate 25

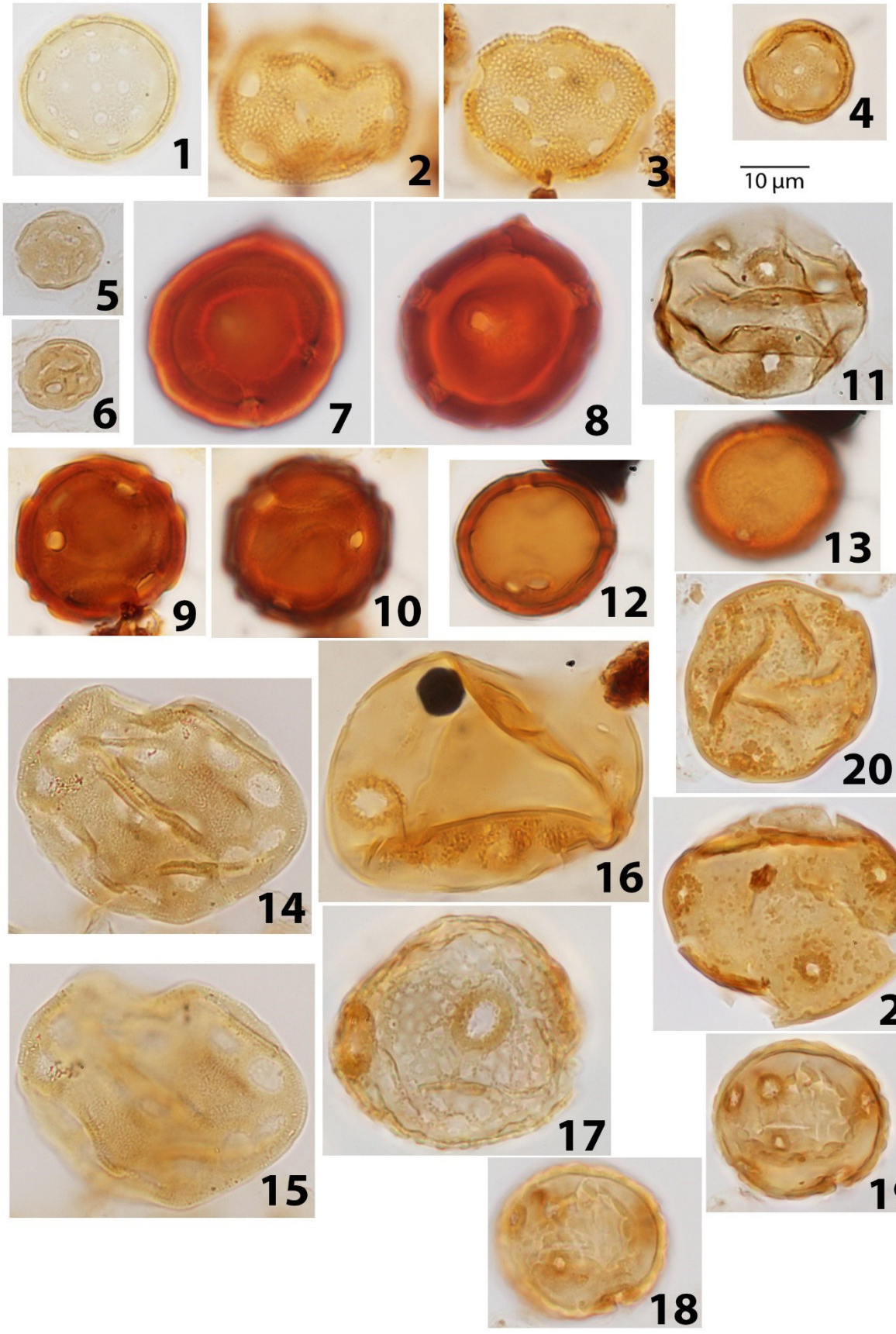

Plate 26

1. *Botryococcus* spp.

2. *Pediastrum* spp.

3*. Foraminiferal lining

4. *Apteodinium? vescum* Matsuoka 1983

5. Rounded Brown Cysts (RBCs)

6-7. *Cleistosphaeridium ancyreum* (Cookson and Eisenack) Eaton *et al*. 2001

8-9. *Cleistosphaeridium placacanthum* (Deflandre and Cookson) Eaton *et al.* 2001

10. *Cribroperidinium* spp.

11. *Cyclopsiella elliptica/granosa* complex sensu de Verteuil and Norris 1996

12-13. *Hystrichokolpoma rigaudiae* Deflandre and Cookson 1955

14-15. *Hystrichokolpoma* spp.

16-17. *Impletosphaeridium prolatum* Head *et al*. 1989

18*. *Leiosphaeridia* "*scabrate*"

19**. *Leiosphaeridia* spp.

20-22. *Lingulodinium machaerophorum* (Deflandre and Cookson) Wall 1967

*picture is doubled-sized

**pictures 18 and 19 were taken with phase contrast

Plate 26

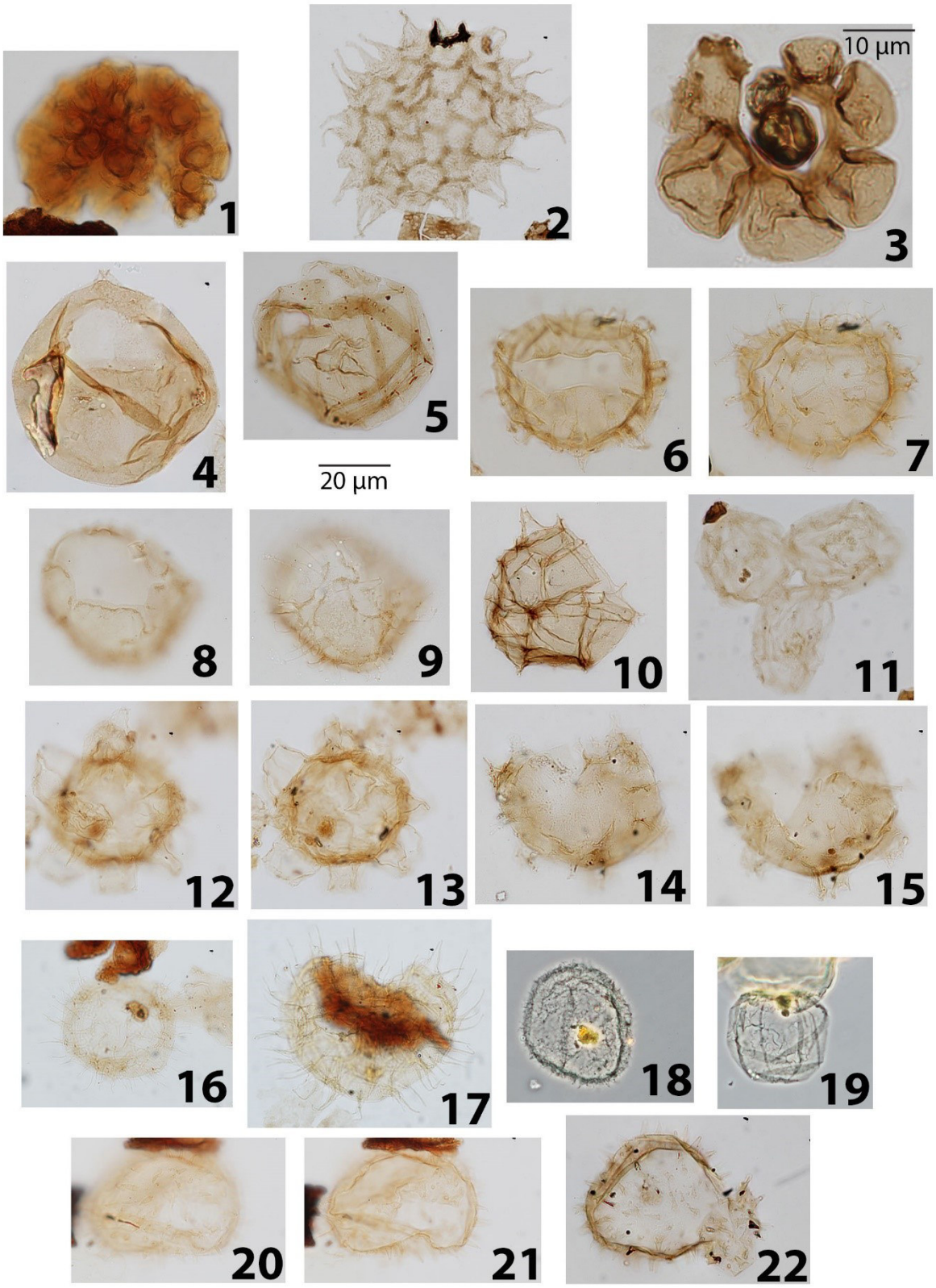

Plate 27

1. *Operculodinium israelianum* (Rossignol) Wall 1967

2-3. *Quadrina*? *condita* de Verteuil and Norris 1996

4. *Quadrina*? "*incerta*" (= Dinocyst XI of Lenoir and Hart, 1986)

5-8. *Spiniferites* "*normalis*"

9-11. *Spiniferites* spp.

12. *Trinovantedinium ferugnomatum* de Verteuil and Norris 1996

13. *Trinovantedinium*? *Xylochoporum* de Verteuil and Norris 1996

14. *Tuberculodinium vancampoae* (Rossignol) Wall 1967

Plate 27

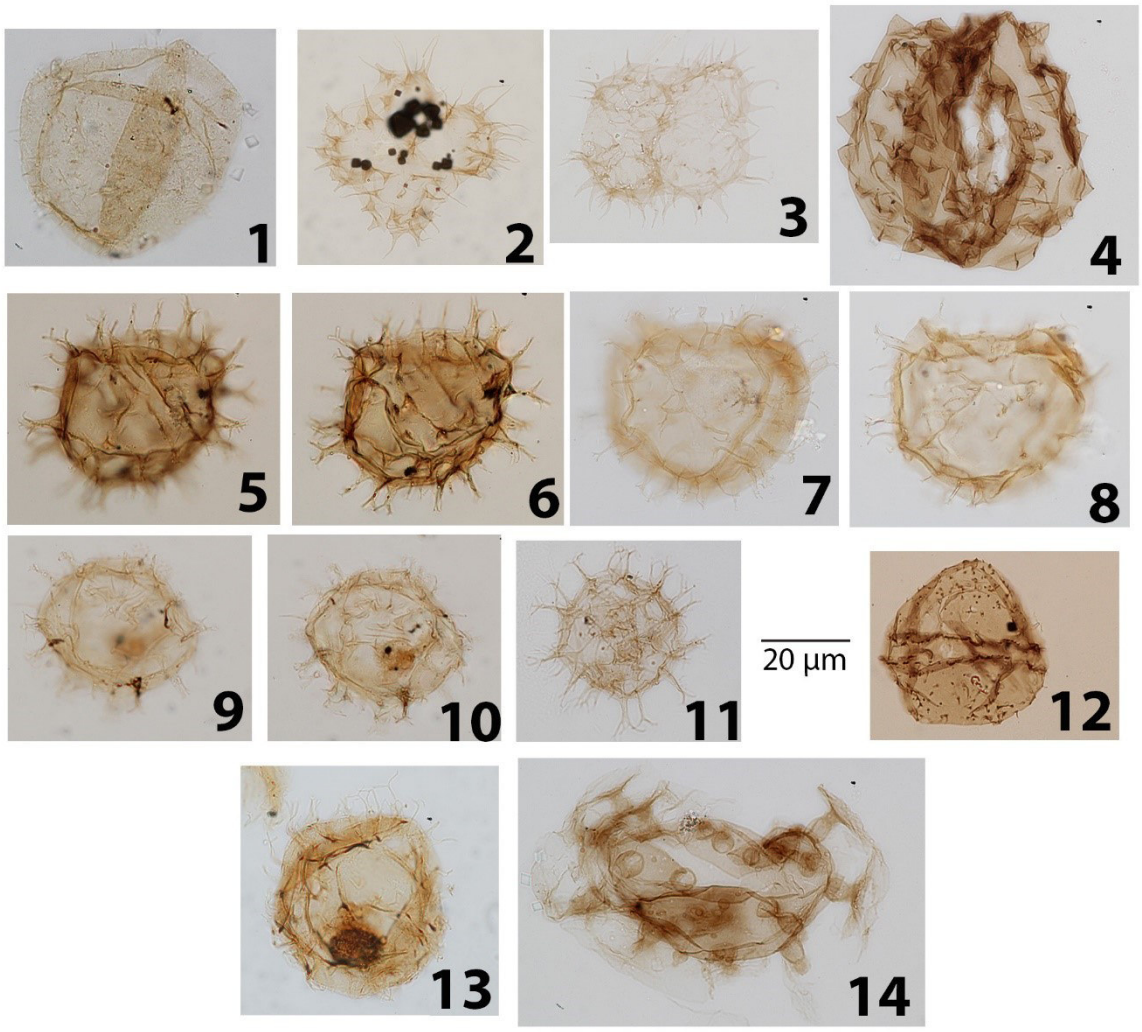

Chapter 5: Biostratigraphy

5.1. Introduction

Dating core 1-AS-105-AM was not only an objective of the current work but also a step without which the subsequent thesis aims could not be reached. In order to build an age model for the core, palynology was used as the main source of information. This was due to pollen data being abundant throughout the complete core and because the most updated biozonation in northwestern South America is based on pollen (Jaramillo *et al*. 2011). Other source of information was dinoflagellates and molluscs, however both of them are heavily controlled by facies and restricted to few samples, so they served only as complementary means of dating. Neverthelss, when these different organism groups agree in their age indications, even if roughly, it gives confidence to the biostratigraphy applied. Pollen data was subject to Graphic Correlation (see methods in Chapter 3), whose results propose an age model against which other sections in the Solimões Formation are compared to.

5.2. Palynostratigraphical framework

The biostratigraphical framework used in western Amazonia has been largely based on work carried out in Venezuela and Colombia. In Venezuela, pollen work was developed by Germeraad *et al.* (1968), Lorente (1986) and Muller *et al.* (1987), their zonations were adapted by Hoorn (1993, 1994a, 1994b) for use in western Amazonia. The sequence of events from Lorente (1986) fitted well the events seen by Hoorn, showing a good correspondence in the overall palynostratigraphical framework in different parts of north-western South America. Nevertheless, some problems arose when regional correlations were made. Inconsistences were pointed by Latrubesse *et al.* (2007, 2010), who also used Lorente's zones to date sections in western Amazonia. Such inconsistencies were related to stratigraphic ranges of marker taxa overlapping zone boundaries. More recently, a zonation

erected by Jaramillo *et al* (2011) and with much better age calibrations showed that some important taxa have older first appearances than what previously postulated, despite also showing good correspondence with the Venezuelan zonations (Germeraad *et al.* 1968, Muller *et al.* 1987). An example is *Grimsdalea magnaclavata*, probably the most used marker taxa in north-western South America. These issues are especially critical when entire sections are placed within one single pollen zone, which is the case with many small outcrops. For instance, zone Grimsdalea (Fig. 5.1) ranges from 16 to 14 Ma, but the taxon *G. magnaclavata*'s range extends from latest early Miocene to the mid-late Pliocene – a significantly longer time interval.

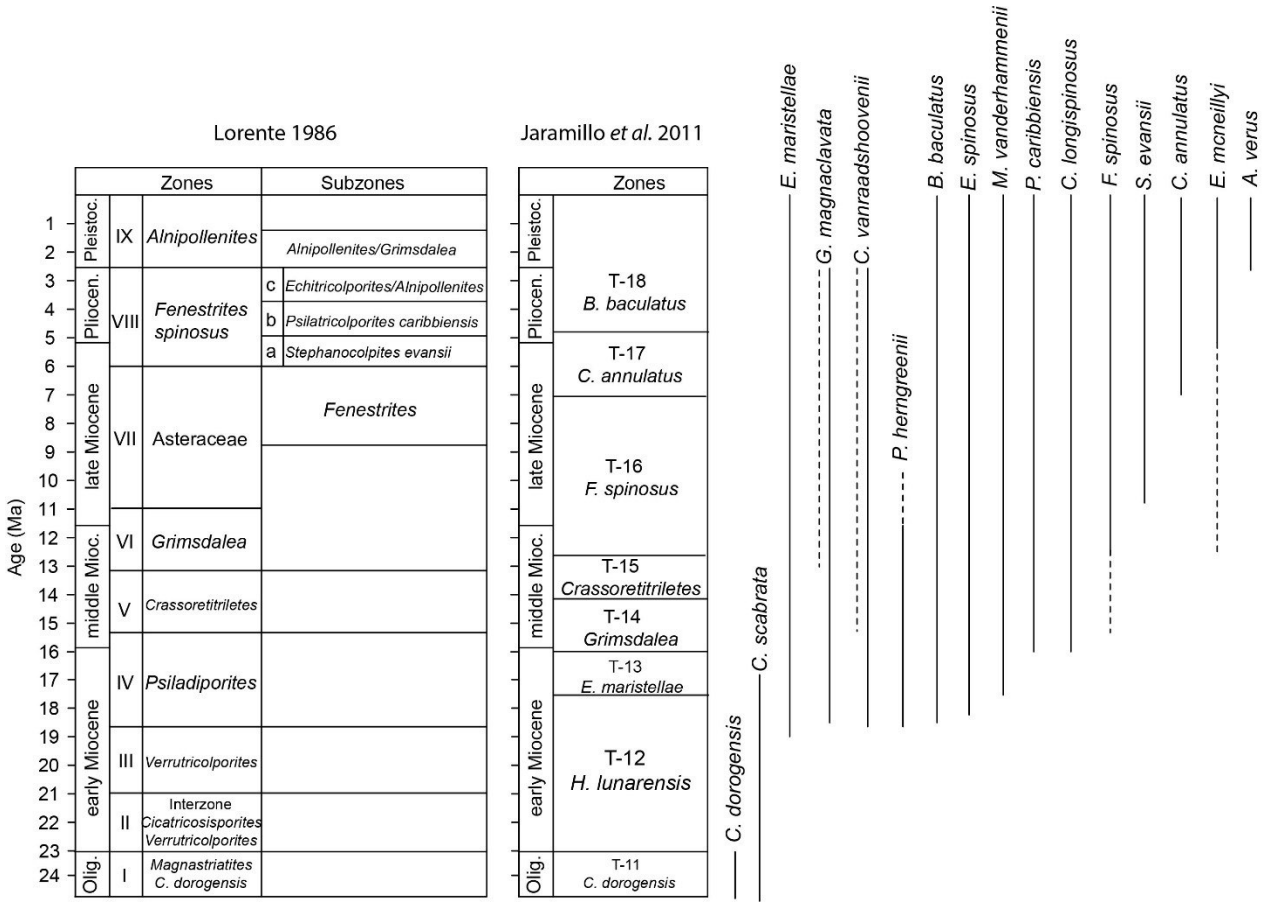

Fig. 5.1. The two principal palynological zonations used in Amazonia, from Venezuela (Lorente 1986) and from the Llanos and Llanos foothills of Colombia (Jaramillo *et al.* 2011). Taxa ranges (on the right) were adapted from Jaramillo *et al.* (2011) with modifications from Jaramillo *et al*. (in prep), some differences are evident. Dashed lines are uncertainties in ranges. *Grimsdalea magnaclavata* and *Crassoretitriletes vanraadshoovenii* have two ranges shown (dashed line: Lorente 1986; solid line: Jaramillo *et al.* 2011). *Echitricolporites maristellae = Malvacipolloides maristelae* (Silva-Caminha *et al*. 2010); *Psilatricolporites caribbiensis = Ladakhipollenites caribbiensis* (Silva-Caminha *et al*. 2010).

As new sites are discovered and analysed, zonations are updated, and the continuous reassessment of ages is necessary. Here, I take advantage of recent developments and inclusion of new sites in the zonation of Jaramillo *et al.* (2011) to date core 105-AM studied herein and correlate it with sites in western Amazonia and from the work of previous authors.

5.3. Graphic Correlation (age model)

Graphic correlation was performed between core 105-AM (this thesis) and the composite section of Jaramillo *et al.* (2011). In its recent update (Jaramillo *et al.* in prep) the composite section included sites in western Amazonia. Of special interest among these sites is Saltarin in the Colombian llanos (Fig. 1.2). Saltarin is a ~700 metres deep cored section ranging from Early Miocene to the Pliocene, it has excellent pollen recovery almost throughout the entire core and marine incursions were detected. Additional events other than first and last appearances of species were also used. These were surfaces of marine incursions, which make excellent correlation points, as well as sequence stratigraphy points (Appendix 9.4). It is important to note that the base of the age model is the Graphic Correlation performed using palynomorphs, and that sequence stratigraphy points were only added to refine the line of correlation, but without major changes. The lower and upper limits of marine incursions were delimited according to the peak abundance of marine elements (i.e. an ACME event). This was done to ensure the peak of the event is isolated from its full stratigraphic cover that can vary among different geographical areas whereas the peak abundance will tend to be more homogeneous over broad areas. The full list of events used for all rounds of correlations can be found in Appendix Tables 9.1.a) to 9.1.d). Codes for producing Line of Correlations (LOC) can be found in the Appendix (9.1.e) and f)). Range-charts with all species counted in the core can be found in Appendix 9.1.g.

Correlation 1-AS-105-AM vs. composite section (Fig. 5.3 Table 5.1):

At the bottom of section 105-AM three FADs of important taxa are in full agreement with the FAD events in the composite section. These taxa are *Ilexpollenites tropicalis*, *Grimsdalea magnaclavata* and *Bombacacidites baculatus*. This established the initial correlation point. Following it, the lower marine incursion and its associated FADs of dinocysts constituted another important step in the line of correlation. Towards the middle and upper parts of the 105-AM section, the key marker taxa *Cichoreacidites longispinosus*, *Retitricolporites crassicostatus* and *Fenestrites spinosus* have their FADs and *Psilastephanoporites herngreenii* and *Echidiporites barbeitoensis* have their LADs. These events constrained the terminal part of the line of correlation. Some useful sequence stratigraphy events were C2-I2, C2-I3H, C1-I1, C1-12, L-12, L-13 and L-15 (their description can be found in the Appendix material), they mostly represent maximum flooding surfaces within parasequences. They were added to the composite section after being also identified in core Saltarin (Fig. 5.3).

After the line of correlation was established, depths in core 105-AM were transformed into composite units. These units have ages associated to them from a calibration of the composite section by means of foraminiferal biostratigraphy, magnetostratigraphy and carbon isotopes (Fig. 5.4; and Jaramillo *et al*. 2011). Therefore, ages for all composite units in core 105-AM could be generated. Samples between each pair of composite units were interpolated linearly. Likewise, samples after the topmost and before the bottommost samples were extrapolated linearly. The final result is an age-depth curve ranging from 18.78 to 10.72 Ma (Fig. 5.4). Sample interval gap has an average time span of 0.08 Ma (min. 0.01 and max. 0.32). These ages are a working model, naturally prone to changes as new calibration points are added to the composite section. Their use is not intended with the same precision as in absolute dating methods, but they provide an age framework so far not tried in western

Amazonia and therefore formulate a baseline on which biostratigraphical hypotheses can be built on for future improvements.

Table 5.1. Key biostratigraphic markers used for graphic correlation (Fig. 5.2). Range charts with the distribution of all species identified can be foun in Appendix 9.1.g.

Event/Taxa	Depth in 105-AM	Depth in S.C.S.	Comments
FAD *G. magnaclavata*	-326.2	-9,777.74	This FAD is widely recognized as a marker of the middle or latest early Miocene*
FAD *I. tropicalis*	-324.9	-9,799.83	Added to the S.C.S. after correlation with Saltarin
FAD *B. baculatus*	-325.3	-9,777.74	This FAD is widely recognized as a marker late early Miocene (ca. 17.35 Ma)
FAD FL EM	-293.3	-9,535.84	Added to the S.C.S. after correlation with Saltarin
LAD FL EM	-284	-8,511.18	Added to the S.C.S. after correlation with Saltarin
FAD *C. longispinosus*	-165.5	-5,492.8	This FAD is at app. 10 Ma in Jaramillo *et al*. (2011), but with uncertainties, now it is clearly older (ca. 16 Ma) after correlation with Saltarin
FAD *R. crassicostatus*	-125.3	-4,647.01	Added to the S.C.S. after correlation with Saltarin
FAD *F. spinosus*	-75.3	-4,039.3	FAD is a zone marker, at app. 10 Ma in Jaramillo *et al*. (2011)
LAD *P. herngreeni*	-359	-9,129.27	This LAD is at ca. 11.8 Ma in Jaramillo *et al*. (2011)
LAD *E. barbeitoensis*	-105.5	-5,194.03	Had not yet been applied in w. Amazonia, in Venezuela it is a mid. Miocene marker
FAD FL MM	-101.2	-5,342.95	Added to the S.C.S. after correlation with Saltarin
LAD FL MM	-96.7	-3,959.46	Added to the S.C.S. after correlation with Saltarin

FAD = First appearance datum; LAD = Last appearance datum; FL = Flooding; EM = early Miocene; MM = middle Miocene. *FAD age is ca. 18 Ma and ca. 16 Ma for consistent FAD.

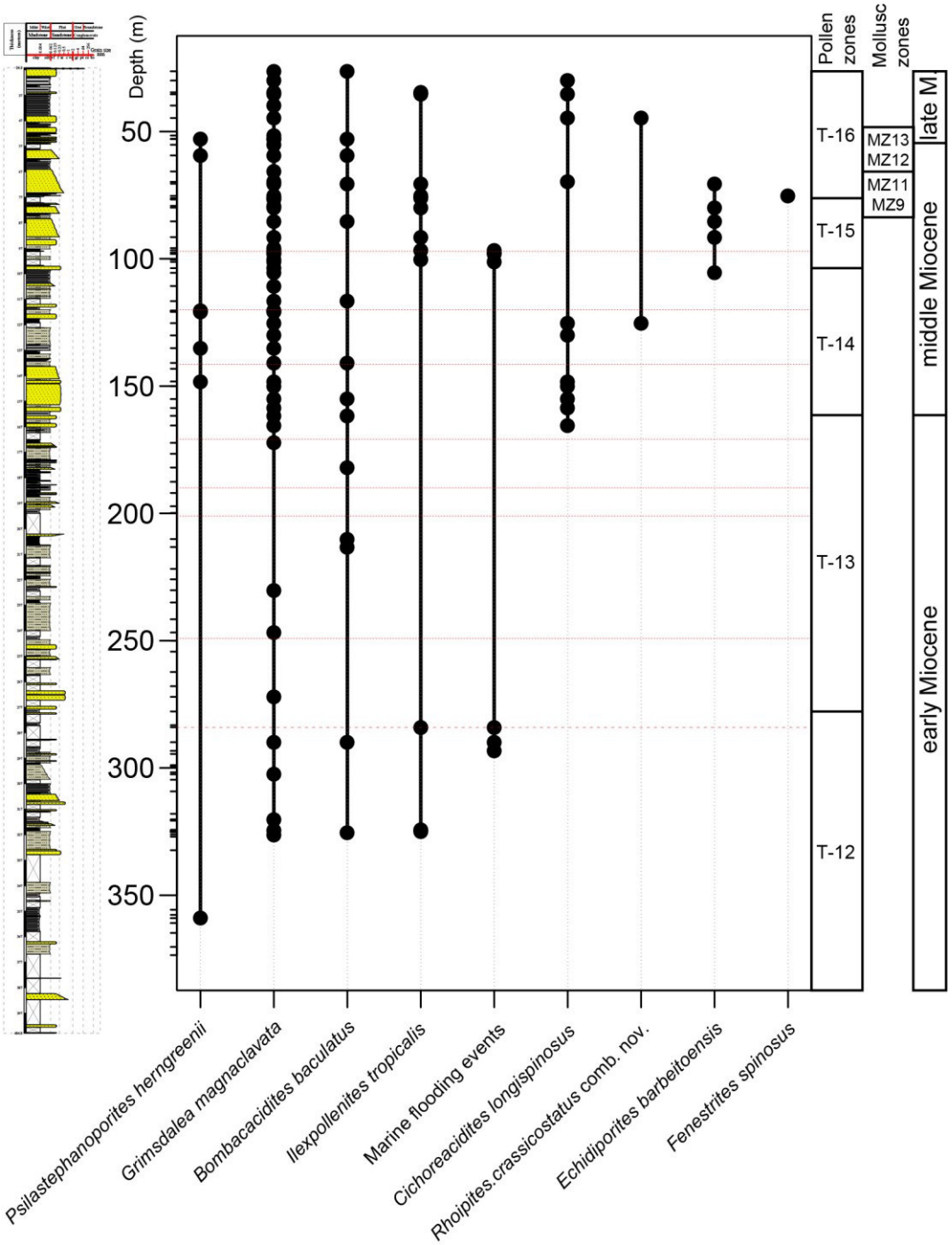

Fig. 5.2. Range chart of selected palynomorphs used for graphic correlation. Pollen zones follow Jaramillo *et al*. (2011), for more details see Fig. 5.1 and Table 5.1. Mollusc zones follow Wesselingh *et al* .2006a, for more details see Fig. 5.6 and Table 5.2 and text below (5.4).

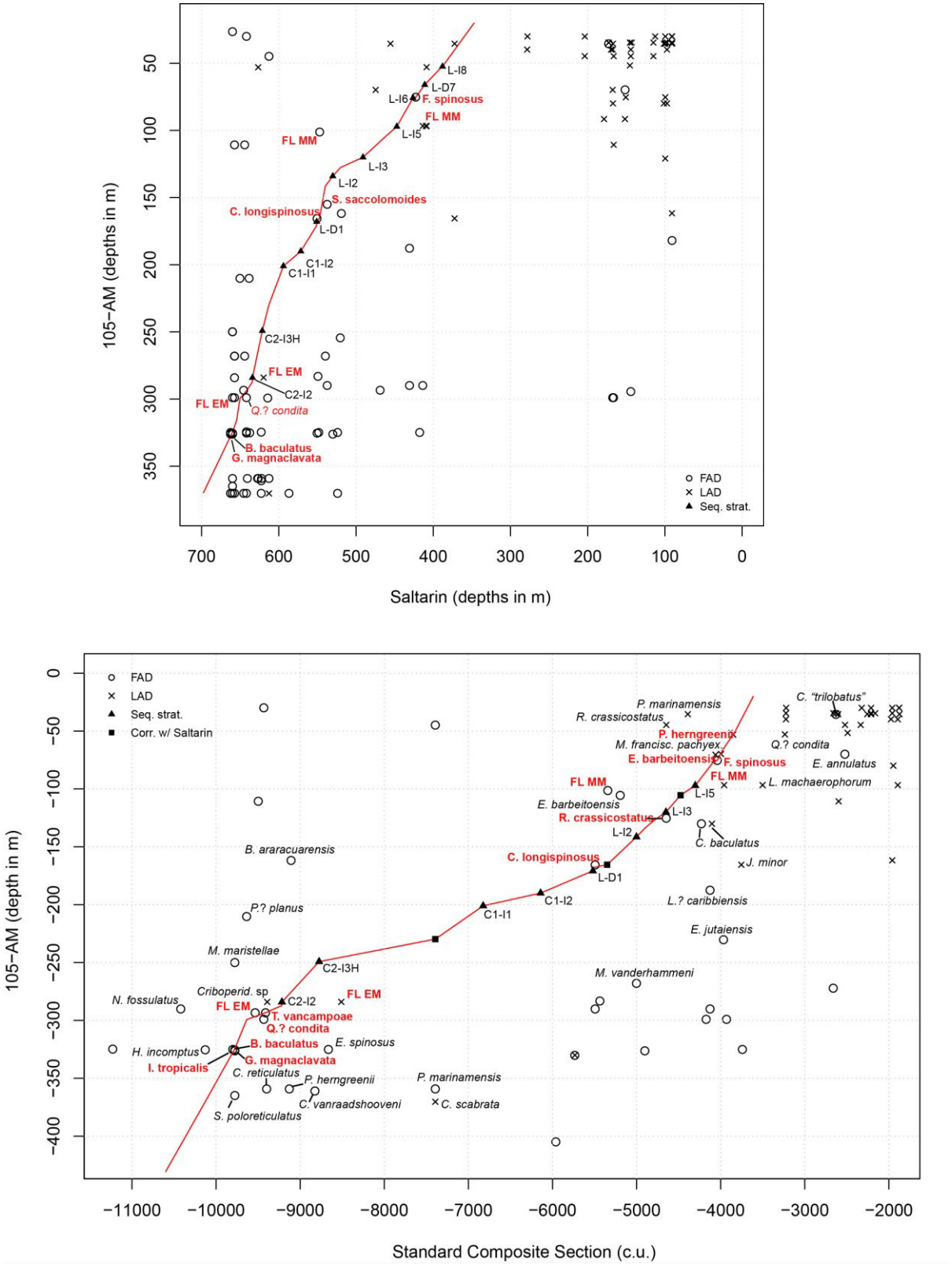

Fig. 5.3. Top: Graphic correlation between cores 105-AM and Saltarin; Bottom: graphic correlation between core 105-AM and the composite section of Jaramillo *et al.* (2011). In this plot, events of the composite section are the final round of correlation not including core 105-AM. The latest sequence of events includes core 105-AM (e.g. taxa range in Figure 5.1).

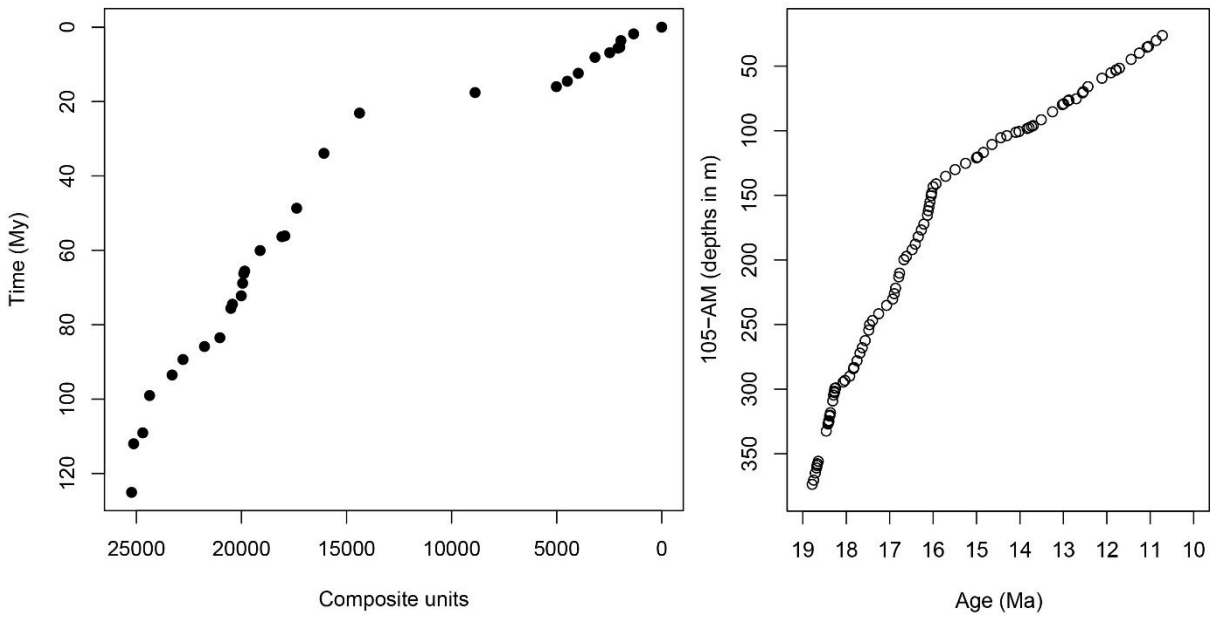

Fig. 5.4. Left: calibration of the pollen zonation of Jaramillo *et al*. (2011). Right: Age vs. Depth model for core 105-AM.

5.4. Molluscs biostratigraphy

Molluscs in core 105-AM were found in four different depths and can be divided into two assemblages: 52.9 to 53 m, and 79.9 to 83 m. Twenty one species in 11 genera were identified (Table 5.2) and photographed (Fig. 5.5). The molluscan biostratigraphic zones follow Wesselingh *et al.* (2006a, 2006b), who erected a molluscan zonation for the Neogene of western Amazonia. The 52.9-53m assemblage could be assigned to either MZ12 zone (the youngest published Pebas fauna so far) but has even more in common with the yet unpublished MZ13 fauna (F. Wesselingh *personal communication*). Age would be latest middle Miocene or earliest late Miocene. The 79.9-83m assemblage seems to contain an admixture of several faunas. *Charadreon intermedius* is known from MZ7-MZ8, but most of the fauna is typical of MZ9-11 (e.g. *Aylacostoma browni*, *Charadreon glabrum*, *Pachydon trigonalis*). Therefore, the assemblage is assigned to zones MZ9-MZ11 (Late Middle Miocene). The age of both assemblages supports the age derived from graphic correlation (Fig 5.6).

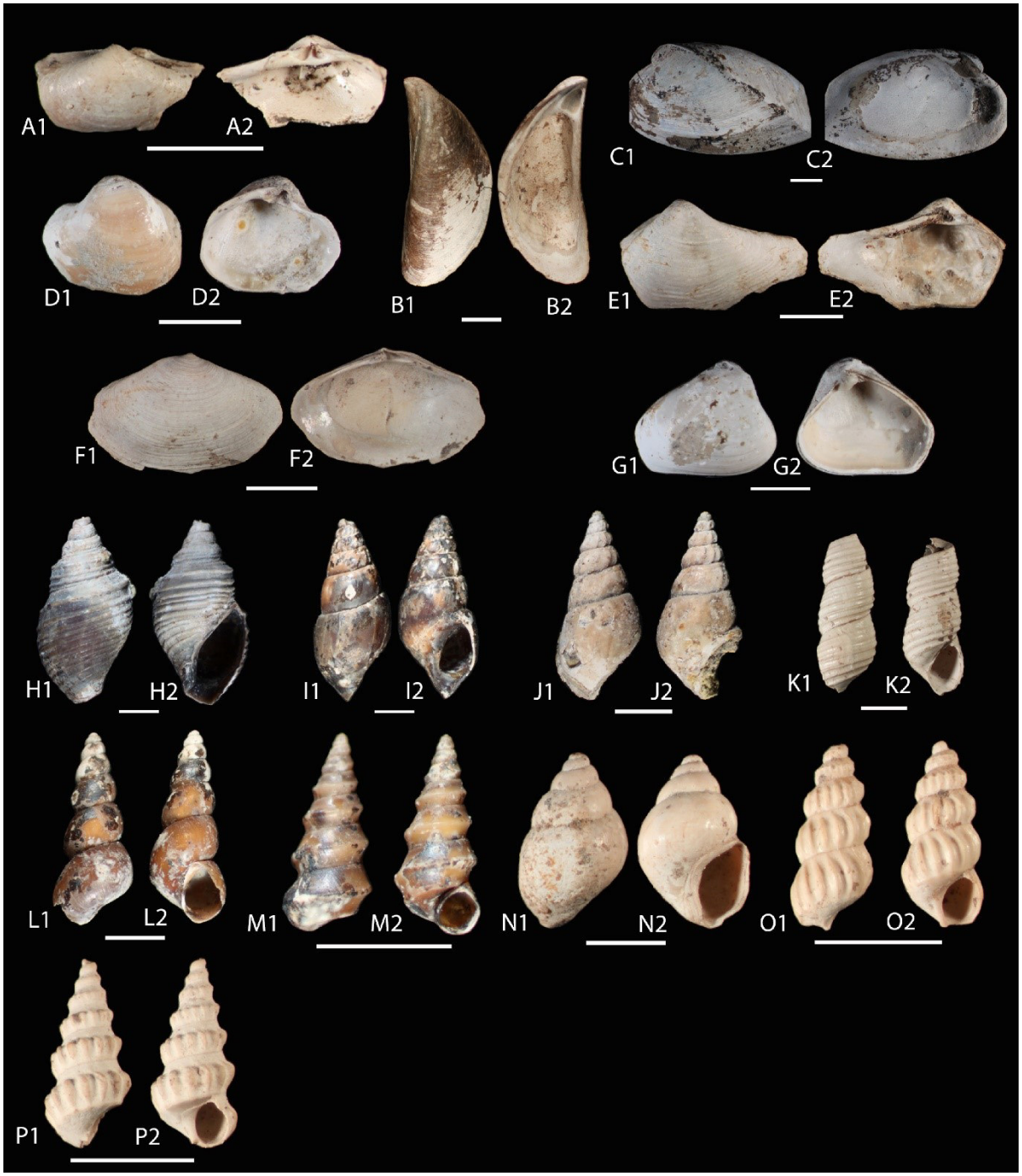

Figure 5.5. Photographs of shells from core 1-AS-105-AM. Scale bar is 2.5 mm. (A) to (G) are bivalves for which exterior and interior views are shown (1's and 2's, respectively). (H) to (P) are gastropods for which rear and front views are shown (1's and 2's, respectively). (A). *Corbula cotuhensis* Wesselingh, 53 m. (B). *Mytilopsis sallei* Récluz, 53m. (C). *Pachydon carinatus* Conrad, 83m. (D). *Pachydon cuneatus* Conrad, 52.9m. (E). *Pachydon ledaeformis* Dall, 53 m. (F). *Pachydon telliniformis* Wesselingh, 53 m. (G). *Pachydon trigonalis* Nuttall, 79.9 m. (H). *Aylacostoma browni* Etheridge, 53 m. (I). *Charadreon glabrum* Wesselingh, 79.9 m. (J). *Charadreon intermedius* Wesselingh, 79.9 m. (K). *Dyris bicarinatus bicarinatus* Wesselingh, 53 m. (L). *Dyris ortoni* Gabb, 79.9 m. (M). *Feliconcha feliconha* Wesselingh, 79.9 m. (N). *Toxosoma grande* Wesselingh, 53 m. (O). *Tryonia nuttalli* Wesselingh, 53 m. (P). *Tryonia scalarioides scalarioides* Etheridge, 53 m. Identifications by F. Wesselingh.

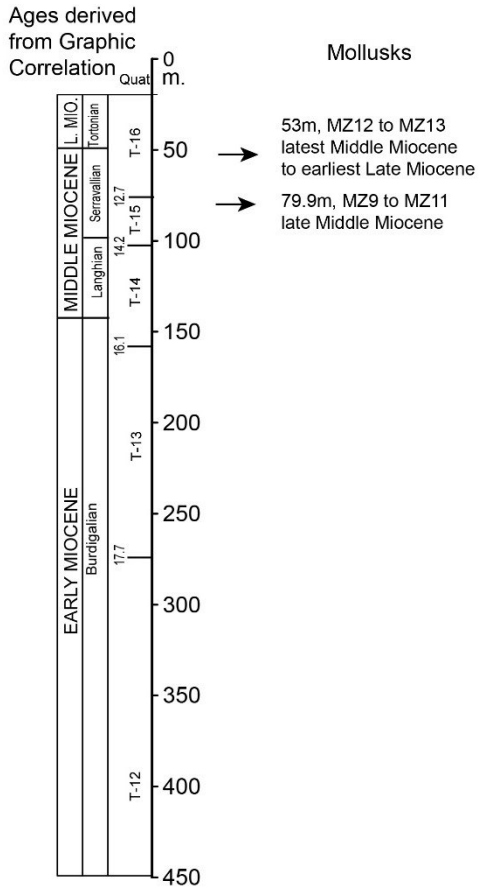

Figure 5.6. Molluscan biostratigraphy of core 105-AM. Molluscs at meter 53 indicate zone MZ12 to MZ13 (latest middle Miocene to earliest late Miocene). Assemblage at meter 79.9m indicates zone MZ9 to MZ11 (molluscan Zones after Wesselingh *et al.* 2006a). Molluscan biostratigraphy supports the ages derived from Graphic Correlation.

Table 5.2. Molluscs in core 1-AS-105-AM.

	Assemblage 1		**Assemblage 2**	
Taxa / Depth (in metres)	**52.9**	**53**	**79.9**	**83**
?*Cochliopina bourguyi*		1		
Aylacostoma browni		1	1	
Charadreon glabrum			1	
Charadreon intermedius			1	
Corbula cotuhensis		1		
Dyris bicarinatus bicarinatus		1		
Dyris ortoni			1	
Dyris sp.		1		
Feliconcha feliconha			1	
Mytilopsis sallei		1		
Pachydon carinatus				1
Pachydon cuneatus	1			
Pachydon ledaeformis		1		
Pachydon telliniformis		1		
Pachydon trigonalis			1	
Sheppardiconcha cf coronata	1	1		
Toxosoma aff. *contortum*		1		
Toxosoma grande		1		
Tryonia cf. *scalarioides scalarioides*			1	
Tryonia nuttalli		1		
Tryonia scalarioides scalarioides		1		

5.5. Dinoflagellate biostratigraphy

Biostratigraphical analysis with dinoflagellate cysts and acritarchs is heavily influenced by facies and therefore can only be used as an accessory source of relative ages. The presence of some key taxa, however, indicates deposition during the early and middle Miocene, in accordance with pollen and mollusc ages. All identified dinoflagellates are listed and illustrated in Chapter 4. Comparisons are made with records of worldwide marine sequences where dinocysts are present.

The lowest marine interval (284 to 293.3 m) holds the marker dinoflagellate cysts species *Apteodinium*? *vescum* (late Burdigalian to early Serravallian or N8-N11 in Matsuoka 1983), *Cleistosphaeridium ancyreum* (early Eocene to mid Miocene in Eaton *et al.* 2001), *Cleistosphaeridium placacanthum* (mid Eocene in Eaton *et al.* 2001 to early Tortonian, 10.6 Ma, in Schreck *et al.* 2012), *Quadrina* "*incerta*" (=Dinocyst XI of Lenoir and Hart 1986, late Burdigalian) and the acritarch *Quadrina*? *condita* (late Burdigalian in Soliman *et al.* 2012 to late Tortonian in de Verteuil 1996). These stratigraphic ranges infer deposition sometime between the late Burdigalian and the early Serravallian, i.e. late early Miocene to late middle Miocene. A late early Miocene is in agreement with pollen ages for the lower marine interval.

The deposition of the upper marine interval (101.2 to 96.7 m) took place sometime between the late Burdigalian and the early late Miocence (i.e. Tortonian) based on the stratigraphic ranges of *Quadrina*? *condita*, the rare dinocyst *Trinovantedinium*? *xylochoporum* (late Oligocene to Tortonian in de Verteuil 1996) and the acritarch *Cyclopsiella elliptica* (late Oligocene to early late Miocene in Matsuoka and Head 1992). These presences only give a rough estimate of age, but the absence of *C. ancyreum* and *C. placanthum* as well as other gonyaulacacean dinoflagellate cysts in the upper marine sequence indicate it may be close to the top ranges of these taxa. In such case, the interval would be late Middle Miocene or younger, which is overall in agreement with the ages derived from graphic correlation. Late

Miocene and Pliocene dinocyst species are absent in the upper marine interval (S. Louwye *personal communication*).

5.6. Regional correlations (and the age of the Solimões Formation)

Other localities in the Solimões Formation and surroundings (Fig. 5.7) where biostratigraphical data are available are herein used for correlation. This correlation aims to assess the total age range of the Formation and its geographical variations. The proposition of large scale paleogeographical models including specific events like fluvial migrations, marine incursions, etc, relies on a consistent biostratigraphical framework. Hence, a reappraisal of dated sequences basinwide is here offered based on the new studied section and its correlations with other sites.

Four cores in the same region as 105-AM were studied by Hoorn (1993), Latrubesse *et al.* (2007, 2010) and Silva-Caminha *et al.* (2010). Three of them reached similar depths to 105-AM (ca. 400 m) and had abundant pollen recovery. One section (32-AM, Latrubesse *et al.* 2010) only had its 133 top metres studied. Many other sections cropping out along rivers and road cuts were studied by Hoorn (1994a, 1994b, 2006), Latrubesse *et al.* (2010), Gross *et al.* (2011) and Nogueira *et al.* (2013), they are much shorter than the cores and have data on pollen and paleovertebrates. I attempted graphic correlation between cores 4a-AM and 27-AM (where longer stratigraphical ranges of taxa are possible), and more general correlations with the other localities using presence of key markers. Graphic correlation with core 32-AM was not performed due to its short range and therefore being completely dominated by edge effect.

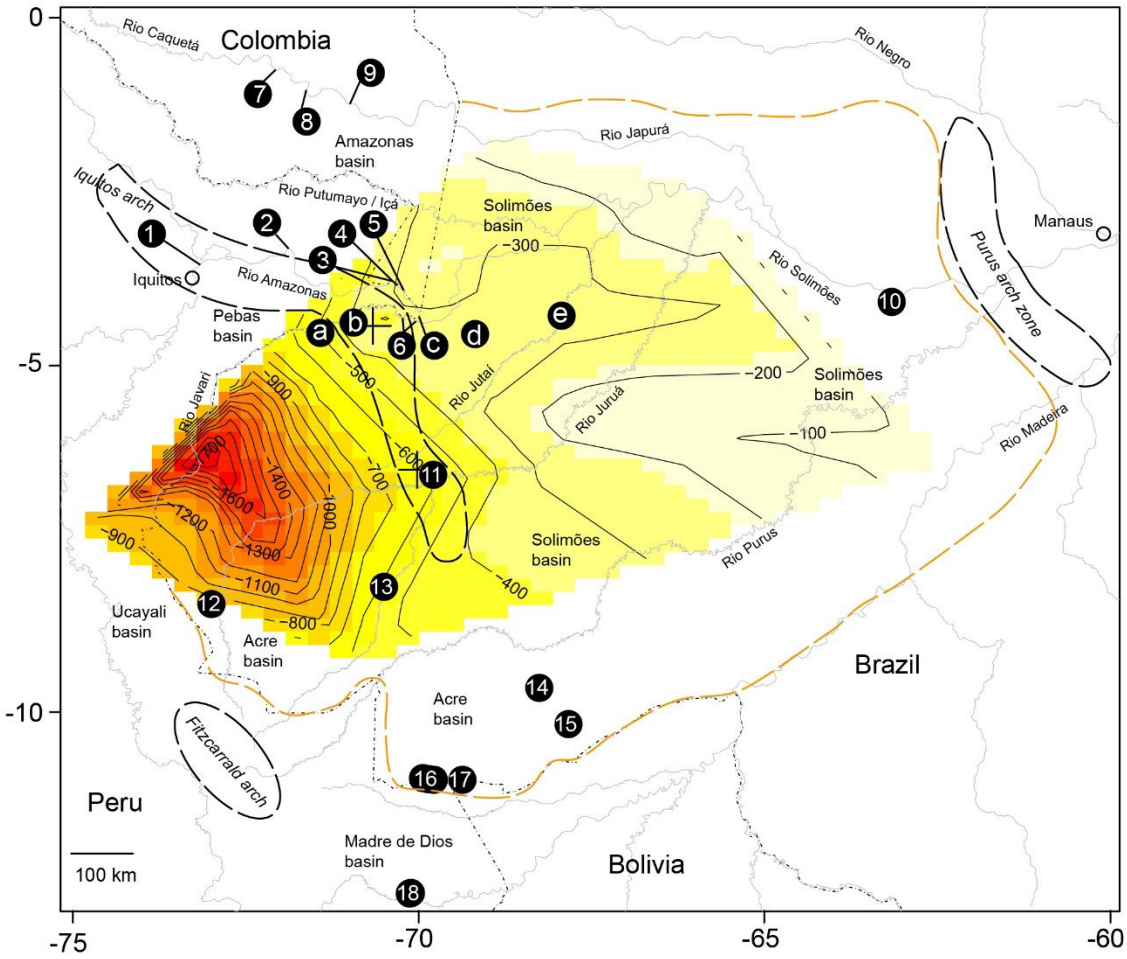

Fig. 5.7. Map showing the Solimões Formation sites discussed in the text and structural features in the area. Letters (a to e) are cores: a) 1-AS-32-AM, b) 1-AS-4a-AM (Hoorn 1993), **c) 1-AS-105-AM (this work)**, d) and e) 1-AS-19-AM and 1-AS-27-AM, respectively (Silva-Caminha *et al.* 2010); numbers 1) to 9) are outcrops studied by Hoorn 1994a, 1994b: 1) Iquitos/Santa Teresa, 2) Pebas, 3) Los Chorros, 4) Mocagua, 5) Santa Sofia, 6) Benjamin Constant, 7) Mariñame, 8) Santa Isabel, 9) Tres Islas, 10) Coari (Nogueira *et al.* 2013), 11) Eirunepé (Gross *et al.* 2011) and 12) to 18) outcrops studied by Latrubesse *et al.* (2010). Isopach lines were plotted using formation thickness measured in 107 boreholes, which includes sites a) to d), from the Brazilian Geological Survey (CPRM) and Petrobrás. Data was linearly interpolated using R package Akima. Positions of arches after Hoorn (1993), Roddaz *et al.* (2005) and Mora *et al.* (2010). Dashed orange outline is approximate limit of the Solimões Fm in Brazil. Crosses (+) are sites were the location of the Iquitos arch was determined by Miura (1972).

Correlation 1-AS-105-AM vs. 1-AS-4a-AM (Hoorn 1993):

Core 4a-AM was originally dated as early to middle-late Miocene by Hoorn (1993) based on presences of key markers *Crassoretitriletes vanraadshoovenii* and *Grimsdalea magnaclavata*. *C. vanraadshoovenii* appears at 181 m and *G. magnaclavata* at 89 m, both are frequent and abundant after their FADs. In core 105-AM *C. vanraadshoovenii* and *G. magnaclavata* appear at 361 and 326, respectively. Towards the top of section 4a-AM, *Retitricolpites lorenteae* (=*Bombacacidites lorentae* nov. comb.) and *Multimarginites vanderhammenii* have the same FAD at 59 m, these species also have very similar FADs in section 105-AM, at 272.1 and 267.9, respectively. Because of these similarities in their sequence of appearances, all four species were chosen to compose the line of correlation. The result of this correlation (Fig. 5.8) shows that core 4a-AM is correlative with the bottom part of core 105-AM and correlates with the early Miocene. This result is similar to the original biostratigraphy of Hoorn (1993) but differs in that middle Miocene is not clearly evident in section 4a-AM. Middle Miocene had been established based on the *Grimsdalea* pollen zone (Lorente 1986) starting at 89 m. However, the FAD of this taxon is late early Miocene (Jaramillo *et al.* 2011, in prep) and given that only ca. 66 m of this range are present in 4a-AM it is possible no middle Miocene or very little of it is present. Other common middle Miocene taxa like *Ladakhipollenites*? *caribbiensis* and *Cichoreacidites longispinosus* which are frequent in 105-AM are completely lacking in 4a-AM. This further supports that core 4a-AM is older than 105-AM and may not extend into the middle Miocene.

The early Miocene marine flooding could be present in 4a-AM, but this is not certain as only rare indeterminate dinoflagellates were reported, therefore the flooding surface was not used in the correlation. In spite of that, the top of the supposed marine flooding is very close to the line of correlation (Fig. 5.8) showing a likely congruence of this event in both sections.

Correlation 1-AS-105-AM vs. 1-AS-27-AM (Silva-Caminha et al. *2010):*

Silva-Caminha *et al.* (2010) studied two cores (1-AS-27-Am and 1-AS-19-AM) that were inter-correlated and appear to represent equal age ranges of late Miocene to early Pliocene. Correlation here is attempted with core 27-AM only. Core 19-AM was not used because it had just eight samples analysed as opposed to 33 of core 27-AM. A large edge effect is predominant in core 27-AM, this is clear when one looks at the many FADs lined up at the bottom of the section (Fig. 5.8). This hampered a reliable choice of where to place the line of correlation. Nevertheless, *C. longispinosus* and *Bombacacidites araracuarensis* were chosen as they have the same FAD in core 27-AM (354.5 m) and nearly the same in 105-AM (165.5 and 161.7 m, respectively) and they are frequent after their FAD. Furthermore, because these taxa have their FADs at ca. 160 m in 105-AM and they are basically present in the entire 27-AM section (from 354 m onwards), this means approximately 200 metres of displacement between the events from one section to the other, and hence 27-AM is younger than 105-AM. The top end of the line of correlation was tentatively set at the FAD of *Retitrescolpites*? *traversei*. This species is a singleton at 44.7 m in core 105-AM and has a FAD at 216 m in core 27-AM followed by two more presences until 137 m. The final correlation shows that 105-AM is older than 27-AM, and that a large proportion of the latter (ca. top 200 m) does not have a tie point. Assuming age assignments by Silva-Caminha *et al.* (2010), this top part of core 27-AM is late-Miocene to early Pliocene. However, no Pliocene marker was found to constraint this interpretation, in fact no late Miocene markers were found either, like *Cyatheacidites annulatus* that has a common presence in surface late Miocene regional outcrops (see section below). Hence, the topmost age of core 27-AM should be around the mid-late Miocene.

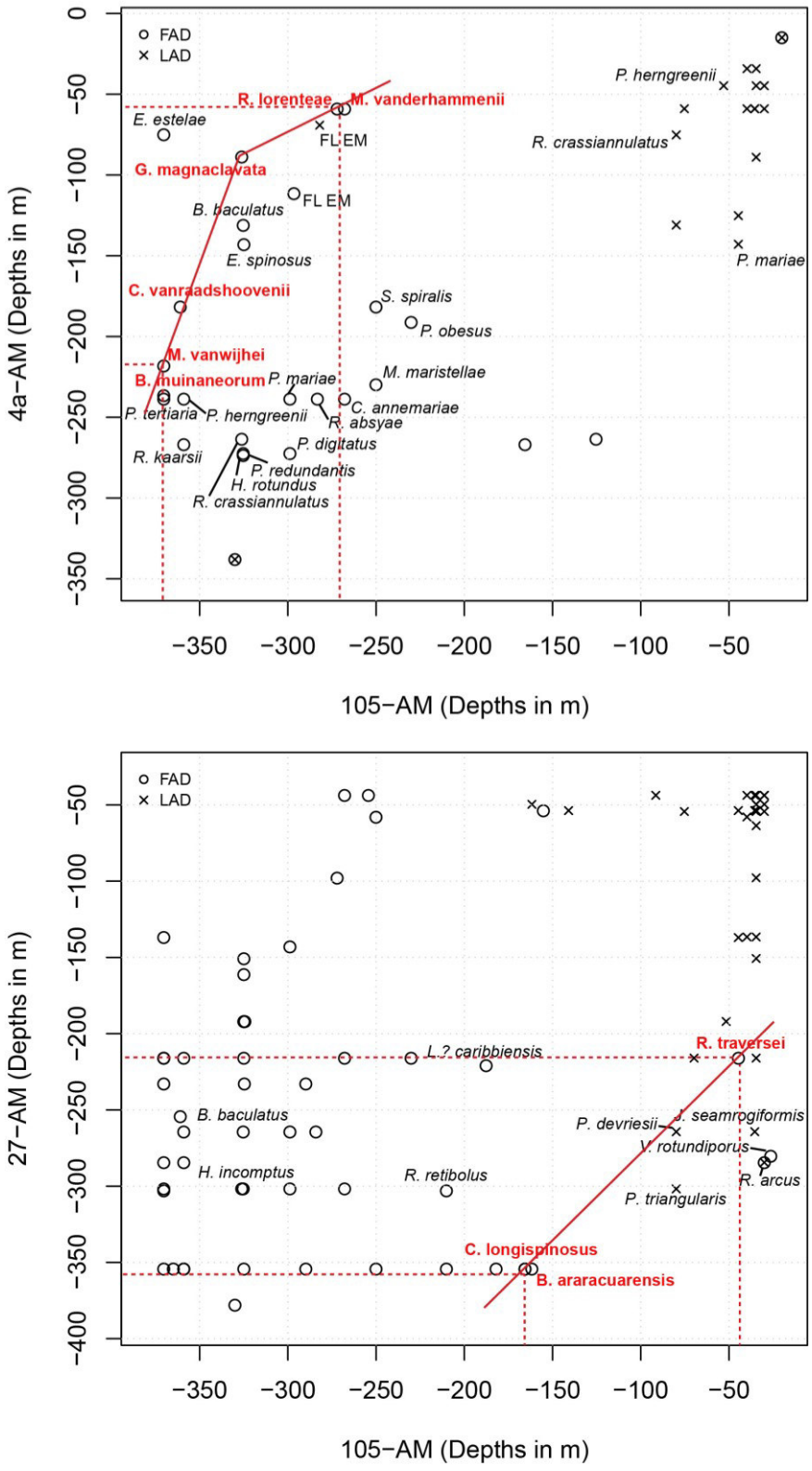

Fig. 5.8. Graphic correlation between cores 105-AM vs. 4a-AM (top), and 105-AM vs. 27-AM (bottom).

Other localities:

Core 32-AM (Latrubesse *et al.* 2010) was placed in the late Miocene-Pliocene Fenestrites zone (Lorente *et al.* 1986) based on the presence of *L.*? *caribbiensis*. However, as shown in the present study, this taxon first appears during the middle Miocene in western Amazonia. That and the lack of other late Miocene-Pliocene markers in core 32-AM makes it more plausible to correlate it with a middle-late Miocene age. It is uncertain how much this site extends into the late Miocene. The short depth (133 m) and the fact that the range of *L.*? *caribbiensis* can be of 187 and 221 metres in cores 105-AM and 27-AM, respectively, show it is possible that the entire core 32-AM is restricted to the middle Miocene. These uncertainties are probably due to the low number of samples (n=13, ~1 sample/10 metres) analysed in this core, thus more data is needed to better constrain its age.

Hoorn (1994a, 1994b) studied several outcrops in the Pebas and Amazonas basins as well as sections in Benjamin Constant/Atalaia do Norte area located between cores 4a-AM and 105-AM in the Solimões basin (Fig. 5.7). In Peru, the sections of Iquitos and Pebas yielded pollen assemblages containing *C. vanraadshoovenii* and lacking all other marker species including *G. magnaclavata*. This led Hoorn (1994a) to place the sections in the middle Miocene Crassoretitriletes pollen zone (Lorente 1986). However, as established by the correlation between 105-AM and the composite section, *C. vanraadshoovenii* like *G. magnaclavata* first appears in the late early Miocene. Thus, it can be deduced that the sections in Iquitos and Pebas area are early Miocene and do not extend into the middle Miocene. The absence of *G. magnaclavata* is quite indicative, because once this species appears it is usually very frequent and abundant. Also in this region is a 12 m long section (Santa Teresa) that does not even contain *C. vanraadshoovenii* and therefore can be attributed to the lower pollen zone Psiladiporites/Crototricolpites of early Miocene age (Lorente 1986). Hence, all sections of the Pebas basin in Peru are of early Miocene. In a more northerly

Amazonas basin of Colombia, three localities were also studied by Hoorn (1994b). Mariñame, Santa Isabel and Tres Islas are outcrops of similar age to the Iquitos/Pebas sections as they do not contain any of the late early and middle Miocene marker taxa and thus they can be also attributed to the lower pollen zone Psiladiporites/Crototricolpites of early Miocene age (Lorente 1986).

The sections of Los Chorros, Mocagua, Santa Sofia (in Colombia) and Benjamin Constant and Atalaia do Norte (in Brazil) (Fig. 5.7) are younger as they contain *G. magnaclavata* apart from *C. vanraadshoovenii*. Hoorn (1994a, 1993) placed these sections in the middle Miocene Grimsdalea zone (Lorente 1986). As shown before, *G. magnaclavata* first appears in the late early Miocene, so it is possible these sections start at this age and extend into the middle Miocene as well. They cannot reach, however, a mid-middle Miocene age since markers common in the nearby cores 105-AM, 27-AM and 19-AM like *C. longispinosus* and *L.*? *caribbiensis* are completely absent.

Other sections in the Solimões Formation are outcrops in Eirunepé, Coari and various sites in the Acre/Madre de Dios basins (Fig. 5.7). In Eirunepé, Gross *et al.* (2011) reported the presence of *G. magnaclavata*, *Echitricolporites spinosus* and *Cyatheacidites annulatus* in two sections. While the first two taxa range from late early Miocene to Pliocene-Modern, C. *annulatus* has a FAD at 7 Ma (Jaramillo *et al.* 2011), henceforth constraining the age of Eirunepé sections to not older than a late late Miocene stage. In Coari (Nogueira *et al.* 2013), six sections yielded a similar pollen assemblage to Eirunepé's, with *C. annulatus* suggesting a late late Miocene age as well, and *Ladakhipollenites*? *caribbiensis* and *Stephanocolpites evansii* suggesting late Miocene (Lorente 1986, Jaramillo *et al.* 2011). These sections in Coari are unconformably overlain by the Içá Formation of Pleistocene age. There is no age for the unconformity, but the continuity of the late late Miocene (7 Ma or younger) towards the Pleistocene suggests that the Pliocene is possibly also present in the region. Many authors

have suggested that the upper Solimões Formation extends to the Pliocene (Latrubesse *et al.* 2010, Silva-Caminha *et al.* 2010, Nogueira *et al.* 2013) based on pollen and mammalian biozones. This needs further study since no definitive Pliocene marker fossils have been established in the region.

In the Acre basin several outcrops (Fig. 5.7) were studied by Latrubesse *et al.* (2010) and Cozzuol (2006). Extensive vertebrate palaeontology and additional palynology analysis place the outcrops in the Huayquerian–Mesopotamian mammalian biozones, which ranges from 9 to 6.5 Ma, hence of late Miocene age.

Other outcrops in the Solimões basin region as well as cores from the 'Solimões Coal project' (CPRM) were studied by Cruz (1984). Unfortunately the pollen data and spatial distribution of sites is not available in the publication. Nevertheless, some interesting insights can be drawn from this work. The report of an association (zone A, Cruz 1984) containing *Cicatricosisporites dorogensis* and completely lacking other late early and middle Miocene markers indicates the existence of Oligocene or earliest early Miocene sediments, most likely among the bottom parts of cores. *C. dorogensis* is known to go extinct at the Oligocene-Miocene boundary (Regali *et al*. 1974, Lorente 1986, Jaramillo *et al.* 2011). Associations B-C established by Cruz (1984) contain *C. vandraashoovenii*, *E. spinosus*, *G. magnaclavata, F. spinosus*, *Retistephanocolpites gracilis* and *C. annulatus* pointing to milddle to late Miocene ages (Germeraad *et al* 1968, Regali *et al*. 1974). Although lacking detailed description of data and samples, Cruz (1984) found late late Miocene to Pliocene beds of sediments are correlatable with those in Eirunepé and Coari based on the presence of *C. annulatus*.

In sum, the Solimões Formation exhibits sediments from early Miocene (ca. 20 Ma) to late Miocene (6.5 Ma). Early Pliocene seems to be present at the eastern parts of the basin (at Coari), a broader extension of Pliocene is possible but needs further testing. Late Oligocene is probable, but further confirmation is needed.

Regarding the possibility of a Pliocene age for the topmost Solimões Formation, a few considerations must be made. First, as exposed above the few metres of sections basinwide in the *C. annulatus* Late Miocene zone (≤ 7 Ma) could naturally extend into the Pliocene. The C. annulatus zone extends into the Pliocene and the taxon is present in the Quaternary as well. Second, in other parts of western Amazonia there are good clues on when the Solimões Formation ceased to accumulate sediments. That is the case of the Acre/Madre de Dios basins. In that region, an important feature controlling watersheds is the Fitzcarrald arch in Peru (Fig. 5.7). It splits apart the Ucayali and the Madre de Dios basins, thus creating the southern limit for the Amazon drainage (Mora *et al* 2010, Latrubesse *et al.* 2010). The Fitzcarrald arch uplifted as a result of a flat slab subduction of the Nazca Ridge, which is dated as Pliocene, to approximately 4 Ma (Espurt *et al.* 2007, 2010). This event lead to the termination of deposition and the initiation of an erosional phase in SW Amazonia. Therefore, if this assumption is correct, the upper Solimões Formation in the region can reach an early Pliocene age. Moreover, assuming a lag between the Fitzcarrald emergence and a full fluvial migration towards eastern Solimões Basin, the upper Solimões Formation in central Amazonia (Coari) could very reasonably be of mid to late Pliocene. This interpretation can reconcile uncertainties regarding the upper Solimões Formation and demonstrate a synchronous depositional phase over an immense geographical area (Fitzcarrald and Coari are ca. 1,200 km apart) as proposed by Latrubesse *et al.* (2010) and Nogueira *et al.* (2013).

A clear pattern among the cores was found – older ages westward and younger ages eastward (Fig. 5.9). This pattern is similar to the overall spatial configuration of the Solimões Formation deposits, which thin out from SW to NE (Fig. 5.7, Maia *et al.* 1977, Latrubesse *et al.* 2010). However, further explanations are necessary to contend this age differences among cores so closely spaced. One idea is that the Iquitos Arch was active and affected

sedimentation in this area during the Miocene (, Latrubesse *et al.* 2007, 2010, Silva-Caminha *et al.* 2010). The Iquitos Arch is the product of a flexural forebulge uplift (Roddaz *et al.* 2005) related to Andean tectonics. Tectono-sedimentary evidences suggests a late Miocene timing for the forebulge growth (Roddaz *et al.* 2005), which coincides with accelerated rates of mountain build in the Andes (Hoorn *et al.* 2010) that in turn is the primary driver of forebulge dynamics. The position of the Iquitos arch was determined by gravimetric anomalies showing strong positive Bouguer values around the Iquitos town in Peru (Roddaz *et al.* 2005) and close to core 4a-AM and the town of Eirunepé in Brazil (Miura 1972) (Fig. 5.7). It is not clear how much of this feature extends in other directions regionally. Assuming the proposed Late Miocene as a time of arch activity, its role could have been to promote exhumation of older sediments rather than influencing their deposition. This would explain the outcrops in the Pebas and Solimões basins studied by Hoorn (1994a, 1994b, Fig. 5.7, Fig. 5.8) which have early to early middle Miocene ages contrasting with other late late Miocene outcrops in other areas (e.g. Coari, Eirunepé). Interestingly, other structures in NW Amazonia are hypothesised to have emerged during the late Miocene-Pliocene like the Vaupés Swell in Colombia (Mora *et al.* 2010) (Fig.1.2). Indeed, some authors (Wesselingh and Salo 2006, Wesselingh 2008) pointed to the difficulties in delineating such subsurface structures and prefer to unite all evidences of uplifts in the Amazonas basin (Colombia) and call it the Iquitos-Araracuara anteclise, a post-Pebasian (late Miocene) broad dome. With this assumption, tectonic activity in the NW Solimões/Pebas/Amazonas basins (Fig. 5.7) during the late Miocene would be the responsible for the discrepancies in outcrop ages seen between this region and elsewhere in the basin.

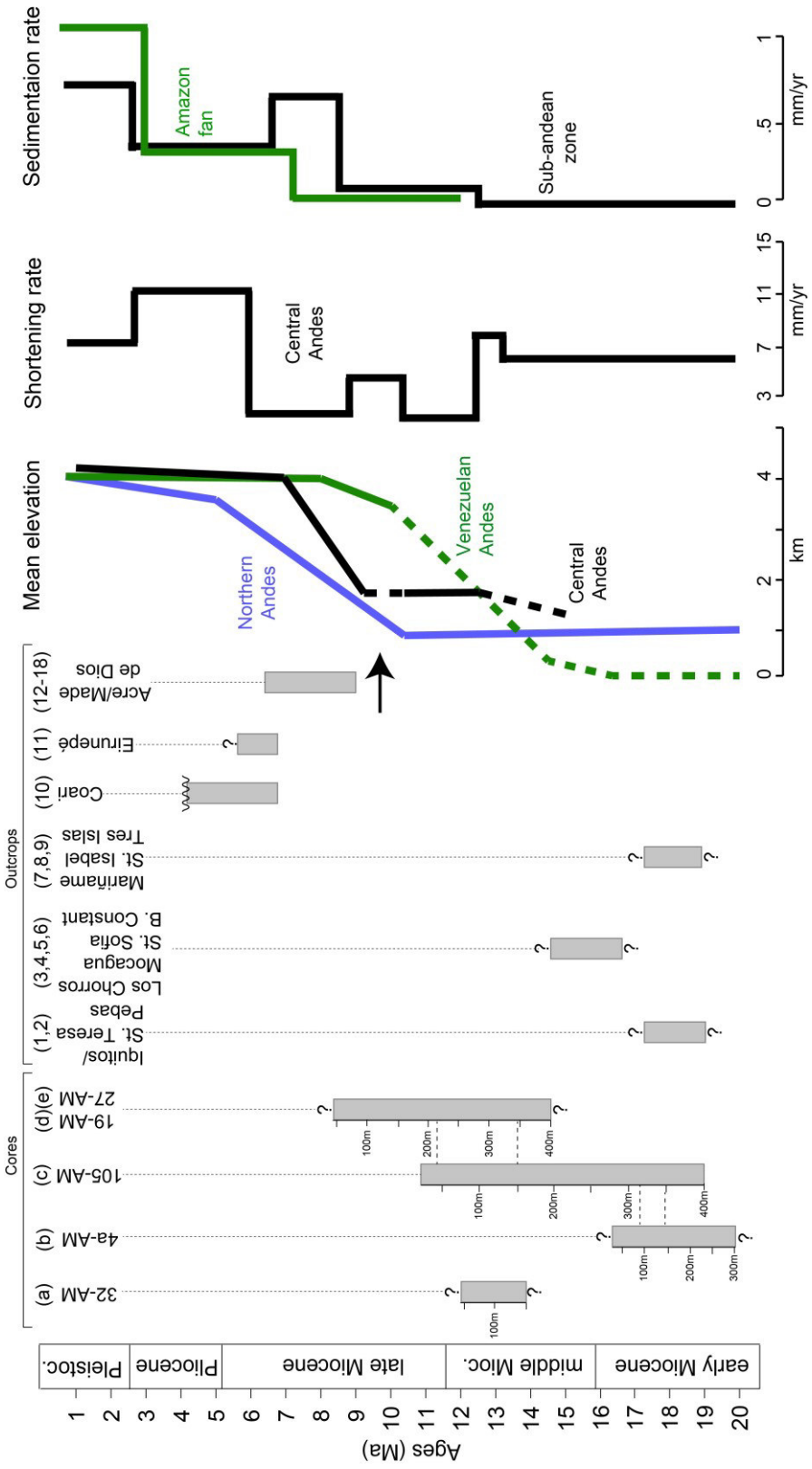

Fig. 5.9. Correlation among sites in the Solimões/Amazonas/Pebas/Acre/Madre de Dios basins (for locations see Fig. 5.6). Schemtaic representation of Mean elevation, shortening and sedimentation in different parts of the Andes are shown (adapted from Hoorn *et al*. 2010), arrow points to late Miocene periods when uplift was pronounced and affected the landscape in western Amazonia by promoting deformation (e.g. Iquitos arch, see text for details).

Chapter 6: Palaeoenvironments in western Amazonia during the late Early to early Late Miocene: evidence from palynology of core 1-AS-105-AM (Solimões Formation)

6.1. Introduction

Amazonia underwent profound landscape changes during the Miocene. Prior to the late Miocene, the Amazon River was split in two with one branch running westward (Figueiredo *et al.* 2009, Hoorn *et al.* 2010). Central Amazonia cratonic areas, as well as the Andes, were drained by rivers that discharged into an immense wetland system that developed during the early, middle and early late Miocene in western Amazonia (Hoorn 1993, Wesselingh *et al*. 2002). This system, often referred to as the Pebas system (or lake), comprised a series of lakes, megalakes, rivers, deltas, estuaries, and floodplains much like the Pantanal of central Brazil, Paraguay and Bolivia are at the present time, but at a much larger spatial scale. When at its full development as a lake, estimates put this system to over one million km^2 in extension, making it one of the largest ever recorded lakes (Wesselingh *et al.* 2002, Wesselingh 2007, 2008). The Andean uplift during the Miocene is a heavy influence on the evolution of the Pebas system. Mountain building created continuous accommodation space in the forelands. This and the lack of other significant relief in western Amazonia resulted in a low gradient and low energy scenario suitable for the development of wetlands. Prior to late Miocene and Pliocene, when Andean tectonism was the strongest and caused most deformation in the foreland basins, important watersheds did not exist (Mora *et al*. 2010). This signifies that the outline of western Amazonia as a whole was larger, extending south into the central Andes in Bolivia, and north through the Llanos basin in Colombia into the Orinoco basin. This Pan-Amazonia area had a long-lived interconnectedness, so much so that episodes of marine incursions are detected from the Caribbean to southwest Amazonia (Hoorn *et al*. 2010, Antoine *et al*. 2016), approximately 2,500 km distant from each other.

The marine incursions into western Amazonia are probably the most debated topic in the Amazon literature (see for instance Latrubesse *et al*. 2010). Their existence is suggested since early works on molluscs from the area (Gabb 1869, Woodward 1871, Boettger 1878). Shells with affinities to North American and Caribbean taxa were indicative of marine connections. This fossil record plus sedimentary characteristics lead authors already in the early twentieth century to postulate inundation theories for the upper Cenozoic in western Amazonia that would only decades later be confirmed. One author wrote that, "the Tertiary rocks appear from their characters and fossils to be of fluviatile, or possibly brackish-water, origin. (…) The rise of the Andes would dam up the ancient [Amazon] river into a lake which would eventually find an outlet eastward, as at present" (Sherlock 1934, pages 115-116). Later, in the early 1950s, T. Van der Hammen in his initial works in Colombia saw wide extensions of sediments with iron oölite and manganite, indicating presence of lacustrine and brackish-water conditions. These were years later confirmed by his finding of mangrove pollen (*Zonocostites*) in Neogene sediments. Finally, in the early 1990s a more refined picture emerged with the studies of Nuttal (1990) and Hoorn (1993, 1994a, 1994b) who dated more precisely sediments of western Amazonia to the Miocene.

Existence of marine indicators in western Amazonia early and middle Miocene beds is irrefutable. Among the most compelling fossils with marine affinities include: molluscs, foraminifera (tests and linings), dinoflagellate cysts (dinocysts), ostracods (*Cyprideis*), bryozoans, decapoda, fish teeth (shark, stingray, sawfish), sea urchins and various ichnofossils (Lorente 1986, Dueñas 1980, Hoorn 1990, 1993, 1994a, 1994b, Monsch 1998, Rull 2001, Wesselingh *et al.* 2002, Salas-Gismondi *et al*. 2006, Antoine *et al.* 2007, 2016, Hovikoski *et al.* 2007, 2010, Bayona *et al.* 2007, Linhares *et al.* 2011, Bianucci *et al.* 2013, Boonstra *et al.* 2015). Other than fossils, strontium isotopes from molluscs (Vonhof *et al.* 1998, 2003), molecular data of Amazon fish with relatives in the Caribbean (Lovejoy *et al.*

1998, 2006, Cooke *et al.* 2012) and preserved tidal sedimentary structures (Hoorn 1994a, Hovikoski *et al.* 2007, 2010) further point to marine connections. Despite this body of evidence, there are still some contentious topics and many unanswered questions in the literature. First, what was the timing, duration and significance of marine incursions? The chronostratigraphic framework used in western Amazonia relies heavily on palynology of the Solimões and Pebas Formations. Pollen zones adapted from Venezuela (Lorente 1986) are used and also served to aid the formulation of other biostratigraphic frameworks like the molluscan zonation of Wesselingh *et al.* (2006a). Such zones are best estimates but do not provide a high temporal resolution to bracket specific events. Furthermore, the great majority of studied sites are outcrops. Because (i) the beds of the Solimões/Pebas and adjacent deposits lie horizontally or sub-horizontally, (ii) the overall landscape is flat and (iii) there is a dense forest cover, exposed sections cannot cover long vertical ranges. These factors, and the lack of good age control, mean basinwide correlations are rendered difficult. Second, what was the geographical extension of the marine incursions? This question, in turn, is directly linked to the first question because age correlation is essential to map spatial and temporal distribution of a given inundation event.

Another issue, which is perhaps the least tested of all, is to what extent these inundations affected the forest structure and composition. Some authors have used the flooding dynamics (flood x dry) to inform theories about biodiversity (Nores 1999, 2004). Large scale inundations potentially create countless islands on high ground that isolated fauna and flora and encouraged allopatric speciation (Nores 1999, 2004). They also allegedly gave rise to novel environments like mangroves and estuaries of variable salinities. If this all is true, we should be able to detect some signal of species changes related to such events. To test some of the questions contended above, a paleoenvironmental analysis was carried out using the pollen data generated from core 1-AS-105-AM. Palynomorphs were grouped in

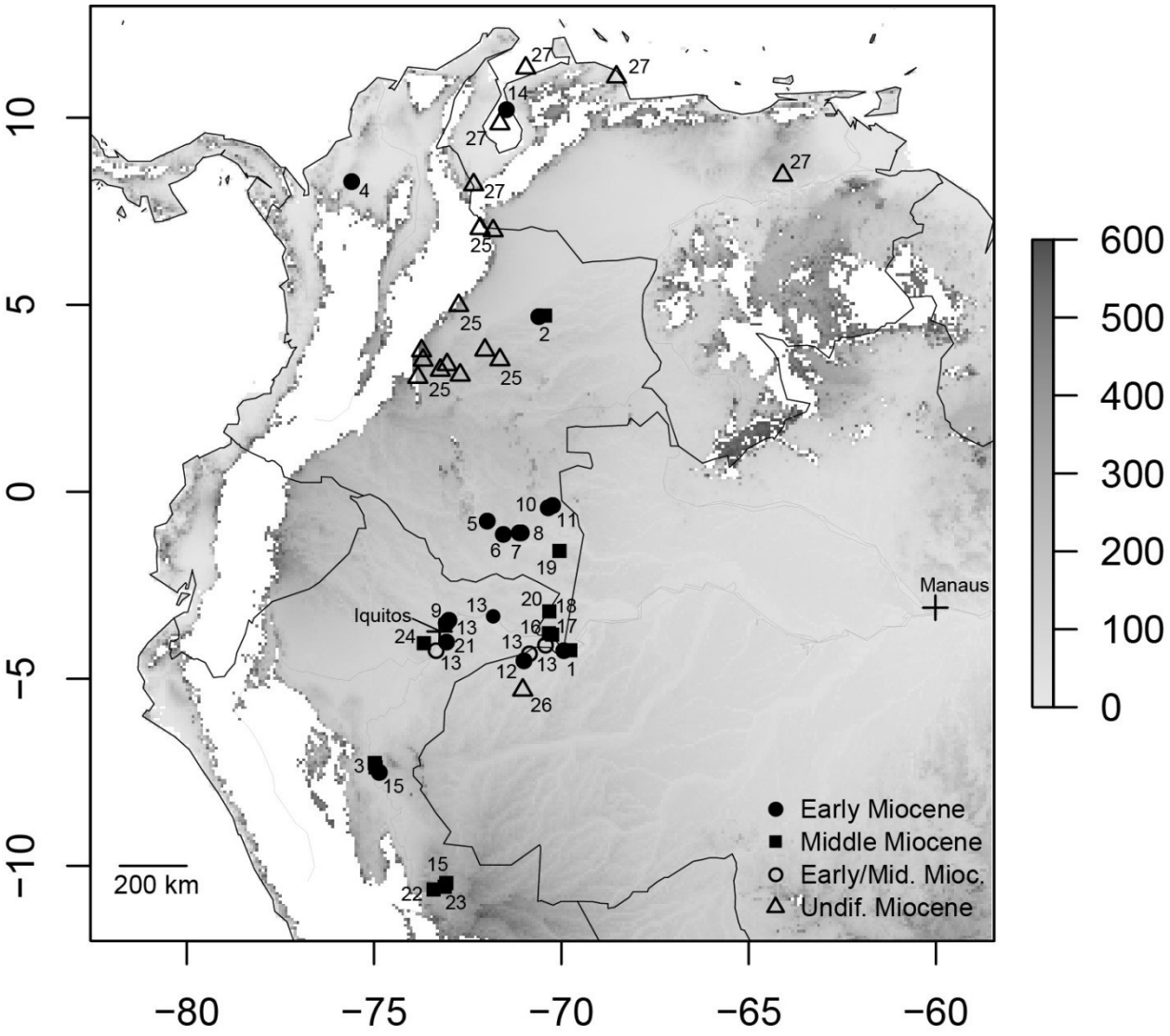

Figure 6.1. Location map of sites where marine incursions have been evidenced by fossils: **1 (core 105-AM, this study)**, 2 (core Saltarin, Jaramillo *et al*. in prep), 3 (Contamana, Antoine *et al.* 2016), 4 (core Q-E-22, Dueñas 1980, Bayona *et al.* 2007), 5 to 8 (various outcrops in Mariñame, Hoorn 1990, 1994b), 9 (outcrop Santa Teresa, Hoorn 1994a), 10 and 11 (outcrops in Apaporis, Hoorn 2006), 12 (core 4a-AM, Hoorn 1993, Vonhof *et al.* 2003), 13 (various outcrops by Hovikoski *et al.* 2005, 2007, 2010), 14 (core Tj, Rull 2001), 15 (sites revisited by Boonstra *et al.* 2015, see text for details), 16 to 20 (various outcrops studied by Hoorn 1994a, 1994b, Wesselingh *et al.* 2002, Vonhof *et al.* 2003), 21 (Loreto locality IQ-115, Monsch 1998, Boonstra *et al.* 2015), 23 and 23 (Fitzcarrald area, Salas-Gismondi *et al.* 2006, Antoine *et al.* 2007, Bianucci *et al.* 2013, Boonstra *et al.* 2015), 24 (Loreto locality N. Horizonte, Wesselingh *et al.* 2002, Vonhof *et al.* 2003), 25 (various cores studies by Bayona *et al.* 2007), 26 (core 33-AM, Linhares *et al*. 2011), 27 (various localities studies by Lorente 1986).

their ecological and botanical affinities, contrasted against the age estimated for the core and finally compared to other published localities. The full methods can be found in Chapter 3.

6.2. Results

Marine incursions

Two conspicuous marine levels were detected in core 105-AM (Fig. 6.2 and Fig. 6.3). They were established on the basis of peak abundances of dinocysts, foraminiferal linings and mangrove pollen (*Zonocostites* + *Lanagiopollis crassa*). The lower incursion (MF1) took place from ca. 18.4 to 17.8 Ma (duration of 0.57 Ma). The maximum extent of marine flooding is at the top of the interval with a 200,000 yrs period from 17.83 to 18.03 revealed by an abundant and rich dinocyst assemblage. At the bottom of MF1 dinocysts are rare (≤1%) but a peak in foraminiferal linings and *Zonocostites* is present. Between the bottom and top of MF1, gaps exist of up to ca. 0.02 Ma (but potentially 0.1 Ma) where samples contain no marine indicators. The upper marine incursion (MF2) took place from ca. 14.10 to 13.73 Ma (duration of 0.37 Ma). It is expressed by spikes in dinocyst and one rare occurrence of an undetermined foraminifera at ca. 98 m or ca. 13.8 Ma (Fig. 6.3), which coincides with the highest dinocyst abundance peak. MF2 also has a gap where no marine evidence was recorded, but estimating its duration is not possible because it is covered by only one sample. Twenty one dinocyst taxa were recorded in total, 14 of which have identification to the species level (Fig. 6.3 and plates 26-27 of Chapter 5). Dinocyst abundance data are distributed in all types of lithologies with no significant differences found (Kruskal-Wallis one way Anova; K=1.5121, p=0.6795). However, dinocyst peak abundances (>40%) are restricted to mudstones (Fig. 6.4), thus suggesting marine incursions occurred during periods of lake development, probably at peak megalake stages when the water table was high throughout the basin.

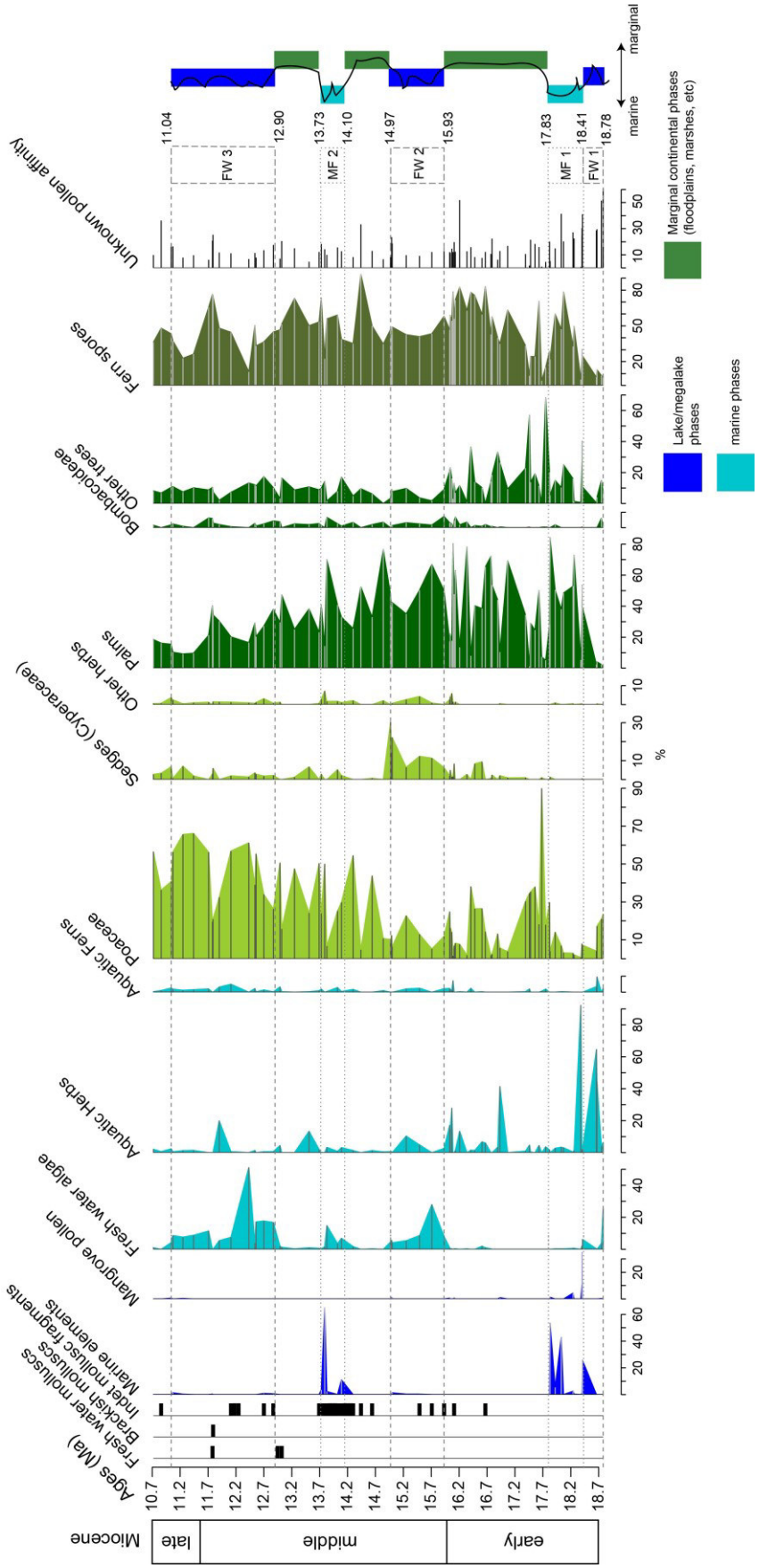

Figure 6.2. Summary percentage diagram of ecological groups. Solid line along the coloured bars represents empirical interpretation of variability in the changing environmental settings.

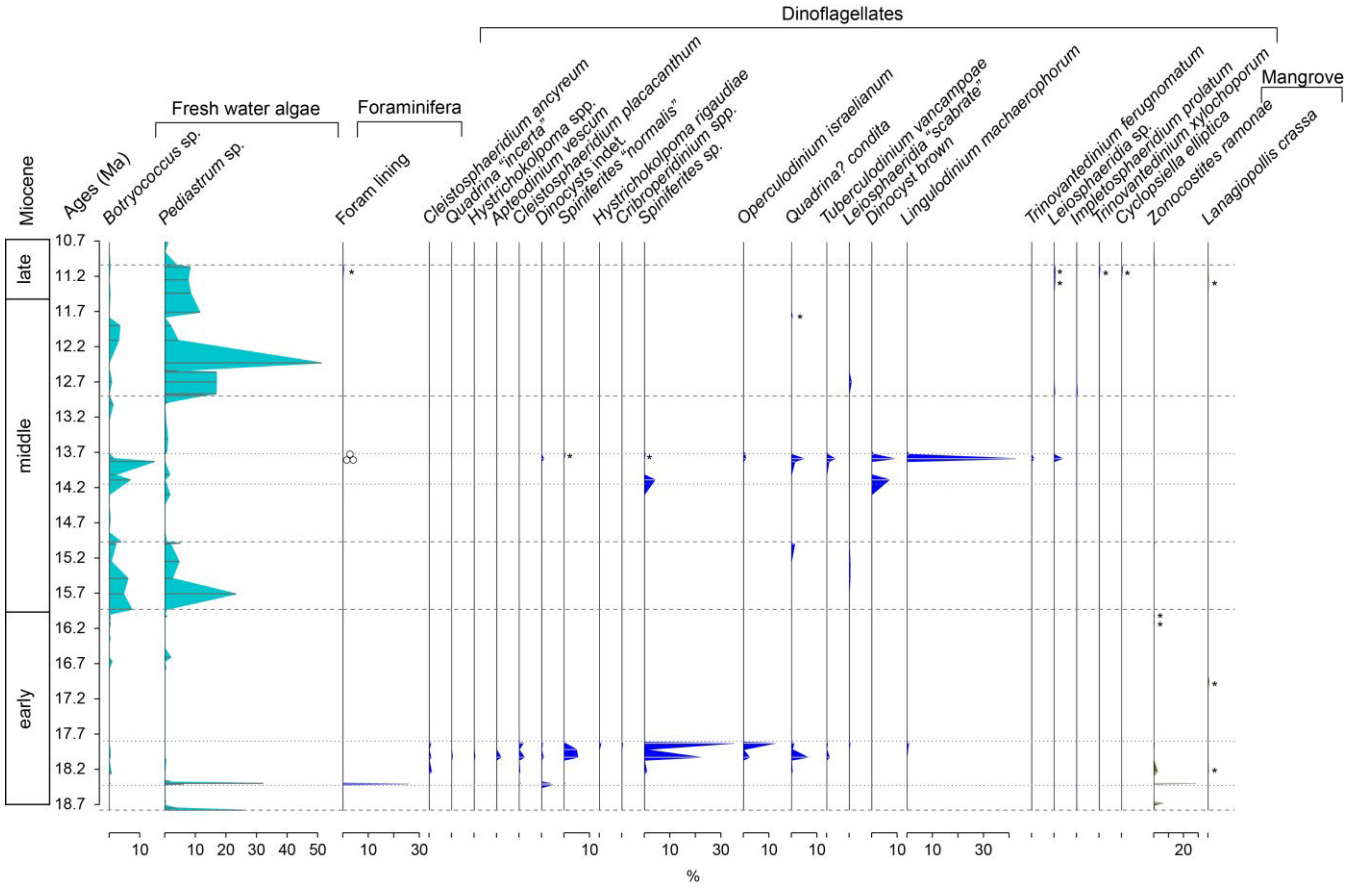

Figure 6.3. Freshwater and marine water indicators, including all dinocyst taxa identified. Rare occurrences (≤1%) are highlighted with a "*". Notice foraminifera symbol at ca. 13.8 Ma (♧).

Fresh and brackish water phases

Whereas clear marine inundations are evident from peak dinocyst abundance (MF1 and MF2), freshwater-dominated phases with occasional brackish conditions also existed. These fresh water phases are spread in three different periods - at the base of the 105-AM sequence (FW1, from 18.78 to 18.41 Ma), at the middle (FW2, from 15.93 to 14.97 Ma) and in the upper part (FW3, from 12.90 to 11.04 Ma). They were established after the continued and abundant presence of fresh water algal cells *Pediastrum* spp and *Botryococcus* spp. These algae are present in all lithologies but in varying quantities, being more abundant in silts and sands (Fig. 6.4). In lignites, significantly less algae were recorded (Kruskal-Wallis one way Anova; K=14.37, df=3, p=0.00244; and Post-hoc Tukey test: lignite vs. sand, p=0.0084 |

lignite vs. silt, p=0.0255). Further support of such lacustrine conditions can be indicated by peaks in aquatic plants pollen (Fig. 6.2) and mollusc taxa found at two levels (Fig. 6.2). Among the mollusc species, *Charadreon*, *Aylacostoma* and *Sheppardiconcha* can be assigned to fluvial or marginal lacustrine ecologies, whereas all other species are Pebasian endemics (Wesselingh *et al.* 2002, Wesselingh 2006) and therefore most likely lacustrine. These include a few informal species from the Benjamin Constant fauna (F. Wesselingh *personal comm*.) A full list of mollusc species can be found in Chapter 5, Table 5.2. Also typical of fresh water flooding, like extant *várzeas* and *igapós*, is Bombacoideae (Bombax trees) with abundant palms.

During FW2 and FW3, rare occurrences of dinocysts point to brackish conditions. Although they are Neogene, moderately well-preserved dinocysts, they could still be reworked since the likely short distance from source to deposition would prevent them from being too damaged. However, at least during MF3, brackish conditions are also supported by the occurrence of brackish water bivalve species *Corbula cotuhensis* (Wesselingh 2006a) at 11.79 Ma (Fig. 6.2) and by the accumulation of carbonate mud (micrite) in thin different levels of the core (Fig. 2.1 and Appendix 9.4). These thin micritic bands can be produced by brackish conditions in an overall freshwater environment common in humid regions (Kelts and Hsü 1978). Calcareous sources could be layers of shells accumulated in lakes, calcareous algal blooms or inorganic inputs from detrital re-deposition. These scenarios could be related to freshwater carbonate accumulation only, like it has been reported in late Miocene Solimões Formation floodplain lakes rich in shells and other fossils (Gross *et al.* 2011). However, the presence of rare dinocysts and brackish bivalves strongly suggests transient fresh-brackish water dynamics during FW2 and FW3.

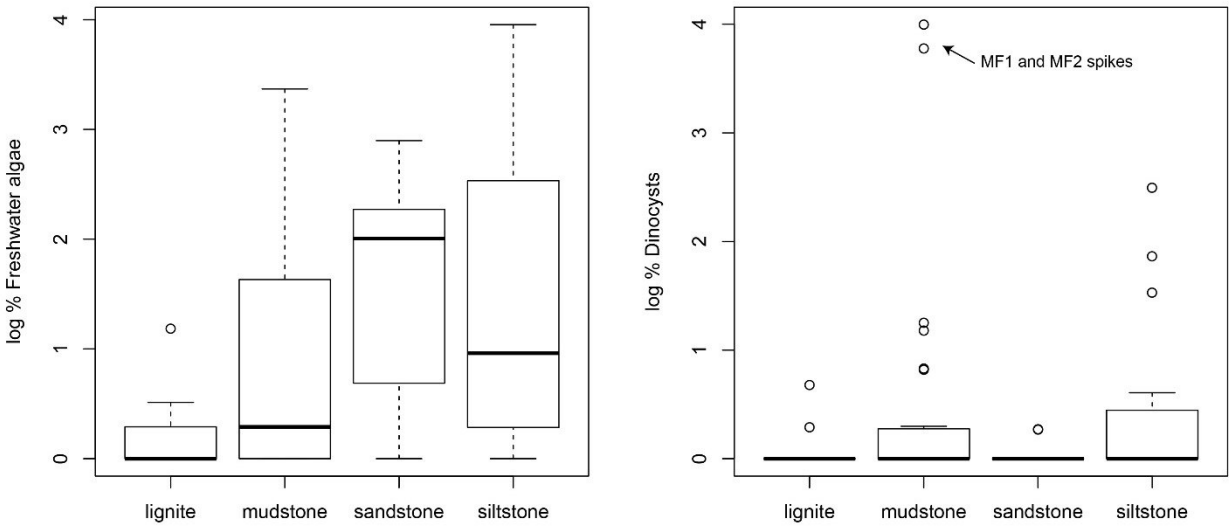

Figure 6.4. Abundance distribution of freshwater algae in comparison to lithology.

Vegetation

Vegetation throughout the entire 105-AM core is typical of Amazonian lowland forests. The extant botanical affinities of fossil pollen, and their ecological significance, was compiled from the literature (see Appendix table 9.2). Of the total pollen species (fern spores excluded), 31.8% had known affinities at least to the family level. When reviewed in terms of abundance, 83% of the pollen counts had a known systematic affinity (Fig. 6.2). Among the most abundant families (Fig. 6.2) are grasses (Poaceae), palms (Arecaceae), Malvaceae (subfamily Bombacoideae), Euphorbiaceae, Melastomataceaae, and Alismataceae (Fig. 6.5.). Except grasses and aquatic/swamp species (Alismataceae, Cyperaceae, Polygalaceae Onagraceae), the overall majority of plants belong to arboreal taxa. The dominance of palms, grasses, aquatic plants, a rich tree assemblage including seasonally flooded forest taxa (Bombacoideae, although not exclusively) as well as abundant ferns, is indicative of floodplains, swamps and *terra firme* forests. Thus, the pollen record points to the constant presence of warm and humid conditions. The presence of Podocarpaceae (*Podocarpus* sp)

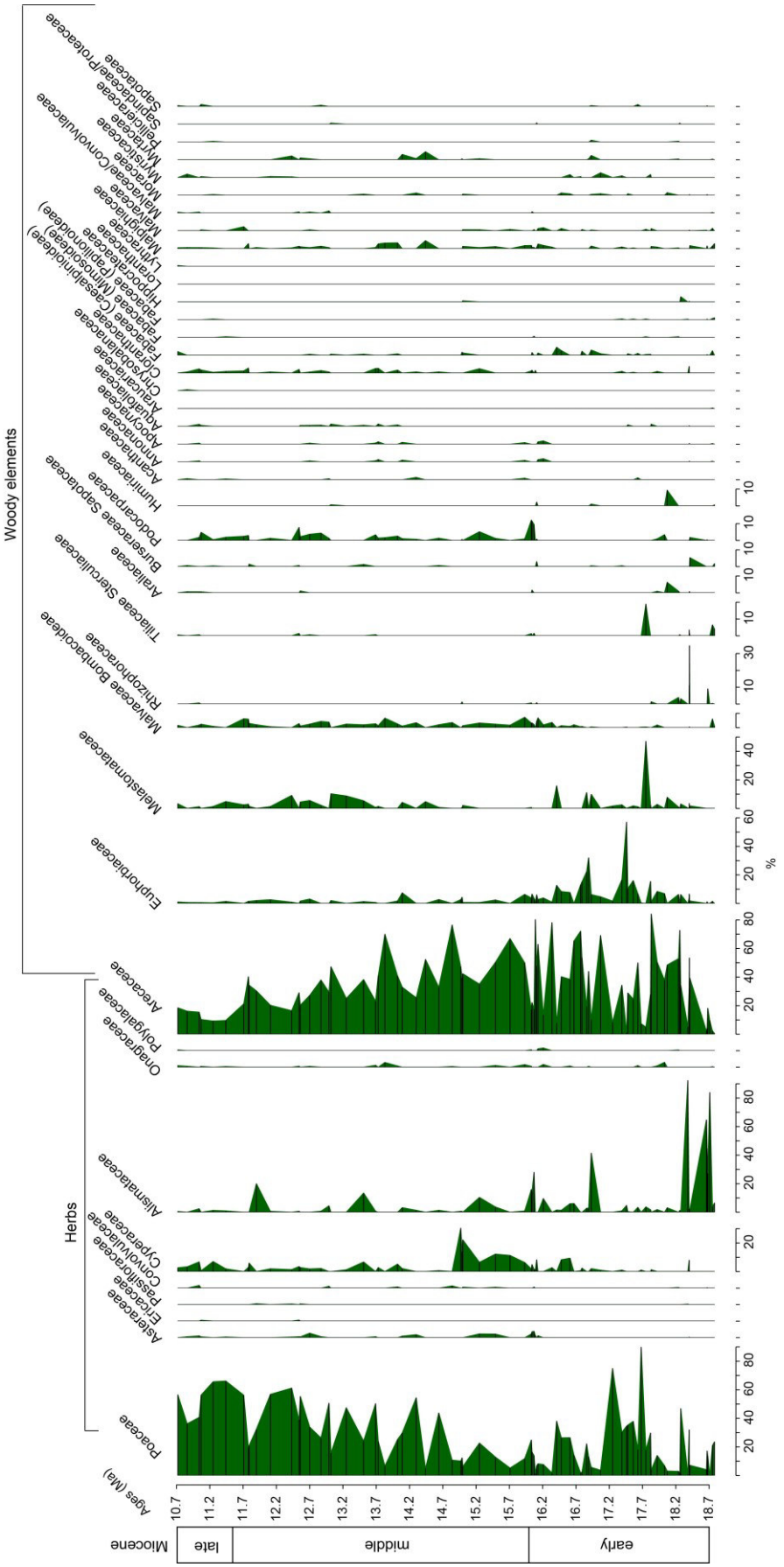

Figure 6.5. Percentage diagram of plant families and subfamilies for which botanical affinity is known.

and Loranthaceae (*Hedyosmum* sp.) could indicate either montane (Andean) sourced pollen carried by rivers or lowland montane-like plant communities in oligotrophic or water-logged soils (Householder *et al.* 2015, Punyasena *et al.* 2011, *personal observation*). *Hedyosmum* sp. invaded South America in the early Miocene, inhabiting lowlands (Martinez *et al*. 2013) during this time. Lineages of lowland tropical *Podocarpus* sp. emerged during warm Tertiary times (Quiroga *et al*. 2015), thus the presence of both taxa in lowland deposits does not necessarily reflect descence from Andean forests.

To test the possible effects of inundations (freshwater/brackish or marine) on the vegetation, a Canonical Correspondence Analysis (CCA) was run on the vegetation data set (species matrix). Environmental variables used for this were the presence of lake conditions (FW1, FW2 and FW3) and marine incursions (MF1 and MF2). Table 6.1 summarises the results of the CCA. *Constrained* CCA is the analysis that used the explanatory variables and *unconstrained* CCA is a correspondence analysis of the residuals of the constrained CCA. Only 3.78% of the inertia is explainable variation, whereas 96.21% is residual. The vegetation matrix transformed into binary data yielded very similar results (Table 6.1., shown in parenthesis). Therefore, nearly no effect on the abundance distribution or composition of plants is explained by the inundations. CCA axis scores (eigenvalues) weigh more on the Fresh/Brackish water inundation (71.4% of variation) than they did on Marine water (28.6%), further showing marine incursions have negligible effects on the vegetation. These axis scores will not be further explored due to the very poor fit of the analysis.

Table 6.1. Summary results of the Canonical Correspondence Analysis (CCA) of vegetation data against environmental variables (fresh/brackish and marine water).

	Inertia	Proportion	Rank
Total	3.81044 (*4.38858*)	100%	--
Constrained	0.14418 (*0.14698*)	3.78% (*3.34%*)	2
Unconstrained	3.66626 (*4.24160*)	96.21% (*96.65%*)	72

cca(formula = veg ~ FreshWater + MarineWater , data = environ); Inertia is mean squared contingency coefficient (to show how good the analysis was). Numbers in parenthesis are CCA run with binary matrix.

6.3. Discussion

Dinocysts ecology and the nature of western Amazonian inundations

The dinoflagellate cysts found here are commonly seen in a number of Neogene marine sequences worldwide and thus their niche occupancy can be interpreted. The majority of identified species from both marine intervals are neritic, cosmopolitan and with a broad tolerance for temperature (see below). No characteristic oceanic species are present. Only *Operculodinium israelianum* and *Tuberculodinium vancampoae* are restricted to subtropical, tropical and equatorial realm, favouring nearshore or coastal areas (Zonneveld *et al.* 2013). The upper marine incursion (MF2) has a spike of *Lingulodinium machaerophorum* (Fig. 6.3), this cyst is euryhaline and tends to attain high abundance in estuaries or in areas of coastal upwelling (Dale 1996). In the upper freshwater/brackish phase, at ca. 11 Ma, *Cyclopsiella elliptica/granosa* complex was recorded in a cluster. This species often form colonial biocoenosis (de Verteuil and Norris 1996), which points to an attached or perhaps encrusted mode of life (Matsuoka and Head 1980) in nearshore, high energetic environments (Louwye and Laga 2008). At the same sample, *Trinovantedinium xylocophorum* was recorded, this species as well as 'rounded brown cysts' (RBCs) of indeterminate Protoperidiniaceae affinity in MF2 is nonphotosynthetic or heterotrophic (Fensome *et al.* 1993). The same goes for *T.*

ferugnomatum present in MF2. The presence of these protoperidiniacean cysts and especially their considerable abundance in MF2 (Fig. 6.3) can be associated with enhanced nutrient levels driven by fluvial/deltaic input (Dale 1996). For instance, some protoperidiniacean dominated dinocyst assemblages are documented from the Oligocene of Nigeria (Biffi and Grignani 1983) and the Miocene of the Gulf of Mexico (Duffield and Stein 1986), both localities receiving high nutrient inputs from the Niger Delta and Mississippi delta complex respectively.

The acritarch species *Quadrina*? *condita* is present in both marine intervals and outside of them as well. Its ecology is still poorly understood but occurrences are seen in warm settings like lower to middle Miocene of the Gulf of Suez (Soliman *et al.* 2012) and productive shallow marine environments of middle to upper Miocene age in the Maryland-Virginia coast (de Verteuil and Norris 1996). Many of the individuals of *Q*.? *condita* seen in core 105-AM had a distinctive cruciform shape that is stronger than the original cruciform outline caused by spines being clustered at the corners of the cyst (see Figure 2 in Plate 27, Chapter 4). Cruciform shape has been shown to be the result of low salinity adaptation in many dinoflagellate species (Wall *et al.* 1973, Kouli *et al*. 2001, Mudie *et al.* 2001, Marret *et al.* 2004). This could be the case of *Q*.? *condita* as well since it is recorded in brackish waters in the Pebas system. Other species do not show signs of cruciform shape.

The lower marine interval (MF1) is dominated by *Spiniferites* species (Fig. 6.3). Unfortunately they could not be identified to the species level. The genus is cosmopolitan (Zonneveld *et al.* 2013), occupying open oceans and coastal regions from all latitudes, thus an ecological assignment to the *Spiniferites* assemblage in MF1 is imprecise. Other dinocysts in this assemblage are more informative, like *O. israelianum* and *T. vancampoae* that tend to be restricted to sub-(tropical) and equatorial nearshore and coastal regions (Zonneveld *et al.* 2013). Therefore, dinoflagellate ecology in both marine incursions is similar and indicative of

nearshore, shallow marine to estuaries, with high energy and high nutrient input in an equatorial setting.

Freshwater/brackish phases

Lake phases were established based on the abundant and consecutive presence of freshwater algae. This interpretations was based essentially on the green alga *Pediastrum* and done at the generic level, given the difficulties in identification of this polymorphic genus (Komarék and Jankovská 2001). *Pediastrum* is representative of low energy environments (Weiler 1985) like lakes. A number of studies have linked *Pediastrum* concentrations to lake level and temperature in the tropics (Rull *et al.* 2008, Gosling *et al.* 2008, Whiteny and Mayle 2012). Different species of the genus can have contrasting water level and other ecological preferences (Komarék and Jankovská 2001). For instance, Whitney and Mayle (2012) studying lowland wetlands in central South America found that some taxa prefer deeper waters while others develop better in shallow water associated with a dense macrophyte cover. In core 105-AM, no relation was found between the relative abundance of aquatic plants and freshwater algae (r^2= -0.010, p=0.667), and therefore a preference of *Pediastrum* to very shallow water like ponds, marshes and bogs where the aquatic plants identified here thrive cannot be suggested. This agrees with the significant lower concentrations of algae in lignite facies (Fig. 6.4, see results), that are deposited in peat forming marshes and bogs. Hence, for the best of our knowledge, *Pediastrum* is pointing to lacustrine environments with a higher water table. This explains the higher amount of algae in coarser facies (Fig. 6.4, see results), that although they do not represent lake deposits (muds), they attest to connection of separate lacustrine systems by the action of avulsion, internal deltas and splays. Evidence of this connections is the occurrence of dinocysts during overall freshwater phases (FW2 and FW3) and full marine phases disrupting what was otherwise freshwater lakes. Full marine

phases are associated with mud facies, when lakes were at high stands and thus covered a wider geographical area.

Comparison with other regional dinocyst records:

(1) Amazonas/Pebas/Solimões basins (sites 5, 6, 10, 16, 17, 18 and 20, in Fig. 6.1)

The early to middle Miocene outcrops of Mariñame, Tres Islas, Apaporis, Los Chorros, Mocagua and Buenos Aires that are all in the southern Colombian Amazon were originally studied by Hoorn (1990, 1994a, 1994b, 2006) and recently revisited by Boonstra *et al.* (2015). They report low counts of dinocysts ranging from 1 to 35 individuals (0.3 to 11.6% of a typical 300 pollen count) what is in contrast with the high percentages attained in the full marine incursions reported herein (>40 % of the total count). Four dinocyst taxa are shared in both studies, *Spiniferites* spp, *T. vancampoae*, *Quadrina*? *condita* and indeterminate RBCs (Protoperidinioid). In addition, Boonstra *et al.* (2015) report *Polysphaeridium zoharyi*, *Brigantedinium* spp. and *Lejeunecysta* spp. *P. zoharyi* is found in subtropical, tropical to equatorial coastal sites (Zonneveld *et al.* 2013) and can be associated with lagoons and estuaries (Wall *et al.* 1977, Marret and Zonneveld 2003). The Protoperidinioids *Brigantedinium* spp. and *Lejeunecysta* spp. are heterotrophic cosmopolitan taxa and their abundance can be associated to high productivity (Zonneveld *et al.* 2013). Altogether, the dinocyst assemblages from 105-AM and the Hoorn outcrops point to the very similar environmental conditions of shallow marine, high-nutrient, and coastal areas.

In addition to dinocysts, Hoorn (2006) and Boonstra *et al.* (2015) report foraminiferal organic linings and calcareous tests as well as mangrove pollen (*Zonocostites*) in some of the above-mentioned localities. In Tres Islas, Los Chorros and Buenos Aires, linings and tests of *Ammonia, Elphidium* and *Trochammina* were found (6 to 49 individuals in 1 cm^3 sediment for linings and 10 to 30 g sediment for tests). Other localities reached counts of 300 tests,

which is the case of Nuevo Horizonte in Peru (number 24 in Fig. 6.1). The organic linings despite lacking definitive systematic identification seem to be produced by the same genera of calcareous tests (Boonstra *et al.* 2015). Some of these calcareous tests (15% of the assemblage) were reported to have abnormalities in shape like extra, protruding chambers, with distorted arrangements and reduced size. The ecology of these organisms point to euryhaline conditions (wide range of salinity toleration) and show they are common in shallow marine environments like ponds, lagoons and mangroves, with such occurrences for instance in the Caribbean (Javaux and Scott 2003, Molinares *et al.* 2012). Their morphological aberration is a response to stressful environmental conditions like salinity, oxygen and organic matter (Boltovskoy 1991, Geslin *et al.* 2000). They represent phenotypic responses to environmental stress. In sum, evidence from foraminifera is in agreement with dinocyst ecology, pointing to shallow marine, productive coastal areas like estuaries or mangroves.

(2) Contamana (site 3 in Fig. 6.1)

The Pebas sediments have been recently described in detail for the Contamana area in Peru (Antoine *et al.* 2016). Two palynological samples of middle Miocene and middle-Late Miocene age yielded rare (~1%) dinocysts belonging to the genera *Brigantedinium*, *Trinovantedinium* (three indeterminate species), *Impletosphaeridium*, *Cleistosphaeridium*, *Lingulodinium*, *Spiniferites* and another unidentified dinocyst. These are the same genera present in the Mariñame/Apaporis/Iquitos area and in core 105-AM. Although without specific identifications, a similar ecological requirement can be inferred. In addition to dinocysts, foraminifera (dominant *Ammonia*), sea urchins, ostracods (mainly *Cyprideis*) and a wealth of ichthyofauna and mammals is also recorded. The fossiliferous content and sedimentology of this section in Contamana is interpreted as representing coastal plains with

marginal marine influence to estuarine embayments. This parallels the situation interpreted for other areas including core 105-AM.

(3) Llanos basin (site 2 in Fig. 6.1)

A newly analysed borehole documented the environmental history of the Llanos basin in Colombia during the late early Miocene to the latest late Miocene (Jaramillo *et al*. in prep). The rich palynological assemblages coupled with numerical age estimates derived from graphic correlation (see Chapter 4) allows a quantitative comparison of environments in the Llanos to those recorded here in the Solimões/Pebas system in western Amazonia (Fig. 6.6). The specific composition of dinocysts from Saltarin is fairly similar to that of core 105-AM, with dominant taxa being the Protoperidinioids (indeterminate RBCs), *Q.*? *condita* and *Spiniferites*. Moreover, *O. israelianum*, *L. machaerophorum*, *P. zoharyi*, *T. vancampoae* and many species of *Tuberculodinium* are present. The ecological requirement of this assemblage is the same discussed for the western Amazonia sites. For instance, *O. israelianum*, *T. vancampoe* and *P. zoharyi* constrain the environment to low latitude shallow waters (Zonneveld *et al.* 2013). Species of the genera *Erymnodinium*, *Selenopemphix*, *Sumatradinium* and *Trinovantedinium* together with the Protoperidinioids attest to a highly productive environment to sustain high numbers of nonphotosynthetic or heterotrophic dinoflagellates (Fensome *et al.* 1993). The abundance of such taxa is especially indicative given that protoperidiniacean cysts are sensitive to post-depositional degradation through oxidation (Hopkins and McCarthy 2002, Zonneveld *et al*. 2007, 2010), which points to two non-mutually exclusive scenarios: (1) blooms of these taxa and consequently high amounts of cysts reaching depositional environments, and (2) a high and stratified water table leading to anoxic or semi-anoxic conditions and therefore cyst preservation. Furthermore, large numbers of heterotrophic cysts in shelfal environments can be related to enhanced nutrient levels through fluvial/deltaic inputs (Dale 1996, Biffi and Grignani 1983, Duffield and Stein 1986).

Considerable spikes of foraminiferal linings were also recovered from the Saltarin core samples (up to 94% of the total sum, whereas dinocysts ranged from ~1% to >50%). Unfortunately they were not identified to any taxonomic level, but their presence in high numbers attests to the pronounced marine influence in the area. Overall, the Saltarin locality corroborates and gives better age constrains to the long known marine advances into northwest South America from the Caribbean sea (Lorente 1986, Rull 2001, Bayona *et al.* 2007), including the Llanos basin that is in a proximal position to the sea and eventually connected it to the western Amazonia region.

The comparison between Saltarin and 1-AS-105-AM shows a good correspondence of events (Fig. 6.6). Both marine incursions detected in 105-AM (MF1 and MF2) are paralleled with similar spikes in marine elements in the Llanos. Differences are also evident. The marine influence at the Llanos is clearly stronger as its episodes lasted longer and supported a richer dinocyst fauna (30 taxa vs. 21 in 105-AM), not to mention remarkably more foraminiferal linings. Two freshwater/brackish events in western Amazonia (FW2 and FW3) coincide with marine peaks in the Llanos. During these phases, freshwater algae were abundant in western Amazonia. The freshwater phases were interpreted as lakes and megalakes. *Pediastrum* is a good indicator of low energy freshwater environments (Weiler 1985), but some of its species can also not only survive but thrive in low salinities (Batten and Grenfell 1996, Head *et al.* 2005). This environmental plasticity could reinforce the brackish nature of the lakes that developed in western Amazonia synchronously with marine peaks in the Llanos. Why more frequent or longer episodes of marine influx did not occur in western Amazonia requires an explanation. Factors hampering the full transgression of the stronger and long-lasting marine phases from Llanos into western Amazonia could be related to (1) local tectonic controls, (2) fluvial migrations increasing the freshwater input into lakes, and (3) higher precipitation, also strengthening the freshwater input. Such mechanisms have

been proposed on the basis of molluscan strontium, oxygen and carbon isotope studies that reconciled low estimated salinities in Pebas deposits (~1 psu or less) with abundant Andean and cratonic freshwater runoff (Vonhof *et al.* 2003). Local uplifts controlling the impact and geographical extension of marine incursions are hard to prove. Not enough detailed reconstructions exist, and the ones available point to late Miocene activity, like those in the Iquitos forbulge area (Roddaz *et al.* 2005, and see Chapter 4) and the Vaupés range (Mora *et al.* 2010), which may represented the northern boundary of the western Amazonas basin and therefore the 'portal' into the Llanos basin (Mora *et al*. 2010).

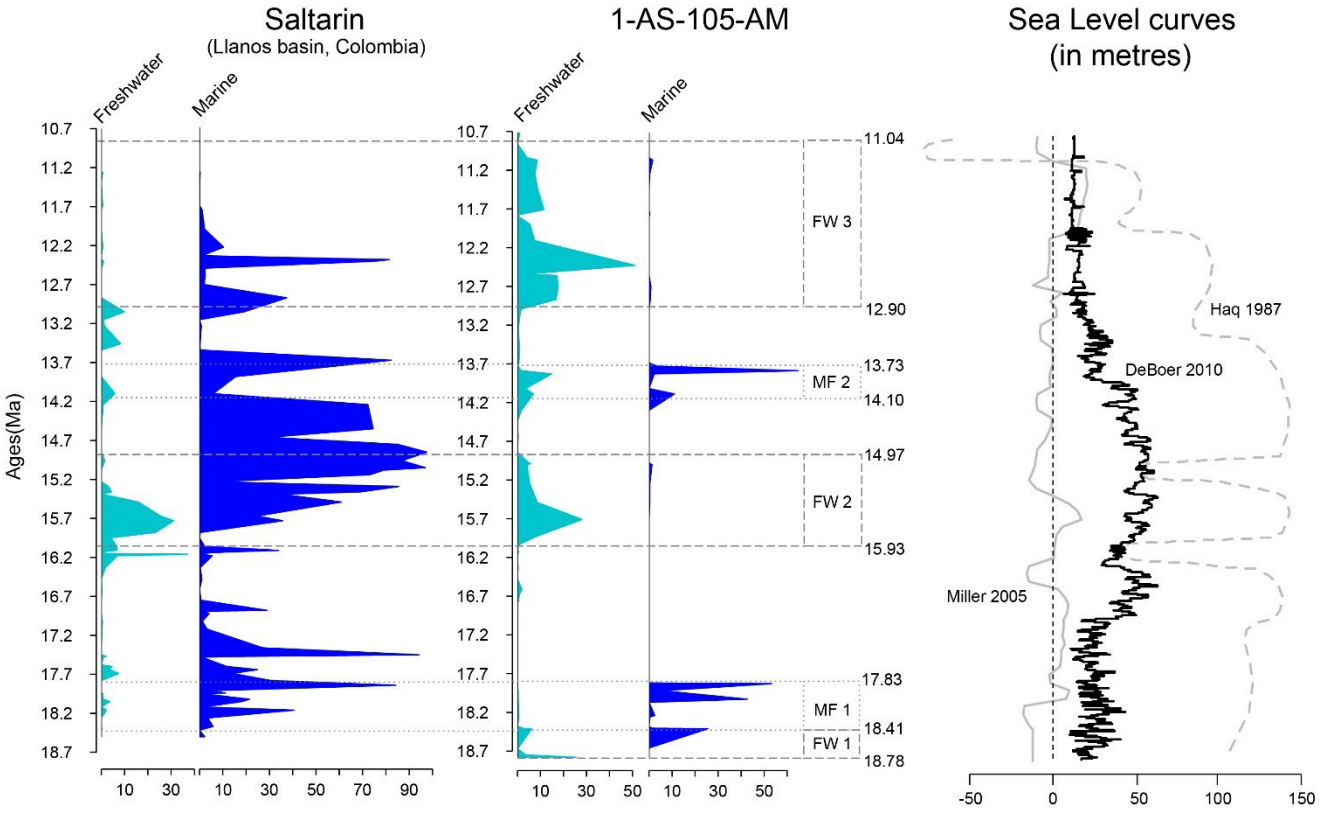

Figure 6.6. Comparison of proxies for freshwater (*Pediastrum* and *Botryococcys*) and marine influence (dinocysts, acritarcs and foram linings) between cores Saltarin in the Colombian Llanos and 1-AS-105-AM in western Solimões Fm. Percentages are in relation to total count (all palynoorphs included). Sea level estimates from the same period from Haq (1987), Miller *et al.* (2005) and De Boer *et al.* (2010). Sea level curve by Müller *et al.* (2008) was not plotted for clarity, it is a nearly flat line ca. 60 m a.s.l. Zones (MF and FW) are bracketed the same way in both cores for comparison purposes.

Geographical extension and frequency of inundations

Boonstra *et al.* (2015) and Antoine *et al.* (2016) recognised three incursion phases in the Pebas deposits: (1) in the early Miocene, (2) in the late early and middle Miocene and (3) in the late Middle to early late Miocene. Their early Miocene inundation can be correlated with MF1 of the present study. Their late early to middle Miocene can be correlated with either MF1, FW2 or MF2 - discrepancies are due to outcrops being short and thus ages cannot be well constrained. Most likely, it is the middle Miocene incursion (MF2) that correlates with middle Miocene sites of Boonstra *et al.* (2015), based on locality Nuevo Horizonte that demonstrates notable spikes of foraminiferal tests. This is the only marine proxy comparable to the dinocyst abundance of MF2. The late middle to early late Miocene inundation is correlated with the brackish conditions found in FW3. A further marine phase during the late Miocene was also suggested by Uba *et al.* (2009), this is outside the scope of the present study. In short, both peak marine phases and the upper brackish conditions of FW3 seem to have regional correlates, pointing to at least three phases of widespread marine/brackish conditions in western Amazonia.

Regarding the total extension of the marine incursions, there is evidence for both events as far south as the Contamana region in Peru (~7°1'S, Fig. 6.1) (Boonstra *et al.* 2015, Antoine *et al.* 2016). For the middle Miocene event (MF2) the evidence suggests as far south as the Fitzcarrald region also in Peru (~10°3'S, Fig. 6.1) (Salas-Gismondi *et al.* 2006, Antoine *et al.* 2007, Bianucci *et al.* 2013, Boonstra *et al.* 2015). Altogether, these extensions account for approximately 1,900 and 2,200 km, respectively, from the Caribbean Sea. The Fitzcarrald arch only uplifted during the Pliocene (Mora *et al.* 2010), in contrast with other late Miocene uplifts (e.g. Iquitos arch, Roddaz *et al.* 2005), so older sediments are probably still buried in the Fitzcarrald area and that explains the lack of early Miocene marine fossils in this area. Moreover, very likely a further marine incursion during the late Miocene reached

as far south as Bolivia (Uba *et al.* 2009). In this case, there should be no physical barrier for either of the marine incursions allowing constraint of their geographical extension during the Miocene. Hence the north-south axis was of the same proportions in all events.

Eastern limit of the marine reach?

Core 105-AM is the easternmost locality where evidence exists for marine incursions in the Pebas system. Maps of the geographical extension of the marine reaches tend not to overpass this area (e.g. Boonstra *et al.* 2015). Two arguments can be used to support this observation. First, the overall morphology of the Solimões/Pebas deposits exhibits decreasing thicknesses eastward (Chapter 4, Fig. 4.6, Maia *et al*. 1977, Silva-Caminha *et al.* 2010, Latrubesse *et al.* 2010). In Northern Peru (Wesselingh *et al.* 2006b) and Acre region (Maia *et al.* 1977), boreholes reached over a thousand metres whereas in the eastern and north-eastern parts of the Pebas system, boreholes reached the basement with less than 200 metres (Hoorn 1993). This configuration represents a migrating depocentre, which is typical of foreland basin systems like western Amazonia (DeCelles and Gilles 1996), and in this case is an east-migrating depocentre. Therefore, with deeper areas westward, it is plausible to assume that full marine incursions would reach preferentially the deeper areas and marginally the eastern parts. The second argument is that two middle-late Miocene cores studied by Silva-Caminha *et al.* (2010) in the Solimões Formation did not contain any marine elements. Cores 1-AS-19-Am and 1-AS-27-AM are 100 to 220 km, respectively, east of the 105-AM core (Fig. 5.6). Sampling effort or methodological differences related to laboratory processing of palynological samples could explain the lack of marine elements in these cores, otherwise they provide good evidence of the geographical limits of the marine incursions.

Effect of tectonics and sea level change

Western Amazonian basins evolved in direct response to Andean uplift. The Andes have uplifted since the late Cretaceous (Martin-Gombojav and Winkler 2008, Roddaz *et al.* 2010, Hoorn *et al.* 2010), but mountain building peaked in the Neogene. The exhumation history of north and central Andes has been revealed by Apatite Fission Track analysis (Hoorn *et al.* 2010) and it shows three main uplift waves: at the Oligocene-Miocene boundary (~23 Ma), at the late Miocene (~12 Ma), and during the Pliocene (~4.5 Ma). During uplift, accommodation space was created in the forelands, which resulted in pronounced subsidence during the Neogene, including the Pebas wetland system. Vast areas of western Amazonia have altitudes of up to 120 m. For example, all 84 CPRM/Petrobrás cores (Figs. 1.2 and 5.6) were drilled in localities ranging from 70 to 120 m over an area of ~13,000 km^2. The record presented here (~18.7 to 10.7 Ma) lies between the two first peaks in uplift (~23 to 12 Ma) and notably it goes across the second and strongest of them at ~12 Ma. This accelerated uplift during the late middle and late Miocene led to higher elevations in the Andes (~2,000 m a.s.l.) and as a result rainfall increased in the eastern flank causing abundant water and sediment supply to the sedimentary foreland basins (Uba *et al.* 2007, Poulsen *et al.* 2010, Hoorn 1993).

Concomitant with the tectonic and sedimentary history in western Amazonia, sea level was also fluctuating. Estimates of sea level evolution are contentious. Some estimates show high uncertainty when using global ocean basin dynamics for proxies (e.g. Müller *et al.* 2008). Others rely on sedimentary records (Haq *et al.* 1987, Miller *et al.* 2005), while other authors apply mathematical models linking sea level to ice volume and temperature derived from oxygen isotopes (De Boer *et al.* 2010) to explain sea level fluctuations. The majority of estimates agree that during the period studied here sea level was higher than present (Fig. 6.6 and references therein). Assuming the rather low gradient topography from western

Amazonia to the oceans and higher than present sea level, it is evident marine incursions could reach the studied sites without great difficulties. A precise comparison is not possible to make because of sea level estimate discrepancies and also due to the lack of an error estimation in the age model used for cores 105-AM and Saltarin. Nevertheless, it is interesting to see that basically the entire record of the wetlands including marine incursions takes place during high sea stands, that the most pronounced sea level rises happen during the late early and early-middle Middle Miocene and this parallels the longest and strongest marine incursion in the Llanos basin, eventually reaching western Amazonia (Fig. 6.6). Although still high, late middle and early late Miocene sea levels dropped, but at this time a peak in uplift renews foreland sedimentary dynamics that can explain the marine incursion in the Llanos and the paralleled freshwater/brackish megalake interpreted for western Amazonia (FW3; Fig. 6.6).

Vegetation

The terrestrial palynomorph assemblage clearly shows humid tropical conditions throughout the entire studied period (Fig. 6.2). The dominance by pollen of grasses, aquatics, palms and other trees (Fig. 6.2, Fig. 6.5) is indicative of floodplains, marshes and surrounding *terra firme* forests. The suite of aquatics, palms, grasses and sedges can be interpreted as swamps and marshes (also known as *chavascal*), this is especially the case of abundant palm species *Mauritiidites* (=*Mauritia*/*Mauritiella*) that tend to form palm swamps (*buritizal*). Grasses, sedges and aquatic plants are also typical of *chavascal* (Junk and Piedade 1997). The combination of abundant grasses with *Ranunculacidites* (=*Alchornea*) is typical of primary succession communities establishing in sand bars and overbanks of *várzeas* (Wittmann *et al.* 2010). These are replaced by secondary or later succession communities represented by some palms, *Bombacacidites* spp (Bombax trees), and other trees like *Retitrescolpites*? *irregularis*

(=*Amanoa*), whose most widely distributed species is typical of *várzea* and riparian forests (Secco *et al.* 2014), *Ilexpollenites* (=*Ilex*) that can be found in late succession *várzeas* (Wittman *et al.* 2010) and *Ladakhipollenites*? *caribbiensis* (=*Sapium*) from both late succession *várzeas* and *terra firme*. Palms combined with other trees also point to *terra firme* forests. The high abundance of ferns can be derived from both floodplains and *terra firme* communities where they tend to be rather abundant in the understory, slopes and near streams (Hopkins 2005, Costa *et al.* 2005, Zuquim *et al*. 2008). In general, pollen is sourced from the nearby flooded systems like *várzeas*, marshes and palm swamps. Besides, the many woody taxa point to contribution from non-flooded forests (*terra firme*) as well. A high number of pollen taxa with unknown affinities (ca. 68% of the pollen species, or 17% of the pollen sum) was composed of tricolporate, reticulate or other ornamentations - such morphologies are more common among woody groups than herbs (Bush *et al*. 2004), so the proportion of trees should be higher than was estimated. A common aspect of tree communities in Amazonia is a strong skewed abundance distribution (ter Steege *et al.* 2013), with a very high proportion of low abundance and rare taxa. This is seen in the pollen spectra under study.

Tha range of forms that were linked to an extant botanical group (Appendix table 9.2) gives confidence to the vegetation reconstruction attempted. Affinities established in most cases are genus-specific (e.g. *Mauritia*, *Alchornea*, *Sapium*, *Crematosperma*, *Aspidosmperma*, *Geissospermum*, *Macoubea*, *Ilex*, *Shcefflera*, *Euterpe*, *Korthalsia*, *Humiria*, *Bombax*, *Catostema*, *Ceiba*, *Pachira*, among many others). Family-level affinities like Arecaceae, Poaceae, Melastomataceae, Cyperaceae, Moraceae, and others, when in association with each other or specific ecological groups (e.g. aquatics) do not leave much room for uncertainty regarding their parental biomes. Therefore, in spite of not complete, the botanical affinity list procuded is confidently robust for paleoenvironmental interpretations.

Poaceae pollen attained high abundances (Fig. 6.5), and is essentially represented by one species, *Monoporopollenites annulatus*, which is a family-level morphology. Although Poaceae can be dominant in open vegetation types like savannahs (e.g. central Brazilian cerrados, Salgado-Laboriau 1979), there are reasons to believe the pollen spectra here identified has no affinitiy with dry environments. First, the lack of a diverse herbaceous community is evidence that no other biome was installed in the area - Poaceae has a bipolar palynological signal and its use as openness (and aridity) indicator is questionable (Bush 2002) and only indicated when associated with other herb groups (Absy *et al.* 2014). When not indicating aridity, Poaceae pollen in high abundances is an evidence of marshy vegetation, primary succession or floating meadows that are rather common in Amazonian rivers nowadays and other Neotropical lakes and wetlands (Absy 1979, Bush 2002, Gosling *et al.* 2009). This interpretation agrees with the overall picture of vast wetlands covering western Amazonia in the early and middle Miocene. Higher Poeaceae counts were observed towards the top of section 105-AM (Fig. 6.5), this can be explained by thicker and more frequent sand deposits (Fig. 2.1) that document fluvial channels that in turn procude bars and creat room for the establishment of pionner and early successional vegetation, that has a dominant grass cover.

Overall, the entire pollen sequence here analysed shows a continued presence of tropical humid-warm conditions. Pollen taxa indicative of open or dry-wooded habitats (like wooded savannahs) were not identified. Although without thorough analytical approaches, other pollen records in the region are in agreement with the data presented presently as they do not show any evidence for floristic changes during the Miocene (Hoorn 1993, 1994a, 1994b, Silva-Caminha *et al.* 2010). A detailed floristic comparison should be performed in order to assess geographical homogeneity of plant associations across inundations. This,

however, will require a much better taxonomic consistency amongst palynologists, who should aim to unify taxa and thus increase among-site comparability.

Presence of mangrove is well defined by spikes of the pollen *Zonocostites ramonae* (=*Rhizophora*). Hoorn (2006) found a dominance of this species in three sections in the Apaporis river area (25 to 85% of the pollen sum) near Mariñame (Fig. 6.1). Other localities with comparable spikes of *Zonocostites* are Tres Islas and Santa Isabel, also in the Mariñame area. Other occurrences of this taxon are given by Hoorn (1994a, 1994b) but with lower amounts (~10% or less in Mariñame, Pijuayal and Los Chorros, and rare in Iquitos, Santa Teresa, Mocagua and core 4a-AM). An early Miocene age can be safely given to Mariñame, Tres Islas, Santa Isabel and core 4a-AM. A late early to middle Miocene stage is proposed to all other localities (see age correlations in Chapter 5). In core 105-AM the only spike of *Zonocostites* is in the early Miocene (MF1) at ~18.4 Ma, what would be in agreement with abundance spikes in early Miocene sequences at Mariñame, Tres Islas and Santa Isabel. In the middle Miocene there are rare to moderate abundances of mangrove pollen in this area, with no spike having been recorded. Given the abundance pattern discussed above, it can be inferred that large areas of mangrove developed during the early Miocene in the region of southern Colombian, western Brazilian and northeast Peruvian Amazonia, but probably spread for a much larger geographical area. Mangrove during the middle Miocene is also suggested but less clear, it is probable that mangrove occurred in other areas of western Amazonia and *Zonocostites* pollen reached the depositional sites mentioned above through water or wind transportation instead of being locally present. This would explain low abundances to rare occurrences where otherwise the taxon attains remarkable spikes.

A striking result found here is that nearly no variation in the vegetation can be explained by the flooding phases whether they are brackish or marine (CCA, Table 6.1). A methodological bias regarding the over-dominance of one environment over the others cannot

account for this result as half of the duration (3.94 Ma or 49.25%) of the studied record is non-inundated. Some imprecision in this interpretation could still exist given that the geographical extent and depth of each freshwater inundation are very hard to estimate. It still is remarkable that marine phases did not affect the vegetation structure at all, except of course by leading to short phases of mangroves. This resilience of the forest can be explained by the marginal character of the studied section. As discussed above, the westernmost part of the Solimões Formation was less affected by the inundations than other parts of the Pebas system. In a landscape context, this translates into a higher proximity of broad areas of *terra firme* forest to the Pebas systems. These *terra firme* forests were installed in central and eastern parts of the Solimões basin, in drainage areas whose rivers ran westwards into the Pebas system. If locally extirpated, forests could regain their composition and structure from the surrounding species pool that was readily available to recolonize drying inundated areas. A stabilising trend of plant communities has been seen in glacial-interglacial cycles in higher latitudes (Clark and McLachlan 2003, Blarquez *et al*. 2014), somewhat comparable to the western Amazonia inundation dynamics. In both, ecosystem divergence does not seem to exist with passing time but stabilisation, thus reinforcing the suggestion of a resilient forest that expands back to its original extent in a short temporal scale (few millennia) when either temperature or habitat/ecosystem is propitious. This idea can also be supported by ecotonal areas bordering Amazonia, where forest re-expanded with ameliorating climatic conditions of the Holocene (Absy *et al*. 1991, Mayle *et al*. 2000). The results found are not surprising given the marginal nature of core 105-AM - a detailed pollen record in a more central part of the Pebas system would be desired to more carefully address the question of whether plant communities are affected by inundations or not.

6.4. Conclusions

The palynomorph assemblage retrieved from core 1-AS-105-AM (18.7 to 10.7 Ma) in western Amazonia revealed vast extensions of wetland, megalakes and marine incursions coming from the Caribbean. This period is referred to as the Pebas system and evolved in response to Andean tectonics and had impacts from seal level fluctuations. Two pronounced marine phases were identified based on dinocyst spikes at 18.4 - 17.8 and 14.1 - 13.7 Ma, they were relatively rapid (0.58 to 0.37 Ma, respectively) and did not affect forest structure and composition, at least not in the marginal areas of the Pebas system. All evidence from dinocyst ecology points to assemblages adapted to shallow waters, coastal areas like estuaries and mangroves in an overall equatorial setting. Indeed, mangroves developed in the early Miocene (~18.4 Ma) and probably during the middle Miocene, as evidenced by *Rhizophora* pollen. The intervening landscape was composed of marshes, floodplains, *terra firme* forests and freshwater lakes with eventual brackish conditions. The brackish conditions are interpreted from dinocysts that point to connection of large areas and therefore megalake conditions. The Pebas system extended from southwestern Amazonia to the Llanos Basin in Colombia where marine incursions were longer and stronger during the same studied period.

Chapter 7: Plant diversity across the Mid Miocene Climatic Optimum in western Amazonia

7.1. Introduction

The origin of the highly diversified Neotropical forests is a topic hotly debated in the literature. Megathermal, angiosperm-dominated biomes may have existed since the mid Cretaceous ~100 Ma in South America (Davis *et al.* 2005), but it is from the late Paleocene (~58 Ma) of north-western South America that fossils assigned to modern plant groups give us the best picture as to when the Neotropical forest structure and diversity first developed (Wing *et al.* 2009). A modern composition of the forest at the family level has remained relatively stable since the early Paleogene (Ricklefs and Renner 2012), which means tropical forests have existed for at least 60 Ma. Throughout this time, the Neotropics have acted as a cradle for species, where speciation and extinction happen rapidly (Antonelli *et al*. 2015). To the best of our knowledge, these originations and extinctions appear not to be random, but positively correlated with temperature (Jaramillo *et al.* 2006, 2010b). That has been the case at least from the Paleocene to early Miocene. Plant diversity as measured by pollen data shows bursts of in diversification during warm phases and, conversely, reductions in species diversity during cooling periods like the onset of Oligocene glaciations ~34 Ma ago (Jaramillo *et al.* 2006). This relationship of temperature and diversification has been used to empirically demonstrate an underlying driver of speciation in tropical forests (i.e. temperature) and to show that these forests have undergone considerable warming without collapse of the ecosystem.

This seemingly direct link between climate and diversity has not, however, been demonstrated for the Neogene period (23-2.5 Ma). Pollen data from the Llanos of Colombia (Hoorn *et al.* 2010) and from western Amazonia (Jaramillo *et al.* 2010a) reveal no apparent

changes of diversity that can be related to climate. An exception might be the recently published pollen record in Panama, where there is an increase in richness from early to late Miocene (Jaramillo *et al.* 2014). Unfortunately a temporal gap covering part of the early and mid-Miocene as well as taphonomic issues related to lithofacies prevent a more detailed picture of when the diversity increase happened. Regardless of change or stability in the Neogene records mentioned above, a more comprehensive study of plant diversity during this period of time is completely lacking in northern South America, including the Amazon forest.

The objectives of this chapter are to describe the pollen diversity (here used as number of species) in core 1-AS-105-AM and to test if there are significant changes of pollen richness across the Mid Miocene Climatic Optimum (MMCO, Zachos *et al.* 2001, 2008), and across the marine incursions already detected (see chapter 6). The studied section constitutes a very good model for the intended analysis since (i) it has a constant and linear accumulation in an overall homogeneous continental environment, (ii) is well sampled, and (iii) it spans the period from 18.7 to 10.7 Ma (see chapter 5) and therefore captures the time before, during and after the MMCO. The full methods applied in this chapter can be found in Chapter 3.

The Miocene climate

The Neogene world is characterised by a long term cooling punctuated by a warming phase (Zachos *et al.* 2001, 2008). Early Miocene (23-16 Ma) global temperature gradually cooled, but at ca. 17 Ma a transient warming event is superimposed on this general cooling trend and lasted until ca. 14 Ma. This 3 Ma period is known as the Mid Miocene Climatic Optimum (MMCO) and temperatures could have risen ~3 to 4 Celsius degrees compared to today (Zachos *et al.* 2001, You *et al.* 2009, Goldner *et al*. 2014). This warming is the last significant one in the planet's geological history and can be compared to modelled late 21st century scenarios (ca. 3°C by 2100, IPCC 2014), hence being a possible analogue for future

climate change, although warming rates were in the millennial-million year scale rather than decade-century scale as presently. Proceeding this warming stage, temperatures cooled down gradually in what is known as the Mid Miocene Climatic Transition (MMCT), when the whole planet got colder and glaciations intensified in the northern hemisphere. Global vegetation responded to this climatic evolution by expanding and compressing biomes in high latitudes (Pound *et al.* 2012). In western Amazonia, vegetation for the period comprised in the MMCO and MMCT is characterised by wetlands, floodplains and evergreen upland forest (*terra firme*) (Hoorn 1993, 1994a, 1994b, Silva-Caminha *et al.* 2010), with no evidences for biome changes. Many important constituents of the present day Amazon lowland plant diversity were already in place during the Miocene (Cuenca *et al.* 2008, Meerow *et al.* 2009, Dick *et al.* 2013).

7.2. Results

Ninety five samples were analysed for their pollen and spores content. From those, 70 were chosen for the diversity analysis as they had pollen counts of at least 226. This ensured samples utilized had a similar size and thus biases related to sample size could be avoided (Fig. 7.1.a). A further three samples were excluded because they clearly were evenness outliers (Fig. 7.1.b), such samples have a hyperdominance by one or two taxa and as a result diversity measurements are largely biased. This procedure guaranteed a fair comparability of sample regarding diversity metrics.

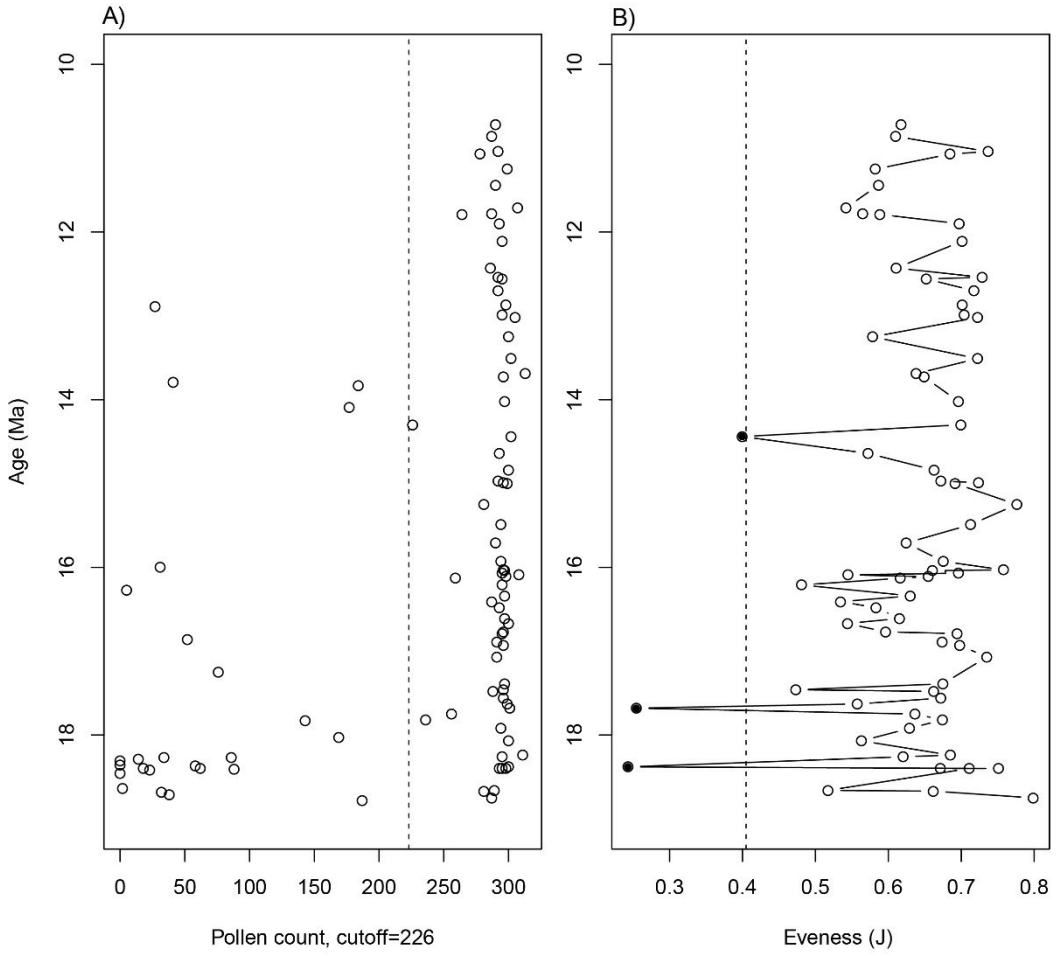

Figure 7.1. A) Pollen counts for the initial 95 samples plotted against age, dashed line is cut off of 226. B) Evenness for the 70 samples chosen for diversity analysis, dashed line is a threshold of 0.4 J below which samples were removed from data set (three solid symbols), number of remaining samples is 67.

Within-sample diversity and ecological ordination

Within sample diversity metrics display an evident pattern of increasing values at ca. 16 Ma (Fig. 7.2. a and b). Rarefied diversity and H' diversity increased 46.8% and 20%, respectively. This diversity increase is accompanied by an even stronger community change at the same age as measured by the ecological ordination (Fig. 7.2. c and d). The DCA results (Table 7.1) reveal that axis one is responsible for most of the variation, totalling 40.3%. Axis two is responsible for 26.8%; however, a good part of this variation is caused by the position of the bottom three samples while the great majority of samples orbit a similar value (Fig. 7.2.c) and there is no significant variation of scores before and after 16 Ma (w=568, p-value=0.9). Hence the exploration of variations is focused on axis one, which indeed accounts for a 70% change from pre to post 16 Ma. Across marine incursions there are no apparent changes in neither diversity nor community scores. In fact, the effect of inundations on plant composition is negligibleor completely undetected (see Chapter 6).

Table 7.1. Summary results of Detrended Correspondence analysis (DCA). Percentages in bold are how much variation each axis explains.

	DCA1	DCA2	DCA3	DCA4
Eigenvalues	0.2263 (**40.3%)**	0.1503(**26.8%**)	0.09987(**17.8%**)	0.08388 (**14.9%**)
Decorana values	0.2309	0.1682	0.08906	0.06850
Axis lengths	2.2032	2.3556	1.30600	1.66649

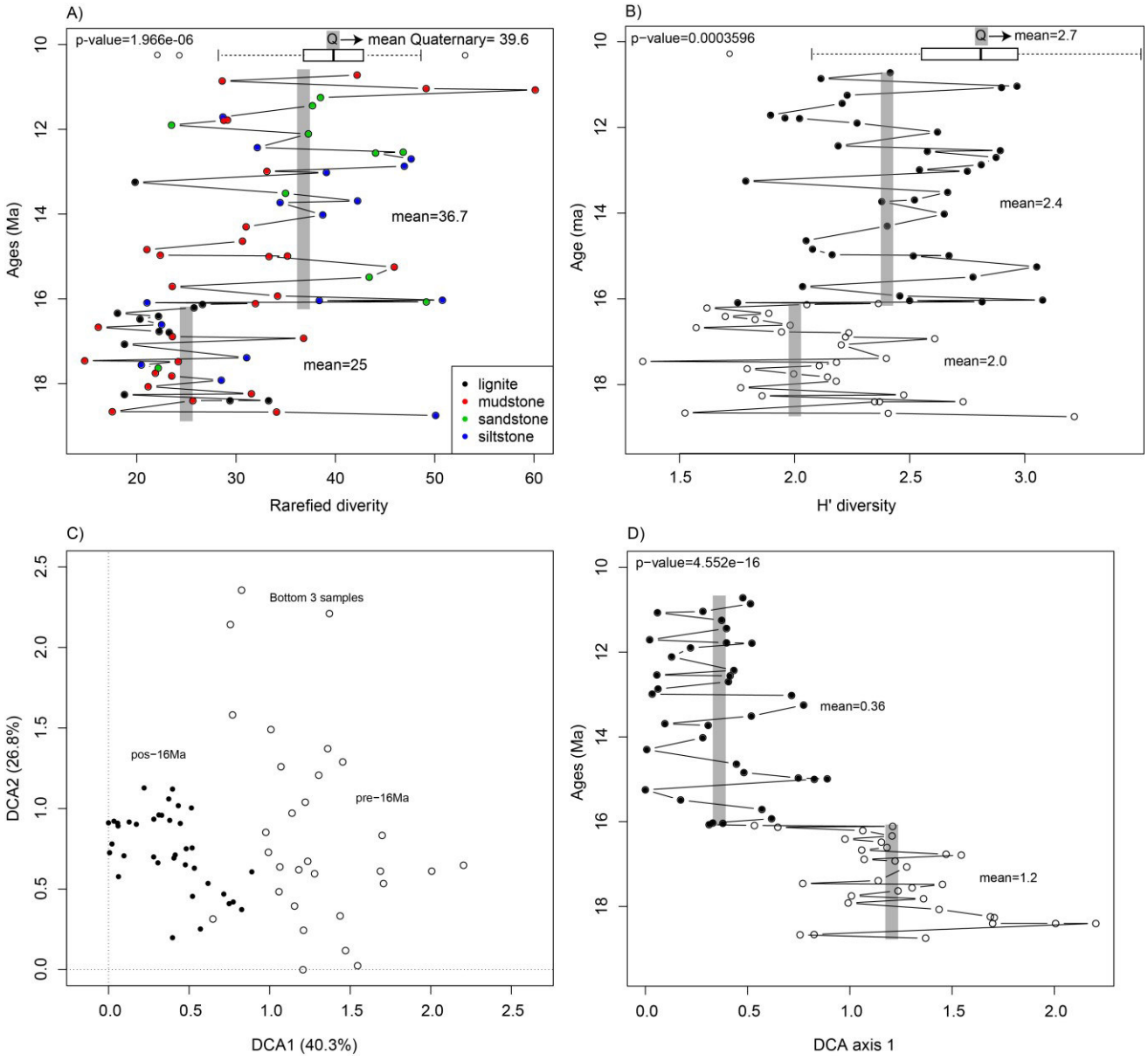

Figure 7.2. A) Rarefied diversity, lithology of samples is colour coded. B) Shannon (H') diversity. C) Detrended correspondence analysis (DCA, Table 7.1) plot of axis 1 and 2, open symbols are samples older than 16 Ma, solid symbols are samples younger than 16 Ma. D) DCA axis 1 scores plotted against time. For all plots: grey bars are mean values for groups pre and post 16 Ma, p-values refer to Mann-Whitney U tests.

Potentially taphonomic biases

An analysis of variance was performed in order to test the effects of strata (age) and lithology on the diversity and ecological metrics. The ANOVA results (Table 7.2) reiterate the significant differences of all diversity and ecological metrics when older (strata >16 Ma) and younger (strata <16 Ma) ages are compared. The ANOVA also shows no significant differences in evenness, thus confirming abundances distributions of taxa are not affecting diversity estimates differentially. What is more, there is a clear effect of lithology on all metrics, but no iteration between lithology and strata was found (Table 7.2). A closer inspection on what generates these significant differences of lithology on the analysed metrics was carried out with a Tukey test (results are summarised in Appendix Table 9.3.4), and the main driver of such results is lignite. Samples of lignite have lower diversities and higher DCA axis one scores than other lithologies (Fig. 7.3). This could be caused by a real underlying vegetation signal, as sediments are capturing the very local vegetation signal, i.e. the immediate surroundings only rather than a larger catchement are - since lignites are formed from peats that accumulate in bogs, marshes and swamps and therefore they tend to be representative of local plant communities (Traverse 2007, Jardine and Harrington 2008). Another issue with the lignites in the present study is that they are concentrated on the lower part of the section and are not distributed evenly in time. Similarly, sands are concentrated in the upper part of the section (Fig. 7.2.a). These distinctions in lithology distribution over the core can be problematic and bias the results as depositional systems may differ and not be evenly represented throughout the core. In order to tackle this, the complete analysis was re-run firstly excluding lignites, and secondly excluding both lignites and sands. This way, a more isotaphonomic subset of the data could reveal if the pattern of diversity increase and community change at 16 Ma is real or a product of taphonomy. The results of these analyses can be seen in Fig. 7.4, they show that all significant differences are maintained when lignites

and sands are removed from the data set. Also, invariably the bottommost sample is a high diversity outlier for the pre-16 Ma stage, and when excluded from the data the differences are even more significant (Fig. 7.4). Furthermore, when siltstones and sandstones are combined (38.8% of the data set) and analysed, they also retain the previous patterns: for rarefied (W=112, p=0.006914) and H' diversity (W=105, p=0.02547), and for DCA axis 1 (W=1, p <0.0001). When only mudstones are analysed (43% of the total data set) the pre and post 16 Ma groups are significant with regard to rarefied within-sample diversity (W=157, p=0.0196) and DCA axis 1 (W=143, p=8.841e-07) but not H' diversity (0.09161).

Table 7.2. Summary results of analysis of variance to test the effect of lithology and strata (age) on diversity, evenness and DCA axis 1 scores. Lithologies tested were lignite, mudstone, siltstone and sandstone; Strata tested were older (pre-16Ma) and younger (post-16Ma). For the Shapiro-Wilk normality test, p-values > 0.05 mean that the null hypothesis (that the data are normally distributed) cannot be rejected, thus the normality assumption was met for the ANOVA.

		Df	Sum sq	Mean sq	F value	Pr(>F)	Shapiro-Wilk
Rarefied diversity	Lithology	3	12.61	4.203	7.739	**0.000192*** **	[1]W=0.97246 p=0.1429
	Strata	1	7.43	7.431	13.685	**0.000477*** **	
	Lithology:strata	3	1.77	0.591	1.089	0.360957	
	Residuals	59	32.04	0.543			
H' diversity	Lithology	3	1.757	0.5856	4.147	**0.00983** **	W=0.99312 p=0.9738
	Strata	1	0.930	0.9301	6.586	**0.01283***	
	Lithology:strata	3	0.271	0.0903	0.639	0.59280	
	Residuals	59	8.332	0.1412			
Evenness	Lithology	3	0.01339	0.004462	0.882	0.448	W=0.97861 p=0.3017
	Strata	1	0.00831	0.008311	1.643	0.205	
	Lithology:strata	3	0.00714	0.002379	0.470	0.704	
	Residuals	59	0.29842	0.005058			
DCA axis 1	Lithology	3	1.9034	0.6345	13.005	**1.26e-06*** **	[1]W=0.97648 p=0.2341
	Strata	1	3.0204	3.0204	61.909	**9.14e-11*** **	
	Lithology:strata	3	0.0924	0.0308	0.631	0.598	
	Residuals	59	2.8784	0.0488			

Signif. codes: 0 '***' 0.001 '**' 0.01 '*' 0.05 '.' 0.1 ' ' 1

[1]square-rooted

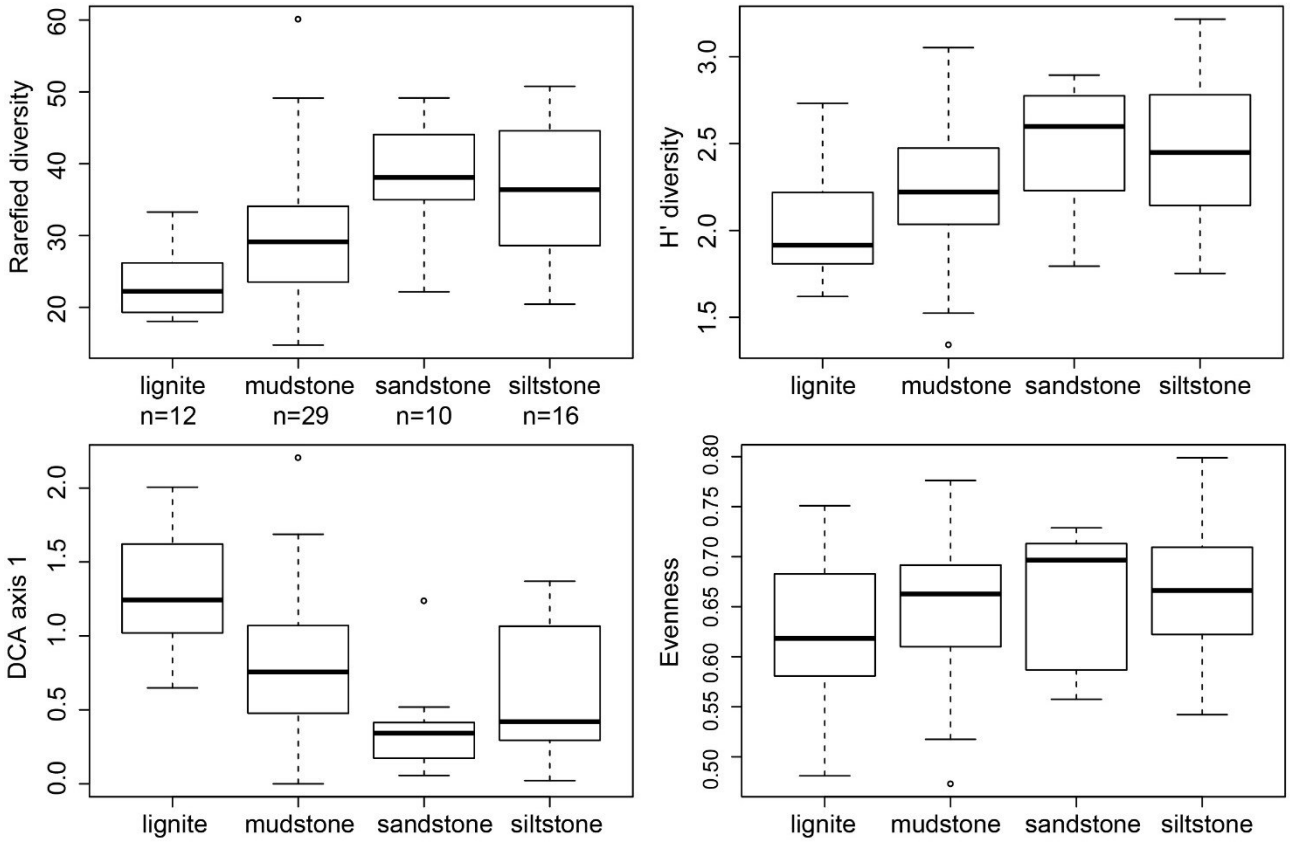

Figure 7.3. Boxplots of diversity metrics, DCA axis 1 scores and evenness for each individual lithology (details of ANOVA in Table 7.2).

Among-sample diversity

Among sample estimates agree with the overall results of the within sample estimates, although with some discrepancies. The following comparisons are at a sample pool of 31 as this is the total number of samples of the smaller group (pre-16Ma). The expected species richness for the rarefaction curves increased 18.3%, from 229 before 16 Ma to 271 after 16 Ma (Fig. 7.5.a). Chao2 estimator increased 14%, from 442 to 504 (Fig. 7.5.b) and Jackknife2 increased 11.4%, from 420 to 468 (Fig. 7.5.c). Except rarefied curves, Chao2 and Jackknife2 display confidence bands that overlap between older and younger groups, implying there is no significant difference of the expected number of species at a comparable sample pool (Fig. 7.5). A remarkable result seen in these estimates is the overall number of species for each

technique used. Because there are many rare taxa in the studied samples and because Chao2 and Jackknife2 estimators weigh singletons and doubletons differentially from common taxa, the total expected richness given by these estimators is greater (ca. twofold) than that given by rarefaction. When the total expected richness is compared between each group, Chao2 yielded 442 and 575 and Jackknife2 yielded 420 and 507 species pre and post 16 Ma, respectively. These results compared are significantly different (Chao2: W=685, p=0.007633; Jackknife2: W=638, p=0.04577). Taking all the above together, there is a weaker evidence, but nevertheless detectable, for higher taxonomic diversity between samples of the younger group (post 16 Ma) than of the older group (pre 16 Ma) than the evidence from these group's within sample estimates.

Standing diversity

The piecewise regression performed with LAD and FAD data resulted in ages of 18.24 Ma for FAD and 11.25 for LAD (Fig.7.6.a). This means that there is a considerable edge effect for originations older than 18.24 Ma and for extinctions younger than 11.25 Ma. Standing diversity, origination and extinction rates are then limited to the interval between these ages. The standing diversity curve (Fig. 7.6.b) has a "D" shape, i.e. increasing at the bottom and decreasing at the top, this is an indication that an edge effect is still present. Taking this into account, it is still noticeable that the maximum standing diversity is reached at 13.7 Ma with 169 taxa. This is explained by consistently higher originations than extinctions up to ca. 13.9 Ma (Fig. 7.6.c).

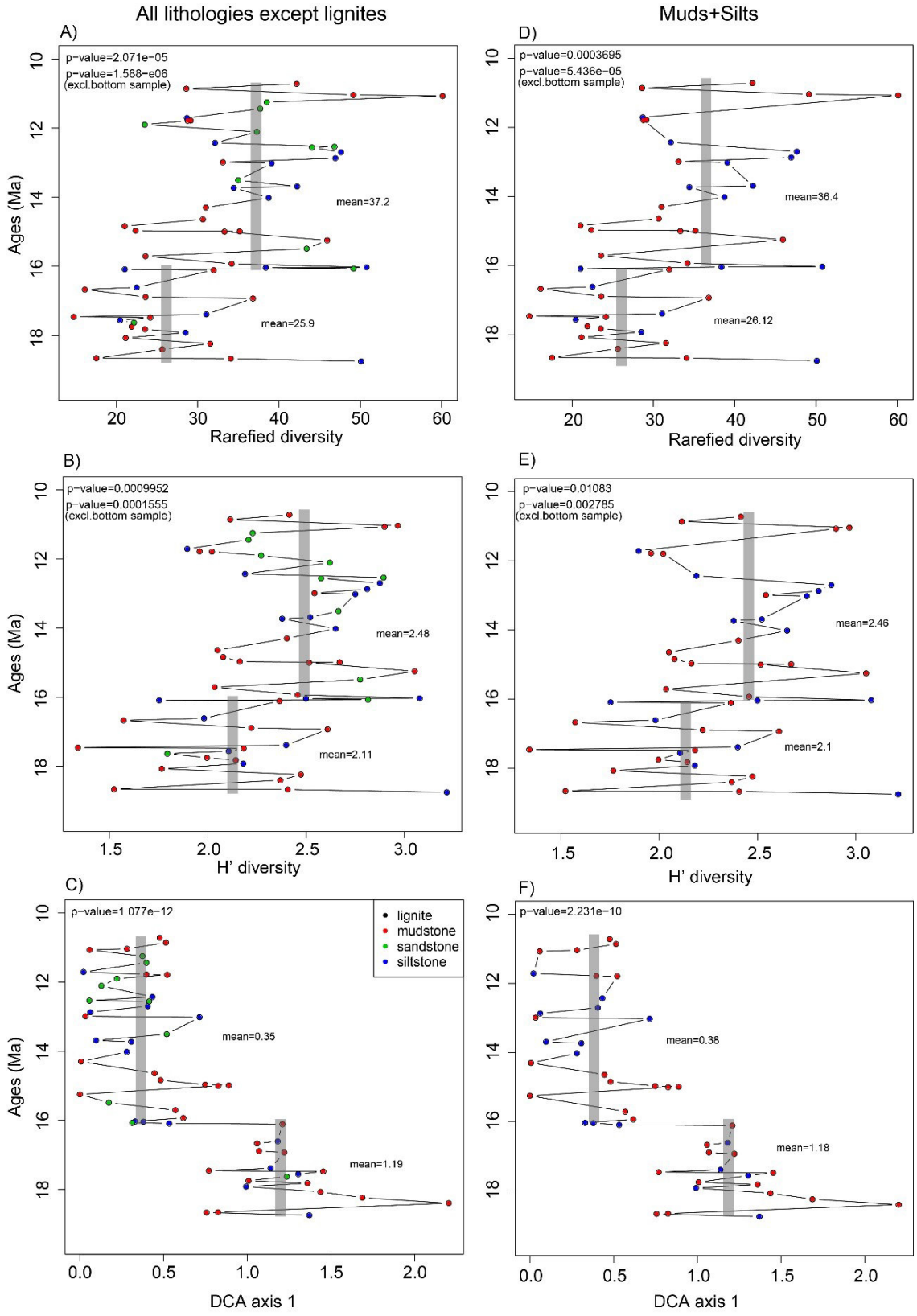

Figure 7.4. Plots of rarefied diversity (A), H' diversity (B) and DCA axis 1 (C) for data set excluding lignites, and for data set formed of muds and silts only (D, E and F). For all plots: grey bars are mean values for groups pre and post 16 Ma, p-values refer to Mann-Whitney U tests.

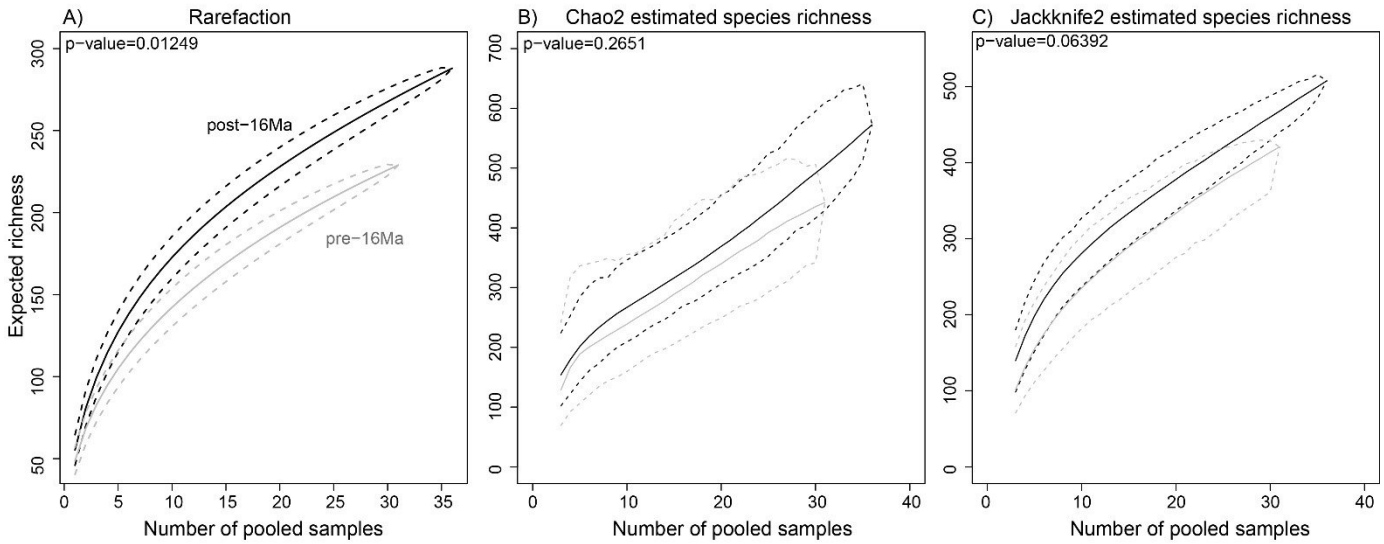

Figure 7.5. Among sample diversity estimates using rarefaction (A) and richness estimators Chao2 (B) and Jackknife2 (C). p-values refer to Mann-Whitney U tests run at a sample pool of 31 samples.

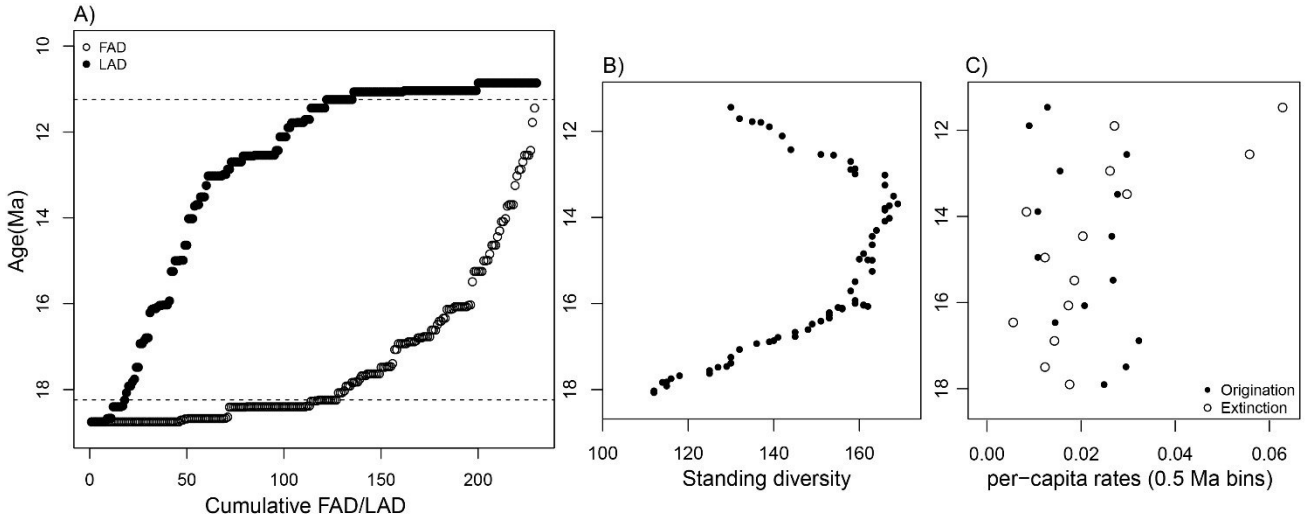

Figure 7.6. A) Cumulative FAD and LAD data plotted against time. Dashed lines are the breakpoints from the piecewise regression used to estimate the edge effect for FAD (18.24 Ma) and LAD (11.25 Ma). B) Standing diversity calculated after range-through assumption of taxa. C) Per-capita rates of origination and extinction in 0.5 Ma bins.

Evolutionary models

Data was binned at every 0.5 Ma and time series analysis run. Unbiased random walk (URW) models fitted the data best. For rarefied diversity, URW is the best model when the full data set is used and also when lignite is excluded (Table 7.3), but in the latter case stasis is a non-negligible model (A.W. of 0.301). When only muds and silts samples are used the rarefied diversity data is fitted best for URW and stasis with similar weights. This is also the case for all data sets used for model fits of H' diversity, although for the full data set there is a non-negligible generalised random walk (GRW) model fit (A.W. of 0.242). These results reflect a nearly complete lack of directionality for diversity over time, but it is clear there is considerable variation. The picture gets more evident for models fitting DCA axis 1 scores, where regardless of the data set used GRW greatly outperforms other models. This indicates a strong directionality of the plant community. All in all, composition changes more significantly than did richness (compare model fits for diversity x DCA in Table 7.3). The evolutionary models are partially confirming the results from the diversity and ecological metrics, but with the main difference that a trajectory in diversity dynamics is not clear and the reason for this is probably a higher variation of the data post 16 Ma than pre 16 Ma.

Table 7.3. Summary of model fits to diversity and ordination metrics for pollen data. K: number of model parametres; AICc: corrected Akaike Information Criterion; A.W.: Akaike Weight; GRW: Generalised random walk; URW: Unbised random walk. Best fits in bold, non-negligible in italic.

			Rarefied diversity		H' diversity		DCA axis 1	
Data	Model	*K*	AICc	A.W.	AICc	A.W.	AICc	A.W.
Full data	GRW	3	112.2393	0.174	8.337407	*0.242*	7.106912	**0.866**
	URW	2	109.4623	**0.699**	7.441643	**0.379**	10.848010	0.133
	Stasis	2	112.8731	0.127	7.441643	**0.379**	25.046422	0.000
Excl. lignites	GRW	3	114.6744	0.135	10.481275	0.196	6.799147	**0.848**
	URW	2	111.8078	**0.565**	9.045207	**0.402**	10.237425	0.152
	Stasis	2	113.0683	*0.301*	9.045207	**0.402**	22.630638	0.000
Muds + Silts	GRW	3	102.58017	0.098	11.050310	0.152	7.938299	**0.848**
	URW	2	99.49092	**0.460**	9.000112	**0.424**	11.389083	0.151
	Stasis	2	99.57422	**0.442**	9.000112	**0.424**	20.840422	0.001

Comparison between Miocene and extant diversity

The four Lateglacial-Holocene cores yielded 75 samples above the cut-off count of 226 grains. Evenness was comparable to Miocene samples (mean J=0.71 and minimum J=0.5), therefore further sample removals were unnecessary. A total number of 237 taxa was found. Mean rarefied diversity was 39.6 (22.3 to 53.2) and H' diversity was 2.7 (1.7 to 3.5). These numbers are higher than middle Miocene values (rarefied: W=1057, p=0.041; H': W=705, p <0.0001) and much higher than early Miocene ones (rarefied: W=138, p <0.0001; H': W=214, p <0.0001) (Fig. 7.2).

7.3. Discussion

The pollen flora of western Amazonia studied here revealed a pattern of richness increase at 16 Ma. Although with high variation (Fig. 7.2a and b), diversity of the post-16 Ma period has a consistent increase of ca. 39 to 46% in the rarefied within-sample diversity, and of ca. 18% in the among-sample diversity (and of ca. 11 to 14% when using Chao2 and Jackknife3 estimators, but potentially more if errors are taken into account). Quantifying the amount of richness increase is not straightforward, but the pattern is evident. This increase in diversity is paralleled by a noticeable shift in the community data (Fig. 7.2c and d, and results of the time series analysis in Table 7.3). Together, both the diversity and community structure seem to occur in a rather sharp fashion. The overall change at ~16 Ma can be explained by a higher number of taxa being restricted to the post 16 Ma period than to the pre 16 Ma (Fig. 7.7). A total of 50 taxa only appear after 16 Ma, whereas 31 go extinct before 16 Ma. Furthermore, amongst the singletons, 92 are restricted to the post 16 Ma period, and 51 to the pre 16 Ma period. Altogether, post 16 Ma restricted taxa account for 35% of the total assemblage, a number that is similar to the within-sample rarefied diversity increase (ca. 39

to 46%). The great majority of the taxa (64%, singletons excluded), however, range through the entire or great part of the record. Another aspect that reinforce the difference between taxa before and after 16 Ma is the longer ranges of taxa after 16 Ma than pre 16 Ma. That translates into a rather discrete standing diversity of the pre 16 Ma restricted assemblage when compared to the post 16 Ma restricted assemblage (Fig. 7.7). It seems therefore that extinctions (or emigrations) are playing are minor role in causing the diversity and community change than are originations (or immigrations). In fact this can be seen in the origination/extinction per capita rates, which show higher originations across the MMCO and up to ~13.9 Ma (Fig. 7.6).

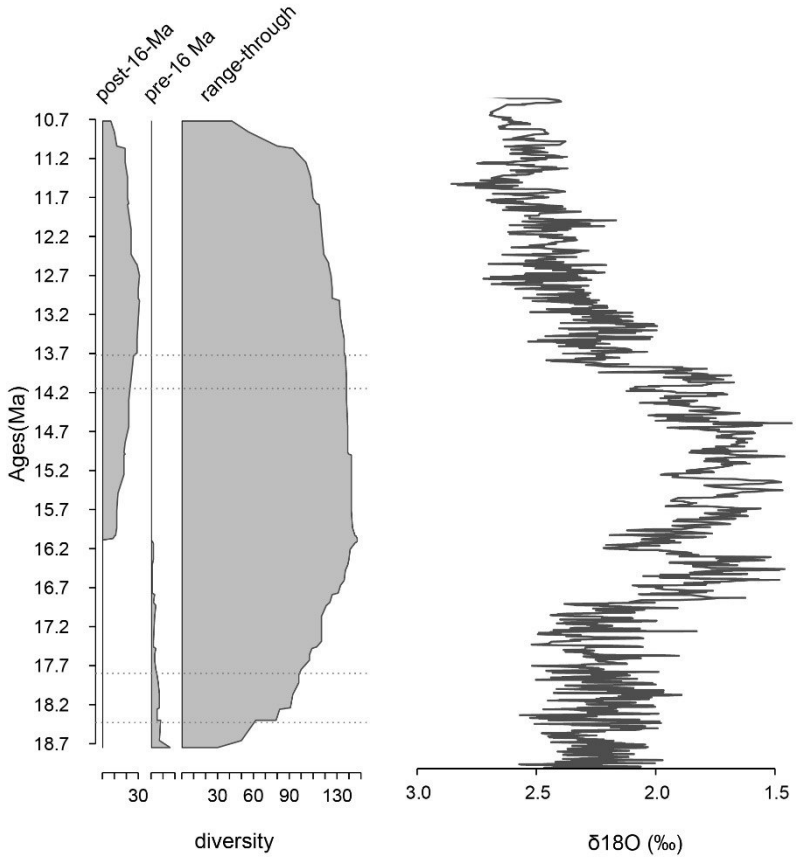

Figure 7.7. Left: Standing diversity for groups of taxa restricted to the period pre and post-16 Ma, and for those ranging-through. Right: Oxygen isotope curve of Zachos *et al*. (2001).

The observed changes in the pollen record are coincident with the beginning and duration of the MMCO (Fig. 7.7), thus suggesting a link between the climatic warming and the pollen record. Other variables do not seem to have a detectable effect on diversity and community, like for instance the inundations (see chapter 6) or taphonomic biases (see results). A statistical artefact exists regarding the edge effect (Foote 2000), however this does not affect within-sample diversity estimates or multivariate scores. Furthermore, after partially controlling for the edge effect (piecewise regression), there is still a consistent trend of higher originations than extinction which overlaps with the duration of the MMCO.

A relationship between plant communities and climate has been broadly reported for the Cenozoic of northern South America (Jaramillo *et al.* 2006, 2010b). Increases in plant diversity take place during warming periods, reminiscent of what is reported here. This relation is more robust for the Palaeogene and lower Neogene (early Miocene), but had only been suggestively shown for the remaining Miocene period, including the MMCO span (Hoorn *et al.* 2010, Jaramillo *et al.* 2014). The data reported here on diversity increase (see results) can now confirm this pattern in detail. Interestingly, the standing diversity of pollen shown by Hoorn *et al*. (2010) peaks at an age of 13 Ma, what is quite similar to the reported herein (13.7 Ma). The data used by Hoorn *et al.* (2010) comes from the Llanos region (Fig. 1.2) approximately 1,000 km from core 105-AM, hence the positive diversity response to the MMCO event is potentially synchronous in a wide geographical area. This area could be even wider if the Panama Miocene data presented by Jaramillo *et al.* (2014) is confirmed. The latter shows the similar significant diversity increase from early to late Miocene, but further studies are needed to understand when exactly this increase takes place. All these examples plus the present study agree with the idea that warmings do affect tropical forests by prompting diversification. Mechanisms underlying speciation are still obscure, they could be

related to latitudinal expansion of the tropical forests during warmer periods (Fine and Ree 2006, Fine *et al.* 2008, Morley 2000) what would lead to richer species pools due to the species-area relationship (Rosenzweig 1995) (but see Jaramillo and Cardenas 2013). Other mechanisms invoke increased metabolic rates in the tropics due to higher energy inputs and consequentially increased mutation rates (Rohde 1992, Wright *et al.* 2006). Another set of ideas contends that organisms in warm environments have accelerated biotic interactions (Dobzhansky 1950, Vermeij 2003, Schemke *et al.* 2009), which leads to stronger pressures in niche occupation and in turn to speciation. Regardless of the mechanisms driving diversification, a response by the forest to increased temperatures is clear. During the MMCO, with an estimated ~3-4°C increase (You *et al*. 2009, Goldner et al. 2014), Amazon forests could have experienced MAT of up to 30.5°C (assuming a present MAT of 27.5°C). This value lies within maximum tolerance of tropical plants (Krause *et al*. 2010), hence a dieback due to heat intolerance can be ruled out. Actually, molecular data for many widespread Neotropical tree species show they already existed during warmer periods, namely the late Miocene (Dick *et al*. 2013). Much stronger warmings during the Palaeogene were not able to destabilize tropical forests, they actually increased diversity (Jaramillo *et al.* 2010b). Moreover, apart from temperature a key factor defining vegetation structure is precipitation (Woodward 1987). During the Miocene in western Amazonia all evidence points to very humid conditions, including molluscan isotopic data that points to a similar seasonal monsoonal system controlled by the Inter Tropical Convergence Zone as it is presently (Kaandorp *et al.* 2005). In terms of CO_2, another constraining factor for plant growth (Taiz and Zeiger 2015), estimates for the MMCO period are controversial with either similar, lower or much higher than present (e.g. Royer and Beerling 2011). Some of these estimates are two to three times present day values (for instance Kürschner *et al*. 2008, Beerling *et al*. 2009, Retallack 2009, Zhang *et al*. 2013). Increased CO_2 can stimulate water

use efficiency and overall plant performance (Lloyd and Farquhar 2008, Cernusak *et al.* 2011). Given that in western Amazonia water was not a limiting factor, higher temperatures and CO_2 can therefore be expected to promote favourable conditions for plant development. Paralleled to this favourable physiological conditions there is a dynamic system in a wide geographical area. Largescale flooding potentially fragmented the forest that would in turn reconnect during lower water tables. This process probably varied in intensity both in time and space, so plant species had the constant opportunity of habitat re-colonisation. The combination of niche dynamics with favourable climatic-physiological conditions during the MMCO resulted in diversification of the plant communities.

A long debate has permeated evolutionary biology of tropical ecosystems – are the tropics a cradle or a museum of diversity (Stebbins 1974, Jablonski *et al*. 2006)? A current view is that the dichotomy be abandoned as evidence places the tropics in both cradle and museum scenarios (Jablonski *et al*. 2006). Antonelli *et al*. (2015) showed that for plants the Neotropics have higher rates of both originations and extinctions when compared to other tropical areas, implying that a more rapid turnover during geological time explains the higher Neotropical diversity. The data presented here agrees with this interpretation. There is a degree of correlation (~35%) between originations and extinctions (see Fig. 7.8), showing a tendency for turnover of the plant community. These dynamics cannot be fully explained by originations and extinctions as they could naturally be immigrations and emigrations in the present study due to the short interval analysed and limited geographic coverage (one borehole only). To solve that question a high number of sites, covering a broad geographical area are needed in order to understand the biogeographical histories of the species found herein. Nonetheless, it is striking that both molecular and distributional (Antonelli *et al*. 2015) and fossil pollen data from western Amazonia have a certain similarity concerning patterns of origination/extinction. The Palaeogene data of Jaramillo *et al*. (2010b) also

showed an increase in extinction in the same time bin that originations attain the highest rate (during the PETM interval), which is similar to the relationship suggested by the current data (Fig. 7.8). In both cases there is a net increase in the total pollen diversity, therefore demonstrating that although there is species replacement (turnover), the final output is a richer assemblage across warming intervals. This proposes the possibility of Neotropical forests in acting as both cradles and museums of biodiversity.

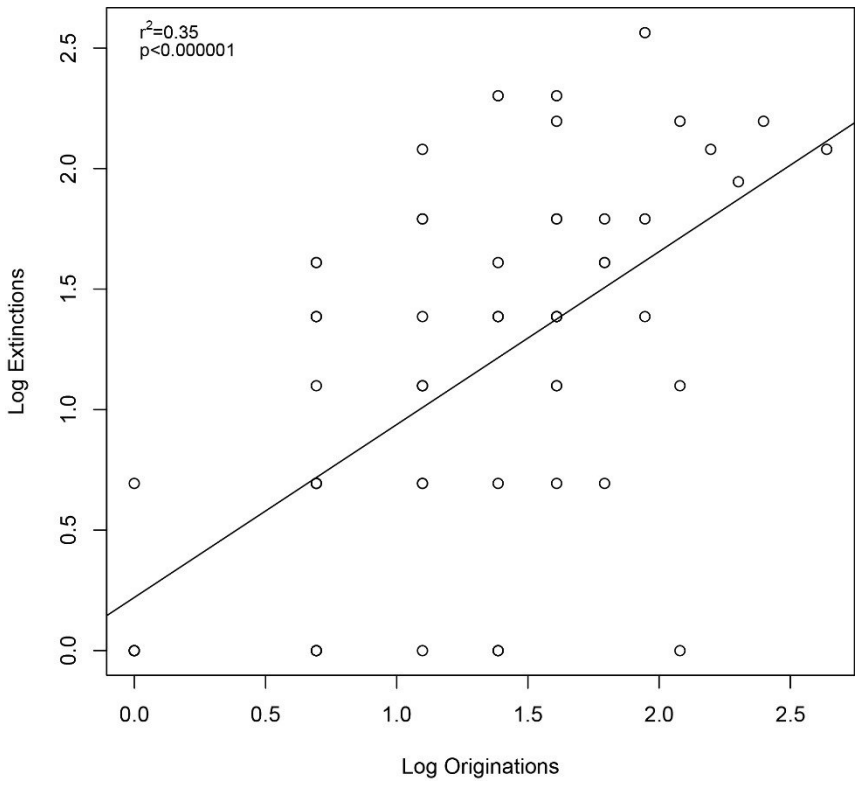

Figure 7.8. Originations and extinction display a certain degree of correlation. Data used is restricted to samples below and above the edge effect (see Fig. 7.6), singletons excluded.

Finally, the Miocene vs. extant (Holocene) comparison showed a richer pollen assemblage at the present time. The very same result had been seen by Jaramillo *et al*. (2006), who stated that diversification should have occurred from early Miocene to present in order to produce a richer extant assemblage. The authors hypothesised that it was the MMCO event that triggered such speciation. This is in full agreement with the present data and also

potentially in line with other studies (Hoorn *et al*. 2010, Jaramillo *et al*. 2014). Van der Hammen and Hooghiemstra (2000), however, claimed the contrary, that the Miocene was more species rich than the present day. They posited this after comparing Holocene with Miocene sediment samples from a similar area (Caquetá River, Hoorn 1994b) and seeing 280 pollen types in the Miocene and 140 in the Holocene. This comparison is nevertheless not possible as the time interval between samples in Holocene and older (e.g. Tertiary) sequences varies vastly (see for instance Wing 1998, Harrington and Jaramillo 2007). With a much longer interval between samples (Miocene) more species can accumulate and therefore the final species pool is richer than when only a few thousand years are comprised between samples (Holocene). A preferable comparison was done here, using the rarefied within-sample estimates that significantly showed a richer extant diversity (Fig. 7.2). Clearly, more fieldwork effort and taxonomic work must be done to improve the comparability of Miocene and extant samples. Howsoever, assuming the diversity trend depicted above it is unexpected that for the remaining period from the late middle Miocene to Pliocene the overall temperature-diversity relationship is not shown (Hoorn *et al.* 2010) as opposed to the rest of the Tertiary. Why did not diversity decrease during cooling periods from the middle Miocene Climatic Transition (MMCT) to the Quaternary (Fig. 1.1)? One possibility is that diversification outweighed extinctions when plant communities invaded the drying Pebas system. By the late Miocene, western Amazonia started to dry out as a consequence of Andean uplift (Wesselingh 2006, Figueiredo *et al*. 2009, Hoorn *et al*. 2010, Sacek 2014), and by the early Pliocene wetland areas had completely vanished (Latrubesse *et al*. 2010). With the demise of inundation, western and eastern parts of Amazonia could reconnect. Plant groups were then able to take advantage of newly formed land ecosystem and colonise or recolonise them. That is the case, for instance, of speciose families Rubiaceae (Antonelli *et al*. 2009) and Arecaceae (Roncal *et al*. 2013). These new land areas were as well uplifting

and exposing sediments very rich in cations that are nowadays reflected in consistently nutrient richer soils in western Amazonia than in eastern parts, not to mention edaphic heterogeneity (Wesselingh and Salo 2006). This difference has a direct influence in plant composition (Higgins *et al*. 2011) and translates into more diverse western forests (ter Steege *et al*. 2006, Hoorn *et al*. 2010).

8. CONCLUSIONS

Palynological analysis of cored sediments from western Amazonia was presented from 95 samples. The intensive taxonomic work from core 1-AS-105-AM from the Solimões Formation in NW Brazil (Chapter 2) yielded 491 different types of pollen, spores, algae, dinoflagellate cysts, acritarchs and foraminiferal linings. Remarkable is the high diversity of pollen and spores that accounted for 402 types. Of these, 76 pollen and 25 spores species were formally described as new (Chapter 4). In addition, 14 formal species from the literature were re-described in new combinations because they had originally been assigned into incorrect form-genera.

The wealth of palynomorphs in the core, meta-analysis of other palynological data from the Amazon region, and well-preserved mollusc shells in some horizons, permitted an age assignment significantly better than previous ones for the region (Objective 1.4.1). First and last appearance events of key taxa were used to perform a Graphic Correlation with a nearby pollen zonation. This zonation (Jaramillo *et al*. 2011, and unpublished results) has a calibration that allowed age assignments for individual samples via interpolation (Chapter 5). The results of this exercise were an age span from 18.7 to 10.7 Ma (late early to earliest-late Miocene) for the studied core. Furthermore, critical comparisons and reassessments of previously published pollen records from western Amazonia supported an age for the entire Solimões Formation and its lateral equivalents (Pebas Fm) of early Miocene to Pliocene. Morphology and local structural controls on the deposits of the Solimões Formation were also discussed and linked to foreland dynamics as a result of the Andean orogeny.

The combination of a more detailed age model proposed for core 105-AM when compared to previous studies (e.g. Hoorn 1993, 1994a, 1994b, Silva-Caminha *et al*. 2010) with a higher sampling resolution and excellent palynomorph recovery permitted an

improved palaeoenvironmental description for the early and middle Miocene in western Amazonia (Chapter 6, Fig. 8.1). By using presence and also relative abundance data of marine elements (dinocysts, foraminiferal linings and acritarchs) two major events of marine incursions into western Amazonia were established (Objective 1.4.2). The first occurred between 18.4 and 17.8 Ma, and the second between 14.1 and 13.7 Ma. The timing and duration for these events is the best estimate so far for the long known marine incursions in the region. Freshwater lake phases were also established in three main periods and they possibly had a minor brackish character as well.

Throughout the whole studied period, vegetation type does not change and consists of typical humid tropical forest elements. A series of statistical analyses were used to test the effect of inundation events and climate evolution on the diversity and structure of the forest (Chapters 6 and 7, Fig. 8.1). Interestingly, inundations had no detectable effect on the composition or structure of the forest as measured in the fossil pollen associations (Objective 1.4.3). This was interpreted as resilience of the forest. The exception is a short period where mangroves developed during the early Miocene. Diversity metrics, however, did show a change from lower to higher diversity at ca. 16 Ma (Objective 1.4.4). This increase occurs during the Middle Miocene Climatic Optimum, when temperature may have risen ca. 3-4° C degrees (You *et al*. 2009, Goldner *et al*. 2014), and it is concluded that this warming event drove diversification. This idea builds on previous records showing a close relationship between plant diversity and temperature in the equatorial humid forests (Jaramillo *et al*. 2006) that had not yet been properly tested for the Miocene period.

Finally, the results and discussions of the present thesis have both regional and wider implications. Regionally, the age model of core 105-AM can help improve the overall biostratigraphical framework. There is still substantial work to be undertaken, but with a more detailed age model such as the one presented here, future studies can build upon it to

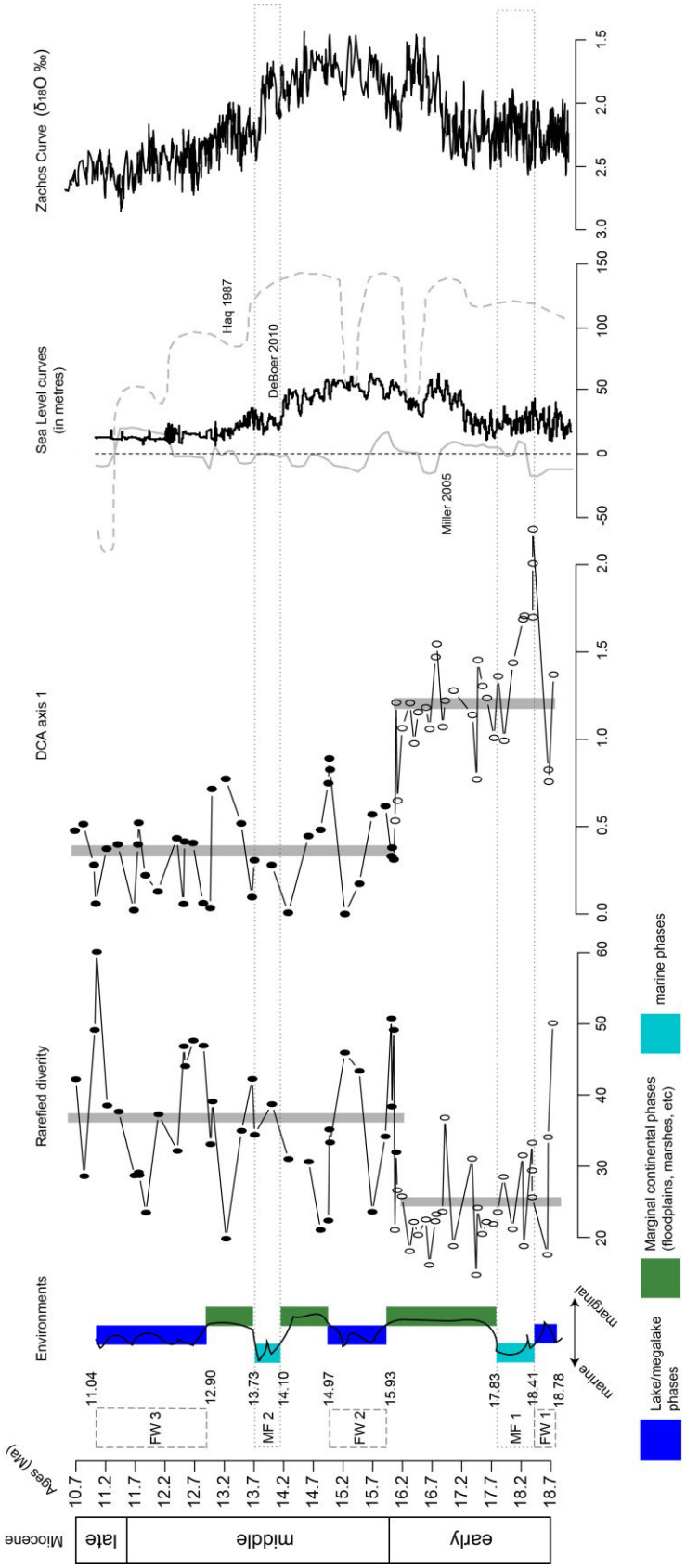

Figure 8.1. Summary schematic diagram with environments, diversity metrics from core 1-AS-105-AM, and independent global measures of sea level and temperature. Marine inundation events (MF1 and MF2) do not coincide with plant community change and diversity increase.

formulate biostratigraphical hypotheses and gradually improve the use of marker taxa in western Amazonia during the Neogene. At a broader scale, studies of diversification processes of various Amazonian organisms can more precisely incorporate the timing and duration of events described herein into their hypotheses. For instance, many aquatic groups entered and adapted to Amazonian waters from the Caribbean Sea (e.g. river dolphin, Hamilton *et al*. 2011). Do dated molecular phylogenies coincide with the inundations events? Does the appearance of certain plant and animal groups in different sites of Amazonia happen before, in-between or only after inundation events? What is the relationship between migration/speciation and the evolution of the Pebas system? These and many other questions can be asked and use the present work as paleogeographical hypotheses. Moreover, climate modellers can incorporate with more detail the lake/marine phases into climatic models of the Neogene, with potential global effects.

9: Appendixes

Tables 9.1. List of LAD and FAD events used in the graphic correlation (Chapter 5), Line of Correlation (LOC) equations and R functions used to derive composite units and ages.

9.1. a). Events of well 1-AS-105-AM and Composite units (CU) from the composite section of Jaramillo *et al*. (2011). FL EM= Early Miocene Flooding, FL MM = Middle Miocene Flooding; species with " " are informal and were added to the composite section from an initial correlation between well Saltarin and the composite section (see Appendix Table 9.1. b).

Event	CU_FAD	FAD105	CU_LAD	LAD105
Areci regio	-19960	-370.3	-1960.1	-30
Bomba araracuarensis	-9108.92	-161.7	-1471.46	-39.8
Bomba baculatus	-9777.74	-325.3	-817.278	NA
Bomba brevis	-18009.4	-324.9	-204.935	-69.8
Bomba muinaneorum	-14393.6	-370.3	-717.273	-35.4
Bomba nacimientoensi	-18335.1	NA	-2602.8	-35.4
Byttn "rugulata"	-9498.44	-110.7	-2256.62	-35.4
Camar "trilobatus"	-2630.87	-35.4	-2212.21	-35.4
Cicat baculatus	-4228.02	-130.1	-4104.23	-130.1
Cicho longispinosus	-5492.8	-165.5	-866.39	-30
Clava microclavatus	-11226.7	-324.6	-102.468	-30
Crass columbianus	-15916.2	NA	-316.93	-39.8
Crass vanraadshooven	-8823.06	-360.9	-1960.1	-34.6
Cribr sp.	-21405.9	-284	-9391.73	-284
Croto annemariae	-18077.2	-267.9	-2597.95	-110.7
Croto reticulatus	-9398.7	-359	-2323.64	-30
Cteno suigeneris	-16076.7	-359	-2163.46	-34.6
Cyclu scabrata	-18077.2	-370.3	-7393.37	-370.3
Echid barbeitoensis	-5194.03	-105.5	-4061.78	-70.5
Echin muelleri	-17465.6	-267.9	-817.278	NA
Echip akanthos	-16427.3	NA	-102.468	NA
Echip estelae	-17606.1	-370.3	-1161.15	NA
Echip intectatus	-2660.24	-272.1	-2660.24	-34.6
Echip jutaiensis	-3966.69	-230.2	-1874.4	-35.4
Echip lophatus	-4126.67	-289.9	-1874.4	NA
Echit mcneillyi	-0.6	-101.2	-573.818	-34.6
Echit spinosus	-8663.71	-324.9	-102.468	-34.6
Erici annulatus	-2522.91	-69.8	-2212.21	-35.4
FL EM	-9535.84	-293.3	-8511.18	-284
FL MM	-5342.95	-101.2	-3959.46	-96.7
Fenes spinosus	-4039.3	-75.3	-174.195	-75.3
Foveo ornatus	-15599.7	-324.9	-1474.08	-34.6
Grims magnaclavata	-9777.74	-326.2	-1874.4	NA

Heter incomptus	-10128.9	-325.3	-174.195	-34.6
Heter rotundus	-4900.76	-326.2	-0.1513	NA
Heter verrucosus	-5492	-289.9	NA	NA
Hydro minor	-5492	NA	NA	NA
Ilexp tropicalis	-9799.83	-324.9	-2212.21	-34.6
Jandu minor	-16778.9	-370.3	-3755.03	-165.5
Jandu seamrogiformis	-16808.2	-284	-1471.13	-35.4
Ladak caribbiensis	-4126.67	-187.6	-2630.87	-34.6
Laevi granulatus	-19177.8	-324.9	-727.52	NA
Lanag crassa	-17590.7	-298.9	-1975.13	-39.8
Lingu machaerophorum	-16835.3	-289.9	-3502.25	-96.7
Longa microfoveolatu	-19875.9	-110.7	-0.0402	NA
Magna grandiosus	-16032.8	-359	-174.195	-34.6
Malva maristellae	-9777.74	-250	-651.906	-34.6
Margo vanwijhei	-17708.5	-370.3	-1471.13	NA
Mauri franciscoifra	-19722.9	-370.3	-286.75	NA
Mauri franciscoimin	-18917.8	-325.3	-0.1513	NA
Mauri franciscoipac	-19482.1	-76.7	-3995.93	-69.8
Monop annulatus	-19904.9	NA	-71.7273	NA
Multi vanderhammenii	-5001.31	-267.9	-789	-30
Nijss fossulatus	-10419.3	-289.9	-758.26	-34.6
Parso brenacii	-3930.96	-298.9	-0.6	-44.7
Perfo digitatus	-17454.6	-298.9	-924.7	-34.6
Peris pokornyi	-17038	NA	-0.1513	NA
Polya mariae	-4173.47	-298.9	-2522.07	-44.7
Polyp planus	-9636.79	-210.1	-1878.11	NA
Polyp pseudopsilatus	-14176.4	-155.1	-143.455	-35.4
Polyp sp.	-19913.1	-324.9	-0.0402	-34.6
Polyp specious_aff	-17818.7	-360.9	-1317.26	-34.6
Polyp usmensis	-16304.6	NA	-789.04	NA
Prote triangulatus	-14548.2	-370.3	-1878.11	-30
Proxa tertiaria	-19987.8	-370.3	-563.571	-34.6
Psila devriesii	-17963.1	NA	-1471.13	-79.9
Psila fissilis	-18346.2	-298.9	-1962.39	NA
Psila garzonii	NA	-298.9	NA	-35.4
Psila herngreenii	-9129.27	-359	-3852	-53
Psila marinamensis	-7393.37	-359	-4390.81	-35.4
Psila minimus	-16849.4	-294.5	-0.4	-120.9
Psila nanus	-16116.9	-359	-917.984	-69.8
Psila obesus	NA	-230.2	NA	NA
Psila redundantis	-16720	-325.3	-14354.3	-39.8
Psila silvaticus	-9334.42	NA	-1878.11	-30
Psila triangularis	-17815.1	-299.3	-1021.17	-79.9
Pteri gemmatus	-17815.1	-254.3	-174.195	-91.5
Quadr condita	-9432.78	-298.9	-3236.33	-52.9
Quaternary	-1415	-20	NA	NA

Ramon	-5958.74	-405	-5733.06	-330
Ranun operculatus	-16685	-370.3	-0.4	NA
Retib retibolus	-19961.8	-210.1	-1975.13	NA
Retib yavarensis	-15549.9	-182	-1960.1	-161.7
Retim absyae	-5437.47	-283.2	-3221.87	-30
Retis crassiannulatu	-16711	-325.3	-1474.08	-75.3
Retit caputoi	-16116.9	-326.2	-1947.27	-79.9
Retit crassicostatus	-4647.01	-125.3	-4647.01	-44.7
Retit irregularis	-17816.1	-370.3	-0.1047	NA
Retit kaarsii	-14637.3	-359	-1894.29	-39.8
Retit lorenteae	NA	-272.1	-1330.73	NA
Retit magnus	-17963.1	-53	-15604	-53
Retit simplex	-18066.4	-370.3	-543.078	-140.9
Retit traversei	-7393.37	-44.7	-2335.18	-44.7
Rhoip guianensis	-18066.4	NA	-1317.26	NA
Rugut arcus	-9432.78	-30	-2212.21	-30
Rugut felix	-17038	-325.1	-0.4	-91.5
Silta dilcheri	-16116.9	-267.9	-3223.84	-39.8
Solimoes	-5733.06	-330	-1415	-20
Spiro spiralis	-18077.2	-250	-1471.13	-44.7
Stria anastomosatus	-3742.15	-324.9	-3223.84	-34.6
Stria catatumbus	-17817.3	-165.5	-789.04	NA
Stria poloreticulatu	-9777.74	-364.8	-0.1513	NA
Stria saccolomoides	-16169.7	-155.1	-563.571	-35.4
Tuber vancampoae	-9411.42	-293.3	-1894.29	-96.7
Verru etayoi	-16114.7	-324.3	-2490.5	-51.6
Verru rotundiporus	-14964	-26.35	-1317.26	NA
Zonoc ramonae	-17372.7	-370.3	-817.278	-34.6

9.1. b). Events of well Saltarin and Composite units (CU) from the composite section of Jaramillo *et al*. (2011). FL EM= Early Miocene Flooding, FL MM = Middle Miocene Flooding; species with " " are informal. Leon and Guayabo are Formations in the Llanos basin.

Taxa	**FAD_CU**	**FAD_Salt**	**LAD_CU**	**LAD_Salt**
Bomba araracuarensis	-9108.92	-518.94	-1471.46	-144.15
Bomba baculatus	-9783.12	-659.93	-817.278	-396.22
Bomba baumfalki	NA	-657.3	-3812	-575.38
Bomba brevis	-18009.4	NA	-204.935	-167.65
Bomba muinaneorum	-14393.6	-662.33	-717.273	-372.38
Bomba nacimientoensi	-18335.1	-396.22	-2777.9	-167.35
Brevi microechinatus	-18314.3	-612.76	-15024.1	-372.38
Byttn "rugulata"	-4540.11	-644.25	-3721.8	-99.53
C1	-9026.57	-608.2	-5453.74	-546.9
C2	-9728.67	-654.6	-9026.57	-608.2

C3	-10506.2	-671	-9728.67	-654.6
Camar "trilobatus"	-3721.8	-172.85	-3721.8	-90.83
Cicho longispinosus	-5492	-550.43	-866.39	-90.83
Clava densiclavatus	-19906.5	-628.61	-10548.9	-406.95
Clava microclavatus	-11226.7	-622.78	-102.468	-90.83
Corsi psilatus	-19944.5	-548.24	-0.1513	-145.35
Corsi undulatus	-17604	-636.8	-0.0402	-99.53
Crass columbianus	-15916.2	-659.93	-316.93	-169.77
Crass vanraadshooven	-10056.7	-622.78	-1960.1	-172.85
Crico guianensis	-19893.8	-638.33	-15878.6	-145.35
Crico macroporus	-17708.5	-622.78	-12096.5	-622.78
Croto annemariae	-18077.2	-657.3	-4093.51	-166.4
Croto reticulatus	-10042.1	-640.65	-3683.21	-112.66
Cyath annulatus	-2661.24	-178.8	-81.974	-90.83
Cyclu scabrata	-18077.2	-641.88	-7393.37	-612.76
Echim gracilis	-16849.4	-178.8	-16068	-167.65
Echim solitarius	-17496.1	-386.52	-16450	-112.66
Echin muelleri	-17465.6	-644.25	-817.278	-90.83
Echip akanthos	-16427.3	NA	-102.468	-112.66
Echip estelae	-17606.1	-523.9	-1161.15	-203.77
Echip lophatus	-9303.38	-430.82	-1874.4	-409.52
Echit "microechinatu	NA	-520.35	NA	-143.07
Echit acanthotrileto	-14764.6	-641.88	-4385.34	-97.29
Echit spinosus	-9780.04	-523.9	-102.468	-90.83
Echit trianguliformiorb	-17598	-372.38	-16068	-372.38
Echit variabilis	-17603.8	-543.38	-15750.4	-90.83
Erici annulatus	-4000.24	-151.7	-3721.8	-90.83
FL EM	-9411.42	-645.6	-9215.71	-619.75
FL MM	-4388.72	-547.18	-4298.46	-408.56
Fenes spinosus	-4039.3	-422.69	-174.195	-99.53
Foveo ornatus	-15599.7	-417.55	-1474.08	-90.83
Grims magnaclavata	-9790.03	-659.93	-1874.4	-99.53
Guayabo	NA	-441.8	NA	NA
Heter incomptus	-10128.9	-550.43	-174.195	-114.92
Heter rotundus	-9790.03	-529.95	-0.1513	-86.3
Horni lunarensis	-18498.1	-638.33	-10294	-622.78
Ilexp tropicalis	-9780.04	-662.33	-3716.09	-90.83
Jandu minor	-16778.9	-662.33	-4399.63	-372.38
Jandu seamrogiformis	-16808.2	-657.3	-1471.13	-101.35
Ladak caribbiensis	-6063.63	-430.82	-3591.72	-172.85
Laevi granulatus	-19177.8	-548.24	-727.52	-143.07
Lanag crassa	-17590.7	-657.3	-1975.13	-97.29
Leon	-5453.74	-546.9	-3893.7	-441.8
Lingu machaerophorum	-16835.3	-413.49	-3502.25	-413.49
Longa microfoveolatu	-19875.9	-657.3	-0.0402	-278.37
Lumin colombianensis	-16755.3	-543.38	-16194	-144.15

Magna grandiosus	-16032.8	-659.93	-174.195	-99.53
Malva maristellae	-9091.86	-659.93	-651.906	-97.29
Malva spinulosa	-15785.1	-657.3	-4408	-99.53
Margo vanwijhei	-17708.5	-622.78	-1471.13	-184.33
Mauri franciscoifra	-19722.9	NA	-286.75	NA
Mauri franciscoimin	-18917.8	-662.33	-0.1513	-144.15
Monop annulatus	-19904.9	-659.93	-71.7273	-90.83
Multi vanderhammenii	-9011.84	-539.77	-789	-90.83
Nijss fossulatus	-10419.3	-537.29	-758.26	-143.07
Pachy diederixi	-3115.55	-654.97	-3047.95	-654.97
Palae cingulatus	-3905.37	-435.01	-1945.49	-90.83
Parso brenacii	-9621	-167.65	-0.6	-144.15
Perfo digitatus	-17454.6	NA	-924.7	-145.35
Perin reticuloacicul	-19979.5	-586.7	-102.468	-145.35
Peris pokornyi	-17038	NA	-0.1513	-97.29
Polor absolutus	-18441.7	-101.35	-16102.8	-101.35
Polya mariae	-9621	-166.4	-2522.07	-166.4
Polyp echinatus	-18586	-539.77	-17563.8	-539.77
Polyp planus	-7004.07	-650.29	-1878.11	-376.26
Polyp sp.	-19913.1	-657.3	-0.0402	-90.83
Polyp usmensis	-16304.6	-662.33	-789.04	-112.66
Polys subtile	-16867.7	-510.03	-817.278	-510.03
Prote dehaani	-20458.8	-586.7	-19732.2	-174.98
Prote triangulatus	-14548.2	-586.7	-1878.11	-99.53
Proxa operculatus	-19976.7	-619.75	-817.278	-396.22
Pseud perfectus	-17538.9	-650.29	-15999.2	-650.29
Psila devriesii	-17963.1	-575.38	-1471.13	-97.29
Psila fissilis	-18346.2	-659.93	-1962.39	-433.27
Psila herngreenii	-10042.1	-626.73	-3852	-626.73
Psila marinamensis	-10042.1	-612.76	-3721.8	-455.4
Psila minimus	-16849.4	-144.15	-0.4	-99.53
Psila nanus	-16116.9	-627.36	-917.984	-474.6
Psila pachydermatus	-15521.1	-662.33	-0.0402	-586.7
Psila robustus	NA	-629.9	-14424.2	-86.3
Psila silvaticus	-3898.56	-638.33	-1878.11	-203.77
Psila tesseroporus	-4363.15	-659.93	-2045.22	-659.93
Psila triangularis	-17815.1	-614.35	-1021.17	-101.35
Psila venezuelanus	-16105	-662.33	-4114.9	-99.53
Pteri gemmatus	-17815.1	-520.35	-174.195	-178.8
Quadr condita	-9621	-641.88	-3236.33	-408.56
Ranun operculatus	-16685	-657.3	-0.4	-90.83
Retib retibolus	-19961.8	-638.33	-1975.13	-372.38
Retib triangulatus	-17589	-184.33	-15794	-184.33
Retib yavarensis	-15549.9	-90.83	-1960.1	-90.83
Retim absyae	-9205.58	-549.23	-3683.21	-278.02
Retip crotonicolumel	-4352.09	-510.03	-866.39	-97.29

Retis angeli	-18863.5	-657.3	-16120.8	-396.22
Retis crassiannulatu	-16711	-641.88	-1474.08	-150.63
Retis festivus	-17608.2	-654.97	-16002.9	-654.97
Retit baculatus	-18586	-638.33	-15896.5	-442.42
Retit caputoi	-16116.9	-662.33	-1947.27	-167.35
Retit irregularis	-17816.1	NA	-0.1047	-90.83
Retit kaarsii	-14637.3	-622.47	-1894.29	-167.65
Retit simplex	-18066.4	-659.93	-543.078	NA
Retit sommeri	-15729.8	-548.24	-604.558	-151.7
Retit traversei	-3966.69	-612.76	-3227.58	-114.92
Retit wijningae	-3355.76	-638.33	-3355.76	-638.33
Rhoip guianensis	-18066.4	NA	-1317.26	-90.83
Rhoip hispidus	-18041.9	-659.93	-1471.46	-550.43
Rugut arcus	-4783.7	-641.88	-3683.21	-90.83
Rugut felix	-17038	-637.73	-0.4	-151.7
Scabr planetensis	-15759.5	-650.29	-1351.05	-278.37
Silta dilcheri	-16116.9	-657.3	-3223.84	-278.37
Spiro spiralis	-18077.2	-659.93	-1471.13	-203.77
Stria catatumbus	-17817.3	NA	-789.04	-97.29
Stria poloreticulatu	-10086.6	-659.93	-0.1513	-386.52
Stria saccolomoides	-16169.7	-537.29	-563.571	-90.83
Tetra maculosus	-17625.2	-662.33	-1351.05	-107.94
Tetra transversalis	-18249.3	-662.33	-727.52	NA
Trico clarensis	-18077.2	-644.25	-7790.69	-251.53
Trico finitus	-15878.6	-638.33	-194.688	-403.39
Tuber vancampoae	-9411.42	-468.84	-1894.29	-409.52
Tuber verrucatus	-17815.1	-645.6	-3655.35	-99.53
Venez distinctus	-16867.7	-550.43	-14429.1	-550.43
Verru etayoi	-16114.7	-641.88	-3742.15	-145.35
Verru rotundiporus	-14964	-659.93	-1317.26	-90.83
Verru rugulatus	-17458	-614.35	-10775.9	-372.38
Zonoc ramonae	-17372.7	-645.6	-817.278	NA

9.1. c). Events of wells 1-AS-105-AM and 1-AS-4a-AM (Hoorn *et al.* 1993). FL EM= Early Miocene Flooding, FL MM = Middle Miocene Flooding. Ramón (not confirmed) is the Formation underlying the Solimões Formation; Quaternary is the top section recent deposits.

Taxa	**FAD105**	**FAD4a**	**LAD105**	**LAD4a**
Bomba baculatus	-325.3	-131	NA	NA
Bomba muinaneorum	-370.3	-236.5	-35.4	-59
Bomba nacimientoensi	NA	-236.5	-35.4	-59
Crass columbianus	NA	-273.6	-39.8	-59
Crass vanraadshooven	-360.9	-181.85	-34.6	NA
Croto annemariae	-267.9	-238.6	-110.7	NA
Echip akanthos	NA	-273.6	NA	-34.2

Echip estelae	-370.3	-75.2	NA	-75.2
Echit spinosus	-324.9	-143.1	-34.6	-89
FL EM	-293.3	115	-284	65
Grims magnaclavata	-326.2	-89	NA	NA
Heter rotundus	-326.2	-263.5	NA	-75.2
Malva maristellae	-250	-229.8	-34.6	-34.2
Margo vanwijhei	-370.3	-218.2	NA	-78.9
Multi vanderhammenii	-267.9	-59	-30	-59
Perfo digitatus	-298.9	-272.6	-34.6	NA
Polya mariae	-298.9	-238.6	-44.7	-142.9
Proxa tertiaria	-370.3	-238.6	-34.6	-44.75
Psila devriesii	NA	NA	-79.9	-75.2
Psila herngreenii	-359	-238.6	-53	-44.75
Psila obesus	-230.2	-191.2	NA	-34.2
Psila redundantis	-325.3	-272.6	-39.8	NA
Psila silvaticus	NA	NA	-30	-44.75
Quaternary	-20	-15	NA	NA
Ramon	-405	-353	-330	-338
Ranun operculatus	-370.3	NA	NA	-44.75
Retim absyae	-283.2	-238.6	-30	NA
Retis crassiannulatu	-325.3	-273.6	-75.3	-59
Retit caputoi	-326.2	NA	-79.9	-131
Retit crassicostatus	-125.3	-263.5	-44.7	NA
Retit irregularis	-370.3	NA	NA	-75.2
Retit kaarsii	-359	-267	-39.8	-34.2
Retit lorenteae	-272.1	-59	NA	NA
Solimoes	-330	-338	-20	-15
Spiro spiralis	-250	-181.85	-44.7	-125.2
Stria catatumbus	-165.5	-267	NA	NA
Verru rotundiporus	-26.35	NA	NA	-44.75

9.1. d). Events of wells 1-AS-105-AM and 1-AS-27-AM (Silva-Caminha *et al*. 2010). Species with " " are informal.

Taxa	**FAD105**	**FAD27**	**LAD105**	**LAD27**
Areci regio	-370.3	NA	-30	-49.6
Bomba araracuarensis	-161.7	-354.5	-39.8	-43.7
Bomba baculatus	-325.3	-264.3	NA	-216
Bomba brevis	-324.9	-354.5	-69.8	NA
Bomba muinaneorum	-370.3	-216	-35.4	-43.7
Cicho longispinosus	-165.5	-354.5	-30	NA
Clava microclavatus	-324.6	-233.1	-30	-43.7
Crass columbianus	NA	-280.2	-39.8	-57.9
Crass vanraadshooven	-360.9	-354.5	-34.6	-49.6

Croto reticulatus	-359	-354.5	-30	NA
Cteno suigeneris	-359	-284.5	-34.6	-63.6
Echin muelleri	-267.9	-301.8	NA	-150.7
Echip estelae	-370.3	-216	NA	NA
Echip intectatus	-272.1	-97.8	-34.6	-97.8
Echip jutaiensis	-230.2	-216	-35.4	-43.7
Echip lophatus	-289.9	-233.1	NA	-63.6
Echit spinosus	-324.9	-150.7	-34.6	-150.7
Foveo ornatus	-324.9	-192	-34.6	-53.7
Grims magnaclavata	-326.2	NA	NA	-43.7
Heter incomptus	-325.3	-301.8	-34.6	-53.7
Heter rotundus	-326.2	-301.8	NA	-53.7
Heter verrucosus	-289.9	-354.5	NA	NA
Ilexp tropicalis	-324.9	-216	-34.6	-216
Jandu minor	-370.3	NA	-165.5	NA
Jandu seamrogiformis	-284	-264.3	-35.4	-264.3
Ladak caribbiensis	-187.6	-221	-34.6	NA
Laevi granulatus	-324.9	-161.2	NA	-161.2
Magna grandiosus	-359	-354.5	-34.6	NA
Malva maristellae	-250	-57.9	-34.6	-43.7
Margo vanwijhei	-370.3	-137	NA	-53.7
Mauri franciscoimin	-325.3	NA	NA	-43.7
Monop annulatus	NA	-354.5	NA	NA
Multi vanderhammenii	-267.9	-43.7	-30	-43.7
Parso brenacii	-298.9	-143.1	-44.7	-53.7
Perfo digitatus	-298.9	-301.8	-34.6	-54.3
Polyp planus	-210.1	-354.5	NA	-49.6
Polyp pseudopsilatus	-155.1	-53.7	-35.4	-53.7
Prote triangulatus	-370.3	-303	-30	-54.3
Proxa tertiaria	-370.3	-233.1	-34.6	-49.6
Psila devriesii	NA	NA	-79.9	-264.3
Psila fissilis	-298.9	-264.3	NA	-221
Psila herngreenii	-359	-264.3	-53	NA
Psila nanus	-359	-216	-69.8	-216
Psila triangularis	-299.3	NA	-79.9	-301.8
Pteri gemmatus	-254.3	-43.7	-91.5	-43.7
Ranun operculatus	-370.3	-301.8	NA	NA
Retib retibolus	-210.1	-303	NA	-137
Retib yavarensis	-182	-354.5	-161.7	-49.6
Retim absyae	-283.2	NA	-30	NA
Retis crassiannulatu	-325.3	NA	-75.3	-54.3
Retit irregularis	-370.3	-354.5	NA	-53.7
Retit simplex	-370.3	-284.5	-140.9	-53.7
Retit traversei	-44.7	-216	-44.7	-137
Rugut arcus	-30	-284.5	-30	-284.5
Silta dilcheri	-267.9	-216	-39.8	-136.6

Solimoes	-330	-378	-20	-13
Spiro spiralis	-250	-354.5	-44.7	NA
Stria anastomosatus	-324.9	-192	-34.6	-136.6
Stria catatumbus	-165.5	-354.5	NA	-43.7
Stria poloreticulatu	-364.8	-354.5	NA	-137
Verru etayoi	-324.3	-192	-51.6	-192
Verru rotundiporus	-26.35	-280.2	NA	-67.9

9.1. e). R codes to produce LOC equations (= intercepts and slopes for various segments in each correlation). Equation results are shown within the codes (in bold). In all codes, Medina is the reference section, which therefore becomes the composite section. Codes written by Jaramillo *et al*. (2011).

```
##code to transfer Saltarin values into Medina values.  Saltarin values in first
#column(depent variable)
locMolino<-read.table("LOC_SaltarinvsMedina.txt",header=T,sep="\t",na.strings =
"NA")##contains the calibration points between both sites, in first column goes the dependent
variable
locMolino = locMolino[order(locMolino$saltarin),]##PMedina ordered from young to old

##Loops that will produce all intercepts and coeff for calibration
intercept.molino <- numeric (nrow(locMolino)-1)
slope.molino <- numeric (nrow(locMolino)-1)
for (i in (1:(nrow(locMolino)-1))) {
segcal.molino=lm(locMolino$medina[i:(i+1)]~locMolino$saltarin[i:(i+1)])## need to change,
first independent
intercept.molino[i]=segcal.molino$coefficients[1]
slope.molino[i]=segcal.molino$coefficients[2]
}

#intercepts for composite section and well Saltarin:
[1]   1748.4964   1650.9603   -503.0868   1553.3205   2137.8087   -525.7042
 [7] -19885.2057 -11199.5390 -90596.3240  -9934.3806  -8350.9091  -4226.5144
[13]   3702.3409
#slopes for composite section and well Saltarin:
[1]   5.104830   5.650334  10.746379   6.308920   5.118516  10.239573
 [7]  46.105778  30.342890 159.915292  30.202429  27.705628  21.318644
[13]   9.206125

calibfun.molino=function(a,b) {  ##lm for any given segment, a is tausa, b is segment to use
c=a*slope.molino[b]+ intercept.molino[b]
```

```
c
}

slopesegmentfun.molino=function(b) {
a=numeric (nrow(locMolino)-1)
segment=numeric(1)
for (i in (1:(nrow(locMolino)-1))) {
a[i]=ifelse(b>=locMolino[i,1] & b<locMolino[(i+1),1],which(locMolino ==
locMolino[i,1]),0)##gives back the segment number
segment=which (a >0)
}
segment
}

molinoforcomposite=read.table("Saltarin_UnknownAges.txt",header=F,sep="\t",na.strings =
"NA")#the depths that we need to translate into composite units
molinoforcomposite=as.matrix(molinoforcomposite)
segmenttouse.molino=as.numeric(apply(molinoforcomposite,1,slopesegmentfun.molino))
write.table(calibfun.molino(molinoforcomposite, segmenttouse.molino), file =
"saltarinTOmedina.csv", sep = ",", col.names = NA, qmethod = "double")##saltarin expressed in
Medina units (or composite units)
----------------------------

##code to transfer 105AM values into Medina values.  105AM values in first column(depent
#variable)
locMolino<-read.table("LOC_105AMvsMedina.txt",header=T,sep="\t",na.strings = "NA")##contains
the calibration points between both sites, in first column goes the dependent variable
locMolino = locMolino[order(locMolino$X1.AS.105.AM.m),]##PMedina ordered from young to old

##Loops that will produce all intercepts and coeff for calibration
intercept.molino <- numeric (nrow(locMolino)-1)
slope.molino <- numeric (nrow(locMolino)-1)
for (i in (1:(nrow(locMolino)-1))) {
segcal.molino=lm(locMolino$Medina[i:(i+1)]~locMolino$X1.AS.105.AM.m[i:(i+1)])## need to
change, first independent
intercept.molino[i]=segcal.molino$coefficients[1]
slope.molino[i]=segcal.molino$coefficients[2]
}

calibfun.molino=function(a,b) {  ##lm for any given segment, a is tausa, b is segment to use
c=a*slope.molino[b]+ intercept.molino[b]
c
}
```

```
#intercepts for composite section and well 1-AS-105-AM:
[1]  3468.82496  3082.37073  3357.69671  3504.48858 -1641.30022  3273.91719
[7]  2265.23883  3220.17700  2305.77440  2752.46484  3126.09072  2944.64659
[13] -5799.04220  5464.31808   -17.37225 -5650.92786  2849.71214 -8962.01604
[19]  5619.39754  8946.81255    91.53890 -1564.43957 -1567.52472  7958.94373
[25]  7958.88723  7283.46514
#slopes for composite section and well 1-AS-105-AM:
[1]  7.1462776 14.5213583  9.3265285  7.1024092 75.4395780 10.5950211
[7] 20.9830578 11.9235250 19.5435467 16.0434962 13.2552434 14.5378060
[13] 67.3697624  0.3259512 32.4147086 62.0650013 19.7732600 71.1759798
[19] 12.6630842  0.9509581 31.7759266 37.4219494 37.4323463  5.6031835
[25]  5.6033623  7.6841451

slopesegmentfun.molino=function(b) {
a=numeric (nrow(locMolino)-1)
segment=numeric(1)
for (i in (1:(nrow(locMolino)-1))) {
a[i]=ifelse(b>=locMolino[i,1] & b<locMolino[(i+1),1],which(locMolino ==
locMolino[i,1]),0)##gives back the segment number
segment=which (a >0)
}
segment
}

molinoforcomposite=read.table("105AM_UnknownAges.txt",header=F,sep="\t",na.strings = "NA")
molinoforcomposite=as.matrix(molinoforcomposite)
segmenttouse.molino=as.numeric(apply(molinoforcomposite,1,slopesegmentfun.molino))
write.table(calibfun.molino(molinoforcomposite, segmenttouse.molino), file =
"105AMTOmedina.csv", sep = ",", col.names = NA, qmethod = "double")##105AM into Medina units
```

9.1. f). R codes to transfer composite units to geological time. This code uses a file "calibration_2011December.txt" from Jaramillo *et al*. (2011).

```
##COMPOSITE UNITS TO GEOLOGIC TIME
calibration<-read.table("calibration_2011December.txt",header=T,sep="\t",na.strings =
"NA")##contains the calibration points
calibration = calibration[order(calibration $CU),]##composite units ordered from young to old

plot(calibration$CU,calibration$time,xlab="composite units",ylab="time (My)", pch=19)

##Loops that will produce all intercepts and coeff for calibration
intercept <- numeric (nrow(calibration)-1)
slope <- numeric (nrow(calibration)-1)
```

```
for (i in (1:(nrow(calibration)-1))) {
segcal=lm(calibration$time[i:(i+1)]~calibration$CU[i:(i+1)])
intercept[i]=segcal$coefficients[1]
slope[i]=segcal$coefficients[2]
}

calibfun=function(a,b) {  ##lm for any given segment, a is composite unit, b is segment to
use
c=a*slope[b]+ intercept[b]
c
}

##function that gives back the segment number
slopesegmentfun=function(b) {
a=numeric (nrow(calibration)-1)
segment=numeric(1)
for (i in (1:(nrow(calibration)-1))) {
a[i]=ifelse(b>=calibration[i,1] & b<calibration[(i+1),1],which(calibration ==
calibration[i,1]),0)##gives back the segment number
segment=which (a >0)
}
segment
}

compositeunits<-as.matrix(read.table("105AM_CU.txt",header=F,sep="\t",na.strings =
"NA"))##the composite units to be transformed into time
segmenttouse=as.numeric(apply(compositeunits,1,slopesegmentfun))## apply to find the segment
for each composite unit, eg.
timeunits=calibfun(compositeunits, segmenttouse)##calculate the time for each composite unit
plot(compositeunits, timeunits)
write.table(timeunits, file = "105AM_timeunits.csv", sep = ",", col.names = NA, qmethod =
"double")

compositeunits<-as.matrix(read.table("Saltarin_CU.txt",header=F,sep="\t",na.strings =
"NA"))##the composite units to be transformed into time
segmenttouse=as.numeric(apply(compositeunits,1,slopesegmentfun))## apply to find the segment
for each composite unit, eg.
timeunits=calibfun(compositeunits, segmenttouse)##calculate the time for each composite unit
plot(compositeunits, timeunits)
write.table(timeunits, file = "saltarin_timeunits.csv", sep = ",", col.names = NA, qmethod =
"double")
```

9.1.g) Range charts with pollen counts from core 1-AS-105-AM (ordered by FAD).

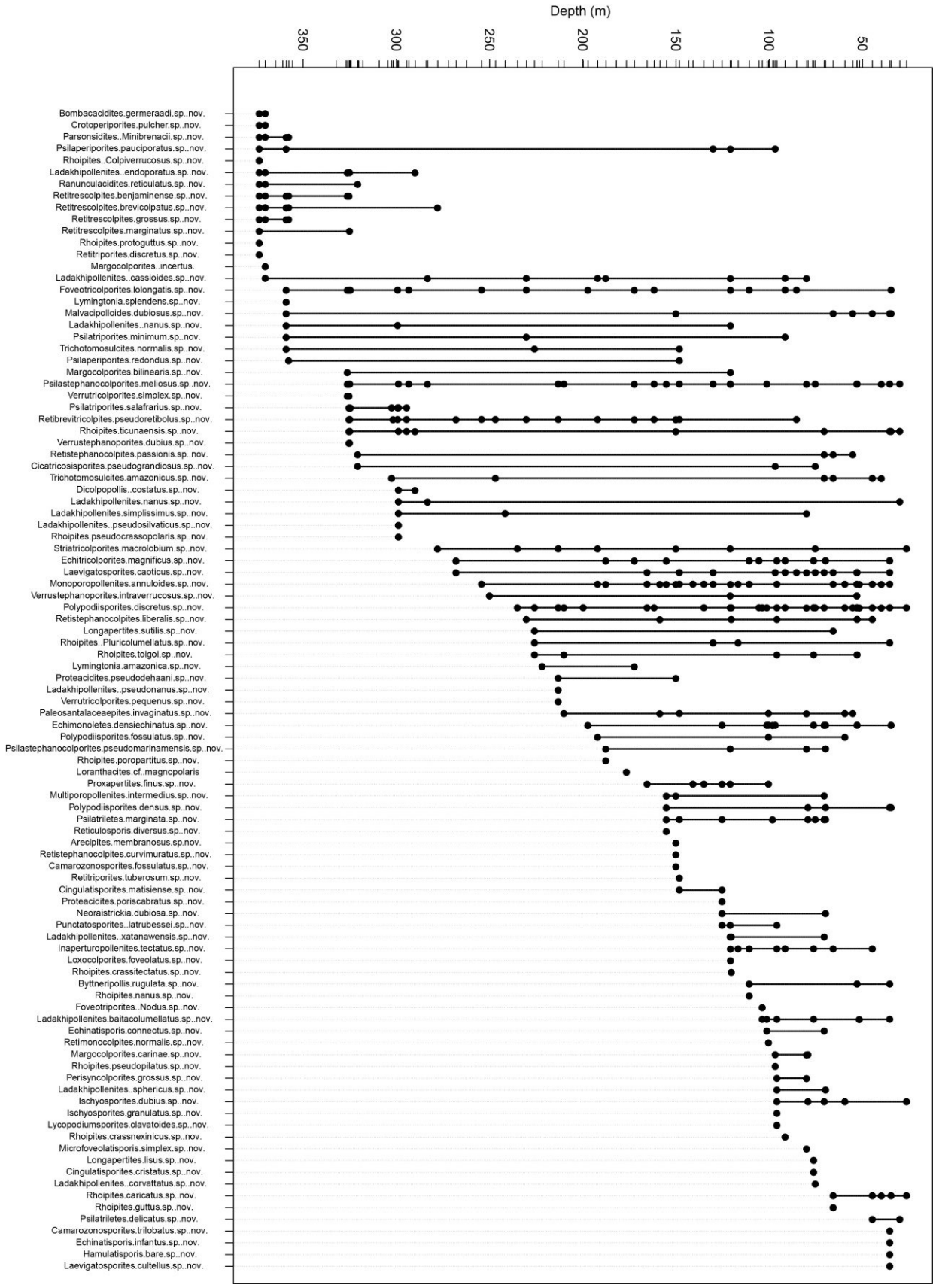

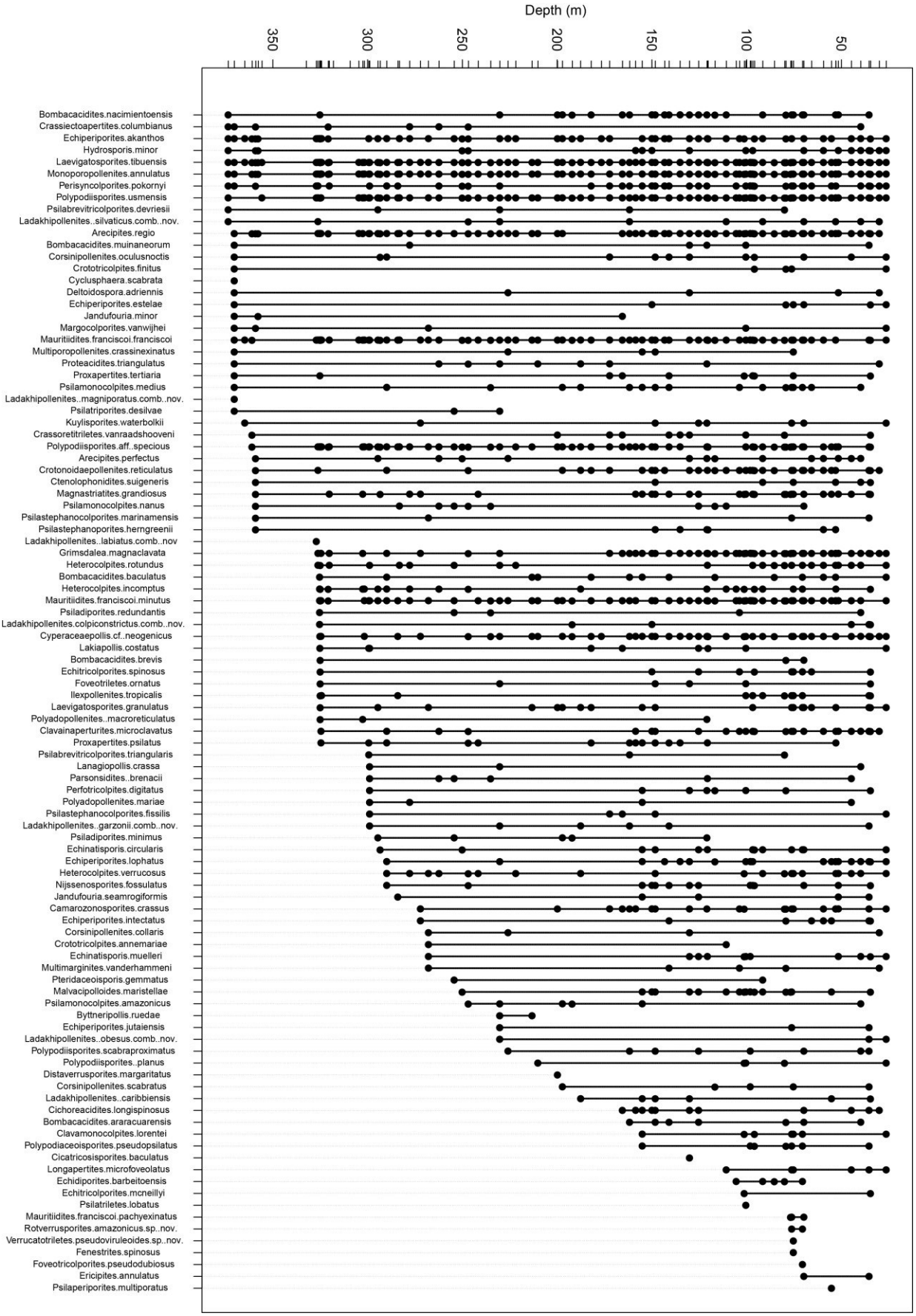
Depth (m)
350
300
250
200
150
100
50
Bombacacidites.nacimientoensis
Crassiectoapertites.columbianus
Echiperiporites.akanthos
Hydrosporis.minor
Laevigatosporites.tibuensis
Monoporopollenites.annulatus
Perisyncolporites.pokornyi
Polypodiisporites.usmensis
Psilabrevitricolporites.devriesii
Ladakhipollenites..silvaticus.comb..nov.
Arecipites.regio
Bombacacidites.muinaneorum
Corsinipollenites.oculusnoctis
Crototricolpites.finitus
Cyclusphaera.scabrata
Deltoidospora.adriennis
Echiperiporites.estelae
Jandufouria.minor
Margocolporites.vanwijhei
Mauritiidites.franciscoi.franciscoi
Multiporopollenites.crassinexinatus
Proteacidites.triangulatus
Proxapertites.tertiaria
Psilamonocolpites.medius
Ladakhipollenites..magniporatus.comb..nov.
Psilatriporites.desilvae
Kuylisporites.waterbolkii
Crassoretitriletes.vanraadshooveni
Polypodiisporites.aff..speciosus
Arecipites.perfectus
Crotonoidaepollenites.reticulatus
Ctenolophonidites.suigeneris
Magnastriatites.grandiosus
Psilamonocolpites.nanus
Psilastephanocolporites.marinamensis
Psilastephanoporites.herngreenii
Ladakhipollenites..labiatus.comb..nov
Grimsdalea.magnaclavata
Heterocolpites.rotundus
Bombacacidites.baculatus
Heterocolpites.incomptus
Mauritiidites.franciscoi.minutus
Psiladiporites.redundantis
Ladakhipollenites.colpiconstrictus.comb..nov.
Cyperaceaepollis.cf..neogenicus
Lakiapollis.costatus
Bombacacidites.brevis
Echitricolporites.spinosus
Foveotriletes.ornatus
Ilexpollenites.tropicalis
Laevigatosporites.granulatus
Polyadopollenites..macroreticulatus
Clavainaperturites.microclavatus
Proxapertites.psilatus
Psilabrevitricolporites.triangularis
Lanagiopollis.crassa
Parsonsidites..brenacii
Perfotricolpites.digitatus
Polyadopollenites.mariae
Psilastephanocolporites.fissilis
Ladakhipollenites..garzonii.comb..nov.
Psiladiporites.minimus
Echinatisporis.circularis
Echiperiporites.lophatus
Heterocolpites.verrucosus
Nijssenosporites.fossulatus
Jandufouria.seamrogiformis
Camarozonosporites.crassus
Echiperiporites.intectatus
Corsinipollenites.collaris
Crototricolpites.annemariae
Echinatisporis.muelleri
Multimarginites.vanderhammeni
Pteridaceoisporis.gemmatus
Malvacipolloides.maristellae
Psilamonocolpites.amazonicus
Byttneripollis.ruedae
Echiperiporites.jutaiensis
Ladakhipollenites..obesus.comb..nov.
Polypodiisporites.scabraproximatus
Polypodiisporites..planus
Distaverrusporites.margaritatus
Corsinipollenites.scabratus
Ladakhipollenites..caribbiensis
Cichoreacidites.longispinosus
Bombacacidites.araracuarensis
Clavamonocolpites.lorentei
Polypodiaceoisporites.pseudopsilatus
Cicatricosisporites.baculatus
Longapertites.microfoveolatus
Echidiporites.barbeitoensis
Echitricolporites.mcneillyi
Psilatriletes.lobatus
Mauritiidites.franciscoi.pachyexinatus
Rotverrusporites.amazonicus.sp..nov.
Verrucatotriletes.pseudoviruleoides.sp..nov.
Fenestrites.spinosus
Foveotricolporites.pseudodubiosus
Ericipites.annulatus
Psilaperiporites.multiporatus

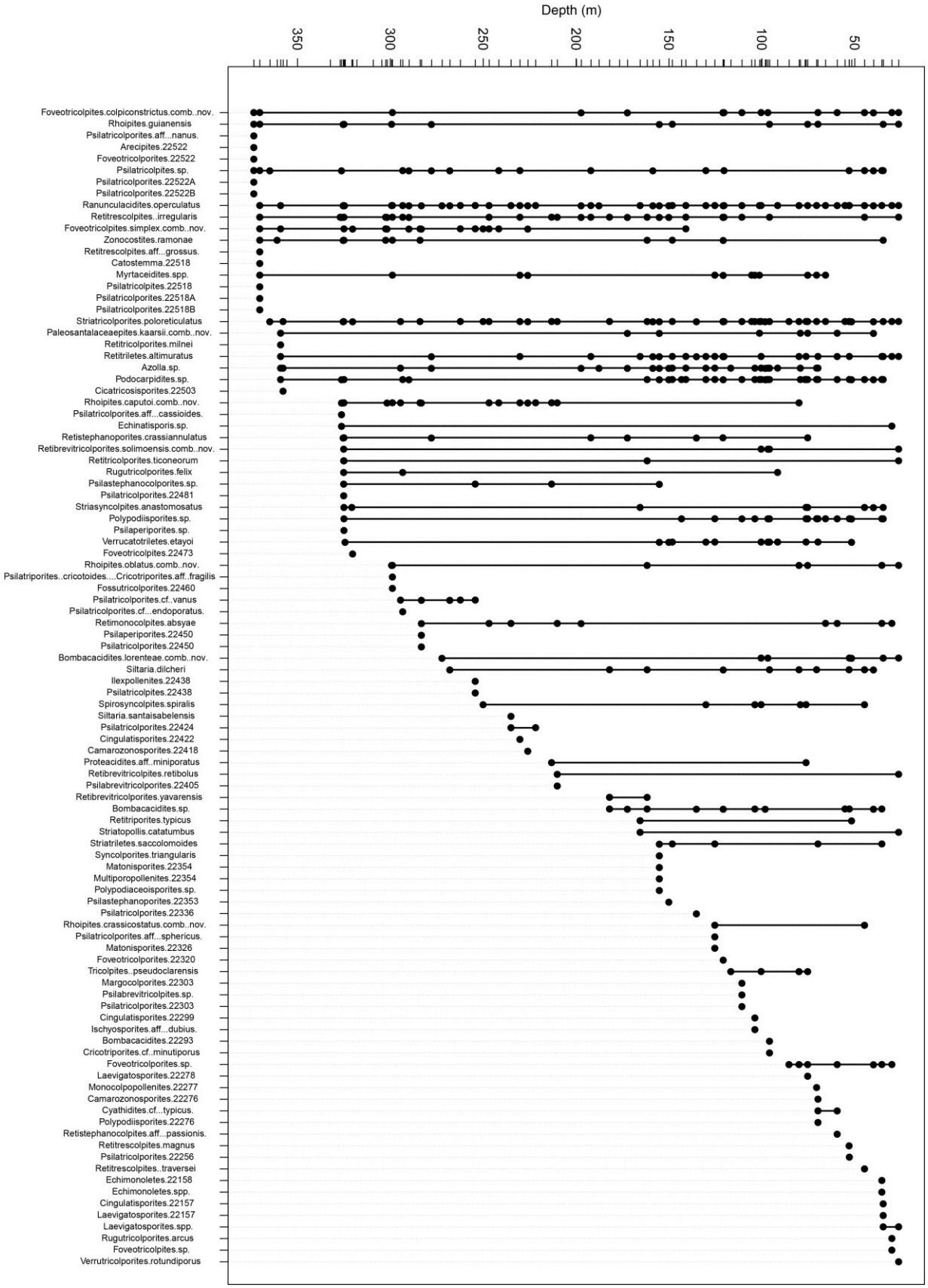
Depth (m)
350
300
250
200
150
100
50
Foveotricolpites.colpiconstrictus.comb..nov.
Rhoipites.guianensis
Psilatricolporites.aff...nanus.
Arecipites.22522
Foveotricolporites.22522
Psilatricolpites.sp.
Psilatricolporites.22522A
Psilatricolporites.22522B
Ranunculacidites.operculatus
Retitrescolpites..irregularis
Foveotricolpites.simplex.comb..nov.
Zonocostites.ramonae
Retitrescolpites.aff...grossus.
Catostemma.22518
Myrtaceidites.spp.
Psilatricolpites.22518
Psilatricolporites.22518A
Psilatricolporites.22518B
Striatricolporites.poloreticulatus
Paleosantalaceaepites.kaarsii.comb..nov.
Retitricolporites.milnei
Retitriletes.altimuratus
Azolla.sp.
Podocarpidites.sp.
Cicatricosisporites.22503
Rhoipites.caputoi.comb..nov.
Psilatricolporites.aff...cassioides.
Echinatisporis.sp.
Retistephanoporites.crassiannulatus
Retibrevitricolporites.solimoensis.comb..nov.
Retitricolporites.ticoneorum
Rugutricolporites.felix
Psilastephanocolporites.sp.
Psilatricolporites.22481
Striasyncolpites.anastomosatus
Polypodiisporites.sp.
Psilaperiporites.sp.
Verrucatotriletes.etayoi
Foveotricolpites.22473
Rhoipites.oblatus.comb..nov.
Psilatriporites..cricotoides....Cricotriporites.aff..fragilis
Fossutricolporites.22460
Psilatricolporites.cf..vanus
Psilatricolporites.cf...endoporatus.
Retimonocolpites.absyae
Psilaperiporites.22450
Psilatricolporites.22450
Bombacacidites.lorenteae.comb..nov.
Siltaria.dilcheri
Ilexpollenites.22438
Psilatricolpites.22438
Spirosyncolpites.spiralis
Siltaria.santaisabelensis
Psilatricolporites.22424
Cingulatisporites.22422
Camarozonosporites.22418
Proteacidites.aff..miniporatus
Retibrevitricolpites.retibolus
Psilabrevitricolporites.22405
Retibrevitricolporites.yavarensis
Bombacacidites.sp.
Retitriporites.typicus
Striatopollis.catatumbus
Striatriletes.saccolomoides
Syncolporites.triangularis
Matonisporites.22354
Multiporopollenites.22354
Polypodiaceoisporites.sp.
Psilastephanoporites.22353
Psilatricolporites.22336
Rhoipites.crassicostatus.comb..nov.
Psilatricolporites.aff...sphericus.
Matonisporites.22326
Foveotricolporites.22320
Tricolpites..pseudoclarensis
Margocolporites.22303
Psilabrevitricolpites.sp.
Psilatricolporites.22303
Cingulatisporites.22299
Ischyosporites.aff...dubius.
Bombacacidites.22293
Cricotriporites.cf..minutiporus
Foveotricolporites.sp.
Laevigatosporites.22278
Monocolpopollenites.22277
Camarozonosporites.22276
Cyathidites.cf...typicus.
Polypodiisporites.22276
Retistephanocolpites.aff...passionis.
Retitrescolpites.magnus
Psilatricolporites.22256
Retitrescolpites..traversei
Echimonoletes.22158
Echimonoletes.spp.
Cingulatisporites.22157
Laevigatosporites.22157
Laevigatosporites.spp.
Rugutricolporites.arcus
Foveotricolpites.sp.
Verrutricolporites.rotundiporus

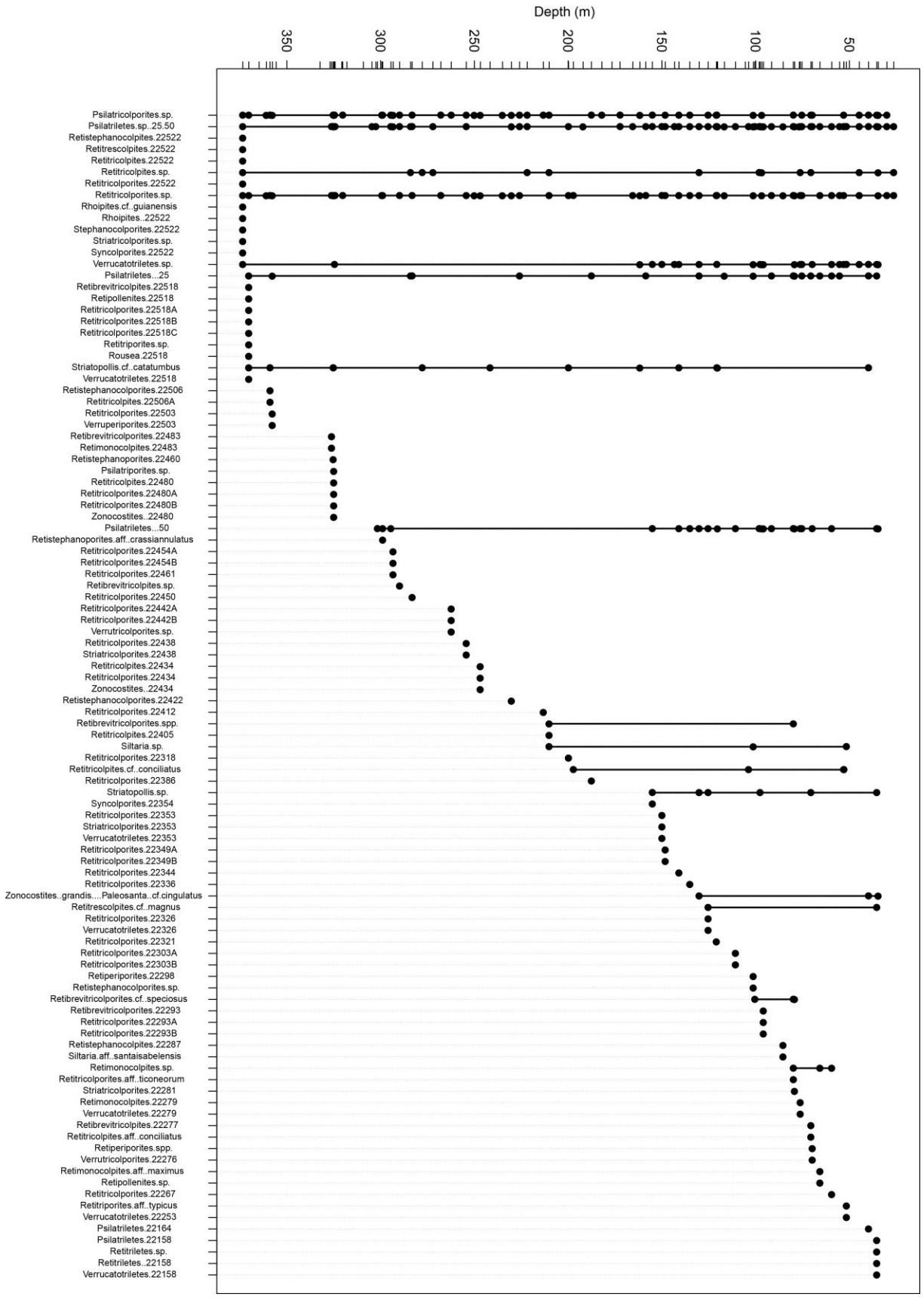
Depth (m)
350
300
250
200
150
100
50
Psilatricolporites.sp.
Psilatriletes.sp..25.50
Retistephanocolpites.22522
Retitrescolpites.22522
Retitricolpites.22522
Retitricolpites.sp.
Retitricolporites.22522
Retitricolporites.sp.
Rhoipites.cf..guianensis
Rhoipites..22522
Stephanocolporites.22522
Striatricolporites.sp.
Syncolporites.22522
Verrucatotriletes.sp.
Psilatriletes...25
Retibrevitricolpites.22518
Retipollenites.22518
Retitricolporites.22518A
Retitricolporites.22518B
Retitricolporites.22518C
Retitriporites.sp.
Rousea.22518
Striatopollis.cf..catatumbus
Verrucatotriletes.22518
Retistephanocolporites.22506
Retitricolpites.22506A
Retitricolporites.22503
Verruperiporites.22503
Retibrevitricolporites.22483
Retimonocolpites.22483
Retistephanoporites.22460
Psilatriporites.sp.
Retitricolpites.22480
Retitricolporites.22480A
Retitricolporites.22480B
Zonocostites..22480
Psilatriletes...50
Retistephanoporites.aff..crassiannulatus
Retitricolporites.22454A
Retitricolporites.22454B
Retitricolporites.22461
Retibrevitricolpites.sp.
Retitricolporites.22450
Retitricolporites.22442A
Retitricolporites.22442B
Verrutricolporites.sp.
Retitricolporites.22438
Striatricolporites.22438
Retitricolpites.22434
Retitricolporites.22434
Zonocostites..22434
Retistephanocolporites.22422
Retitricolporites.22412
Retibrevitricolporites.spp.
Retitricolpites.22405
Siltaria.sp.
Retitricolporites.22318
Retitricolpites.cf..conciliatus
Retitricolporites.22386
Striatopollis.sp.
Syncolporites.22354
Retitricolporites.22353
Striatricolporites.22353
Verrucatotriletes.22353
Retitricolporites.22349A
Retitricolporites.22349B
Retitricolporites.22344
Retitricolporites.22336
Zonocostites..grandis....Paleosanta..cf.cingulatus
Retitrescolpites.cf..magnus
Retitricolporites.22326
Verrucatotriletes.22326
Retitricolporites.22321
Retitricolporites.22303A
Retitricolporites.22303B
Retiperiporites.22298
Retistephanocolporites.sp.
Retibrevitricolporites.cf..speciosus
Retibrevitricolporites.22293
Retitricolporites.22293A
Retitricolporites.22293B
Retistephanocolpites.22287
Siltaria.aff..santaisabelensis
Retimonocolpites.sp.
Retitricolporites.aff..ticoneorum
Striatricolporites.22281
Retimonocolpites.22279
Verrucatotriletes.22279
Retibrevitricolpites.22277
Retitricolpites.aff..conciliatus
Retiperiporites.spp.
Verrutricolporites.22276
Retimonocolpites.aff..maximus
Retipollenites.sp.
Retitricolporites.22267
Retitriporites.aff..typicus
Verrucatotriletes.22253
Psilatriletes.22164
Psilatriletes.22158
Retitriletes.sp.
Retitriletes..22158
Verrucatotriletes.22158

9.2. Table with all known botanical affinities (Chapter 6).

taxa name	type	family/ subfamily	genus/ species	life habit	ecology	author
Multimarginites vanderhammeni	pollen	Acanthaceae	Trichantera/ Bravaisia	tree	terra firme	Germeraad et al. 1968
Retitrescolpites? traversei	pollen	Acanthaceae	Teliostachya	tree	lowland	Silva-Caminha et al 2010
Echiperiporites akanthos	pollen	Alismataceae	Sagittaria/ Echinodorus	herb	swamp, lake	This study
Proxapertites tertiaria	pollen	Annonaceae	Crematosperma	tree	lowland	Van der Hammen and Garcia Mutis 1965
Ctenolophonidites suigeneris	pollen	Apocynaceae	Geissospermum	tree	terra firme	Silva-Caminha et al 210
Dicolpopollis? "costatus"	pollen	Apocynaceae	Macoubea	tree	terra firme	This study
Margocolporites "carinae"	pollen	Apocynaceae	Aspidosperma	tree	terra firme	This study
Psilastephanoporites herngreenii	pollen	Apocynaceae	unknown	tree	unknown	Hoorn 1993
Verrustephanoporites "intraverrucosus"	pollen	Apocynaceae	Forteronia/ Prestonia/ Odontadenia	lowland liana	lowland forest	Dessaune-Rodrigues et al 2016
Ilexpollenites 22438	pollen	Aquafoiliaceae	Ilex	tree	terra firme, white-sand	Thiergart 1937 ex Potonie 1960
Ilexpollenites tropicalis	pollen	Aquafoiliaceae	Ilex	tree	terra firme, white-sand	Silva-Caminha et al 2010, Thiergart 1937 ex Potonie 1960
Rhoipites ticunaensis	pollen	Araliaceae	Schefflera	tree	lowland	This study
Cyclusphaera scabrata	pollen	Araucariaceae	unknown	tree	montane	Jaramillo and Dilcher 2001
Arecipites "membranosus"	pollen	Arecaceae	unknown	tree	unknown	This study
Arecipites 22522	pollen	Arecaceae	unknown	tree	unknown	This study
Arecipites perfectus	pollen	Arecaceae	unknown	tree	unknown	Silva-Caminha et al 2010
Arecipites regio	pollen	Arecaceae	unknown	tree	unknown	Van der Hammen and Garcia, 1966
Clavamonocolpites lorentei	pollen	Arecaceae	Iriartea(?)	tree	terra firme	Gonzalez 1967
Echidiporites barbeitoensis	pollen	Arecaceae	Korthalsia ferox	tree	terra firme	Muller et al 1987
Grimsdalea magnaclavata	pollen	Arecaceae	extinct genus	tree	unknown	Germeraad et al. 1968
Longapertites microfoveolatus	pollen	Arecaceae	unknown	tree	unknown	Jaramillo and Rueda 2013
M. franciscoi pachyexinatus	pollen	Arecaceae	Mauritia/ Mauritiella	tree	varzea, swamp	(Van der Hammen 1956) Van Hoeken-Klinkenberg 1964
Mauritiidites franciscoi franciscoi	pollen	Arecaceae	Mauritia	tree	varzea, swamp	(Van der Hammen 1956) Van Hoeken-Klinkenberg 1964
Mauritiidites franciscoi minutus	pollen	Arecaceae	Mauritia	tree	varzea, swamp	(Van der Hammen 1956) Van Hoeken-Klinkenberg 1964
Psilamonocolpites amazonicus	pollen	Arecaceae	Euterpe	tree	lowland	Hoorn 1993
Psilamonocolpites medius	pollen	Arecaceae	unknown	tree	lowland	(Van der Hammen 1956) Van der Hammen and Garcia 1966
Psilamonocolpites nanus	pollen	Arecaceae	unknown	tree	lowland	Hoorn 1993
Trichotomosulcites "amazonicus"	pollen	Arecaceae	unknown	tree	lowland	This study
Trichotomosulcites "normalis"	pollen	Arecaceae	unknown	tree	lowland	This study
Longapertites "lisus"	pollen	Arecaceae (?)	unknown	tree	unknown	This study
Longapertites "sutilis"	pollen	Arecaceae (?)	unknown	tree	unknown	This study
Cichoreacidites longispinosus	pollen	Asteraceae	unknown	herb	bars, swamps, savannahs	Lorente 1986
Echitricolporites mcneillyi	pollen	Asteraceae	unknown	herb	bars, swamps, savannahs	Germeraad et al. 1968
Echitricolporites spinosus	pollen	Asteraceae	unknown	herb	bars, swamps, savannahs	Germeraad et al. 1968
Fenestrites spinosus	pollen	Asteraceae	unknown	herb	bars, swamps, savannahs	Van der Hammen 1956 ex Lorente, 1986
Ladakhipollenites? silvaticus	pollen	Burseraceae/ Sapotaceae	unknown	tree	unknown	Hoorn 1993
Rugutricolporites arcus	pollen	Chrysobalanaceae	Licania	tree	lowland	Hoorn 1993
Clavainaperturites microclavatus	pollen	Cloranthaceae	Hedyosmum	tree	montante, riparian forests in cerrados	Hoorn et al 1994, D'Apolito et al 2013
Lymingtonia "splendens"	pollen	Convolvulaceae	Evolvulus/ Jacquemontia	herb	lowland liana	This study
Perfotricolpites digitatus	pollen	Convolvulaceae	Merremia	herb	lowland liana	Gonzalez 1967
Echiperiporites lophatus	pollen	Convolvulaceae (?)	unknown	herb	liana?	This study

Cyperaceaepollis cf. neogenicus	pollen	Cyperaceae	unknown	herb	bars, swamps, savannahs	Krutzsch 1970
Ericipites annulatus	pollen	Ericaceae	unknown	unknown	unknown	Gonzalez 1967
Crototricolpites annemariae	pollen	Euphorbiaceae	Croton	tree	terra firme, montane	Leidelmeyer 1966
Foveotricolpites simplex	pollen	Euphorbiaceae	Sapium	tree	lowland	Gonzalez 1967
Ladakhipollenites? caribbiensis	pollen	Euphorbiaceae	Sapium	tree	terra firme, varzea	Muller et al. 1987
Ranunculacidites operculatus	pollen	Euphorbiaceae	Alchornea	tree	lowland, varzea	(Van der Hammen & Wymstra, 1964) Jaramillo & Dilcher 2001
Retitrescolpites? irregularis	pollen	Euphorbiaceae	Amanoa	tree	lowland	(Van der Hammen & Wymstra 1964) Jaramillo & Dilcher 2001
Ladakhipollenites? cassioides	pollen	Fabaceae, Caesalpinioideae	Cacia?	tree	unknown	This study
Margocolporites vanwijhei	pollen	Fabaceae, Caesalpinioideae	Caesalpinea	tree	terra firme	Germeraad et al. 1968
Psilatriporites desilvae	pollen	Fabaceae, Caesalpinioideae	unknown	tree	lowland	Hoorn 1993
Striatopollis catatumbus	pollen	Fabaceae, Caesalpinioideae	unknown	tree	lowland	(Gonzalez 1967) Takahashi and Jux 1989
Striatricolporites "macrolobium"	pollen	Fabaceae, Caesalpinioideae	unknown	tree	lowland	This study
Polyadopollenites mariae	pollen	Fabaceae, Mimosoideae	Acacia	tree	lowland	Dueñas 1980
Crassiectoapertites columbianus	pollen	Fabaceae, Papilionoideae	unknown	tree	terra firme	Dueñas 1980
Ladakhipollenites? magniporatus	pollen	Fabaceae?	unknown	unknown	unknown	Hoorn 1993
Polyadopollenites macroreticulatus	pollen	Hippocrateaceae	Hippocratea (volubilis?)	tree	lowland	Salard-Cheboldaeff 1974
Psilabrevitricolporites devriesii	pollen	Humiriaceaecaee	Humiria	tree	lowland, montane, white-sand	Lorente 1986
Loranthacites cf. "magnopolaris"	pollen	Loranthaceae	unknown	tree	unknown	Jaramillo and Rueda 2013
Verrutricolporites rotundiporus	pollen	Lythraceae	Crenea	tree	lowland	Van der Hammen and Wymstra 1964
Perisyncolporites pokornyi	pollen	Malpighiaceae	unknown	unknown	lowland	Germeraad et al 1968
Byttneripollis ruedae	pollen	Malvaceae	Byttneria	tree	terra firme	Silva-Caminha et al 210
Catostemma 22518	pollen	Malvaceae	Catostema	tree	terra firme	
Jandufouria minor	pollen	Malvaceae	Catostema (?)	tree	terra firme, varzea	Germeraad et al. 1968
Jandufouria seamrogiformis	pollen	Malvaceae	Catostema	tree	terra firme, varzea	Germeraad et al. 1968
Retistephanoporites crassiannulatus	pollen	Malvaceae	Quararibea	tree	lowland	Lorente 1986, Roubik and Moreno 1991
Malvacipolloides "dubiosus"	pollen	Malvaceae (?)	unknown	unknown	unknown	This study
Bombacacidites "germeraadi"	pollen	Malvaceae, Bombacoideae	unknown	tree	unknown	
Bombacacidites 22293	pollen	Malvaceae, Bombacoideae	unknown	tree	unknown	
Bombacacidites araracuarensis	pollen	Malvaceae, Bombacoideae	Ceiba sp	tree	terra firme, varzea	Hoorn 1994
Bombacacidites baculatus	pollen	Malvaceae, Bombacoideae	Pachira aquatica	tree	terra firme, swamp	Muller et al. 1987
Bombacacidites brevis	pollen	Malvaceae, Bombacoideae	unknown	tree	unknown	(Dueñas, 1980) Muller et al., 1987
Bombacacidites lorenteae	pollen	Malvaceae, Bombacoideae	Bombax	tree	varzea	Hoorn 1993
Bombacacidites muinaneorum	pollen	Malvaceae, Bombacoideae	Bombacopsis	tree	terra firme, varzea	Hoorn 1993
Bombacacidites nacimientoensis	pollen	Malvaceae, Bombacoideae	Bombax	tree	terra firme, varzea	Anderson 1960, Elsik 1968
Bombacacidites sp.	pollen	Malvaceae, Bombacoideae	unknown	tree	unknown	
Malvacipolloides maristellae	pollen	Malvaceae, Bombacoideae	unknown	tree	terra firme	Muller et al. 1987
Echiperiporites estelae	pollen	Malvaceae/ Convolvulaceae	unknown	unknown	unknown	Germeraad et al. 1968
Heterocolpites incomptus	pollen	Melastomataceae	unknown	tree	terra firme	Hoorn 1993
Heterocolpites rotundus	pollen	Melastomataceae	unknown	tree	terra firme	Hoorn 1993
Heterocolpites verrucosus	pollen	Melastomataceae	unknown	tree	terra firme	Hoorn 1993
Psiladiporites minimus	pollen	Moraceae	Ficus/ Artocarpus/ Sorocea	tree	lowland	Van der Hammen & Wijmstra 1964
Psiladiporites redundantis	pollen	Moraceae	unknown	tree	lowland	Gonzalez 1967

Psilatriporites "minimum"	pollen	Moraceae	unknown	tree	lowland	This study
Retimonocolpites absyae	pollen	Myristicaceae	Virola	tree	lowland, varzea	Hoorn 1993
Myrtaceidites spp.	pollen	Myrtaceae	Myrtaceae	tree	lowland	This study
Corsinipollenites collaris	pollen	Onagraceae	Ludwigia	herb	swamp, lake	(Thiergart 1940); Nakoman 1965
Corsinipollenites oculusnoctis	pollen	Onagraceae	Ludwigia	herb	swamp, lake	(Thiergart 1940); Nakoman 1965
Corsinipollenites scabratus	pollen	Onagraceae	Ludwigia	herb	swamp, lake	(Thiergart 1940); Nakoman 1965
Retistephanocolpites "passionis"	pollen	Passifloraceae	Passiflora	herb	lowland liana	This study
Lanagiopollis crassa	pollen	Pellicieraceae	Pelliciera	tree	mangrove	Jaramillo and Rueda 2013
Monoporopollenites "annuloides"	pollen	Poaceae	unknown	herb	bars, swamps, savannahs	This study
Monoporopollenites annulatus	pollen	Poaceae	unknown	herb	bars, swamps, savannahs	(Van der Hammen, 1954) Jaramillo & Dilcher 2001
Podocarpidites sp.	pollen	Podocarpaceae	Podocarpus	tree	lowland, montane	Punyasena et al 2011, D'Apolito et al in prep
Psilastephanocolporites fissilis	pollen	Polygalaceae	Polygala	herb	swamp, lake	Lorente 1986
Zonocostites ramonae	pollen	Rhizophoraceae	Rhizophora	tree	mangrove	Dueñas 1980
Proteacidites triangulatus	pollen	Sapindaceae/ Proteaeceae	unknown	tree	lowland	Lorente 1986
Psilabrevitricolporites triangularis	pollen	Sapindaceae?	unknown	unknown	unknown	Lorente 1986
Ladakhipollenites? obesus	pollen	Sapotaceae	unknown	tree	lowland	Hoorn 1993
Psilastephanocolporites marinamensis	pollen	Sapotaceae	unknown	tree	lowland	Hoorn 1994
Ladakhipollenites? labiatus	pollen	Sapotaceae, Pouteria	unknown	tree	lowland	Hoorn 1993
Ladakhipollenites? pseudosilvaticus	pollen	Sapotaceae?	unknown	tree	unknown	This study
Rhoipites guianensis	pollen	Tiliaceae/ Sterculiaceae	unknown	tree	lowland	(Van der Hammen & Wymstra 1964) Jaramillo & Dilcher 2001
Nijssenosporites fossulatus	spore	Adianthaceae	Pityrogramma	fern	lowland	Jaramillo and Rueda 2013
Cicatricosisporites baculatus	spore	Anemiaceae	Anemia	fern	terra firme	Regali et al 1974
Cyathidites cf. "typicus"	spore	Cyatheaceae	unknown	fern	unknown	Couper 1953
Kuylisporites waterbolkii	spore	Cyatheaceae	Cyathea horrida	fern	montane	Potonie 1956
Lycopodiumsporites "clavatoides"	spore	Lycopodiaceae (?)	unknown	fern	unknown	This study
Distaverrusporites margaritatus	spore	Ophioglossaceae (?), Lindsaeaceae (?)	unknown	fern	unknown	Jaramillo and Rueda 2013
Polypodiisporites aff. specious	spore	Polypodiaceae	unknown	fern	lowland	Sah 1967
Polypodiisporites usmensis	spore	Polypodiaceae, Blechnaceae	unknown	fern	unknown	(Van der Hammen, 1956a) Khan and Martin 1972
Deltoidospora adriennis	spore	Pteridaceae	Acrostichum aureum	fern	swamp, mangrove	(Potonie & Gelletich 1933) Frederiksen
Magnastriatites grandiosus	spore	Pteridaceae	Ceratopteris	fern	aquatic	(Kedves & Sole de Porta 1963) Dueñas 1980
Polypodiaceoisporites pseudopsilatus	spore	Pteridaceae	Pteris	fern	lowland	Jaramillo and Rueda 2013
Azolla sp.	spore	Salviniaceae	Azolla	fern	aquatic	
Hydrosporis minor	spore	Salviniaceae	Salviniaceae, Salvinia	fern	aquatic	Silva-Caminha et al 2010
Crassoretitriletes vanraadshooveni	spore	Schizaceae	Lygodium microphyllum	fern	swamp	Germeraad et al. 1968
Cingulatisporites "cristatus"	spore	Selaginellaceae	Selaginella	fern	unknown	This study
Echinatisporis "connectus"	spore	Thelypteraceae/ Athyriaceae/ Marathiaceae	unknown	fern	unknown	Krutzsch 1967
Echinatisporis "infantus"	spore	Thelypteraceae/ Athyriaceae/ Marathiaceae	unknown	fern	unknown	Krutzsch 1967
Echinatisporis circularis	spore	Thelypteraceae/ Athyriaceae/ Marathiaceae	unknown	fern	unknown	Krutzsch 1967
Echinatisporis muelleri	spore	Thelypteraceae/ Athyriaceae/ Marathiaceae	unknown	fern	unknown	Krutzsch 1967
Echinatisporis sp.	spore	Thelypteraceae/ Athyriaceae/ Marathiaceae	unknown	fern	unknown	Krutzsch 1967

9.3. R scripts for all figures and analyses (organised by chapter), except scripts for the age model that are in Appendix Tables 9.1. (Excel files are stored in the electronic supplement of this thesis – CD).

9.3.1 - Chapter 1 (Introduction), Fig. 1.1 and 1.2:

```
data<-read.csv("zachos2008.csv",head=T)
plot(data$Age,data$d18O.5pt,xlim=c(0,65), ylim=c(5,-1),type="l",col="blue",lwd=1.5,
ylab="d18O",xlab="Age (Ma)")
abline(v=66,lty=2) #Maastrichtian
abline(v=56,lty=2) #paleogene
abline(v=33.9,lty=2) #eocene
abline(v=23.03,lty=2) #oligocene
abline(v=20.44,lty=2) #Aquitanian
abline(v=15.97,lty=2) #Burdigalian
abline(v=13.82,lty=2) #Langhian
abline(v=11.63,lty=2) #Serravalian
abline(v=7.25,lty=2) #Tortonian
abline(v=5.33,lty=2) #Messianian
abline(v=2.59,lty=2) #Pliocene

###sea levels:
haq<-read.csv("haq_sealevel_curve.csv",head=T)
plot(haq$age,haq$seaLevel,type="l", xlim=c(0,65),ylim=c(-100,220),
xlab="",ylab="Sea Level curve", col="darkviolet")
abline(h=0,lty=2,col="grey")

miller<-read.csv("MillerCurve2005.csv",head=T)
points(miller[,2],miller[,1],type="l", xlim=c(0,65),ylim=c(-100,200),
ylab="",col="red")

muller<-read.csv("MullerCurve2008.csv",head=T)
points(muller[,1],muller[,2],type="l", xlim=c(0,65),xlim=c(-100,400),
xlab="",col="black")
points(muller[,1],muller[,2]-muller[,3],type="l", xlim=c(0,65),
ylab="",col="grey")
points(muller[,1],muller[,2]+muller[,4],type="l", xlim=c(0,65),
ylab="",col="grey")


DeBoer<-read.csv("DeBoer_data.csv",head=T)
points(DeBoer[,1]*-0.001,DeBoer[,2],type="l",ylab="",col="green3") #notice *-0.001 to
standarize scale
```

```
text(31,-18,"Miller",pch=.3,col="red")
text(32,208,"Haq",pch=.3,col="darkviolet")
text(2,101,"Müller",pch=.3)
text(7,-82,"DeBoer",pch=.3,col="green3")

### Temp  records
library(zoo)
Beerling<-read.csv("BeerlingTempCO2.csv",head=T)
plot(Beerling$age,Beerling$CO2,type="p",xlim=c(0,65),xlab="",ylab="Atmospheric CO2 (ppm)",
col="black",pch=19)
ma<-rollmean(Beerling$CO2,3,fill = list(NA, NULL, NA))
lines(Beerling$age,ma,col="orange",lwd=2)
abline(h=390, lty=2)
points(DeBoer[,1]*-0.001,DeBoer[,3],type="l",xlim=c(0,65),ylab="",col="blue") #Temp
points(DeBoer[,1]*-0.001,DeBoer[,4],type="l",xlim=c(0,65),ylab="",col="blue") #DeepWater Temp
```

9.3.2 - Chapter 5 (Age model):

Fig. 5.2 graphic correlation biplot:

```
## 105 vs SALTARIN
GCSALTARIN_105AM<-read.table("GCSALTARIN_105AM.txt",header=T,sep="\t",na.strings = "NA") #LOC
Salt vs 105
plot(GCSALTARIN_105AM$Saltarin.m,GCSALTARIN_105AM$ X1.AS.105.AM.m, ylab="105-AM (Depths in
m)",
xlab="Saltarin (Depths in m)", ylim=c(380,20),xlim=c(700,0),type="l",col="red")
grid()
events105Saltarin<-read.csv("105AM_Saltarin_events.csv",header=T,na.strings = "NA")
points(events105Saltarin$FADSalt*-1,events105Saltarin$FAD105*-1)
points(events105Saltarin$LADSalt*-1,events105Saltarin$LAD105*-1,pch=4, cex=.7)
#legend
library(gplots)
smartlegend("right","bottom",c("FAD", "LAD","Seq.
strat."),pch=c(1,4,17),inset=0.01,bty="n",cex=.7)
```

Fig. 5.6 Isopach map (kriging):

```
library(maps) #package for basic map
library(mapdata) #package for basic map
library(maptools) #package for basic map

map("worldHires", xlim=c(-75,-60),ylim=c(-12.7,0), border = 0.01,
interior=T,lwd=0.5,lty=4)
box()
```

```
data.s<-read.csv2("para isopach.csv",header=T)
library(akima) #package to perform Kriging
akima.li <- interp(data.s$x*-1,data.s$y*-1,data.s$z*-1,duplicate="mean")
akima.li.2<-interp(data.s$x*-.1,data.s$y*-.1,data.s$z*-.1,duplicate="mean")

image(akima.li, add=T)

contour(akima.li, nlevels= 20, add=TRUE,lwd=.5)
map("worldHires", xlim=c(-75,-60),ylim=c(-13,0), border = 0.01,
interior=T,lwd=0.5,lty=4,add=T) #repeat map outline

shape <- readShapeLines("lineaire_1km.shp") #shapefile for rivers
plot(shape,add=T,col="grey",lwd=0.4) #rivers

sites2<-read.csv("sites_Acre_Gross.csv",h=T)
points(sites2[1:1,2:3],pch=19,cex=2) #Gross et al 2011 sites
points(sites2[7:16,2:3],pch=19,cex=2) #Latrubesse et al 2010 sites
points(-70.916,-4.383,pch=19,cex=2) #4a
points(-69.933,-4.25,pch=19,cex=2) #105am
points(-67.916,-4.283,pch=19,cex=2) #27am
points(-69.166,-4.55,pch=19,cex=2) #19am
points(-71.4,-4.533,pch=19,cex=2) #32am
points(-63.140833,-4.085,pch=19,cex=2) #Coari
points(-60.077478,-3.117606) #Manaus
points(-73.25,-3.75) #Iquitos
points(-70.639236OO, -4.438224OO,pch=3,cex=2) #well 2-RC-1 (Miura 1972)
points(-70,-6.5,pch=3,cex=2) #2-EP-1 (approx. location) (Miura 1972)

#adding scale: 1 degree = 111 km//1'=1.85 Km//5'=.83 decimals
xe<-c(-74.104,-75)
ye<-c(-12,-12)
lines(xe,ye)  #0.896 = 100km
text(-74.5,-12.3,"100 km",cex=.7)
```

 # Fig. 5.7 graphic correlation biplots:

```
## Corr 105 vs 27:
Events105.27<-read.csv("105AM_27AM_events.csv",header=T,na.strings = "NA")
plot(Events105.27$FAD105,Events105.27$FAD27,ylab="27-AM (Depths in m)",
xlab="105-AM (Depths in m)", ylim=c(-390,-30),xlim=c(-380,-20))
points(Events105.27$LAD105,Events105.27$LAD27,pch=4,cex=.7)
grid()
```

```
#legend
library(gplots)
smartlegend("left","top",c("FAD", "LAD"),pch=c(1,4),inset=0.01,bty="n",cex=.7)
text(locator(1),"R. traversei",cex=.7)
text(locator(1),"R. arcus",cex=.7)
text(locator(1),"V. rotundiporus",cex=.7)
text(locator(1),"B. araracuarensis",cex=.7)
text(locator(1),"C. longispinosus",cex=.7)
text(locator(1),"L.? caribbiensis",cex=.7)
text(locator(1),"R. retibolus",cex=.7)
text(locator(1),"B. baculatus",cex=.7)
text(locator(1),"H. incomptus",cex=.7)
text(locator(1),"G. magnaclavata",cex=.7)
text(locator(1),"P. triangularis",cex=.7)

## Corr 105 vs 4a:
Events105.4a<-read.csv("105AM_4aAM_events.csv",header=T,na.strings = "NA")
plot(Events105.4a$FAD105,Events105.4a$FAD4a,ylab="4a-AM (Depths in m)",
xlab="105-AM (Depths in m)", ylim=c(-350,-10),xlim=c(-380,-20))
points(Events105.4a$LAD105,Events105.4a$LAD4a,pch=4,cex=.7)
grid()
#legend
library(gplots)
smartlegend("left","top",c("FAD", "LAD"),pch=c(1,4),inset=0.01,bty="n",cex=.7)
text(locator(1),"B. baculatus",cex=.7)
```

9.3.3 - Chapter 6 (Paleoenvironments):

 # Fig. 6.1 location map with sites from literature:

```
sites<-read.csv("table_map.csv",h=T)
sal_105<-sites[1:2,1:2]
e.m<-sites[3:19,1:2]        #early Miocene sites
em.m<-sites[20:22,1:2]      #early-middle Miocene sites
m.m<-sites[23:37,1:2]       #middle Miocene sites
Mio_indet<-sites[38:54,1:2] #Indet Miocene sites

library(raster) #package to import geotiff file with topography data
library(rgdal) #package to import geotiff file (etopo) with topography data
library(maps) #package to plot basic maps.
library(mapdata) #package to plot basic maps.
library(maptools) #package to plot basic maps.
etopo<-"map.files/ETOPO1_Ice_g_geotiff.tif"
```

```
r.etopo<-raster(etopo)
r.etopo[r.etopo<0]<-NA
r.etopo[r.etopo>600]<-NA

#col=bpy.colors(225)#rainbow, heat.colors, topo.colors, bpy.colors,gray.colors
ext <- extent(-82.5,-58.5,-12,13)

#Map:
zoom(r.etopo, ext=ext,col=rev(gray.colors(225)))
map("worldHires", xlim=c(-82.5,-58.5),ylim=c(-12,13), border = 0.01,
interior =T,lwd=0.5,add=T)
map("rivers", add=T, col="grey50",lwd=0.03)
points(-60.016667,-3.1,pch=3) #Manaus
points(-73.25,-3.733333,pch=3) #Iquitos

points(sal_105,pch=19,cex=0.8)
points(e.m,pch=19,cex=0.8)
points(m.m,pch=15,cex=0.8)
points(em.m,pch=1,cex=0.8)
points(Mio_indet,pch=2,cex=0.8)
numbers<-sites[,13]
text(sites[,1:2]*1.003,labels=c(numbers),cex=.5)

#scale: 1 degree = 111 km//1'=1.85 Km//5'=.83 decimals
xe<-c(-80,-81.792)
ye<-c(-10,-10)
lines(xe,ye)  #1.792 = 200km
text(-80.8,-10.5,"200 km",cex=.7)

library(gplots)
smartlegend("right","bottom",
c("Early Miocene","Middle Miocene","Early/Mid. Mioc.","Undif. Miocene"),
pch=c(19,15,1,2),inset=0.001,bty ="n",cex=.7)
```

 # Fig. 6.2 pollen groups diagrams:

```
rawdata<-read.csv("Chart_groups.csv",h=T) #counts start in column 8
rawdata[is.na(rawdata)] <- 0 #replace NAs with zeros
data<-cbind(rawdata[3:4],rawdata[6:7],rawdata[9:103]) #gets rid of unimportant columns
(author names, etc)

## Creating objects of sum based on groups:

library(data.table)  #for groups sums using data.table()
```

```
DT <- data.table(data)

type<-DT[, lapply(.SD, sum), by = type]
FW<-as.data.frame(type[1,])
FW<-FW[5:99]
MW<-as.data.frame(type[2,])
MW<-MW[5:99]
pollen<-as.data.frame(type[3,])
pollen<-pollen[5:99]
spores<-as.data.frame(type[4,])
spores<-spores[5:99]
#paleoz.acrit<-as.data.frame(type[5,])
#paleoz.acrit<-paleoz.acrit[5:99]
#other.age<-as.data.frame(type[6,])
#other.age<-other.age[5:99]
#cretaceous<-as.data.frame(type[7,])
#cretaceous<-cretaceous[5:99]
#tertiary<-as.data.frame(type[8,])
#tertiary<-tertiary[5:99]
#juras.Cretac.<-as.data.frame(type[9,])
#juras.Cretac.<-juras.Cretac.[5:99]

lifeHabit<-DT[, lapply(.SD, sum), by = life.habit]
tree<-as.data.frame(lifeHabit[3])
tree<-tree[5:99]
herb<-as.data.frame(lifeHabit[4])
herb<-herb[5:99]
RW<-as.data.frame(lifeHabit[8])
RW<-RW[5:99]
unknown<-as.data.frame(lifeHabit[5]) #unknown pollen life habit affinities
unknown<-unknown[5:99]

family<-DT[, lapply(.SD, sum), by = family.subfamily]
poaceae<-as.data.frame(family[40,])
poaceae<-poaceae[5:99]
palms<-as.data.frame(family[9,])
palms<-palms[5:99]
bombac<-as.data.frame(family[31,])
bombac<-bombac[5:99]
sedges<-as.data.frame(family[17,])
sedges<-sedges[5:99]

ecology<-DT[, lapply(.SD, sum), by = ecology]
mangrove<-as.data.frame(ecology[20,])
```

```
mangrove<-mangrove[5:99]
aquaticFern<-as.data.frame(ecology[23,])
aquaticFern<-aquaticFern[5:99]
aquaticHerb<-as.data.frame(ecology[5,])
aquaticHerb<-aquaticHerb[5:99]

other.herb<-herb-poaceae-sedges-aquaticHerb
other.tree<-tree-palms-bombac

## Calculating percentage for each group:
ages<-read.csv("Chart_groups.csv",h=F) #reading excel sheet again w/ h=F (to select ages)
ages<-as.numeric(ages[1,9:103])

groups<-rbind(ages,FW,MW,pollen,spores,tree,herb,poaceae,palms,bombac,
other.herb,other.tree,mangrove,unknown,aquaticFern,aquaticHerb,sedges)

rownames(groups)<-c("ages","FW","MW","pollen","spores","tree","herb",
"poaceae","palms","bombac","other.herb","other.tree","mangrove","unknown",
"aquaticFern","aquaticHerb","sedges")

groups<-as.data.frame(t(groups))
groups<-groups[rowSums(groups[2:5])>100,] #eliminate sums <100

totalSum<-apply(groups[2:5],1,sum) #total sum = algae+dinos+pollen+spores
pollenSum<-apply(groups[4:4],1,sum)
sporesSum<-apply(groups[5:5],1,sum)

FW.P<-groups$FW/totalSum*100
MW.P<-groups$MW/totalSum*100
mangrove.P<-groups$mangrove/pollenSum*100
aquaticHerb.P<-groups$aquaticHerb/pollenSum*100
aquaticFern.P<-groups$aquaticFern/totalSum*100
poaceae.P<-groups$poaceae/pollenSum*100
sedges.P<-groups$sedges/pollenSum*100
palms.P<-groups$palms/pollenSum*100
bombac.P<-groups$bombac/pollenSum*100
other.tree.P<-groups$other.tree/pollenSum*100
other.herb.P<-groups$other.herb/pollenSum*100
spores.P<-groups$spores/totalSum*100
unknown.P<-groups$unknown/pollenSum*100
tree.P<-groups$tree/pollenSum*100

groups.P<-rbind(groups$ages,MW.P,mangrove.P,FW.P,aquaticHerb.P,aquaticFern.P,poaceae.P,
```

```
sedges.P,other.herb.P,palms.P,bombac.P,other.tree.P,spores.P,unknown.P,tree.P) #new groups
using percentages

rownames(groups.P)<-c("ages","Marine elements","Mangrove pollen","Fresh water algae",
"Aquatic Herbs","Aquatic Ferns","Poaceae","Sedges (Cyperaceae)","Other herbs","Palms",
"Bombacoideae","Other trees","Fern spores","Unknown pollen affinity","Tres total")

groups.P<-as.data.frame(t(groups.P))

## Relation Aquatics~Algae:
aquatics<-aquaticHerb.P+aquaticFern.P
plot(log(FW.P+1),log(aquatics+1))
summary(lm(log(FW.P+1)~log(aquatics+1)))

#Molluscs data for diagram below:
molluscs<-read.csv("molluscs.csv",h=T)
molluscs[is.na(molluscs)] <- 0 #replace NAs with zeros

###Diagram (Fig. 6.2) part 1
library(rioja) # package that plots diagrams.
y.tks<-seq(10.7,18.8,0.5)
depths<-groups.P$ages

x<-strat.plot (molluscs[2:4],yvar=depths,scale.percent=F,
    graph.widths=1, minmax=NULL,
    scale.minmax = F, xLeft = 0.05, xRight = .1,
    yBottom = 0.07, yTop = 0.8, title = "", cex.title=1.2,
    y.axis=T, min.width = 5, ylim = NULL, y.rev = T,
    y.tks=y.tks, ylabel = "Ages(Ma)", cex.ylabel=1, cex.yaxis=.8,
    xSpace = 0.006, wa.order = "none",plot.line=F,
    col.line = "black", lwd.line=1,plot.bar=T,
    lwd.bar = 4, col.bar = "black", sep.bar = FALSE,
    plot.poly =F,col.poly="blue",col.poly.line="blue",
    lwd.poly = 1, x.names=NULL, cex.xlabel = .88, srt.xlabel=45,
    cex.axis=.8, clust.width=0.1,
    orig.fig=NULL, add=T)


addZone(x,13.72,col="grey50",lty=3) #MM top
addZone(x,14.15,col="grey50",lty=3) #MM bottom
addZone(x,17.8,col="grey50",lty=3)#EM top
addZone(x,18.43,col="grey50",lty=3)#EM bottom
addZone(x,18.78,col="grey50",lty=2) #FW1 bottom
addZone(x,15.93,col="grey50",lty=2) #FW2 bottom
```

```
addZone(x,14.97,col="grey50",lty=2) #FW2 top
addZone(x,12.90,col="grey50",lty=2) #FW3 bottom
addZone(x,11.04,col="grey50",lty=2) #FW3 top

par(tcl=-.25)
x<-strat.plot (groups.P[2:3],yvar=depths,scale.percent=T,
    graph.widths=1, minmax=NULL,
    scale.minmax = F, xLeft = 0.1, xRight = .21,
    yBottom = 0.07, yTop = 0.8, title = "", cex.title=1.2,
    y.axis=F, min.width = 5, ylim = NULL, y.rev = T,
    y.tks=y.tks, ylabel = "Ages(Ma)", cex.ylabel=1, cex.yaxis=.8,
    xSpace = 0.006, wa.order = "none",plot.line=F,
    col.line = "black", lwd.line=1,plot.bar=T,
    lwd.bar = 1, col.bar = "grey", sep.bar = FALSE,
    plot.poly =T,col.poly="blue",col.poly.line="blue",
    lwd.poly = 1, x.names=NULL, cex.xlabel = .88, srt.xlabel=45,
    cex.axis=.8, clust.width=0.1,
    orig.fig=NULL, add=T)

addZone(x,13.72,col="grey50",lty=3) #MM top
addZone(x,14.15,col="grey50",lty=3) #MM bottom
addZone(x,17.8,col="grey50",lty=3)#EM top
addZone(x,18.43,col="grey50",lty=3)#EM bottom
addZone(x,18.78,col="grey50",lty=2) #FW1 bottom
addZone(x,15.93,col="grey50",lty=2) #FW2 bottom
addZone(x,14.97,col="grey50",lty=2) #FW2 top
addZone(x,12.90,col="grey50",lty=2) #FW3 bottom
addZone(x,11.04,col="grey50",lty=2) #FW3 top

par(tcl=-.25)
x<-strat.plot (groups.P[4:6],yvar=depths,scale.percent=T,
    graph.widths=1, minmax=NULL,
    scale.minmax = F, xLeft = 0.20, xRight = .40,
    yBottom = 0.07, yTop = 0.8, title = "", cex.title=1.2,
    y.axis=F, min.width = 5, ylim = NULL, y.rev = T,
    y.tks=y.tks, ylabel = "", cex.ylabel=1, cex.yaxis=.8,
    xSpace = 0.006, wa.order = "none",plot.line=F,
    col.line = "black", lwd.line=1,plot.bar=T,
    lwd.bar = 1, col.bar = "grey40", sep.bar = FALSE,
    plot.poly =T,col.poly="turquoise3",col.poly.line="turquoise3",
    lwd.poly = 1, x.names=NULL, cex.xlabel = .88, srt.xlabel=45,
    cex.axis=.8, clust.width=0.1,
    orig.fig=NULL, add=T)
```

```
addZone(x,13.72,col="grey50",lty=3) #MM top
addZone(x,14.15,col="grey50",lty=3) #MM bottom
addZone(x,17.8,col="grey50",lty=3)#EM top
addZone(x,18.43,col="grey50",lty=3)#EM bottom
addZone(x,18.78,col="grey50",lty=2) #FW1 bottom
addZone(x,15.93,col="grey50",lty=2) #FW2 bottom
addZone(x,14.97,col="grey50",lty=2) #FW2 top
addZone(x,12.90,col="grey50",lty=2) #FW3 bottom
addZone(x,11.04,col="grey50",lty=2) #FW3 top

par(tcl=-.25)
x<-strat.plot (groups.P[7:9],yvar=depths,scale.percent=T,
    graph.widths=1, minmax=NULL,
    scale.minmax = F, xLeft = 0.40, xRight = .60,
    yBottom = 0.07, yTop = 0.8, title = "", cex.title=1.2,
    y.axis=F, min.width = 5, ylim = NULL, y.rev = T,
    y.tks=y.tks, ylabel = "", cex.ylabel=1, cex.yaxis=.8,
    xSpace = 0.006, wa.order = "none",plot.line=F,
    col.line = "black", lwd.line=1,plot.bar=T,
    lwd.bar = 1, col.bar = "grey30", sep.bar = FALSE,
    plot.poly =T,col.poly="yellowgreen",col.poly.line="yellowgreen",
    lwd.poly = 1, x.names=NULL, cex.xlabel = .88, srt.xlabel=45,
    cex.axis=.8, clust.width=0.1,
    orig.fig=NULL, add=T)

addZone(x,13.72,col="grey50",lty=3) #MM top
addZone(x,14.15,col="grey50",lty=3) #MM bottom
addZone(x,17.8,col="grey50",lty=3)#EM top
addZone(x,18.43,col="grey50",lty=3)#EM bottom
addZone(x,18.78,col="grey50",lty=2) #FW1 bottom
addZone(x,15.93,col="grey50",lty=2) #FW2 bottom
addZone(x,14.97,col="grey50",lty=2) #FW2 top
addZone(x,12.90,col="grey50",lty=2) #FW3 bottom
addZone(x,11.04,col="grey50",lty=2) #FW3 top

par(tcl=-.25)
x<-strat.plot (groups.P[10:12],yvar=depths,scale.percent=T,
    graph.widths=1, minmax=NULL,
    scale.minmax = F, xLeft = 0.60, xRight = .80,
    yBottom = 0.07, yTop = 0.8, title = "", cex.title=1.2,
    y.axis=F, min.width = 5, ylim = NULL, y.rev = T,
    y.tks=y.tks, ylabel = "", cex.ylabel=1, cex.yaxis=.8,
    xSpace = 0.006, wa.order = "none",plot.line=F,
    col.line = "black", lwd.line=1,plot.bar=T,
```

```
    lwd.bar = 1, col.bar = "grey", sep.bar = FALSE,
    plot.poly =T,col.poly="darkgreen",col.poly.line="darkgreen",
    lwd.poly = 1, x.names=NULL, cex.xlabel = .88, srt.xlabel=45,
    cex.axis=.8, clust.width=0.1,
    orig.fig=NULL, add=T)

addZone(x,13.72,col="grey50",lty=3) #MM top
addZone(x,14.15,col="grey50",lty=3) #MM bottom
addZone(x,17.8,col="grey50",lty=3)#EM top
addZone(x,18.43,col="grey50",lty=3)#EM bottom
addZone(x,18.78,col="grey50",lty=2) #FW1 bottom
addZone(x,15.93,col="grey50",lty=2) #FW2 bottom
addZone(x,14.97,col="grey50",lty=2) #FW2 top
addZone(x,12.90,col="grey50",lty=2) #FW3 bottom
addZone(x,11.04,col="grey50",lty=2) #FW3 top

par(tcl=-.25)
x<-strat.plot (groups.P[13:13],yvar=depths,scale.percent=T,
    graph.widths=1, minmax=NULL,
    scale.minmax = F, xLeft = 0.80, xRight = .89,
    yBottom = 0.07, yTop = 0.8, title = "", cex.title=1.2,
    y.axis=F, min.width = 5, ylim = NULL, y.rev = T,
    y.tks=y.tks, ylabel = "", cex.ylabel=1, cex.yaxis=.8,
    xSpace = 0.006, wa.order = "none",plot.line=F,
    col.line = "black", lwd.line=1,plot.bar=T,
    lwd.bar = 1, col.bar = "grey", sep.bar = FALSE,
    plot.poly =T,col.poly="darkolivegreen",col.poly.line="darkolivegreen",
    lwd.poly = 1, x.names=NULL, cex.xlabel = .88, srt.xlabel=45,
    cex.axis=.8, clust.width=0.1,
    orig.fig=NULL, add=T)

addZone(x,13.72,col="grey50",lty=3) #MM top
addZone(x,14.15,col="grey50",lty=3) #MM bottom
addZone(x,17.8,col="grey50",lty=3)#EM top
addZone(x,18.43,col="grey50",lty=3)#EM bottom
addZone(x,18.78,col="grey50",lty=2) #FW1 bottom
addZone(x,15.93,col="grey50",lty=2) #FW2 bottom
addZone(x,14.97,col="grey50",lty=2) #FW2 top
addZone(x,12.90,col="grey50",lty=2) #FW3 bottom
addZone(x,11.04,col="grey50",lty=2) #FW3 top

par(tcl=-.25)
x<-strat.plot (groups.P[14:14],yvar=depths,scale.percent=T,
    graph.widths=1, minmax=NULL,
```

```
    scale.minmax = F, xLeft = 0.89, xRight = 0.99,
    yBottom = 0.07, yTop = 0.8, title = "", cex.title=1.2,
    y.axis=F, min.width = 5, ylim = NULL, y.rev = T,
    y.tks=y.tks, ylabel = "", cex.ylabel=1, cex.yaxis=.8,
    xSpace = 0.006, wa.order = "none",plot.line=F,
    col.line = "black", lwd.line=1,plot.bar=T,
    lwd.bar = 1, col.bar = "black", sep.bar = T,
    plot.poly =F,col.poly="",col.poly.line="",
    lwd.poly = 1, x.names=NULL, cex.xlabel = .88, srt.xlabel=45,
    cex.axis=.8, clust.width=0.1,
    orig.fig=NULL, add=T)

addZone(x,13.72,col="grey50",lty=3) #MM top
addZone(x,14.15,col="grey50",lty=3) #MM bottom
addZone(x,17.8,col="grey50",lty=3)#EM top
addZone(x,18.43,col="grey50",lty=3)#EM bottom
addZone(x,18.78,col="grey50",lty=2) #FW1 bottom
addZone(x,15.93,col="grey50",lty=2) #FW2 bottom
addZone(x,14.97,col="grey50",lty=2) #FW2 top
addZone(x,12.90,col="grey50",lty=2) #FW3 bottom
addZone(x,11.04,col="grey50",lty=2) #FW3 top


###### Family diagram (individual Families are isolates and a data set is created with them
to build the diagram) - Fig. 6.5.

family<-DT[, lapply(.SD, sum), by = family.subfamily]

Acanthaceae<-as.data.frame(family[2,])
Acanthaceae<-Acanthaceae[5:99]
Alismataceae<-as.data.frame(family[3,])
Alismataceae<-Alismataceae[5:99]
Annonaceae<-as.data.frame(family[4,])
Annonaceae<-Annonaceae[5:99]
Apocynaceae<-as.data.frame(family[4,])
Apocynaceae<-Apocynaceae[5:99]
Aquafoliaceae<-as.data.frame(family[6,])
Aquafoliaceae<-Aquafoliaceae[5:99]
Araliaceae<-as.data.frame(family[7,])
Araliaceae<-Araliaceae[5:99]
Araucariaceae<-as.data.frame(family[8,])
Araucariaceae<-Araucariaceae[5:99]
Arecaceae<-as.data.frame(family[9,])
Arecaceae<-Arecaceae[5:99]
```

```
Asteraceae<-as.data.frame(family[11,])
Asteraceae<-Asteraceae[5:99]
Burseraceae.Sapotaceae<-as.data.frame(family[12,])
Burseraceae.Sapotaceae<-Burseraceae.Sapotaceae[5:99]
Chrysobalanaceae<-as.data.frame(family[13,])
Chrysobalanaceae<-Chrysobalanaceae[5:99]
Cloranthaceae<-as.data.frame(family[14,])
Cloranthaceae<-Cloranthaceae[5:99]
Convolvulaceae<-as.data.frame(family[15,])
Convolvulaceae<-Convolvulaceae[5:99]
Cyperaceae<-as.data.frame(family[17,])
Cyperaceae<-Cyperaceae[5:99]
Ericaceae<-as.data.frame(family[18,])
Ericaceae<-Ericaceae[5:99]
Euphorbiaceae<-as.data.frame(family[19,])
Euphorbiaceae<-Euphorbiaceae[5:99]
Fabaceae.Caesalpinioideae<-as.data.frame(family[20,])
Fabaceae.Caesalpinioideae<-Fabaceae.Caesalpinioideae[5:99]
Fabaceae.Mimosoideae<-as.data.frame(family[21,])
Fabaceae.Mimosoideae<-Fabaceae.Mimosoideae[5:99]
Fabaceae.Papilionoideae<-as.data.frame(family[22,])
Fabaceae.Papilionoideae<-Fabaceae.Papilionoideae[5:99]
Hippocrateaceae<-as.data.frame(family[24,])
Hippocrateaceae<-Hippocrateaceae[5:99]
Humiriaceae<-as.data.frame(family[25,])
Humiriaceae<-Humiriaceae[5:99]
Loranthaceae<-as.data.frame(family[26,])
Loranthaceae<-Loranthaceae[5:99]
Lythraceae<-as.data.frame(family[27,])
Lythraceae<-Lythraceae[5:99]
Malpighiaceae<-as.data.frame(family[28,])
Malpighiaceae<-Malpighiaceae[5:99]
Malvaceae<-as.data.frame(family[29,])
Malvaceae<-Malvaceae[5:99]
Malvaceae.Bombacoideae<-as.data.frame(family[31,])
Malvaceae.Bombacoideae<-Malvaceae.Bombacoideae[5:99]
Malvaceae.Convolvulaceae<-as.data.frame(family[32,])
Malvaceae.Convolvulaceae<-Malvaceae.Convolvulaceae[5:99]
Melastomataceae<-as.data.frame(family[33,])
Melastomataceae<-Melastomataceae[5:99]
Moraceae<-as.data.frame(family[34,])
Moraceae<-Moraceae[5:99]
Myristicaceae<-as.data.frame(family[35,])
Myristicaceae<-Myristicaceae[5:99]
```

```
Myrtaceae<-as.data.frame(family[36,])
Myrtaceae<-Myrtaceae[5:99]
Onagraceae<-as.data.frame(family[37,])
Onagraceae<-Onagraceae[5:99]
Passifloraceae<-as.data.frame(family[38,])
Passifloraceae<-Passifloraceae[5:99]
Pellicieraceae<-as.data.frame(family[39,])
Pellicieraceae<-Pellicieraceae[5:99]
Poaceae<-as.data.frame(family[40,])
Poaceae<-Poaceae[5:99]
Podocarpaceae<-as.data.frame(family[41,])
Podocarpaceae<-Podocarpaceae[5:99]
Polygalaceae<-as.data.frame(family[42,])
Polygalaceae<-Polygalaceae[5:99]
Rhizophoraceae<-as.data.frame(family[43,])
Rhizophoraceae<-Rhizophoraceae[5:99]
Sapindaceae.Proteaceae<-as.data.frame(family[45,])
Sapindaceae.Proteaceae<-Sapindaceae.Proteaceae[5:99]
Sapotaceae<-as.data.frame(family[46,])
Sapotaceae<-Sapotaceae[5:99]
Sapotaceae.Pouteria<-as.data.frame(family[47,])
Sapotaceae.Pouteria<-Sapotaceae.Pouteria[5:99]
Sapotaceae<-Sapotaceae+Sapotaceae.Pouteria
Tiliaceae.Sterculiaceae<-as.data.frame(family[49,])
Tiliaceae.Sterculiaceae<-Tiliaceae.Sterculiaceae[5:99]

## Calculating percentage for each family:
ages<-read.csv("Chart_groups.csv",h=F) #reading excel sheet again w/ h=F (to select ages)
ages<-as.numeric(ages[1,9:103])

groups<-
rbind(pollen,ages,Poaceae,Asteraceae,Ericaceae,Passifloraceae,Convolvulaceae,Cyperaceae,
Alismataceae,Onagraceae,Polygalaceae,Arecaceae,Euphorbiaceae,Melastomataceae,Malvaceae.Bombac
oideae,Rhizophoraceae,Tiliaceae.Sterculiaceae,Araliaceae,Burseraceae.Sapotaceae,Podocarpaceae
,Humiriaceae,Acanthaceae,Annonaceae,Apocynaceae,Aquafoliaceae,Araucariaceae,
Chrysobalanaceae,Cloranthaceae,Fabaceae.Caesalpinioideae,Fabaceae.Mimosoideae,Fabaceae.Papili
onoideae,Hippocrateaceae,Loranthaceae,Lythraceae,Malpighiaceae,Malvaceae,Malvaceae.Convolvula
ceae,Moraceae,Myristicaceae,Myrtaceae,Pellicieraceae,Sapindaceae.Proteaceae,Sapotaceae)

rownames(groups)<-
c("pollen","ages","Poaceae","Asteraceae","Ericaceae","Passifloraceae","Convolvulaceae"
,"Cyperaceae","Alismataceae","Onagraceae","Polygalaceae","Arecaceae","Euphorbiaceae","Melasto
mataceae","Malvaceae.Bombacoideae","Rhizophoraceae","Tiliaceae.Sterculiaceae","Araliaceae","B
urseraceae.Sapotaceae","Podocarpaceae","Humiriaceae","Acanthaceae","Annonaceae","Apocynaceae"
```

```
,"Aquafoliaceae","Araucariaceae","Chrysobalanaceae","Cloranthaceae","Fabaceae.Caesalpinioidea
e","Fabaceae.Mimosoideae","Fabaceae.Papilionoideae","Hippocrateaceae","Loranthaceae","Lythrac
eae","Malpighiaceae","Malvaceae","Malvaceae.Convolvulaceae","Moraceae","Myristicaceae","Myrta
ceae","Pellicieraceae","Sapindaceae.Proteaceae","Sapotaceae")

groups<-as.data.frame(t(groups))
groups<-groups[rowSums(groups[3:43])>13,] #eliminate sums <13 (one of lowest numbers of count
w/o excluding any family)
depths<-groups$ages
groups<-groups[3:43]/groups$pollen*100

y.tks<-seq(10.7,18.8,0.5)

par(tcl=-.25)
x<-strat.plot (groups[1:13],yvar=depths,scale.percent=T,
    graph.widths=1, minmax=NULL,
    scale.minmax = F, xLeft = 0.05, xRight = .55,
    yBottom = 0.07, yTop = 0.8, title = "", cex.title=1.2,
    y.axis=TRUE, min.width = 5, ylim = NULL, y.rev = T,
    y.tks=y.tks, ylabel = "Ages(Ma)", cex.ylabel=1, cex.yaxis=.8,
    xSpace = 0.006, wa.order = "none",plot.line=F,
    col.line = "black", lwd.line=1,plot.bar=T,
    lwd.bar = 1, col.bar = "grey40", sep.bar = FALSE,
    plot.poly =T,col.poly="darkgreen",col.poly.line="darkgreen",
    lwd.poly = 1, x.names=NULL, cex.xlabel = .88, srt.xlabel=45,
    cex.axis=.8, clust.width=0.1,
    orig.fig=NULL)

par(tcl=-.25)
x<-strat.plot (groups[14:41],yvar=depths,scale.percent=T,
    graph.widths=1, minmax=NULL,
    scale.minmax = F, xLeft = 0.55, xRight = .95,
    yBottom = 0.07, yTop = 0.8, title = "", cex.title=1.2,
    y.axis=F, min.width = 5, ylim = NULL, y.rev = T,
    y.tks=y.tks, ylabel = "Ages(Ma)", cex.ylabel=1, cex.yaxis=.8,
    xSpace = 0.006, wa.order = "none",plot.line=F,
    col.line = "black", lwd.line=1,plot.bar=T,
    lwd.bar = 1, col.bar = "grey40", sep.bar = FALSE,
    plot.poly =T,col.poly="darkgreen",col.poly.line="darkgreen",
    lwd.poly = 1, x.names=NULL, cex.xlabel = .88, srt.xlabel=45,
    cex.axis=.8, clust.width=0.1,
    orig.fig=NULL,add=T)
```

```
#### Dinocysts diagram (Fig. 6.3)

rawdata<-read.csv("dinos.only.csv",h=T) #counts start in column 8
rawdata[is.na(rawdata)] <- 0 #replace NAs with zeros

FW<-as.data.frame(type[1,])
FW<-FW[5:99]
MW<-as.data.frame(type[2,])
MW<-MW[5:99]
pollen<-as.data.frame(type[3,])
pollen<-pollen[5:99]
spores<-as.data.frame(type[4,])
spores<-spores[5:99]

totalSum<-as.numeric(FW+MW+pollen+spores)

aquatic<-rawdata[2:25]/totalSum*100 #2 first FW, rest is MW
aquatic[is.na(aquatic)] <- 0 #replace NAs with zeros
mangrove<-rawdata[26:27]/totalSum*100
mangrove[is.na(mangrove)] <- 0 #replace NAs with zeros
ages<-as.numeric(rawdata$X)

y.tks<-seq(10.7,18.8,0.5)

par(tcl=-.25)
x<-strat.plot (aquatic[1:2],yvar=ages,scale.percent=T,
    graph.widths=1, minmax=NULL,
    scale.minmax = F, xLeft = 0.15, xRight = .3,
    yBottom = 0.07, yTop = 0.8, title = "", cex.title=1.2,
    y.axis=T, min.width = 5, ylim = NULL, y.rev = T,
    y.tks=y.tks, ylabel = "Ages(Ma)", cex.ylabel=1, cex.yaxis=.8,
    xSpace = 0.006, wa.order = "bottomleft",plot.line=F,
    col.line = "black", lwd.line=1,plot.bar=T,
    lwd.bar = 1, col.bar = "grey40", sep.bar = FALSE,
    plot.poly =T,col.poly="turquoise3",col.poly.line="turquoise3",
    lwd.poly = 1, x.names=NULL, cex.xlabel = .88, srt.xlabel=45,
    cex.axis=.8, clust.width=0.1,
    orig.fig=NULL,add=T)

addZone(x,13.72,col="grey50",lty=3) #MM top
addZone(x,14.15,col="grey50",lty=3) #MM bottom
addZone(x,17.8,col="grey50",lty=3)#EM top
addZone(x,18.43,col="grey50",lty=3)#EM bottom
addZone(x,18.78,col="grey50",lty=2) #FW1 bottom
```

```
addZone(x,15.93,col="grey50",lty=2) #FW2 bottom
addZone(x,14.97,col="grey50",lty=2) #FW2 top
addZone(x,12.90,col="grey50",lty=2) #FW3 bottom
addZone(x,11.04,col="grey50",lty=2) #FW3 top

par(tcl=-.25)
x<-strat.plot (aquatic[3:24],yvar=ages,scale.percent=T,
    graph.widths=1, minmax=NULL,
    scale.minmax = F, xLeft = 0.3, xRight = .8,
    yBottom = 0.07, yTop = 0.8, title = "", cex.title=1.2,
    y.axis=F, min.width = 5, ylim = NULL, y.rev = T,
    y.tks=y.tks, ylabel = "Ages(Ma)", cex.ylabel=1, cex.yaxis=.8,
    xSpace = 0.006, wa.order = "bottomleft",plot.line=F,
    col.line = "black", lwd.line=1,plot.bar=T,
    lwd.bar = 1, col.bar = "grey", sep.bar = FALSE,
    plot.poly =T,col.poly="blue",col.poly.line="blue",
    lwd.poly = 1, x.names=NULL, cex.xlabel = .88, srt.xlabel=45,
    cex.axis=.8, clust.width=0.1,
    orig.fig=NULL,add=T)

addZone(x,13.72,col="grey50",lty=3) #MM top
addZone(x,14.15,col="grey50",lty=3) #MM bottom
addZone(x,17.8,col="grey50",lty=3)#EM top
addZone(x,18.43,col="grey50",lty=3)#EM bottom
addZone(x,18.78,col="grey50",lty=2) #FW1 bottom
addZone(x,15.93,col="grey50",lty=2) #FW2 bottom
addZone(x,14.97,col="grey50",lty=2) #FW2 top
addZone(x,12.90,col="grey50",lty=2) #FW3 bottom
addZone(x,11.04,col="grey50",lty=2) #FW3 top

par(tcl=-.25)
x<-strat.plot (mangrove,yvar=ages,scale.percent=T,
    graph.widths=1, minmax=NULL,
    scale.minmax = F, xLeft = 0.8, xRight = .85,
    yBottom = 0.07, yTop = 0.8, title = "", cex.title=1.2,
    y.axis=F, min.width = 5, ylim = NULL, y.rev = T,
    y.tks=y.tks, ylabel = "Ages(Ma)", cex.ylabel=1, cex.yaxis=.8,
    xSpace = 0.006, wa.order = "bottomleft",plot.line=F,
    col.line = "black", lwd.line=1,plot.bar=T,
    lwd.bar = 1, col.bar = "grey", sep.bar = FALSE,
    plot.poly =T,col.poly="darkolivegreen",col.poly.line="darkolivegreen",
    lwd.poly = 1, x.names=NULL, cex.xlabel = .88, srt.xlabel=45,
    cex.axis=.8, clust.width=0.1,
    orig.fig=NULL,add=T)
```

```
addZone(x,13.72,col="grey50",lty=3) #MM top
addZone(x,14.15,col="grey50",lty=3) #MM bottom
addZone(x,17.8,col="grey50",lty=3)#EM top
addZone(x,18.43,col="grey50",lty=3)#EM bottom
addZone(x,18.78,col="grey50",lty=2) #FW1 bottom
addZone(x,15.93,col="grey50",lty=2) #FW2 bottom
addZone(x,14.97,col="grey50",lty=2) #FW2 top
addZone(x,12.90,col="grey50",lty=2) #FW3 bottom
addZone(x,11.04,col="grey50",lty=2) #FW3 top
```

 # Boxplots (Fig. 6.4) of %algae and %dinocysts and kruskal/ANOVA tests (results of chapter 6)

of %algae and %dinocysts and %aquatic pollen against lithology:

```
data<-read.csv("data_divers.csv", head=T)
data[is.na(data)] <- 0
litho<-data[1]
FW<-data[3]
MW<-data[4]
pollenSum<-rowSums(data[5:403])
totalSum<-pollenSum+FW+MW
data2<-cbind(litho,FW/totalSum*100,MW/totalSum*100,pollenSum)
data2<-data2[pollenSum>100,] #eliminate pollen sums <100

par(mfrow=c(1,2))
boxplot(log(FreshWaterAlgae+1)~lithology,data=data2,
ylab="log % Freshwater algae")

shapiro.test(data2$FreshWaterAlgae) #not normal, thus a Kruskal-Wallis will be used
kruskal.test(FreshWaterAlgae~lithology,data=data2)

library(PMCMR) #to run KW post hoc Tukey test
posthoc.kruskal.nemenyi.test(FreshWaterAlgae~lithology,data=data2,dist="Tukey")

boxplot(log(Dinocysts+1)~lithology,data=data2,ylab="log % Dinocysts")
shapiro.test(data2$Dinocysts) #not normal, thus a Kruskal-Wallis will be used
kruskal.test(Dinocysts~lithology,data=data2) #there are no sig. differences

text(2.572,3.917,"MF1 and MF2
Dinocyst spikes", cex=.8)

##Aquatic vs Litho:
```

```
data<-read.csv("Aquatic_vs_litho.csv", head=T)
data[is.na(data)] <- 0

litho<-data[1]
aquatic<-data[3]
FW<-data[4]
MW<-data[5]
pollenSum<-rowSums(data[6:404])
totalSum<-pollenSum+FW+MW

data2<-cbind(litho,aquatic/totalSum*100,pollenSum)
data2<-data2[pollenSum>100,] #eliminate pollen sums <100

boxplot(log(totalAquatic+1)~lithology,data=data2,
ylab="log % Fresh water algae")

shapiro.test(data2$totalAquatic) #normal
aov<-aov(totalAquatic~lithology,data=data2)
summary(aov)
```

 # Canonical Correspondence Analysis (Table 6.1) location map with sites from literature:

```
data<-read.csv("Chart_CCA.csv",h=T)
data[is.na(data)]<-0
data<-data[rowSums(data[9:410])>100,]
data<-data[,colSums(data)>3]

environ<-data[1:8]  #environmental variables
veg<-log(data[9:178]+1) #vegetation matrix

library(vegan)
cca.1<-cca(veg~FreshWater+PeakMarine,data=environ) #runs cca
cca.1 #CCA summary

#cca w binary data set:
veg<-data[9:178]
veg<-ifelse(veg[,-1]>=1,1,0) #transforming data into binary

cca.1<-cca(veg~FreshWater+PeakMarine,data=environ) #runs cca
cca.1 #CCA summary
```

 # Diagram (Fig. 6.6) of marine-freshwater elements from Saltarin and 105-am, plus sea level curves:

```
##Saltarin:
rawdata<-read.csv("DataSaltarin.csv",h=T)
rawdata[is.na(rawdata)] <- 0
data<-rawdata[rowSums(rawdata[8])>100,] #eliminate sums <100
FWperc<-data$FW/data$Total.Sum*100
Marine<-(data$Dinos+data$Foram.lining)/data$Total.Sum*100
groups.P<-cbind(data$age, FWperc, Marine)
groups.P<-as.data.frame(groups.P[21:96,]) #excl. Late Mioc samples

###Diagrama parte 1
library(rioja) #package that plots diagram
y.tks<-seq(10.7,18.7,0.5)
depths<-groups.P[,1]

par(tcl=-.25)
x<-strat.plot (groups.P[2:3],yvar=depths,scale.percent=T,
    graph.widths=1, minmax=NULL,
    scale.minmax = F, xLeft = 0.1, xRight = .51,
    yBottom = 0.07, yTop = 0.8, title = "", cex.title=1.2,
    y.axis=TRUE, min.width = 5, ylim = NULL, y.rev = T,
    y.tks=y.tks, ylabel = "Ages(Ma)", cex.ylabel=1, cex.yaxis=.8,
    xSpace = 0.006, wa.order = "none",plot.line=F,
    col.line = "black", lwd.line=1,plot.bar=F,
    lwd.bar = 1, col.bar = "grey", sep.bar = FALSE,
    plot.poly =T,col.poly=c("turquoise3","blue"),col.poly.line=c("turquoise3","blue"),
    lwd.poly = 1, x.names=NULL, cex.xlabel = .88, srt.xlabel=45,
    cex.axis=.8, clust.width=0.1,
    orig.fig=NULL, add=T)

addZone(x,13.72,col="grey50",lty=3) #MM top
addZone(x,14.15,col="grey50",lty=3) #MM bottom
addZone(x,17.8,col="grey50",lty=3)#EM top
addZone(x,18.43,col="grey50",lty=3)#EM bottom

##105-AM:
rawdata<-read.csv("FWMW_105.csv",h=T)
rawdata[is.na(rawdata)] <- 0
data<-rawdata[rowSums(rawdata[6])>100,] #eliminate sums <100

FWperc<-data$FW/data$TotalSum*100
Marine<-(data$Dinocysts+data$Forams)/data$TotalSum*100
```

```
groups.P<-cbind(data$age, FWperc, Marine)

y.tks<-seq(10.7,18.7,0.5)
depths<-groups.P[,1]

par(tcl=-.25)
x<-strat.plot (groups.P[,2:3],yvar=depths,scale.percent=T,
    graph.widths=1, minmax=NULL,
    scale.minmax = F, xLeft = 0.6, xRight = .95,
    yBottom = 0.045, yTop = 0.85, title = "", cex.title=1.2,
    y.axis=TRUE, min.width = 5, ylim = NULL, y.rev = T,
    y.tks=y.tks, ylabel = "", cex.ylabel=1, cex.yaxis=.8,
    xSpace = 0.006, wa.order = "none",plot.line=F,
    col.line = "black", lwd.line=1,plot.bar=F,
    lwd.bar = 1, col.bar = "grey", sep.bar = FALSE,
    plot.poly =T,col.poly=c("turquoise3","blue"),col.poly.line=c("turquoise3","blue"),
    lwd.poly = 1, x.names=NULL, cex.xlabel = .88, srt.xlabel=45,
    cex.axis=.8, clust.width=0.1,
    orig.fig=NULL, add=T)

addZone(x,13.72,col="grey50",lty=3) #MM top
addZone(x,14.15,col="grey50",lty=3) #MM bottom
addZone(x,17.8,col="grey50",lty=3)#EM top
addZone(x,18.43,col="grey50",lty=3)#EM bottom

###sea levels:
haq<-read.csv("haq_sealevel_curve.csv",head=T)
par(mfrow=c(1,2))
plot(haq$seaLevel,haq$age,type="l", ylim=c(18.7,10.7),xlim=c(-80,160),
xlab="Sea Level curve",ylab="Age (Ma)", col="grey",lty=2,lwd=2)

miller<-read.csv("MillerCurve2005.csv",head=T)
points(miller[,1],miller[,2],type="l", ylim=c(18.7,10.7),xlim=c(-80,160),
ylab="",col="grey",lwd=2)

muller<-read.csv("MullerCurve2008.csv",head=T)
#points(muller[,2],muller[,1],type="l", ylim=c(18.7,10.7),xlim=c(-80,160),
xlab="",col="black")
#points(muller[,2]-muller[,3],muller[,1],type="l", xlim=c(0,65),
ylab="",col="grey")
#points(muller[,2]+muller[,4],muller[,1],type="l", xlim=c(0,65),
ylab="",col="grey")

DeBoer<-read.csv("DeBoer_data.csv",head=T)
```

```
points(DeBoer[,2],DeBoer[,1]*-0.001,type="l",ylab="",col="black",lwd=2) #notice *-0.001 to
standarize scale
abline(v=0,lty=2)
text(31,-18,"Miller",pch=.3,col="red")
text(32,208,"Haq",pch=.3,col="darkviolet")
text(2,101,"Müller",pch=.3)
text(7,-82,"DeBoer",pch=.3,col="green3")

##Zachos
data<-read.csv("zachos2008.csv",head=T)
plot(data$d18O.5pt,data$Age,ylim=c(18.7,10.7), xlim=c(3,1.3),type="l",col="blue",lwd=1.5,
xlab="d18O",ylab="")
#plot(data$d13C.5pt,data$Age,ylim=c(18.7,10.7),type="l",col="green4",lwd=1.5,
ylab="d13C",xlab="Age (Ma)")
abline(h=18.7)
abline(h=10.7)
```

9.3.4 - Chapter 7 (Diversity). Codes for figures and analyses.

```
# preparing the data plus Fig. 7.1 (abundance and eveness distribution over ages):
data<-read.csv("data_divers.csv", h=T)
data300<-data[1:405] #selects pollen+spores counts only
data300[is.na(data300)] <- 0 #replace NAs with zeros
data300.sum<-apply(data300[3:405], 1, sum) #row sums

plot(data300.sum,data300[,2],ylim=c(19,10), ylab="Age (ma)",
xlab="Pollen count, cutoff=226")
abline(v=223,lty=2)

data226<-data300[rowSums(data300[3:405])>225,] #excludes rows < 226 count. Note first column
(ages) is not included in the row sum
data226.sum<-apply(data226[3:405], 1, sum) #new row sums
points(data226.sum,data226[,2],ylim=c(19,10.5),cex=.5, col="red") #plotting to confirm subset
was correctly made
#At this point, a new dataset has been produced with pollen counts >= 226. Now, some
diversity metrics will be calculated including evenness, after that a new dataset will be
produced excluding samples with very low evenness:

library(vegan)
ages<-data226[,2]
raremin<-min(rowSums(data226[3:405])) #shows lowest count, which I know already from the
routine (and plot) above
H<-diversity(data226[3:405],index="shannon") #shannon index
```

```
S<-specnumber(data226[3:405]) #number of species (richness)
J<-H/log(S) #eveness

plot(J, ages,ylim=c(19,10),type="b",xlab="eveness",ylab="ages (ma)") #plotting eveness vs
age:
abline(v=0.405,lty=2)
points(J[25],ages[25],pch=20)
points(J[57],ages[57],pch=20)
points(J[64],ages[64],pch=20)

data226$J<-J #adds "J" column of eveness values to data.frame (which is now 405 columns long)
data226<-data226[data226["J"]>0.4,] #excludes rows < 0.4 evenness (3 samples)

##### New diversity indexes and eveness
ages<-data226[,2]
Srare<-rarefy(data226[3:405], 226)
H<-diversity(data226[3:405],index="shannon") #shannon index
S<-specnumber(data226[3:405]) #number of species (richness)
J<-H/log(S) #eveness

plot(J, ages,ylim=c(19,10),type="b",xlab="eveness",ylab="ages (ma)") #plotting eveness vs
age:
abline(v=0.405,lty=2)
mean(J[1:36])
mean(J[37:67])
wilcox.test(J[1:37],J[38:70])
text(0.77,13.3,"mean=0.66",cex=.8)
text(0.77,17.3,"mean=0.63",cex=.8)
legend("topleft","p-value=0.09",cex=.8,box.lty=0)
abline(v=0.66)
abline(v=0.63)

############### Rarefied diversity (Fig. 7.2-a)
plot(Srare,ages,ylim=c(19.5,10),type="b", ylab="ages (Ma)",
xlab="Rarefied diverity")
points(Srare[1:36],ages[1:36],pch=20)
mean(Srare[1:36])
mean(Srare[37:67])
wilcox.test(Srare[1:37],Srare[38:70])
text(50.5,13.4,"mean=36.7",cex=.8)
text(50.5,17.3,"mean=25",cex=.8)
legend("topleft","p-value=1.966e-06",cex=.8,box.lty=0)
abline(v=36.7)
abline(v=25)
```

```
##########Diversity Shannon (Fig. 7.2-b)
plot(H,ages,ylim=c(19,10),type="b",ylab="Age (ma)",xlab="H' diversity")
points(H[1:37],ages[1:37],pch=20)

mean(H[1:36])  #2.4
mean(H[37:67]) #2.0
text(3,13,"mean=2.4",cex=.8)
text(3,17,"mean=2.0",cex=.8)
abline(v=2.4)
abline(v=2.0)

wilcox.test(H[1:37],H[38:70]) #p-value=0.0003596
legend("topleft","p-value=0.0003596",cex=.8,box.lty=0)

############# DCA (Table 7.1 and Fig. 7.2-c and d)
dataDCA<-log(data226[3:405]+1)
#dataDCA2<-log(data226[,colSums(data226[3:405])>1]+1) #exlc. singletons
DCA<-decorana(dataDCA,iweigh=1)
axis1<-DCA$rproj[,1]
axis2<-DCA$rproj[,2]

plot(DCA, display="none",xlim=c(0,2.5),ylim=c(0,2.5))
points(axis1[1:37],axis2[1:37],xlim=c(0,2.5),ylim=c(0,3),pch=20)
points(axis1[38:70],axis2[38:70],xlim=c(0,2.5),ylim=c(0,3))
text(0.31,1.33,"pos-16Ma",cex=.8)
text(1.7,1.06,"pre-16Ma",cex=.8)
text(1.6,2.4,"Bottom 3 samples",cex=.8)

mean(axis1[1:36])
mean(axis1[37:67])
wilcox.test(axis1[1:36],axis1[37:67])

plot(axis1, ages,ylim=c(19.5,10),type="b",ylab="ages (Ma)",xlab="DCA axis 1")
text(1,12.70,"mean=0.35",cex=.8)
text(1.8,17,"mean=1.24",cex=.8)
text(2,10,"p-value=2.2e-16",cex=.8)
abline(v=0.35)
abline(v=1.24)
points(axis1[1:36], ages[1:36],pch=20)

mean(axis2[1:36])
mean(axis2[37:67])
wilcox.test(axis2[1:36],axis2[37:67])
```

```
plot(axis2, ages,ylim=c(19.5,10),type="b",ylab="",xlab="DCA axis 2")
points(axis2[1:37], ages[1:37],pch=20)
text(1.9,13.4,"mean=0.83",cex=.8)
text(1.9,17.36,"mean=0.90",cex=.8)
text(2.2,10,"p-value=0.5696",cex=.8)
abline(v=0.83)
abline(v=0.90)

#################### Lithology (data preparation, boxplots and analyses) (Fig. 7.3 and 7.4)
younger<-rep("younger",35)
older<-rep("older",32)
strata<-matrix(c(rep("younger",35),rep("older",32)))

litho.data<-data.frame(data226[2:2],data226[1:1],Srare,axis1,axis2,H,J,strata)

library(plyr)
count(litho.data$lithology) #counts how many samples per lithology

par(mfrow=c(3,2))
boxplot(litho.data$Srare~litho.data$lithology,ylab="Rarefied diversity",
main="n=12            n=29      n=10            n=16")
boxplot(litho.data$H~litho.data$lithology,ylab="H' diversity")
boxplot(litho.data$axis1~litho.data$lithology,ylab="DCA axis 1")
boxplot(litho.data$axis2~litho.data$lithology,ylab="DCA axis 2")
boxplot(litho.data$J~litho.data$lithology,ylab="Eveness")

plot(litho.data$Srare,litho.data$ages,ylim=c(19.5,10),type="b",ylab="ages (Ma)",
xlab="Rarefied diversity")
points(litho.data$Srare,litho.data$ages,col=litho.data$lithology,pch=20)
legend('topleft',legend=levels(litho.data$lithology),col=1:4,cex=0.8,pch=20)
abline(h=17.8,lty=2)
abline(h=18.03,lty=2)
abline(h=14.09,lty=2)
abline(h=13.73,lty=2)

plot(litho.data$axis1,litho.data$ages,ylim=c(19.5,10),type="b",ylab="ages (Ma)",
xlab="DCA axis 1")
points(litho.data$axis1,litho.data$ages,col=litho.data$lithology,pch=20)
legend('topright',legend=levels(litho.data$lithology),col=1:4,cex=0.8,pch=20)

plot(litho.data$axis2,litho.data$ages,ylim=c(19.5,10),type="b",ylab="ages (Ma)",
xlab="DCA axis 2")
points(litho.data$axis2,litho.data$ages,col=litho.data$lithology,pch=20)
```

```
legend('topright',legend=levels(litho.data$lithology),col=1:4,cex=0.8,pch=20)
```

ANOVA diversity metrics vs lithologies (results of a post-hoc Tukey test is at the end of this appendix):

```
#shapiro.test() = The null hypothesis for this test is that the data are
normally distributed. The Prob < W value listed in the output is the p-value.
If the chosen alpha level is 0.05 and the p-value is less than 0.05, then the
null hypothesis that the data are normally distributed is rejected. If the
p-value is greater than 0.05, then the null hypothesis is not rejected.

shapiro.test(sqrt(litho.data$Srare))    #p=0.1429 sqrt-ed to meet ANOVA assumptions
shapiro.test(litho.data$H)              #p=0.9738
shapiro.test(litho.data$J)              #p=0.3017
shapiro.test(sqrt(litho.data$axis1))    #p=0.2341  sqrt-ed to meet ANOVA assumptions

aov<-aov(sqrt(Srare)~lithology*strata, data=litho.data)
summary(aov)
print(model.tables(aov,"means",digit=3))
TukeyHSD(aov,order=T)
shapiro.test(aov$residuals)   #p=0.2423

aov<-aov(H~lithology*strata, data=litho.data)
summary(aov)
print(model.tables(aov,"means",digit=3))
TukeyHSD(aov,order=T)
shapiro.test(aov$residuals)   #p=0.8008

aov<-aov(J~lithology*strata, data=litho.data)
summary(aov)
print(model.tables(aov,"means",digit=3))
TukeyHSD(aov,order=T)
shapiro.test(aov$residuals)   #p=0.3137

aov<-aov(sqrt(axis1)~lithology*strata, data=litho.data)
summary(aov)
print(model.tables(aov,"means",digit=3))
TukeyHSD(aov,order=T)
shapiro.test(aov$residuals)   #p=0.04856
```

#############creates subsets by lithology:

```
mudstone<-subset(litho.data,lithology=="mudstone")
siltstone<-subset(litho.data,lithology=="siltstone")
sandstone<-subset(litho.data,lithology=="sandstone")
lignite<-subset(litho.data,lithology=="lignite")
```

```
fines<-rbind(mudstone,lignite)    #creates data.frame w muds and lignites
fines<-fines[order(fines$ages),]  #orders by ages

plot(fines$Srare,fines$ages,ylim=c(19.5,10),type="b",ylab="ages (Ma)",
xlab="Rarefied diversity", main="Mudstones+lignites")
points(fines$Srare,fines$ages,col=fines$lithology,pch=20)
text(18,10,"p-value=0.003013",cex=.8)
wilcox.test(fines$Srare[1:17],fines$Srare[18:41])

plot(fines$H,fines$ages,ylim=c(19.5,10),type="b",ylab="ages (Ma)",
xlab="H diversity", main="Mudstones+lignites")
points(fines$H,fines$ages,col=fines$lithology,pch=20)
text(1.46,10,"p-value=0.02787",cex=.8)
wilcox.test(fines$H[1:17],fines$H[18:41])

plot(fines$axis1,fines$ages,ylim=c(19.5,10),type="b",ylab="ages (Ma)",
xlab="DCA axis 1", main="Mudstones+lignites")
points(fines$axis1,fines$ages,col=fines$lithology,pch=20)
text(2,10,"p-value=3.589e-09",cex=.8)
wilcox.test(fines$axis1[1:17],fines$axis1[18:41])

#testing differences of mudstones only:
wilcox.test(mudstone$Srare[1:16],mudstone$Srare[17:29]) #p-value = 0.0196
wilcox.test(mudstone$axis1[1:16],mudstone$axis1[17:29]) #p-value = 8.841e-07
wilcox.test(mudstone$H[1:16],mudstone$H[17:29])         #p-value = 0.09161

siltsand<-rbind(siltstone,sandstone)          #creates data.frame w silts and sandss
siltsand<-siltsand[order(siltsand$ages),]     #orders by ages

plot(siltsand$Srare,siltsand$ages,ylim=c(19.5,10),type="b",ylab="ages (Ma)",
xlab="Rarefied diversity", main="Silts+Sands")
points(siltsand$Srare,siltsand$ages,col=siltsand$lithology,pch=20)
text(23,10,"p-value=0.05397",cex=.8)
text(23,10.6,"p-value=7.905e-05
(excl.bottom sample)",cex=.8)
wilcox.test(siltsand$Srare[1:19],siltsand$Srare[20:26])

plot(siltsand$H,siltsand$ages,ylim=c(19.5,10),type="b",ylab="ages (Ma)",
xlab="H diversity", main="Silts+Sands")
points(siltsand$H,siltsand$ages,col=siltsand$lithology,pch=20)
text(1.86,10,"p-value=0.02547",cex=.8)
text(1.87,10.6,"p-value=0.001016
(excl.bottom sample)",cex=.8)
```

```
wilcox.test(siltsand$H[1:19],siltsand$H[20:26])

plot(siltsand$axis1,siltsand$ages,ylim=c(19.5,10),type="b",ylab="ages (Ma)",
xlab="DCA axis 1", main="Silts+Sands")
points(siltsand$axis1,siltsand$ages,col=siltsand$lithology,pch=20)
text(.15,10,"p-value=6.081e-06",cex=.8)
wilcox.test(siltsand$axis1[1:19],siltsand$axis1[20:26])

exclign<-rbind(siltstone,sandstone,mudstone) #creates data.frame excl. lignites
exclign<-exclign[order(exclign$ages),]     #orders by ages

plot(exclign$Srare,exclign$ages,ylim=c(19.5,10),type="b",ylab="ages (Ma)",
xlab="Rarefied diversity", main="All except lignites")
points(exclign$Srare,exclign$ages,col=exclign$lithology,pch=20)
text(19,10,"p-value=2.071e-05",cex=.8)
text(19,10.6,"p-value=1.588-e06
(excl.bottom sample)",cex=.8)
wilcox.test(exclign$Srare[1:35],exclign$Srare[36:55])
abline(v=mean(exclign$Srare[1:35]))
abline(v=mean(exclign$Srare[36:55]))

plot(exclign$H,exclign$ages,ylim=c(19.5,10),type="b",ylab="ages (Ma)",
xlab="H diversity", main="All except lignites")
points(exclign$H,exclign$ages,col=exclign$lithology,pch=20)
text(1.5,10,"p-value=0.0009952",cex=.8)
text(1.5,10.6,"p-value=0.0001555
(excl.bottom sample)",cex=.8)
wilcox.test(exclign$H[1:35],exclign$H[36:55])
abline(v=mean(exclign$H[1:35]))
abline(v=mean(exclign$H[36:55]))

plot(exclign$axis1,exclign$ages,ylim=c(19.5,10),type="b",ylab="ages (Ma)",
xlab="DCA axis 1", main="All except lignites")
points(exclign$axis1,exclign$ages,col=exclign$lithology,pch=20)
text(.15,10,"p-value=1.077e-12",cex=.8)
wilcox.test(exclign$axis1[1:35],exclign$axis1[36:55])
abline(v=mean(exclign$axis1[1:35]))
abline(v=mean(exclign$axis1[36:55]))

MUDsilt<-rbind(siltstone,mudstone)        #creates data.frame w muds and silts
MUDsilt<-MUDsilt[order(MUDsilt$ages),]     #orders by ages

plot(MUDsilt$Srare,MUDsilt$ages,ylim=c(19.5,10),type="b",ylab="ages (Ma)",
xlab="Rarefied diversity", main="Muds+Silts")
```

```
points(MUDsilt$Srare,MUDsilt$ages,col=MUDsilt$lithology,pch=20)
text(19,10,"p-value=0.0003695",cex=.8)
text(19,10.6,"p-value=5.436e-05
(excl.bottom sample)",cex=.8)
wilcox.test(MUDsilt$Srare[1:26],MUDsilt$Srare[27:45])
abline(v=mean(MUDsilt$Srare[1:26]))
abline(v=mean(MUDsilt$Srare[27:45]))

plot(MUDsilt$H,MUDsilt$ages,ylim=c(19.5,10),type="b",ylab="ages (Ma)",
xlab="H diversity", main="Muds+Silts")
points(MUDsilt$H,MUDsilt$ages,col=MUDsilt$lithology,pch=20)
text(1.5,10,"p-value=0.01083",cex=.8)
text(1.5,10.6,"p-value=0.002785
(excl.bottom sample)",cex=.8)
wilcox.test(MUDsilt$H[1:26],MUDsilt$H[27:45])
abline(v=mean(MUDsilt$H[1:26]))
abline(v=mean(MUDsilt$H[27:45]))

plot(MUDsilt$axis1,MUDsilt$ages,ylim=c(19.5,10),type="b",ylab="ages (Ma)",
xlab="DCA axis 1", main="Muds+Silts")
points(MUDsilt$axis1,MUDsilt$ages,col=MUDsilt$lithology,pch=20)
text(.15,10,"p-value=2.231e-10",cex=.8)
wilcox.test(MUDsilt$axis1[1:26],MUDsilt$axis1[27:45])
abline(v=mean(MUDsilt$axis1[1:26]))
abline(v=mean(MUDsilt$axis1[27:45]))



######### Among sample Diversity (Fig. 7.5-a and difference tests):
#two groups:
spK<-specaccum(data226[1:36,3:405],ci=1,method="rarefaction")
spK2<-specaccum(data226[37:67,3:405],ci=1,method="rarefaction")

par(mfrow=c(1,3))
plot(spK,ylab="Number of species", xlab="Number of pooled samples",ci.lty=2,
ci.type="line",lwd=1.5,ylim=c(45,300))
plot(spK2,ylab="Number of species", xlab="Number of pooled samples",ci.lty=2,
ci.type="line",lwd=1.5,col="grey",ci.col="grey",add=T)

wilcox.test(spK$richness[1:31], spK2$richness)  #at 31 samples
text(17.4, 258,"post-16Ma",cex=.8)
text(23.8,167,"pre-16Ma",cex=.8,col="grey40")
text(4.25,300,"p-value=0.01249",cex=.8)

#among sample divers. using Chao2 and Jackknife2 (Fig. 7.5-b and c, and difference tests)
```

```
Chao2.estimates<-poolaccum(data226[1:36,3:405],permutations=1000)#calc. diversities estimates
Chao2.estimates<-summary(Chao2.estimates,display="chao")  #selects chao2
Chao2.estimates2<-poolaccum(data226[37:67,3:405],permutations=1000)
Chao2.estimates2<-summary(Chao2.estimates2,display="chao")

plot(Chao2.estimates[[1]][,1],Chao2.estimates[[1]][,2],type="l",xlim=c(0,40),ylim=c(0,700)
,xlab="Number of pooled samples",ylab ="Chao2 estimated species richness")
lines(Chao2.estimates[[1]][,1],Chao2.estimates[[1]][,3], lty = 2)
lines(Chao2.estimates[[1]][,1],Chao2.estimates[[1]][,4], lty = 2)

lines(Chao2.estimates2[[1]][,1],Chao2.estimates2[[1]][,2],type="l",col ="grey",add=T)
lines(Chao2.estimates2[[1]][,1],Chao2.estimates2[[1]][,3], lty = 2, col="grey")
lines(Chao2.estimates2[[1]][,1],Chao2.estimates2[[1]][,4], lty = 2, col="grey")
text(3.5,700,"p-value=0.2651",cex=.8)
wilcox.test(Chao2.estimates[[1]][1:29,2],Chao2.estimates2[[1]][,2])

Jack2.estimates<-poolaccum(data226[1:36,3:405],permutations=1000) #calc.diversities estimates
Jack2.estimates<-summary(Jack2.estimates,display="jack2")  #selects chao2
Jack2.estimates2<-poolaccum(data226[37:67,3:404],permutations=1000)
Jack2.estimates2<-summary(Jack2.estimates2,display="jack2")

plot(Jack2.estimates[[1]][,1],Jack2.estimates[[1]][,2],type="l",xlim=c(0,40),ylim=c(0,550)
,xlab="Number of pooled samples",ylab ="Jackknife2 estimated species richness")
lines(Jack2.estimates[[1]][,1], Jack2.estimates[[1]][,3], lty = 2)
lines(Jack2.estimates[[1]][,1],Jack2.estimates[[1]][,4], lty = 2)

lines(Jack2.estimates2[[1]][,1],Jack2.estimates2[[1]][,2],type="l",col ="grey",add=T)
lines(Jack2.estimates2[[1]][,1],Jack2.estimates2[[1]][,3], lty = 2, col="grey")
lines(Jack2.estimates2[[1]][,1],Jack2.estimates2[[1]][,4], lty = 2, col="grey")
text(3.2,555,"p-value=0.06392",cex=.8)
wilcox.test(Jack2.estimates[[1]][1:29,2],Jack2.estimates2[[1]][,2])

#amount of singletons pre and post-16
full<-data226[3:405]
full<-full[,colSums(full)==1]
SumPOS16<-colSums(full[1:36,])
sum(SumPOS16) #92 taxa
SumPRE16<-colSums(full[37:67,])
sum(SumPRE16) #51 taxa

############ Piecewise regression and Fig. 7.6-a:
#cumulative FAD-LAD plot:
data<-data[2:91,] #excludes topmost and bottommost samples (where FAD-LAD accumulates
disproportionally)
```

```
data<-data[,colSums(data)>1] #exclue singletons (it is now 90x231)
counts<-data[2:231]
depths<-data$age
sample.labels<-data$age
edge=strat.column(counts=counts,depths=depths,sample.labels=sample.labels)

FAD=fads(edge,increasing.down=T)#FAD, singles excluded
LAD=lads(edge,increasing.down=T)#LAD, singles excluded

plot(rev(sort(FAD)), ylim=c(19,10), ylab="Age(Ma)",xlab="Cumulative FAD/LAD")
points(rev(sort(LAD)),pch=19) #used rev() to make plot similar to range chart
legend("topleft",legend=c("FAD","LAD"),pch=c(1,19),box.lty=0,cex=.8)
abline(h=18.24,lty=2) #fad.edge[breakpoint]
abline(h=11.25,lty=2) #lad.edge[breakpoint]
,decreasing=T

###Piecewise regression (codes from Jaramillo et al. 2006, 2010)

(max(depths)+min(depths))/2 #age central point=14.805

##FAD EDGE
fad.edge<-FAD[which(FAD>14.8)]##time restricted to edge effect for FAD
fad.edge<-sort(fad.edge,decreasing=T)##fad arranged from oldest to youngest
span=length(fad.edge)#length of the analysis, to be included in the next line
cumuedge.fad<-c(1:span)
step1<-numeric(span)##first segment of piecewise
for (i in (1:span)){
step1[i]<-sum(resid(lm(fad.edge[1:i]~cumuedge.fad[1:i]))^2)
}
step2<-numeric(span)##last segment of piecewise
for (i in (1:span)){
step2[i]<-sum(resid(lm(fad.edge[i:span]~cumuedge.fad[i:span]))^2)
}
piecewise<-step1+step2## sum of first and second segment
breakpoint=which(piecewise==min(piecewise))## the position of the minimum value
fad.edge[breakpoint]##18.24 Ma

##LAD EDGE
lad.edge<-LAD[which(LAD<14.8)]##time restricted to edge effect for FAD
lad.edge<-sort(lad.edge)##lad arranged from youngest to oldest
span=length(lad.edge)#length of the analysis, to be included in the next line
cumuedge.lad<-c(1:span)
step1<-numeric(span)##first segment of piecewise
for (i in (1:span)){
```

```
step1[i]<-sum(resid(lm(lad.edge[1:i]~cumuedge.lad[1:i]))^2)
}
step2<-numeric(span)##last segment of piecewise
for (i in (1:span)){
step2[i]<-sum(resid(lm(lad.edge[i:span]~cumuedge.lad[i:span]))^2)
}
piecewise<-step1+step2## sum of first and second segment
breakpoint=which(piecewise==min(piecewise))## the position of the minimum value
lad.edge[breakpoint]##11.25

############# Originations and extinction rates and standing diversity (Fig. 7.6-b and c)
data.oe<-data300[3:404]
ages.oe<-as.character(data300["ages"])
ages.oe<-data300$ages

library(stratigraph)
oe<-oe.rates(data.oe, depths = NULL, breaks = NULL,
per.capita = T, remove.below = 2) #function that calculates standing diversity, origination
#and extinction
divers<-oe$basic[,1] #isolates standing diversity
origin<-oe$basic[,2] #isolates origination
extinc<-oe$basic[,3] #isolates extinction

plot(divers,ages.oe,pch=20, ylim=c(19.5,10),xlim=c(60,170),
ylab="Age (Ma)",xlab="Standing diversity")
abline(h=18.24,lty=2) #fad.edge[breakpoint]
abline(h=11.25,lty=2) #lad.edge[breakpoint]

plot(origin,ages.oe,pch=20, ylim=c(19.5,10),xlim=c(0,0.2),
ylab="Age (Ma)",xlab="per-capita rates")
points(extinc,ages.oe, ylim=c(19.5,10),ylab="Age (Ma)",col="gray50")
abline(v=0)
library(gplots)
smartlegend("right","top",c("Origination", "Extinction"),pch=c(20,1),inset=0.001,
bty ="n",cex=.8)
abline(h=18.24,lty=2) #fad.edge[breakpoint]
abline(h=11.25,lty=2) #lad.edge[breakpoint]

# Origin~extinc (Fig. 7.8)
#First, run oe.rates(...per.capita=F). Second, excl. samples below/above edge effect (8
bottom samples + 5 top samples = from sample 6 to sample 71)

plot(log(origin[6:71]+1), log(extinc[6:71]+1), xlab="Log Originations", ylab="Log
Extinctions")
```

```
x<-lm(log(extinc[6:71]+1)~ log(origin[6:71]+1))
abline(x)
rs<-expression(paste(,r^2 ,"=0.35", sep = ""))
p<-"p<0.000001"
smartlegend("left","top",c(rs,
p),inset=0,bty ="n",cex=.85)
```

Time Series Analysis (Table 7.3):

```
bin.dataTS<-data.frame(ages,Srare,axis1,axis2,H)  #creates dataframe with ages, originations
and extinctions
bin.dataTS$bin<-cut(bin.dataTS$ages,breaks=seq(10.72,18.75,by=0.5),labels=1:16,
include.lowest=T)   #adds a 'bin' variable to the dataframe above, bins every 0.5 Ma
bin.dataTS[67,"bin"]<-16  #replacing last bin number which was NA for a 16

library(plyr) #to use ddply() in order to calculate means

#calculates means for each variable based on factor bin:
bin.meansTS<-ddply(bin.dataTS,.(bin), function(x) data.frame(ages=mean(x$ages),
Srare=mean(x$Srare),axis1=mean(x$axis1),axis2=mean(x$axis2),H=mean(x$H)))

#calculates sd for each variable based on factor bin
bin.sdTS<-ddply(bin.dataTS,.(bin), function(x) data.frame(ages=sd(x$ages),
Srare=sd(x$Srare),axis1=sd(x$axis1),axis2=sd(x$axis2),H=sd(x$H)))

#preparing data.frame for PaleoTS() run (on rar. diversity):
fullsize<-c(4,3,4,4,3,3,2,2,4,3,8,5,5,5,4,8)
fullmean<-bin.meansTS$Srare
fullvar<-bin.sdTS$Srare
age<-bin.meansTS$ages
dataTS<-data.frame(fullsize,fullmean,fullvar,age)

library(paleoTS)
PALEO.data<-as.paleoTS(mm=dataTS$fullmean,vv=dataTS$fullvar,
nn=dataTS$fullsize,tt=dataTS$age)
x<-fit3models(PALEO.data)

#preparing data.frame for PaleoTS() run (on H' diversity):
 fullmean<-bin.meansTS$H
fullvar<-bin.sdTS$H
dataTS<-data.frame(fullsize,fullmean,fullvar,age)
PALEO.data<-as.paleoTS(mm=dataTS$fullmean,vv=dataTS$fullvar,
nn=dataTS$fullsize,tt=dataTS$age)
x<-fit3models(PALEO.data)
```

```
#preparing data.frame for PaleoTS() run (DCAaxis1):
fullmean<-bin.meansTS$axis1
fullvar<-bin.sdTS$axis1
dataTS<-data.frame(fullsize,fullmean,fullvar,age)
PALEO.data<-as.paleoTS(mm=dataTS$fullmean,vv=dataTS$fullvar,
nn=dataTS$fullsize,tt=dataTS$age)
x<-fit3models(PALEO.data)
```

#####Evolutionary models (on All excl. lignites and MUDS+SILTS):

```
bin.dataTS<-data.frame(ages,data226$lithology, Srare,H,axis1)  #creates dataframe with ages,
originations and extinctions

SS<-subset(bin.dataTS,data226$lithology=="sandstone")
TT<-subset(bin.dataTS,data226$lithology=="siltstone")
LL<-subset(bin.dataTS,data226$lithology=="lignite")
MM<-subset(bin.dataTS,data226$lithology=="mudstone")

excLig<-rbind(SS,TT,MM)    #dataframe all excl. lignites
excLig<-excLig[order(excLig$ages),]
excLig$bin<-cut(excLig$ages,breaks=seq(10.72,18.75,by=0.5),labels=1:16,
include.lowest=T)   #adds a 'bin' variable to the dataframe above, bins every 0.5 Ma
excLig[55,"bin"]<-16  #replacing last bin number which was NA for a 16

library(plyr) #to use ddply() in order to calculate means

#calculates means for each variable based on factor bin:
bin.meansTS<-ddply(excLig,.(bin), function(x) data.frame(ages=mean(x$ages),
Srare=mean(x$Srare),axis1=mean(x$axis1),H=mean(x$H)))

#calculates sd for each variable based on factor bin
bin.sdTS<-ddply(excLig,.(bin), function(x) data.frame(ages=sd(x$ages),
Srare=sd(x$Srare),axis1=sd(x$axis1),H=sd(x$H)))

#preparing data.frame for PaleoTS() run (on rar. diversity):
fullsize<-as.numeric(count(excLig$bin)$freq)
fullmean<-bin.meansTS$Srare
fullvar<-bin.sdTS$Srare
age<-bin.meansTS$ages
dataTS<-data.frame(fullsize,fullmean,fullvar,age)
library(paleoTS)
PALEO.data<-as.paleoTS(mm=dataTS$fullmean,vv=dataTS$fullvar,
nn=dataTS$fullsize,tt=dataTS$age)
x<-fit3models(PALEO.data)
```

```
#preparing data.frame for PaleoTS() run (on H' diversity):
fullmean<-bin.meansTS$H
fullvar<-bin.sdTS$H
dataTS<-data.frame(fullsize,fullmean,fullvar,age)
PALEO.data<-as.paleoTS(mm=dataTS$fullmean,vv=dataTS$fullvar,
nn=dataTS$fullsize,tt=dataTS$age)
x<-fit3models(PALEO.data)

#preparing data.frame for PaleoTS() run (DCAaxis1):
fullmean<-bin.meansTS$axis1
fullvar<-bin.sdTS$axis1
dataTS<-data.frame(fullsize,fullmean,fullvar,age)
PALEO.data<-as.paleoTS(mm=dataTS$fullmean,vv=dataTS$fullvar,
nn=dataTS$fullsize,tt=dataTS$age)
x<-fit3models(PALEO.data)
```

##Time Series analysis on MUDS+SILTS:

```
MudSilt<-rbind(TT,MM)    #dataframe w MUDS+SILTS
MudSilt<-MudSilt[order(MudSilt$ages),]
MudSilt$bin<-cut(MudSilt$ages,breaks=seq(10.72,18.75,by=0.5),labels=1:16,
include.lowest=T)   #adds a 'bin' variable to the dataframe above, bins every 0.5 Ma

MudSilt[45,"bin"]<-16  #replacing last bin number which was NA for a 16
#Bins with only one sample will be merged with above or below bin (the one with less samples)
MudSilt[5,"bin"]<-3
MudSilt[13,"bin"]<-7

library(plyr) #to use ddply() in order to calculate means

#calculates means for each variable based on factor bin:
bin.meansTS<-ddply(MudSilt,.(bin), function(x) data.frame(ages=mean(x$ages),
Srare=mean(x$Srare),axis1=mean(x$axis1),H=mean(x$H)))

#calculates sd for each variable based on factor bin
bin.sdTS<-ddply(MudSilt,.(bin), function(x) data.frame(ages=sd(x$ages),
Srare=sd(x$Srare),axis1=sd(x$axis1),H=sd(x$H)))

#preparing data.frame for PaleoTS() run (on rar. diversity):
fullsize<-as.numeric(count(MudSilt$bin)$freq)
fullmean<-bin.meansTS$Srare
fullvar<-bin.sdTS$Srare
age<-bin.meansTS$ages
dataTS<-data.frame(fullsize,fullmean,fullvar,age)
```

```
library(paleoTS)
PALEO.data<-as.paleoTS(mm=dataTS$fullmean,vv=dataTS$fullvar,
nn=dataTS$fullsize,tt=dataTS$age)
x<-fit3models(PALEO.data)

#preparing data.frame for PaleoTS() run (on H' diversity):
fullmean<-bin.meansTS$H
fullvar<-bin.sdTS$H
dataTS<-data.frame(fullsize,fullmean,fullvar,age)
PALEO.data<-as.paleoTS(mm=dataTS$fullmean,vv=dataTS$fullvar,
nn=dataTS$fullsize,tt=dataTS$age)
x<-fit3models(PALEO.data)

#preparing data.frame for PaleoTS() run (DCAaxis1):
fullmean<-bin.meansTS$axis1
fullvar<-bin.sdTS$axis1
dataTS<-data.frame(fullsize,fullmean,fullvar,age)
PALEO.data<-as.paleoTS(mm=dataTS$fullmean,vv=dataTS$fullvar,
nn=dataTS$fullsize,tt=dataTS$age)
x<-fit3models(PALEO.data)


### Comparison between Miocene and recent diversities (results Chapter 7):
Monica1<-read.csv("Data from Behling and Berrio/Monica1.csv", h=T)
Monica1[is.na(Monica1)] <- 0 #replace NAs with zero

Monica2<-read.csv("Data from Behling and Berrio/Monica2.csv", h=T)
Monica2[is.na(Monica2)] <- 0 #replace NAs with zero
Monica3<-read.csv("Data from Behling and Berrio/Monica3.csv", h=T)
Monica3[is.na(Monica3)] <- 0 #replace NAs with zero
Qamor<-read.csv("Data from Behling and Berrio/Quebrada del Amor.csv", h=T)
Qamor[is.na(Qamor)] <- 0 #replace NAs with zero

library(vegan)

#Within-sample rarefied diversity Holcoene (before running, run read.csv again)
Monica1R<-rarefy(Monica1[-1],226,se=TRUE)
Monica2<-Monica2[rowSums(Monica2[-1])>225,] #Monica 2 has samples below cutoff
Monica2R<-rarefy(Monica2[-1],226,se=TRUE)
Monica3R<-rarefy(Monica3[-1],226,se=TRUE)
Qamor<-Qamor[rowSums(Qamor[-1])>225,]#Qamor has samples below cutoff
QamorR<-rarefy(Qamor[-1],226,se=TRUE)

quat226<-c(Monica1R[1,],Monica2R[1,],Monica3R[1,],QamorR[1,])##TOTAL HOLOCENE
```

```
quat226<-as.numeric(quat226)
mean(quat226) #39.6 mean divers
wilcox.test(Srare[1:37],quat226)
wilcox.test(Srare[38:67],quat226)

#Within-sample H' diversity Holcoene:
Monica1H<-diversity(Monica1[-1])
Monica2<-Monica2[rowSums(Monica2[-1])>225,] #Monica 2 has samples below cutoff
Monica2H<-diversity(Monica2[-1])
Monica3H<-diversity(Monica3[-1])
Qamor<-Qamor[rowSums(Qamor[-1])>225,]#Qamor has samples below cutoff
QamorH<-diversity(Qamor[-1])

quat226<-c(Monica1H,Monica2H,Monica3H,QamorH)##TOTAL HOLOCENE
quat226<-as.numeric(quat226)
mean(quat226) #2.7 mean divers
wilcox.test(H[1:37],quat226)
wilcox.test(H[38:67],quat226)

##checking evennes of Quater. sites:
S1<-specnumber(Monica1)
S2<-specnumber(Monica2)
S3<-specnumber(Monica3)
S4<-specnumber(Qamor)

J1<-Monica1H/log(S1)
J2<-Monica2H/log(S2)
J3<-Monica3H/log(S3)
J4<-QamorH/log(S4)
J<-c(J1,J2,J3,J4)
mean(J)
min(J)

#'Violin' plot: (construct data matrix of spp+ DCA1 taxa scores and plots Fig. 7.7)
new_data<-read.csv("data_violin_RangeT.csv",h=T)
new_data[is.na(new_data)] <- 0
S_pos<-new_data[1:67,2:2]
S_pre<-new_data[1:67,3:3]
S_thr<-new_data[1:67,4:4]
df<-data.frame(S_pos, S_pre, S_thr)
library(rioja)

y.tks<-seq(10.7,18.8,0.5)
```

```
par(tcl=-.25)
x<-strat.plot (df,yvar=ages,scale.percent=T,
    graph.widths=1, minmax=NULL,
    scale.minmax = F, xLeft = 0.1, xRight = .5,
    yBottom = 0.07, yTop = 0.8, title = "", cex.title=1.2,
    y.axis=TRUE, min.width = 5, ylim = NULL, y.rev = T,
    y.tks=y.tks, ylabel = "Ages(Ma)", cex.ylabel=1, cex.yaxis=.8,
    xSpace = 0.01, wa.order = "none",plot.line=F,
    col.line = "black", lwd.line=1,plot.bar=F,
    lwd.bar = 1, col.bar = "grey", sep.bar = FALSE,
    plot.poly =T,col.poly="grey",col.poly.line="grey30",
    lwd.poly = 1, x.names=NULL, cex.xlabel = .88, srt.xlabel=45,
    cex.axis=.8, clust.width=0.1,
    orig.fig=NULL)

addZone(x,13.72,col="grey50",lty=3) #MM top
addZone(x,14.15,col="grey50",lty=3) #MM bottom
addZone(x,17.8,col="grey50",lty=3)#EM top
addZone(x,18.43,col="grey50",lty=3)#EM bottom

##Zachos curve for this plot:
data_z<-read.csv("zachos2008.csv",head=T)
plot(data_z$d18O.5pt,data_z$Age,ylim=c(18.7,10.7), xlim=c(3,1.3),type="l",
col="grey30",lwd=1.5,xlab="d18O",ylab="")
```

Results of the Post-hoc TukeyHSD multiple comparisons of means (95% family-wise confidence level) for ANOVA testing lithology vs. diversity metrics. Boldface means significant differences.

a)Rarefied diversity:

```
Fit: aov(formula = sqrt(Srare) ~ lithology * strata, data = litho.data)

$lithology
                          diff         lwr       upr     p adj
mudstone-lignite    0.6144801 -0.05424940 1.2832096 0.0825708
siltstone-lignite   1.1278650  0.38385875 1.8718712 0.0009789
sandstone-lignite   1.3039071  0.46970963 2.1381046 0.0006496
siltstone-mudstone  0.5133849 -0.09334506 1.1201148 0.1252095
sandstone-mudstone  0.6894270 -0.02503879 1.4038929 0.0623881
sandstone-siltstone 0.1760422 -0.60932881 0.9614131 0.9339280

$strata
                 diff       lwr       upr    p adj
younger-older 0.5978294 0.2371717 0.9584871 0.001562

$`lithology:strata`
                                       diff          lwr      upr     p adj
lignite:older-lignite:younger       0.37389534 -2.044624015 2.792415 0.9996865
mudstone:older-lignite:younger      0.48382691 -1.919139105 2.886793 0.9982498
```

siltstone:older-lignite:younger	0.85383807	-1.647248254	3.354924	0.9600036
mudstone:younger-lignite:younger	1.34184730	-1.044973182	3.728668	0.6444602
sandstone:older-lignite:younger	1.40582427	-1.430141051	4.241790	0.7728189
sandstone:younger-lignite:younger	1.70684957	-0.749168436	4.162868	0.3762490
siltstone:younger-lignite:younger	1.84066092	-0.587914685	4.269237	0.2694982
mudstone:older-lignite:older	0.10993157	-0.838689766	1.058553	0.9999547
siltstone:older-lignite:older	0.47994273	-0.695246434	1.655132	0.9014362
mudstone:younger-lignite:older	**0.96795196**	**0.061007205**	**1.874897**	**0.0284750**
sandstone:older-lignite:older	1.03192893	-0.748053113	2.811911	0.6082942
sandstone:younger-lignite:older	**1.33295424**	**0.257007558**	**2.408901**	**0.0058555**
siltstone:younger-lignite:older	**1.46676559**	**0.455026355**	**2.478505**	**0.0006698**
siltstone:older-mudstone:older	0.37001116	-0.772827135	1.512849	0.9699598
mudstone:younger-mudstone:older	0.85802039	-0.006594314	1.722635	0.0531731
sandstone:older-mudstone:older	0.92199736	-0.836793665	2.680788	0.7200251
sandstone:younger-mudstone:older	**1.22302267**	**0.182507865**	**2.263537**	**0.0107452**
siltstone:younger-mudstone:older	**1.35683402**	**0.382859649**	**2.330808**	**0.0012236**
mudstone:younger-siltstone:older	0.48800923	-0.620478806	1.596497	0.8611304
sandstone:older-siltstone:older	0.55198620	-1.338657344	2.442630	0.9831831
sandstone:younger-siltstone:older	0.85301151	-0.397531653	2.103555	0.4003633
siltstone:younger-siltstone:older	0.98682286	-0.208925115	2.182571	0.1791372
sandstone:older-mudstone:younger	0.06397697	-1.672690018	1.800644	1.0000000
sandstone:younger-mudstone:younger	0.36500228	-0.637662876	1.367667	0.9440526
siltstone:younger-mudstone:younger	0.49881363	-0.434616834	1.432244	0.7002793
sandstone:younger-sandstone:older	0.30102531	-1.529582436	2.131633	0.9995288
siltstone:younger-sandstone:older	0.43483665	-1.358785301	2.228459	0.9944162
siltstone:younger-sandstone:younger	0.13381135	-0.964553298	1.232176	0.9999364

B) H’ diversity:

Fit: aov(formula = H ~ lithology * strata, data = litho.data)

$lithology

	diff	lwr	upr	p adj
mudstone-lignite	0.23594426	-0.10507244	0.5769610	0.2701357
siltstone-lignite	**0.43909364**	**0.05968978**	**0.8184975**	**0.0170751**
sandstone-lignite	**0.46853541**	**0.04313877**	**0.8939321**	**0.0253795**
siltstone-mudstone	0.20314938	-0.10625083	0.5125496	0.3146567
sandstone-mudstone	0.23259115	-0.13174867	0.5969310	0.3391978
sandstone-siltstone	0.02944177	-0.37105592	0.4299395	0.9973692

$strata

	diff	lwr	upr	p adj
younger-older	**0.2115019**	**0.02758555**	**0.3954183**	**0.024935**

$`lithology:strata`

	diff	lwr	upr	p adj
lignite:older-lignite:younger	0.24921766	-0.984099422	1.4825347	0.9982092
mudstone:older-lignite:younger	0.28686655	-0.938519148	1.5122522	0.9954945
siltstone:older-lignite:younger	0.48485960	-0.790562274	1.7602815	0.9303606
sandstone:older-lignite:younger	0.51696066	-0.929231802	1.9631531	0.9490638
mudstone:younger-lignite:younger	0.60863465	-0.608517680	1.8257870	0.7650683
sandstone:younger-lignite:younger	0.74199100	-0.510448416	1.9944304	0.5819083
siltstone:younger-lignite:younger	0.77715330	-0.461291943	2.0155985	0.5090664
mudstone:older-lignite:older	0.03764889	-0.446097866	0.5213957	0.9999970
siltstone:older-lignite:older	0.23564194	-0.363642440	0.8349263	0.9177890
sandstone:older-lignite:older	0.26774301	-0.639953786	1.1754398	0.9821651
mudstone:younger-lignite:older	0.35941699	-0.103076913	0.8219109	0.2411265
sandstone:younger-lignite:older	0.49277334	-0.055902616	1.0414493	0.1090397
siltstone:younger-lignite:older	**0.52793564**	**0.012002088**	**1.0438692**	**0.0413216**
siltstone:older-mudstone:older	0.19799305	-0.384794098	0.7807802	0.9610248
sandstone:older-mudstone:older	0.23009411	-0.666796379	1.1269846	0.9921339
mudstone:younger-mudstone:older	0.32176810	-0.119139716	0.7626759	0.3147029
sandstone:younger-mudstone:older	0.45512445	-0.075483123	0.9857320	0.1445454
siltstone:younger-mudstone:older	0.49028675	-0.006388719	0.9869622	0.0554517
sandstone:older-siltstone:older	0.03210107	-0.932027244	0.9962294	1.0000000
mudstone:younger-siltstone:older	0.12377505	-0.441495276	0.6890454	0.9970260
sandstone:younger-siltstone:older	0.25713140	-0.380579534	0.8948423	0.9072283
siltstone:younger-siltstone:older	0.29229370	-0.317474585	0.9020620	0.8010490
mudstone:younger-sandstone:older	0.09167398	-0.793934418	0.9772824	0.9999790
sandstone:younger-sandstone:older	0.22503033	-0.708482888	1.1585436	0.9946073
siltstone:younger-sandstone:older	0.26019263	-0.654459794	1.1748451	0.9855223
sandstone:younger-mudstone:younger	0.13335635	-0.377949900	0.6446626	0.9913165
siltstone:younger-mudstone:younger	0.16851865	-0.307481567	0.6445189	0.9515555
siltstone:younger-sandstone:younger	0.03516230	-0.524945637	0.5952702	0.9999993

c) DCA axia 1:

```
Fit: aov(formula = sqrt(axis1) ~ lithology * strata, data = litho.data)

$lithology
                         diff         lwr       upr     p adj
siltstone-sandstone 0.1313210 -0.10407913 0.3667211 0.4589390
mudstone-sandstone  0.2414952  0.02734759 0.4556429 0.0211041
lignite-sandstone   0.5483123  0.29827735 0.7983473 0.0000017
mudstone-siltstone  0.1101742 -0.07168161 0.2920301 0.3855842
lignite-siltstone   0.4169913  0.19398948 0.6399931 0.0000389
lignite-mudstone    0.3068171  0.10637802 0.5072561 0.0008613

$strata
                  diff       lwr       upr p adj
older-younger 0.381128 0.2730277 0.4892283     0

$`lithology:strata`
                                              diff        lwr       upr     p adj
siltstone:younger-sandstone:younger  0.001115733 -0.3280984 0.3303298 1.0000000
mudstone:younger-sandstone:younger   0.077810468 -0.2227195 0.3783404 0.9916889
sandstone:older-sandstone:younger    0.324344018 -0.2243461 0.8730342 0.5846405
lignite:younger-sandstone:younger    0.368634654 -0.3675104 1.1047797 0.7637788
siltstone:older-sandstone:younger    0.521313265  0.1464865 0.8961400 0.0012533
mudstone:older-sandstone:younger     0.587660773  0.2757861 0.8995355 0.0000047
lignite:older-sandstone:younger      0.635412619  0.3129179 0.9579073 0.0000017
mudstone:younger-siltstone:younger   0.076694735 -0.2030834 0.3564729 0.9883370
sandstone:older-siltstone:younger    0.323228286 -0.2143761 0.8608326 0.5635771
lignite:younger-siltstone:younger    0.367518922 -0.3604008 1.0954387 0.7562881
siltstone:older-siltstone:younger    0.520197532  0.1617946 0.8786004 0.0006577
mudstone:older-siltstone:younger     0.586545040  0.2946146 0.8784755 0.0000011
lignite:older-siltstone:younger      0.634296887  0.3310471 0.9375466 0.0000004
sandstone:older-mudstone:younger     0.246533550 -0.2739996 0.7670667 0.8105383
lignite:younger-mudstone:younger     0.290824186 -0.4245802 1.0062286 0.9035598
siltstone:older-mudstone:younger     0.443502797  0.1112544 0.7757512 0.0022405
mudstone:older-mudstone:younger      0.509850304  0.2506984 0.7690023 0.0000017
lignite:older-mudstone:younger       0.557602151  0.2857626 0.8294417 0.0000006
lignite:younger-sandstone:older      0.044290636 -0.8057365 0.8943178 0.9999998
siltstone:older-sandstone:older      0.196969247 -0.3697155 0.7636540 0.9560059
mudstone:older-sandstone:older       0.263316754 -0.2638477 0.7904812 0.7660604
lignite:older-sandstone:older        0.311068601 -0.2224474 0.8445846 0.6014210
siltstone:older-lignite:younger      0.152678611 -0.5969748 0.9023321 0.9981174
mudstone:older-lignite:younger       0.219026118 -0.5012176 0.9392699 0.9787957
lignite:older-lignite:younger        0.266777965 -0.4581276 0.9916835 0.9408542
mudstone:older-siltstone:older       0.066347507 -0.2761967 0.4088917 0.9986341
lignite:older-siltstone:older        0.114099354 -0.2381414 0.4663401 0.9698788
lignite:older-mudstone:older         0.047751847 -0.2365795 0.3320832 0.9994588
```

9.4 Sedimentology and Sequence Stratigraphy analysis of core 1-AS-105-AM (the text and analysis below are from Jaramillo *et al. in prep*)

Methods:

Saltarin (Jaramillo *et al*. in prep) and 105-AM cores were described at a scale of 1:50 for identification of grain-size trends, sedimentary structures, clast composition, thickness of lamination, bioturbation patterns, and macrofossil identification, which are the support of identification of individual lithofacies. The association of lithofacies within a vertical and conformable succession is the support for depositional environment interpretation, following the criteria James and Dalrymple (2010) and Miall (1996). Sequence stratigraphy analysis follows the criteria described in Catuneanu *et al*. (2009) for definition of flooding surfaces, maximum flooding surfaces and sequence boundaries, as well as the identification of aggradational, progradational and retrogradational stacking patterns of deposition for marginal deposits. For fluvial strata, we used the terms "low accommodation" and "high accommodation" system tracts, as discussed in Catuneanu *et al*. (2009). For homogeneous fine-grained strata accumulated in shallow waters, we used a combination of lithofacies and biostratigraphy data to identify the stratigraphic surfaces of correlation. The detailed sedimentological, biostratigraphic and sequence stratigraphic analyses allowed the identification of stratigraphic sequences of less than 1 Ma of duration. All sedimentological, bioestratigraphic and stratigraphic data are storage and displayed using SDAR software (Ortiz *et al*., 2015).

Well 1-AS-105-AM drilled the Solimões (26.2 to 332.7 m) and Ramón formations (332.7-405 m). Three informal members were identified within the Solimões Formation (Sedimentary log is attached below):

•The lower member (332.7 – 267.5 m) includes three sequences that consists of very thick beds of massive to laminated claystones, siltstones and carbonaceous siltstones passing upsection to medium to thick bedded sublitharenites, locally with cross beds, and thin to medium beds of lignite. A similar succession is documented for the uppermost sequence for the Ramón Formation (358.8-332.7), but the arenites are quartzose in composition.

•The middle member (168.2-267.5 m) includes two very thick sequences that are characterized by laminated and carbonaceous siltstones in the retrogradational segment, with an important increment of decimeter- to meter-scale lignite beds interbedded with siltstones in the aggradational to progradational segment, and lithic-bearing, upward fining and coarsening sandstones and paleosols are part of the progradational interval.

•The upper member (26.2-168.2 m) includes five sequences whose lower retrogradational segment includes gastropods, bivalves and other shell fragments in fine-grained laminated, bioturbated to massive siliciclastic strata and biomicrites that passes upsection to upward-fining sublitharenites with thin to medium beds of lignite; the abundance of fossil content decreases upsection, whereas thickness of sandstone interbeds increases upsection.

The two marine incursions are recorded in claystones with organic matter of the lower member (284-293 m) and in mollusk-rich carbonaceous siltstones of the upper member (96-98 m). These marine incursions correspond to the retrogradational segment and maximum flooding surfaces of two major sequences. The lower sequence involves the lower and middle member of the Solimoes Formation that accumulated mainly in marginal plains with anoxic conditions that allowed the preservation of organic material and development of lignite. The upper sequence accumulated in oxygen-rich marginal settings with broad development of lacustrine systems that allowed the record of gastropods and bivalves. Both sequences have the record of thin fluvial conditions to the top.

A summary of lithology associations, depositional environment interpretation and stacking patterns of stratigraphic sequences identified in the Ramón and Solimoes units from meters 26.2 to 358.8, with emphasis in the two marine intervals documented in this study, is given below:

Unit (depth interval in meters)	Lithofacies association	Marine, lacustrine and pollen indicators	Depositional environment interpretation	Sequence stratigraphy analysis
Solimões Formation (26.2-53.1 m)	From base to top: 45-53.1 m: upward-coarsening siltstones to fine-grained litharenites and one medium-bed lignite; 32.8-45 m: silty mudstone; 26.2-32.8m: calcareous siltstone grading upsection to upward-fining conglomeratic sublitharenite	Lacustrine 0 - 11.5%; Marine 0 - 1.3%; Gastropods and bivalves at the base of the interval. Macroscopic organic matter and plant remains. Excellent palynomorph recovery.	Marginal: extensive development of plains surrounding lacustrine systems. Advance of fluvial channels to the top	Base is a maximum flooding surface. Stacking pattern of three parasequences indicate aggradation at the base to progradation toward the top.
Solimões Formation (53.1-66 m)	Upward-coarsening laminated siltstones grading to fine-grained sublitharenites	Lacustrine 0 - 51.2%; Gastropods, bivalves and shell fragments. Macroscopic organic matter and plant remains. Moderate to excellent palynomorph recovery.	Marginal: deltaic plains with shallow channels ending in shallow lacustrine systems	Base is a sequence boundary. Parasequences defined in this interval show a retrogradational pattern of deposition, and allow the identification of a maximum flooding surface at the top
Solimões Formation (66-85.2 m)	From base to top: 75.7-85.2 m: Calcareous siltstones and fine-grained sandstones, biomicrite and two thick-bedded lignite; 66-75.7 m: upward-fining medium-grained sublitharenite to laminated siltstone	Lacustrine indicators ranges from 1.3 to 17.1 %. Gastropods, bivalves and shell fragments. Macroscopic organic matter and plant remains. Moderate to excellent palynomorph recovery.	Marginal: Subaqueous marginal system (75.7-85.2) with advance of deltaic plains with shallow channels (66-75.7)	A complete sequence is defined for this interval; fossil-rich interval records the retrogradation and the Maximum flooding surface, whereas the sandstone interval records the progradation of the system
Solimões Formation (85.2-105.4 m)	From base to top: 95.7-105.4 m: fossil-rich interval with fine-grained sandstones, siltstones, biomicrite and a medium bedded peat interval; 85.2-95.7 m is a upward-fining, fine-grained sandstones to planar- to wavy-laminated siltstone, and a thin bed of lignite at the top	Marine incursion with 64.8% at 97.6 m and ranging from 3.5-11% from 96.7 to 101.2 m. Lacustrine indicators ranging from 0.3 - 14.9%. Gastropods and bivalves fragments; Macroscopic organic matter at different levels. Excellent palynomorph recovery.	Marginal to marine: Subaqueous marginal system (95.7-105.4 m) with a short period of marine incursion. Upper segment records the advance of deltaic plains with shallow channels (85.2 - 95.7)	A complete sequence is defined for this interval; fossil-rich interval records the retrogradational stacking pattern. The maximum flooding surface is recorded by the marine incursion, whereas the upper sandstone segment records the progradational stacking pattern.
Solimões Formation (105.4-141.1 m)	From base to top: 141.1-137 m: Laminated claystones and siltstones with shell fragments. 120-137 m: planar to wavy laminated fine-grained sublitharenite, siltstone and planar laminated mudstone; 105.4-120 m: upward-fining successions of fine-grained sublitharenite and siltstones with thin lignite beds at the top, and localized shell fragments	Lacustrine indicators from 120.3 to 125.3 m ranges from 4.1 - 5.7%; from 130.1 to 135.1 m ranges from 8-28%: with 1.3% of marine indicators at 120.9 m; localized shell fragments. Macroscopic organic matter in the 120-127 m interval. Excellent palynomorph recovery.	Marginal: dominantly subaqueous lacustrine and marginal plains with migration of shallow channels and adjacent plains with lignite accumulation	A complete sequence is defined for this interval; lower fossiliferous interval records the retrogradation with the maximum flooding surface at 134 m (in the interval of high lacustrine indicators). The upper segment records progradation of marginal plains over lacustrine system

Solimões Formation (141.1-168.2 m)	From base to top: 164-168.2 m: a coarsening-upward siltstone to litharenite and a meter scale siltstone with shell fragments. 141.1-164 m: interbedding of fine- to medium grained litharenites to sublitharenites, thickenning upsection and localized planar to wavy lamination to the top; laminated to bioturbated mudstones, localized paleosol development.	Moderate to excellent palynomorph recovery. 164 to 165.7 m: gastropods, bivalves, and bioturbation; abundant organic matter in 161 to 162.6 m.	Marginal plains with record of migrating channels on floodplains with short periods of subaerial exposure	A complete sequence is defined by a retrogradational stacking pattern at the base with the maximum flooding surface at the interval with shell fragments (the thinnest in comparison with the overlying two sequences). The upper segment records the progradation of migrating channels on marginal plains.
Solimões Formation (168.2-209.1 m)	From base to top: 199.5 to 200.9 m: laminated siltstones, bioturbated with shell fragments; 168.2-199.5 m: dominates laminated and carbonaceous siltstone, locally bioturbated followed by **decimeter to meter-thick lignites** interbedded with meter-scale upward-fining fine-grained sublitharenites. Two thin layers of paleosol toward the top.	Moderate to excellent palynomorph recovery. 199.5 to 200.9 m: bivalves, gastropods, shell fragments.	Migration of: (1) subaqueous marginal lacustrine at the base, to (2) a marginal plains with abundant ponds and oxbows, and (3) to a continental fluvial system with channels and subaerial exposure of the adjacent floodplains	A complete sequence is defined by the retrogradation of Siltstones with shell fragments recording the maximum flooding surface; lignite-rich interval records the aggradation, whereas arenites and paleosols record the progradation of the continental system.
Solimões Formation (209.1-249.2 m)	Fine-grained succession with massive to locally laminated and bioturbated siltstones; carbonaceous siltstone to the top; **decimeter to meter-thick lignites** interbedded with meter-scale upward-coarsening sublitharenites, locally laminated.	Moderate to excellent palynomorph recovery.	Marginal coastal plains with presence of ponds, oxbows and channel migration toward the top	Thick fine-grained succession at the base records the maximum flooding surface and onset of aggradation. Lignite and channel interbeds record the progradation of the system. Top is a sequence boundary,
Solimões Formation (249.2-267.5 m)	Siltstones changing from massive at the base to laminated and organic rich to the top. An upward-fining litharenite and a thin-bedded paleosol layer to the top	Excellent palynomorph recovery.	Marginal plains with channel at the base a more subaqueous conditions to the top	Base is a sequence boundary. This succession records an increase of base level (high accommodation stacking pattern) and retrogradational pattern, allowing the thick record of fine-grained successions.
Solimões Formation (267.5-295.2 m)	From base to top: 277.7-295.2: Poor preserved segment of claystones with organic matter grading to sublitharenite with paleosol developmen and locally bioturbated. 267.5-277.7: Mainly sublitharenites with a upward-coarsening trend and localized organic matter	Marine indicators at 284 (53.4%), 289.9 (5.4%), 293.3 (42.8%). All the succession has an excellent palynomorph recovery.	Lower interval represents a marine flooded marginal plain, whereas the sandy interval at the top records the migration of a sandy deltaic plain	Marine incursions in the lower interval records the retrogradational stacking pattern and maximum flooding system at 284 m, whereas the sandy interval records the progradation of marginal conditions

Solimões Formation (295.2-311 m)	Four-meter thick claystone at the base passing upsection to laminated carbonaceous siltstones with a medium bed of lignite, and a medium-bedded sublitharenite at the top.	Marine and lacustrine indicators in 298.9-299.3 m are less than 2.5%. Palynomorph recovery increases upsection	Marginal subaqueous system	Lower interval of claystones records the retrogradational (high accommodation) stacking pattern and maximum flooding surface, whereas the upper interval shows the progradation of a higher energy subaqueous marginal system
Solimões Formation (311-332.7 m)	From base to top: 323.3-332.7 m: seven-meter thick laminated siltstones at the base passing to a medium bed of lignite to the top interbedded with the siltstones. 311-323.3 m: upward-fining medium-grained sublitharenites with cross beds and planar lamination.	Marine indicators (25.6%) and lacustrine indicators (6.2%) in 326.2 m; minor influence in 324.9 (1 and 2.3%). Poor to moderate palynomorph recovery.	Marginal conditions with a short period of marine incursions at the base changing to a fluvial-deltaic system to the top	This succession is a complete sequence with retrogradational (high accommodation) stacking pattern and maximum flooding surface in the lower interval passing to a progradational fluvial deltaic system to the top
Ramón Formation (332.7-358.8 m)	Three meter-thick claystone at the base passing to siltstones in the middle and medium- to fine- to medium grained quartzarenites to the top	Lacustrine indicators of 0.3% at 357.7m. Poor to moderate palynomorph recovery.	Marginal at the base passing to fluvial channel systems to the top	This succession is a complete sequence with retrogradational (high accommodation) stacking pattern and maximum flooding surface in the lower marginal interval passing to a progradational fluvial system to the top

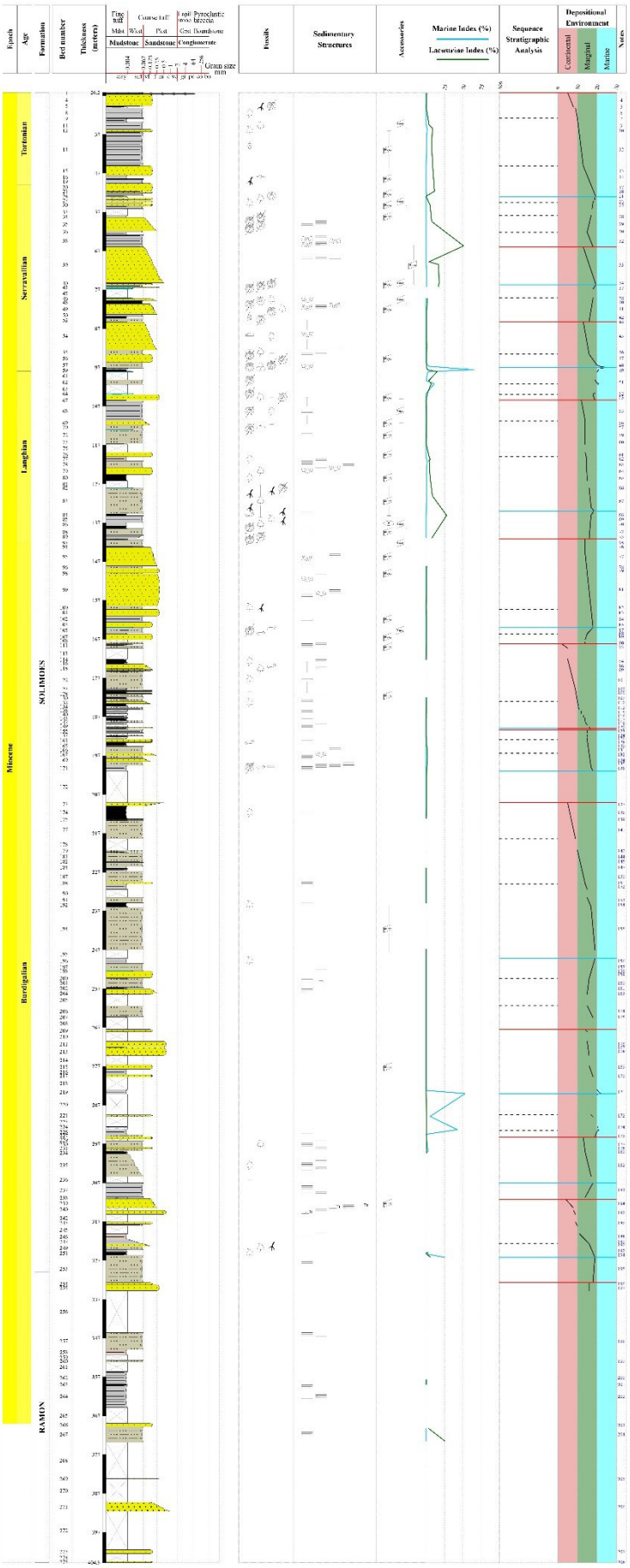
Epoch
Age
Formation
Bed number
Thickness (meters)
Fine tuff
Coarse tuff
Lapilli tuff
Pyroclastic breccia
Mdst
Wkst
Pkst
Grst
Boundstone
Mudstone
Sandstone
Conglomerate
Grain size mm
Fossils
Sedimentary Structures
Accessories
Marine Index (%)
Lacustrine Index (%)
Sequence Stratigraphic Analysis
Depositional Environment
Continental
Marginal
Marine
Notes
Tortonian
Serravallian
Langhian
Burdigalian
Miocene
SOLIMOES
RAMON

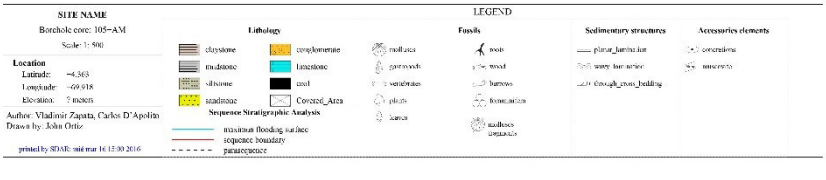
SITE NAME
Borehole core: 105-AM
Scale: 1: 900
Location
Latitude: -4.363
Longitude: -69.918
Elevation: 0 meters
Author: Vladimir Zapata, Carlos D'Apolito
Drawn by: John Ortiz
printed by SDAR: mié mar 16 15:00 2016
LEGEND
Lithology
claystone
mudstone
siltstone
sandstone
conglomerate
limestone
coal
Covered_Area
Sequence Stratigraphic Analysis
transition flooding surface
sequence boundary
paraconcordance
Fossils
mollusca
gymnosperm
vertebrates
plants
leaves
roots
wood
burrows
foraminifera
Sedimentary structures
planar_lamination
wavy_lamination
through_cross_bedding
Accessories elements
concretions
unconform

Footnote	base_depth	top_depth	Comments / Notes
1	26.45	26.2	Sparse oxidized organic matter.
2	26.6	26.45	Polymict conglomerate and sublitharenite. Clasts up to 1.5 cm wide
3	26.7	26.6	Sparse oxidized organic matter.
4	29.6	26.7	Sublitharenite. Sparse fragments of organic matter− quartz grains and lithics.
5	30	29.8	Organic rich.
6	32.8	30.2	Organic rich− carbonized plant remains. Light in weight− possible bioturbation− slight content of carbonate towards the base.
7	32.95	32.8	Abundant muscovite.
8	33.8	32.95	Sparse organic matter.
9	35.7	33.8	Organic matter and abundant fragments of leaves and carbonized plant remains. Sparse lithics.
10	36.3	35.7	Sublitharenite. Organic matter and carbonized plant remains.
11	36.6	36.3	Abundant organic matter.
12	45.1	36.6	Organic matter.
13	47.6	45.1	Sublitharenite. Abundant organic matter and oxidized nodules. Low content of carbonate.
14	48.3	47.6	Organic rich and sparse fragments of carbonized wood.
15	48.4	48.3	Abundant organic matter.
16	48.6	48.4	Lignite.
17	51.6	49.6	Sublitharenite. First 20 cm are slightly carbonated. Abundant organic matter− lithics and micas. Frequent oxidation.
18	51.8	51.6	Organic matter.
19	52.1	51.8	Sublitharenite. Organic matter.
20	52.7	52.1	Organic matter.
21	53.1	52.7	Milimetric fragments of bivalves and gastropods (matrix is non calcareous).
22	53.8	53.3	Sublitharenite. Abundant organic matter− plant bioturbation− sulfur. Contains carbonized plant remains.
23	54.5	54.1	Sublitharenite. Organic matter.
24	54.9	54.5	Abundant organic matter and carbonized plant remains.
25	55.4	54.9	Sublitharenite. Abundant organic matter.
26	55.6	55.4	Lignite (oxidized).
27	56.1	55.6	Abundant organic matter. Possible hard ground.
28	58.4	57.9	Organic matter and shell fragments.
29	61.8	58.4	Sublitharenite. Slightly calcareous− sporadic shell fragments. Sporadic organic matter and sulfur. Planar laminations 1 to 3 mm.
30	62.2	61.8	Organic matter and sulfur.
31	62.9	62.2	Thin planar and slightly wavy lamination− 1 to 3 mm. Organic matter and sulfur.
32	66	62.9	Slight oxidation. Sporadic organic matter and millimetric shell fragments. Thin planar stratification− clay laminae of up to 2 mm.
33	75.2	66	Sublitharenite. Contains lithics− quartz and organic matter. Thin planar and slitghly wavy stratification.
34	75.4	75.2	Shell fragments− opaques.
35	75.7	75.4	Sublitharenite. Organic matter.
36	76.3	75.7	Slighlty calcareous− shell fragments.
37	76.8	76.4	Biomicrite. Bivalves and millimetric calcite veins.
38	79.3	79.1	Biomicrite− impure− contains terrigenous mud and abundant shell fragments.
39	79.8	79.3	Sublitharenite. Abundant fragments of shells and carbonized plant remains. Thin slightly wavy lamination.
40	80.6	79.8	Peat. Multiple shell fragments.
41	83.3	80.6	Sublitharenite. Abundant fragments of shells and carbonized plant remains. Thin slightly wavy lamination.
42	84.4	83.85	Peat. Abundant bivalves in life position− some fragments− and gastropods.

43	85.2	84.4	Shell fragments.
44	85.4	85.2	Lignite. Contains sulfur.
45	92.5	85.4	Sublitharenite to silt– very thin wavy to irregular lamination– abundant carbonized plant remains. Contains sulfur and organic matter.
46	93.6	92.5	Abundant carbonized plant remains and sulfur.
47	95.7	93.6	Sublitharenite. Quartz– lithics– opaques. Sporadic shell fragments and molluscs.
48	97.2	95.7	Bivalve fragments and little organic matter.
49	98	97.5	Peat. Calcareous– shell fragments– thin way stratification– sulfur– opaques.
50	98.2	98	Biomicrite. Shell fragments and foraminifera.
51	101.4	100.2	Multiple shell fragments (bivalve and gastropod)– opaques. Color has reddish stains.
52	103.9	103.65	Biomicrite– shell fragments– millimetric calcite veins.
53	105.4	104	Sublitharenite. Abundant shell fragments– opaques– carbonized plant remains.
54	105.6	105.4	Lignite. Contains sulfur.
55	110.8	105.6	Abundant shell fragments and carbonized plant remains– sulfur. Very thin planar lamination.
56	111.8	110.8	Sublitharenite.
57	112.9	111.8	Micas– opaques– organic matter– carbonized wood.
58	113.05	112.9	Impure micrite– with shell fragments.
59	115.8	113.05	Thin planar lamination.
60	116.6	115.8	Sulfur.
61	120	118.9	Sublitharenite. Opaques– sporadic organic matter.
62	121.1	120	Peat. Carbonized plant remains.
63	122.8	121.1	Sporadic organic matter– micas.
64	124.6	122.8	Sublitharenite. Thin planar to slitghly way lamination– non–continuous. Sporadic organic matter– carbonized plant remains– little sulfur.
65	126.2	124.6	Fisile– organic matter– carbonized plant remains.
66	128.1	128	Biomicrite. Shell fragments and calcite veins. Contains terrigenous silt.
67	134.7	128.1	Bioturbation by roots (centimetric)– carbonized plant remains– opaques (very fine sand).
68	135.2	134.7	Peat. Thin planar lamination.
69	137	135.2	Peat. Organic matter– bioturbation by roots– carbonized plant remains.
70	137.8	137	Peat. Organic matter– bioturbation– carbonized plant remains and sporadic intraclasts.
71	138.5	137.8	Peat. Thin planar lamination– fragmented and few entire bivalves and gastropods.
72	140.2	138.5	Organic matter.
73	141.1	140.2	Millimetric bivalves and gastropods– organic matter.
74	141.3	141.2	Shell fragments.
75	143.1	141.4	Little organic matter– muscovite and some opaques.
76	143.3	143.1	Micrite.
77	148.1	143.3	Sublitharenite. Opaques– quartz– lithics– little oganic matter.
78	148.8	148.1	Oxidizied organic matter. Sporadic fragments of mica.
79	149.9	148.8	Sublitharenite. Quartz– opaques– lithics and organic matter.
80	150.1	149.9	Carbonized organic matter. (possible paleosoil).
81	158.4	150.1	Sublitharenite. Quartz– opaques– lithics and organic matter.
82	159.3	158.4	Carbonized plant remains– organic matter– lithics– plant bioturbation by roots.
83	161	159.3	Sublitharenite– 80% quartz grains– lithics– micas– sporadic organic matter.
84	162.6	161	Planar stratification– slightly wavy– laminae 3 mm to 1 cm. Abundant organic matter– some lithics.

85	163.9	162.6	Sublitharenite. Quartz– opaques– lithics– poor organic matter– and micas.
86	164	163.9	Siderite.
87	165.4	164	Shell fragments and entire millimetric shells. organic matter.
88	165.7	165.4	Shell fragments. Centimetric burrow filled with top lithology.
89	167.1	165.7	Sublitharenite. Organic matter.
90	168.2	167.7	Thin planar lamination. Organic matter– opaques.
91	168.35	168.2	Siderite.
92	168.7	168.35	Slighlty calcareous– very thin lamination.
93	169.3	168.7	Organic matter– lithics– thin lamination 1 to 3 mm.
94	173	172.3	Lignite with silt laminae (up to 1 cm). Carbonized plant remains.
95	173.4	173	Peat.
96	174.4	173.4	Sublitharenite. Burrows filled with top lithology.
97	174.5	174.4	Siderite.
98	174.7	174.5	Carbonized plant remains– organic matter. Thin lamination.
99	175.1	174.7	Sublitharenite. Quartz and opaques.
100	175.3	175.1	Lignite (pure). Carbonized plant remains and sulfur.
101	179.7	175.3	Organic matter and carbonized plant remains.
102	180	179.7	Organic matter. Very thin lamination.
103	180.1	180	Opaques.
104	180.3	180.1	Lignite.
105	180.5	180.3	Sublitharenite. Micas– opaques.
106	180.9	180.5	Lignite. (original sediments missing).
107	181.1	180.9	Sublitharenite with silty laminae of light gray color.
108	181.9	181.1	Sporadic organic matter. Lamination of 1 to 3 mm.
109	182.3	181.9	Lignite.
110	183.6	183	Sublitharenite. Organic matter– carbonized plant remains– quartz– opaques.
111	184.2	183.6	Lignite.
112	184.65	184.5	Very fine sand nodules– organic matter.
113	184.7	184.65	Lignite.
114	185.1	184.7	Very fine sand nodules– organic matter.
115	186.1	185.5	Abundant organic matter– thin lignite laminae.
116	187.1	186.6	Abundant organic matter– thin lignite laminae.
117	187.9	187.5	Lignite.
118	188.1	187.9	Organic matter– micas.
119	189.1	188.4	Micas– organic matter.
120	189.7	189.6	Thin lamination.
121	189.8	189.7	Sublitharenite. Micas– quartz– opaques– lithics.
122	190.1	189.9	Lignite.
123	191.1	190.3	Very fine black sand of indet composition.
124	191.9	191.6	Abundant organic matter and sulfur.
125	192.1	191.9	Lignite.
126	192.8	192.4	Organic matter– laminae 1 to 3 mm.
127	193.3	192.8	Sublitharenite. Organic matter– micas.
128	193.6	193.4	Sublitharenite. Organic matter and micas.
129	194.3	193.6	Lignite– with thin purplish mud laminae. (the bottom 40 cm are missing from the original sediments).
130	194.6	194.3	Organic matter and sulfur.
131	196.4	194.6	Thin planar lamination. Contains indet black fine to coarse sand grains in its matrix.
132	197	196.4	Quartz– micas– opaques– lithics.
133	197.7	197	Contains sand planar laminae.
134	198.5	197.7	Organic matter– lithics– micas and sulfur.
135	199.5	198.5	Bioturbation of millimetric traces. Stratification poorly preserved– planar to slightly wavy lamination.

136	200.9	199.5	Millimetric shells and traces– organic matter– opaques and mica fragments.
137	209.9	209.1	Sublitharenite. Organic matter– abundant micas and opaques.
138	213.3	209.9	Lignite. Very thin planar laminae of green to purplish mud– carbonized plant remains.
139	213.5	213.3	Organic matter– micas.
140	213.7	213.5	Lignite. Very thin planar laminae of purplish mud.
141	218.4	213.7	Lithic fragments– micas.
142	221.7	221.3	Lithic fragments– micas.
143	221.9	221.7	Organic matter.
144	224	221.9	Lithic fragments– micas.
145	224.5	224	Light organic matter.
146	225.5	224.5	Lithic fragments– micas.
147	226	225.5	Organic matter– color darkens towards base.
148	226.2	226	Lignite.
149	226.7	226.2	Abundant organic matter.
150	229.6	226.7	Fine to medium sand sized lithics– organic matter and sulfur.
151	230	229.6	Sublitharenite. Organic matter– very thin planar stratification.
152	231.4	230	Abundant organic matter– planar stratification.
153	234.9	233.5	Organic matter– has thin layers of gray mud laminae.
154	235.9	234.9	Thin laminae of 3 to 5 mm. Carbonized plant remains.
155	247	236.1	Thick homogeneous bed with few preserved structures. Some thin planar laminae– 1 to 3 mm. Sporadic organic matter– poorly preserved and oxidezied. Very fine sand sized muscovite fragments. Slight color variation– with some 5 to 10 cm bands of yellowish–orangeish colors. Abundant globular oxides of dark red to black color– in two bands of ca. 20 cm at 244.2 m and 245.1 m. Sediments get slightly finer towards base– with sporadic organic matter.
156	250.5	249.2	Organic matter– oxidized organic matter– carbonized plant remains.
157	252.4	250.5	Sporadic organic matter. Planar to slightly wavy lamination.
158	252.5	252.4	Siderite.
159	254.2	252.5	Sublitharenite. Organic matter– micas– opaques– lithics and quartz.
160	256.7	254.4	Sporadic organic matter.
161	257.1	256.7	Low oxidation.
162	258.1	257.1	Sublitharenite.
163	258.4	258.1	Sublitharenite.
164	264.2	261.4	Organic matter.
165	264.45	264.2	Organic matter.
166	272	270.55	Sublitharenite. Abundant quartz– lithics.
167	272.2	272	Oxidezied organic matter.
168	274.2	272.2	Sublitharenite. Abundant quartz– lithics.
169	277.7	276.6	Sublitharenite. Carbonized organic matter– opaques– lithics.
170	279.7	279.2	Bioturbated sublitharenite. Hardground.
171	284.2	283.05	Little organic matter.
172	289.8	289.5	Sublitharenite. Hard ground.
173	290	289.8	Organic matter.
174	292.7	292.55	Organic matter.
175	295.2	294.6	Little organic matter.
176	295.7	295.2	Sublitharenite.
177	297.9	296.2	Sulfur– organic matter– very thin laminae– carbonized plant remains.
178	298.2	297.9	Sublitharenite.
179	298.8	298.2	Little organic matter.
180	299.1	298.8	Thin lamination– some organic matter.

181	299.5	299.1	Lignite (impure)− with thin black mud laminae. Organic matter and sulfur.
182	305.35	299.5	Carbonized plant remains− red oxidation nodules. Sporadic sulfur− very thin lamina− 1 to 4 mm.
183	310.7	307	Sporadic organic matter− lithics of coarse to medium sand size. Sporadic micas (~1%)− discrete planar lamination.
184	313.5	311.05	Sublitharenite. Opaques (5%)− lithics (5%)− muscovite (~3%)− abundant quartz.
185	315.1	314.1	Sublitharenite. Quartz (85%)− lithics (10%).
186	317.6	317.1	Sublitharenite. Quartz (85%)− lithics (10%).
187	318.1	317.6	Little organic matter.
188	321.6	320.15	Sporadic organic matter. Very thin silty laminae− 1 to 2 mm.
189	322.7	321.6	Little organic matter.
190	323.3	322.7	Sublitharenite. Little organic matter.
191	324.2	323.3	Sporadic millimetric carbonized plant remains.
192	324.8	324.2	Organic matter
193	325.4	324.8	Lignite. Carbonized plant remains− sulfur.
194	325.6	325.4	Sulfur.
195	332.7	325.6	Very thin laminae− 1 to 2 mm− sporadic organic matter. Contains some very fine sand accumulations (<5 cm).
196	333.3	332.7	Quartzarenite. No organic matter.
197	334.8	333.3	Quartzarenite.
198	349.9	345.6	Sporadic very thin planar lamination.
199	353.2	352.7	Sporadic organic matter.
200	358.8	355.6	Lamianted− little organic matter.
201	359.1	358.8	Peat. High content of organic matter− sulfur.
202	364.9	359.1	Sporadic organic matter. Thin planar laminae− <1 mm.
203	369.8	368.95	Sublitharenite. Silty matrix.
204	373.8	369.8	Organic matter− very fine sand sized quartz.
205	383.3	383.2	Quartzarenite.
206	391.6	389.3	Sublitharenite.
207	402.5	401.5	Sublitharenite.
208	404.8	404.55	Sublitharenite. Silty matrix− some opaques.

Reference list

Absy M.L. (1979) **A palynological study of Holocene sediments in the Amazon Basin**. Ph.D. Thesis. Amsterdam: University of Amsterdam, 86 p.

Absy M.L., Cleef A.M., Fournier M., Martin L., Servant M., Sifeddine A., Silva M.F.F., Soubiès F., Suguio K., Turcq B., Van der Hammen T. (1991) Mise en évidence de quatre phases d'ouverture de la forêt dense dans le sud-est de 1'Amazonie au cours des 60.000 dernières années. Première comparaison avec d'autres regions tropicales. **Comptes Rendus de l'Académiedes Sciences**, 312: 673–678.

Absy M.L., Cleef A.M., D'Apolito C., Silva, M.F.F. (2014) Palynological differentiation of savanna types in Carajás, Brazil (southeastern Amazonia). **Palynology**, 38 (1): 78-89

Adegoke, O.S., Jan du Chene, R.E., Agumanu, E.A., Ajayi, P.O. (1978) Palynology and age of the Kerikeri Formation, Nigeria. **Revista Espanola de Micropaleontologia**, 10(2): 267-283.

Adeney J.M., Christensen, N.L., Vicentini, A., Cohn-Haft, M. (2016) White-sand Ecosystems in Amazonia. **Biotropica**, 48(1): 7-23.

Amante, C., Eakins, B.W. (2009) ETOPO1 1 Arc-minute Global Relief Model: Procedures, Data Sources and Analysis. **NOAA Technical Memorandum NESDIS NGDC-24**, 19 p.

Anderson, R.Y. (1960) Cretaceous-Tertiary palynology, eastern side of the San Juan Basin, New Mexico. **New Mexico Bureau of Mines and Mineral Resources memoir**, 6: 58 p.

Antoine, P.-O., Baby, P., Benammi, M., Brusset, S., De Franceschi, D., Espurt, N., Goillot, C., Pujos, F., Salas Gismondi, R., Tejada, J., Urbina, M. (2007) The Laventan Fitzcarrald local fauna, Amazonian Peru. **4th European Meeting on Paleontology and Stratigraphy of Latin America, Madrid. Cuadernos del Museo Geominero**, 8: 19–24.

Antoine, P.-O., Abello, M.A., Adnet, S., Sierra, A.J.A., Baby, P., Billet, G., Boivin, M., Calderóne, Y., Candela, A., Chabain, J., Corfui, F., Croft, D.A., Ganerød, M., Jaramillo, C., Klaus, S., Marivaux, L., Navarrete, R.E., Orliac, M.J., Parra, F., Pérez, M.E., Pujos, F., Rage, J-C., Ravel, A., Robinet, C., Roddaz, M., Tejada-Lara, J.V., Vélez-Juarbe, J., Wesselingh, F.P., Salas-

Gismondi, R. (2016) A 60-million-year Cenozoic history of western Amazonian ecosystems in Contamana, eastern Peru. **Gondwana Research**, 31: 60-59.

Antonelli, A., Nylander, J.A.A., Persson, C., Sanmartín, I. (2009) Tracing the impact of the Andean uplift on Neotropical plant evolution. **Proceedings of the National Academy of Sciences**, 106 (24): 9749-9754.

Antonelli, A., Zizka, A., Silvestro, D., Scharn, R., Cascales-Miñana, B., Bacon, C.D. (2015) An engine for global plant diversity highest evolutionary turnover and emigration in the American tropics. **Frontiers in Genetics**, 6: 1-14.

Anzótegui, L.M. and Garralla, S.S. (1986) Estudio palinológico de la Formación Paraná (Mioceno Superior) (Pozo Josefina, provincia de Santa Fe, Argentina). Parte 1. Descripciones sistemáticas. **Facena** 6: 101-176.

Archangelsky, S. and Villar de Seoane, L. (1998) Estudios palinológicos de la Formación Baqueró (Cretácico), Provincia de Santa Cruz, Argentina. VIII. **Ameghiniana**, 35 (1): 7-19.

Aureliano, T., Ghilardi, A.M., Guilherme, E., Souza-Filho, J.P., Cavalcanti, M., Riff, D. (2015) Morphometry, bite-force, and paleobiology of the Late Miocene caiman *Purussaurus brasiliensis*. **PLOS ONE**, 10 (2): e0117944.

Balme, B.E. (1957) Spores and pollen grains from the Mesozoic of Western Australia. **Commonwealth Scientific and Industrial Research Organisation, Australia, Coal Research,** Section T.C. 25, 48 p.

Barry, R.G. and Chorley, R.J. (1995) **Atmosphere, weather and climate.** 6th edition. London: Routledge, 392 p.

Batten, D.J. and Grenfell, H.R. (1996) "*Botryococcus*" In Jansonius, J. and McGregor, D.C. (eds.) **Palynology: Principles and Applications**. Vol.1. Dallas: American Association of Stratigraphic Palynologists Foundation, pp. 205-212.

Bayona, G., Jaramillo, C., Rueda, M., Reyes-Harker, A., Torres, V., (2007) Paleocene-middle Miocene flexural-margin migration of the nonmarine Llanos foreland basin of Colombia. **Ciencia, Tecnologia y Futuro**, 3 (3): 51–70.

Beerling, D.J. and Royer, D.L. (2011) Convergent Cenozoic CO_2 history. **Nature Geoscience**, 4: 418-420.

Beerling, D.J., Fox, A., and Anderson, C.W. (2009) Quantitative uncertainty analyses of ancient atmospheric CO2 estimates from fossil leaves: **American Journal of Science**, 309: 775-787.

Behling, H., Berrio, J.C., Hooghiemstra, H. (1999) Late Quaternary pollen records from the middle Caquetá river basin in central Colombian Amazon. **Palaeogeography, Palaeoclimatology, Palaeoecology** 145: 193–213.

Berrio, J.C., Arbeláez, M.A., Duivenvoorden, J.F., Cleef, A.M., Hooghiemstra, H. (2003) Pollen representation and successional vegetation change on the sandstone plateau of Araracuara, Colombian Amazonia. **Review of Palaeobotany and Palynology** 126: 163-181.

Bianucci, G., Lambert, O., Salas-Gismondi, R., Tejada, J., Pujos, F., Urbina, M., Antoine, P.-O. (2013) A Miocene relative of the Ganges River dolphin from the Amazonian basin. **Journal of Vertebrate Paleontology**, 33: 741–745.

Biffi, U., and Grignani, D. (1983) Peridinioid dinoflagellate cysts from the Oligocene of the Niger Delta, Nigeria. **Micropaleontology**, 29: 126-145.

Biswas, R. R. (1962) Stratigraphy of the Mahadev, Langpar, Cherra and Tura Formations, Assam, India. **Bull. Geol. Miner. Metallurg. Soc. India**, 25: 1–48

Dutta, S.K., and Sah, S.C.D. (1970) Palyno-stratigraphy of the Tertiary sedimentary formations of Assam: 5. Stratigraphy and palynology of South Shillong Plateau. **Palaeontographica Abteilung B,** 131: 1-72.

Black, G. A., Dobzhansky, T.H., Pavan, C. (1950) Some attempts to estimate the species diversity and population density of trees in Brazilian forests. **Botanical Gazette**, 111 (4): 413-425.

Blarquez, O., Carcaillet, C., Frejaville, T., Bergeron, Y. (2014) Disentangling the trajectories of alpha, beta and gamma plant diversity of North American boreal ecoregions since 15,500 years. **Frontiers in Ecology and Evolution**, 2: 1-8.

Boettger, O. (1878) Die Tertiarfauna von Pebas am oberen Maraõn. **Jahrbuch der Kaiserlich-Kèoniglichen Geologischen Reichsanstalt**, 28 (3): 485-504.

Boltenhagen, E. (1967) Spores et pollen du Cretace Superieur Gabon. **Pollen et spores**, 9: 335-355.

Boltovskoy, E. (1991) Ihering's hypothesis in the light of forminiferological data. **Lethaia**, 24 (2): 191–198.

Boltovsky, D. (1998) The range-through method of first-last appearance data in paleontological surveys. **Journal of Paleontology**, 62 (1): 157-159.

Boonstra, M., Ramos, M.I.F., Lammertsma, E.I., Antoine, P-O., Hoorn, C. (2015) Marine connections of Amazonia: Evidence from foraminifera and dinoflagellate cysts (early to middle Miocene, Colombia/Peru). **Palaeogeography, Palaeoclimatology, Palaeoecology**, 417: 176–194.

Borcard D., Gillet, F., Legendre, P. (2011) **Numerical Ecology with R**. Dordrecht: Springer, 318 p.

Brenner, G.J. (1963) The spores and pollen of the Potomac Group of Maryland. **Maryland Department of Geology, Mines and Water Resources Bulletin** 27, 215 pp.

Brenner, G.J. and Bickoff, I.S. (1992) Palynology and age of the Lower Cretaceous basal Kurnub Group from the coastal plain to the northern Negev of Israel. **Palynology**, 16: 137-185.

Bush, M.B. (2002) On the interpretation of fossil Poaceae pollen in the lowland humid neotropics. **Palaeogeography, Palaeoclimatology, Palaeoecology**, 177: 5–17.

Bush, M.B., De Oliveira, P.E., Miller, M.C., Moreno, E., Colinvaux, P.A. (2004) Amazonian paleoecological histories: one hill, 3 watersheds. **Palaeogeography, Palaeoclimatology, Palaeoecology**, 214: 359–393.

Burger, D. (1966) Palynology of uppermost Jurassic and lowermost Cretaceous strata in the eastern Netherlands. **Leidse geologische mededelingen**, 35: 209-276.

Burger, D. (1976) Some Early Cretaceous plant microfossils from Queensland. **Bulletin of the Bureau of Mineral Resources, Geology and Geophysics Australia**, 160: 1-22.

Campacci, M.A. (ed.) (2010) **Coletânea de orquídeas brasileiras – novas espécies**. Sãp Paulo: Editora Brasil Orquideas, 48 p.

Caputo, M.V. (1973) Relatório preliminar de exploração – Bacia do Acre. **Relatório 665-A da Petrobrás**.

Caputo M.V. (2011) “Discussão sobre a Formação Alter do Chão e o Alto de Monte Alegre” In Nascimento, R.S.C., Horbe A.M.C., Almeida C.M. (coord.) **Contribuições à Geologia da Amazônia**, Manaus: Sociedade Brasileira de Geologia. pp. 7-23.

Carrillo, J.D., Forasiepi, A., Jaramillo, C., Sánchez-Villagra, M.R. (2015) Neotropical mammal diversity and the Great American Biotic Interchange: spatial and temporal variation in South America's fossil's record. **Frontiers in genetics**, 5 (451): 1-11.

Catuneanu, O., Abreu, V., Bhattacharya, J. P., Blum, M. D., Dalrymple, R. W., Eriksson, P. G., Fielding, C. R., Fisher, W. L., Galloway, W. E., Gibling, M. R., Giles, K. A., Holbrook, J. M., Jordan, R., Kendall, C. G. S. C., Macurda, B., Martinsen, O. J., Miall, A. D., Neal, J. E., Nummedal, D., Pomar, L., Posamentier, H. W., Pratt, B. R., Sarg, J. F., Shanley, K. W., Steel, R. J., Strasser, A., Tucker, M. E., and Winker, C. (2009) Towards the Standardization of Sequence Stratigraphy. **Earth-Science Reviews**, 92: 1-33.

Cernusak, L.A., Winter, K., Martínez, C., Correa, E., Aranda, J., Garcia, M., Jaramillo, C., Turner, B. L. (2011) Responses of legume versus nonlegume tropical tree seedlings to elevated CO2 concentration. **Plant Physiology**, 157: 372–85

Clark, J. S., and McLachlan, J. S. (2003) Stability of forest biodiversity. **Nature**, 423: 635–638.

Coates, A.G., Collins, L.S., Aubry, M-P., Berggren, W.A. (2004) The Geology of the Darien, Panama, and the late Miocene-Pliocene collision of the Panama arc with northwestern South America. **GSA Bulletin**, 116 (11/12): 1327–1344.

Cookson, I.C. (1950) Fossil pollen grains of Proteaceous type from Tertiary deposits in Australia. **Australian Journal of Science, series B**, 3: 166-177.

Cookson, I.C. (1953) Difference in microspore composition of some samples from a bore at Comaum, South Australia. **Australian Journal of Botany**, 1: 462-473.

Colinvaux, P.A., De Oliveira, P.E., Moreno, J.E. (1999) Amazon Pollen Manual and Atlas. New York: Harwood Academic Press, 399 p.

Cooke, G.M., Chao, N.L., Beheregaray, L.B. (2011) Marine incursions, cryptic species and ecological diversification in Amazonia: the biogeographic history of the croaker genus *Plagioscion* (Sciaenidae). **Journal of Biogeography**, 39 (4): 724-738.

Cookson, I. C., and Eisenack, A. (1960) Upper Mesozoic Microplankton from Australia and New Guiena. **Palaeontology**, 2 (2): 243-261.

Copeland, P. and Harrison, T.M. (1990) Episodic rapid uplift in the Himalaya revealed by $^{40}Ar/^{39}Ar$ analysis of detrital K-feldspar and muscovite, Bengal fan. **Geology,** 18: 354-357

Costa, F.R.C., Magnusson, W.E., Luizão, R. (2005) Mesoscale distribution patterns of Amazonian understorey herbs in relation to topography, soil and watersheds. **Journal of Ecology**, 93: 863-878.

Couper, R.A. (1953) Upper Mesozoic and Cainozoic spores and pollen grains from New Zealand. **New Zealand Geological Survey Palaeontological Bulletin**, 22: 77 pp.

Couper, R.A. (1958) British Mesozoic microspores and pollen grains. A systematic and stratigraphic study. **Palaeontographica Abteilung B**, 103: 75-179.

Couper, R.A. (1960) New Zealand Mesozoic and Cainozoic plant microfossils. **New Zealand Geological Survey Palaeontological Bulletin**, 32: 87 pp.

Couto, C. (1981) "Fossil Mammals from the Cenozoic of Acre, Brazil IV – Notoungulata, Notohippidae and Toxodontidae Nesodontinae" In **Anais Congresso Brasileiro de Paleontologia**. Porto Alegre: Sociedade Brasileira de Paleontologia, 461-477

Cozzuol, M. (2006) The Acre vertebrate fauna: diversity, geography and time. **Journal of South American Earth Sciences**, 21: 185–203.

Cruz, N.M.C. (1984) "Palinologia do Linhito do Solimões no Estado do Amazonas" In **Simpósio de Geologia da Amazônia 2**. Manaus: Departamento Nacional de Produção Mineral, pp. 473-480.

Cuenca, A., Asmussen-Lange, C.B., Borchsenius, F. (2008) A dated phylogeny of the palm tribe Chamaedoreeae supports Eocene dispersal between Africa, North and South America. **Molecular Phylogenetics and Evolution**, 46 (2): 760-775.

D'Apolito, C., Absy, M.L., Latrubesse, E.M. (2013) The Hill of Six Lakes revisited: new data and re-evaluation of a key Pleistocene Amazon site. **Quaternary Science Reviews,** 76: 140-155.

Dale, B. (1996) "Dinoflagellate cyst ecology: modelling and geological applications" In Jansonius, J. and McGregor, D.C., (eds.) **Palynology: Principles and Applications**. Dallas: American Association of Stratigraphic Palynolologists Foundation, 3: 1249–1275.

Dalponte, J.C., Silva, F.E., Silva-Júnior, S.S. (2014) New species of titi monkey, genus *Callicebus* Thomas, 1903 (Primates, Pitheciidae), from Southern Amazonia, Brazil. **Papéis Avulsos de Zoologia**, 54 (32): 457-475.

Davis, C.C., Bell, C.D., Mathews, S., Donoghue, M.J. (2002) Laurasian migration explains Gondwanan disjunctions: Evidence from Malpighiaceae. **Proceedings of the National Academy of Science**, 99:6833-6837.

Davis, C.C., Webb, C.O., Wurdack, K.J., Jaramillo, C., Donoghue, M. (2005) Explosive Radiation of Malpighiales Supports a Mid-Cretaceous Origin of Modern Tropical Rain Forests. **The American Naturalist**, 165 (3): 36-65.

DeCelles, P. and Giles, K.A. (1996) Foreland basin systems. **Basin Research**, 8: 105-123.

de Jersey, N.J. (1962) Triassic spores and pollen grains from the Ipswich Coalfield. **Geological Survey of Queensland publication,** 307: pp. 18.

de Verteuil, L and Norris, G. (1996) Miocene dinoflagellate stratigraphy and systematics of Maryland and Virginia. **Micropaleontology** 42, 1–172.

De Boer, B., van De Wal, R.S.W., Bintanja, R., Lourens, L.J., Tuenter, E. (2010) Cenozoic global ice-volume and temperature simulations with 1-D ice-sheet models forced by benthic $\delta^{18}O$ records. **Annals of Glaciology**, 51 (55): 23-33.

Deflandre, G. and Cookson, I.C. (1955) Fossil microplankton from Australian Late Mesozoic and Tertiary sediments. **Australian Journal of Marine and Freshwater Research**, 6 (2): 242-313.

Dessaune-Rodrigues, I., Absy, M.L., Silva-Caminha, S.A.F., Esteves, V.G., Mendonça, C.B.F., Ferreira, M.G., Moura, C.O. (2016) Pollen morphology of 25 Apocynaceae species in the Adolpho Ducke Forest Reserve, Amazonas (Brazil). **Palynology**, in press.

Dick, C.W., Lewis, S.L., Maslin, M., Bermingham, E. (2013) Neogene origins and implied warmth tolerance of Amazon tree species. **Ecology and Evolution**, 3 (1): 162-169.

Dino, R., Soares, E.A.A., Antonioli, L., Riccomini, C., Nogueira, A.C.R. (2012) Palynostratigraphy and sedimentary facies of Middle Miocene fluvial deposits of the Amazonas Basin, Brazil. **Journal of South American Earth Sciences**, 34:61-80.

Dobzhansky, T. (1950) Evolution in the tropics. **American Scientist**, 38: 209–21

Döring, H. (1964) Trilete Sporen aus dem Oberen Jura und dem Wealden Norddeutschlands. **Geologie Beihefte**, 13 (9): 1009-1129.

Krutzsch, W. (1963) **Atlas der mittel- und jungtertiaren dispersen Sporen- und Pollen-sowie der Mikroplanktonformen des nordlichen Mitteleuropas. Lieferung 3: Sphagnaceoide und Selaginellaceoide Sporenformen**. Berlin: Veb Gustav Fischer Verlag Jena, pp. 128.

Drugg, W.S. (1967) Palynology of the Upper Moreno Formation (Late Cretaceous-Paleocene) Escarpado Canyon, California. **Palaeontographica Abteilung B**, 120: 1-71.

Dueñas, H. (1980) Palynology of Oligocene-Miocene strata of borehole Q-E-22, Planeta Rica, Northern Colombia. **Review of Palaeobotay and Palynology**, 10: 318–328.

Duenas, H. (1986) Geologia y palinologia de la formacion Cienaga de Oro, region caribe Colombiana. **Publicaciones Geologicas Especiales del Ingeominas**, 18: 1-51.

Duffield, S.L., and Stein, J. A. (1986) Peridiniacean-dominated dinoflagellate cyst assemblages from the Miocene of the Gulf of Mexico shelf, offshore Louisiana. **American Association of Stratigraphic Palynologists Contribution Series** 17, p. 27-45.

Eaton, G.L., Fensome, R.A., Riding, J.B., Williams, G.L. (2001) Re-evaluation of the status of the dinoflagellate cyst genus *Cleistosphaeridium*. **Neues Jahrbuch für Geologie und Paläontologie, Abhandlungen**, 219 (1–2): 171–205.

Edwards, L.E. (1984) Insights on why graphic correlation (Shaw's method) works. **Journal of Geology**, 92: 583-587.

Edwards, L.E. (1989) Supplemented graphic correlation: a powerful tool for palaeontologists and nonpaleontologists. **Palaios**, 4: 127-143.

Eiras, J. F., Becker, C.R., Souza, E.M., Gonzaga, F.G., Silva, J.G.F., Daniel, L.M.F., Matsuda, N.S., Feijó, F.J. (1994) Bacia do Solimões. **Boletim de Geociências da Petrobrás**, 8 (1): 17–45.

Elsik, W.C. (1968) Palynology of a Paleocene Rockdale Lignite, Milam County, Texas. II. Morphology and taxonomy. **Pollen et spores**, 10: 559-664.

Erdtman, G. (1960) On three new genera from the L. Headon Beds. **Botaniska Notiser**, 113: 46-48.

Espurt, N., Baby, P., Brusset, S., Roddaz, M., Hermoza, W., Regard, V., Antoine, P-O., Salas-Gismondi, R. (2007) How does the Nazca Ridge subduction influence the modern Amazonian foreland basin? **Geology**, 35: 515–518.

Espurt, N., Baby, P., Brusset, S., Roddaz, M., Hermoza, W., Barbarand, J. (2010) "The Nazca Ridge and uplift of the Fitzcarrald arch: implications for regional geology in northern South America" In Hoorn, C and Wesselingh, F.P. (eds.) **Amazonia: landscape and species evolution – a look into the past**. Oxford: Blackwell Publishing, p. 89-100.

Fensome, R. A., Taylor, F. J. R., Norris, G., Sarjeant, W. A. S., Wharton, D. I., Williams, G. L. (1993) A classification of fossil and living dinoflagellates. **Micropaleontology Press Special Paper**, 7: 1-351.

Ferreira, C. A. C. (2009) **Análise comparativa de vegetacãao lenhosa do ecossistema campina na Amazônia Brasileira**. PhD thesis, Manaus: National Institute for Amazon Research, 277 pp.

Figueiredo, J., Hoorn, C., Van der Ven, P., Soares, E. 2009. Late Miocene onset of the Amazon River and the Amazon deep-sea fan: evidence from the Foz do Amazonas Basin. **Geology**, 37: 619–622.

Fine, P.V.A., Ree, R.H. (2006) Evidence for a time-integrated species-area effect on the latitudinal gradient in tree diversity. **The American Naturalist**, 168:796–804

Fine, P.V.A., Ree, R.H., Burnham, R.J. (2008) "Disparity in tree species richness between tropical, temperate and boreal biomes: the geographic area and age hypothesis" In Carson, W.P. and Schnitzer, S.A. (eds.) **Tropical Forest Community Ecology**. London: Blackwell, pp. 31–45.

Flantua, S.G.A., Hooghiemstra, H., Grimm, E.C., Behling, H., Bush, M.B., González-Arango, C., Gosling, W.D., Ledru, M-P., Lozano-García, S., Maldonado, A., Prieto, A.R., Rull, V., Boxel, J.H.V. (2015) Updated site compilation of the Latin American Pollen Database. **Review of Palaeobotany and Palynology**, 223: 104-115.

Foote, M. (2000) "Origination and extinction components of taxonomic diversity: general problems" In Erwin D.H., and Wing, S.L. (eds.) **Deep time: Paleobiology's perspective.** Chicago: The Paleontological Society, pp. 74-102.

Foster, G.L., and Rohling, E. J. (2013) Relationship between sea level and climate forcing by CO_2 on geological timescales. **Proceedings of the National Academy of Sciences**, 110 (4): 1209-1214.

Foster, G.L., Lear, C.H., Rae, J.W.B. (2012) The evolution of pCO_2, ice volume and climate during the middle Miocene. **Earth and Planetary Science Letters**, 341-344: 243–254

Frailey, C.D. (1986) **Late Miocene and Holocene mammals, exclusive of the Notoungulata, of the Río Acre region, Western Amazonia. Contribution in Science.** Los Angeles: Natural History Museum, 374, pp. 1–46.

Franzinelli, E. and Potter, P.E. (1984). Petrology, chemistry, and texture of modern river sands, Amazon River system. **Journal of Geology**, 91: 23-39.

Frederiksen, N.O. (1983) Middle Eocene palynomorphs from San Diego, California. Part II. Angiosperm pollen and miscellanea. **American Association of Stratigraphic Palynologists contribution series**, 12: 32-155.

Gabb, W.M. (1869) Descriptions of fossils from the clay deposits of the Upper Amazon. **American Journal of Conchology**, 4: 197–200.

Germeraad, J. H., Hopping, C. A. and Muller, J. (1968) Palynology of Tertiary sediments from tropical areas. **Review of Palaeobotany and Palynology**, 6: 189–348

Geslin, E., Stouff, V., Debenay, J.P., Lesourd, M., (2000) "Environmental variations and foraminiferal test abnormalities" In Martin, R.E. (ed.) **Environmental Micropaleontology: The Application of Microfossils to Environmental Geology**. New York: Kluwer Academic/Plenum Publishers, pp. 191–215.

Gilinsky, N.L. (1991) "Boostrapping and the fossil record" In Gilinsky, N.L. and Signor, P.W. (eds.) **Analytical paleobiology**: Pittsburgh: Paleontological Society, pp. 185-206.

Gonzalez-Guzman, A.E. (1967) **A palynological study on the Upper Los Cuervos and Mirador Formations (Lower and Middle Eocene; Tibu area, Colombia)**. Leiden: E.J. Brill, pp. 68.

Gosling, W.D., Bush, M.B., Hanselman, J.A., Chepstow-Lusty, A. (2008) Glacial-interglacial changes in moisture balance and the impact on vegetation in the southern hemisphere tropical Andes (Bolivia/Peru). **Palaeogeography, Palaeoclimatology, Palaeoecology**, 259: 35–50.

Gosling, W.D., Mayle, F.E., Tate, N.J., Killeen, T.J. (2009) Differentiation between Neotropical rainforest, dry forest, and savannah ecosystems by their modern pollen spectra and implications for the fossil pollen record. **Review of Palaeobotany and Palynology**, 153: 70–85.

Goulding, M., Barthem, R., Ferreira, E. (2003) **The Smithsonian Atlas of the Amazon.** Washington: Smithsonian books, 256 pp.

Grace, J., Malhi, Y., Higuchi, N. & Meir, P. (2001) "Productivity of tropical rain forests" In "**Terrestrial global productivity: past, present and future**" Mooney, H., Roy, J., Saugier, B. (eds.). Sand Diego: Academic Press, pp. 401–426.

Gradstein, F.M., Ogg, J.G., Schmitz, M., Ogg, G. (2012) **The Geologic time scale**. Cambridge: Cambdirge University Press, pp. 1176.

Green, W.A. (2015) **stratigraph: Toolkit for the plotting and analysis of stratigraphic and palaeontological data**. R package version 0.66. https://CRAN.R project.org/package=stratigraph

Gross, M., Piller, W.E., Ramos, M.I., Silva Paz, J.D. (2011) Late Miocene sedimentary environments in south-western Amazonia (Solimões Formation; Brazil). **Journal of South American Earth Sciences**, 32: 169-181.

Hamilton, H., Caballero, S., Collins, A.G., Brownell Jr., R.L. (2001) Evolution of river dolphins. **Proceedings of the Royal Society of London B**, 268: 549–556.

Haq, B.V., Hardenbol, J., Vail, P.R. (1987) Chronology of fluctuating sea levels since the Triassic (250 million years ago to present). **Science**, 235: 1156-1167.

Head, M. J., Norris, G., Mudie, P., J. (1989) "Palynology and dinocyst stratigraphy of the Miocene in ODP Leg 105, Hole 645E, Baffin Bay" In Srivastava, S.P., Arthur, M., Clement, B., et al. (eds.) **Proceedings of the Ocean Drilling Program, Scientific Results**. Texas: College Station (Ocean Drilling Program), 105: 467-514.

Head, M.J., Seidenkrantz, M.-S., Janczyk-Kopikowa, Z., Marks, L., Gibbard, P.L. (2005) Last Interglacial (Eemian) hydrographic conditions in the southeastern Baltic Sea, NE Europe, based on dinoflagellate cysts. **Quaternary International**, 130: 3-30.

Hedlund, R. W. (1966) Palynology of the Red Branch Member (Woodbine Formation): **Oklahoma Geological Survey Bulletin**, 112: 1–69

Herngreen, G. F. W. (1973) Palynology of Albian-Cenomanian strata of Borehole 1-QS-1-MA, State of Maranhao, Brazil: **Pollen et Spores**, 15 (3-4): 515-555.

Higgins, M.A., Ruokolainen, K., Tuomisto, H., Llerena, N. Cardenas, G., Phillips, O.L., Vásquez, R., Räsänen, M. (2011) Geological control of floristic composition in Amazonian forests. **Journal of Biogeography**, 38: 2136-2149.

Hijmans, R. J., Phillips, S., Leathwick, J., Elith, J. 2013. Dismo: Species distribution modeling. R package version 0.8-17, http://cran.r-project.org/web/packages/ dismo/dismo.pdf.

Hood, K. C. (1998) **GraphCor Interactive Graphic Correlation Software**. Houston: Hood, K.C.

Hooghiemstra, H., Van Der Hammen, T. (1998) Neogene and Quaternary development of the neotropical rain forest: the forest refugia hypothesis, and a literature overview. **Earth Sciences Reviews**, 44: 147–183.

Hoorn, C. (1990) Evolucion de loa ambientes sedimentarios durante el terciario y el Cuaternario en la Amazonia Colombiana. **Colombia Amazonica**, 4 (2): 97–126.

Hoorn, C. 1993. Marine incursions and the influence of Andean tectonics on the Miocene depositional history of northwestern Amazonia: results of a palynostratigraphic study. **Palaeogeography, Palaeoclimatology, Palaeoecology**, 105: 267–309.

Hoorn, C. (1994a) An environmental reconstruction of the palaeo-Amazon River system (Middle–Late Miocene, NW Amazonia). **Palaeogeography, Palaeoclimatology, Palaeoecology**, 112: 187–238.

Hoorn, C. (1994b) Fluvial palaeoenvironments in the intracratonic Amazonas Basin (Early Miocene–early Middle Miocene, Colombia). **Palaeogeography, Palaeoclimatology, Palaeoecology**, 109: 1–54.

Hoorn, C. (2006) Mangrove forests and marine incursions in Neogene Amazonia (Lower Apaporis River, Colombia). **Palaios**, 21: 197–209.

Hoorn, C., Wesselingh, F.P., ter Steege, H., Bermudez, M.A., Mora, A., Sanmartín, J.S.I., Sanchez-Meseguer, A., Anderson, C.L., Figueiredo, J.P., Jaramillo, C., Riff, D.D., Negri, F.R.,

Hooghiemstra, H., Lundberg, J., Stadler, T., Sarkinen, T., Antonelli, A. (2010a). Amazonia through time: Andean uplift, climate change, landscape evolution and biodiversity. **Science**, 330: 927–931.

Hopkins, M.J.G. (2005) Flora da Reserva Ducke, Amazonas, Brasil. **Rodriguésia**, 56 (86): 9-25.

Hopkins, M.J.G. (2007) Modelling the known and unknown plant biodiversity of the Amazon basin. **Journal of Biogeography**, 34: 1400–1411.

Hopkins, J.A. and McCarthy, F. M. G. (2002) Post-depositional palynomorphs degradation in Quaternary shelf sediments: a laboratory experiment studying the effects of progressive oxidation. **Palynology**, 26, 167-184.

Householder, J.E., Wittmann, F., Tobler, M.W., Janovec, J.P. (2015) Montane bias in lowland Amazonian peatlands: plant assembly on heterogeneous landscapes and potential significance to palynological inference. **Paleogeography, Paleoclimatology, Paleoecology**, 423: 138-148.

Hovikoski, J., Räsänen, M.E., Gingras, M.K., Roddaz, M., Brusset, S., Hermoza, W., Pittman, L.R. (2005) Miocene semi-diurnal tidal rhythmites in Madre de Dios, Peru. **Geology**, 33: 177–180.

Hovikoski, J., Räsänen, M., Gingras, M., Lopéz, S., Romero, L., Ranzi, A., Melo, J. (2007) Palaeogeographical implications of the Miocene Quendeque Formation (Bolivia) and tidally-influenced strata in southwestern Amazonia. **Palaeogeography, Palaeoclimatology, Palaeoecology**, 243: 23–41.

Hovikoski, J., Räsänen, M.E., Gingras, M., Ranzi, A., Melo, J. (2008) Tidal and seasonal controls in the formation of late Miocene HIS deposits, western Amazonian Foreland Basin. **Sedimentology**, 55: 499–530.

Hovikoski, J., Wesselingh, F.P., Räsänen, M., Gingras, M., Vonhof, H.B. (2010) "Marine influence in Amazonia: evidence from the geological record" In Hoorn, C. and Wesseling, F.P. (eds.) **Amazonia: Landscape and Species Evolution, a Look into the Past**. Oxford: Wiley-Blackwell, pp. 143-161.

Miranda, L.A., Aleixo, A.B.M., Whitney, L.F., Silveira, E., Guilherme, M. P., Dantas Santos, Schneider, M. P. C. (2013) "Molecular systematics and taxonomic revision of the Ihering's Antwren complex (*Myrmotherula iheringi*: Thamnophilidae), with description of a new species

from southwestern Amazonia" In Hoyo, J. (ed.) **Handbook of the Birds of the World. Special Volume: New Species and Global Index**. Barcelona: Lynx Edicions, pp. 268-271.

Harrington, G.J. and Jaramillo, C. (2007) Paratropical floral extinction in the Late Palaeocene-Early Eocene. **Journal of the Geological Society**, 164: 323–332.

Hubbell, S.P., He, F., Condit, R., Borda-de-Água, L., Kellner, J., ter Steege, H. (2008) How many tree species are there in the Amazon and how many of them will go extinct? **Proceedings of the National Academy of Sciences**, 105(1): 11489-11504.

Hunt, G. (2006) Fitting and comparing models of phyletic evolution: random walks and beyond. **Paleobiology**, 32:578–601.

Hunt, G. (2008) Gradual or pulsed evolution: when should punctuational explanations be preferred? **Paleobiology**, 34:360–377.

Hunt, G. (2015) paleoTS: Analyze Paleontological Time-Series. R package version 0.5-1. https://CRAN.R-project.org/package=paleoTS

Hunt, G. and Carrano, M.T. (2010) "Models and methods for analysing phenotypic evolution in lineages and clades" In Alroy, J. and Hunt, G. (eds.) **Quantitative Methods in Paleobiology.** The Paleontological Society Papers 16, pp. 245-269.

Ibrahim, A.C. (1933) **Sporenformen des Aegir-horizonts des Ruhr-Reviers**. Dissertation, University of Berlin. Wurzburg: Konrad Triltsch, 47 pp.

IPCC (2014) **Climate Change 2014: Synthesis Report. Contribution of Working Groups I, II and III to the Fifth Assessment Report of the Intergovernmental Panel on Climate Change.** Core Writing Team, Pachauri, R.K. and Meyer, L.A. (eds.). IPCC, Geneva, Switzerland, 151 pp.

Jablonski, D., Roy, K., Valentine, J. W. (2006) Out of the Tropics: Evolutionary dynamics of the latitudinal diversity gradient. **Science**, 314: 102-106.

Jablonski, D., Belanger, C.L., Berke, S.K., Huang, S., Krug, A.Z., Roy, K., Tomasovych, A., Valentine, J.W. (2013) Out of the tropics, but how? Fossils, bridge species, and thermal ranges in the dynamics of the marine latitudinal diversity gradient. **Proceedings of the National Academy of Sciences,** 110 (26): 10487-10494.

James N.P., Dalrymple, R.W. (2010) **Facies Models 4, Kingston,** ON, GEotext 6, 586 p.

Jan du Chene, R.E., Klasz, I., Archibong, E.E. (1978) Biostratigraphic study of the Borehole Ojo-1, SW Nigeria, with special emphasis on the Cretaceous microflora. **Revue de micropaleontology**, 21: 123-139.

Jansonius, J. and Hills, L.V. (1976) **Genera File of Fossil Spores and Pollen.** 3287 cards; Special Publication, Department of Geology, University of Calgary, Calgary, Canada.

Jansonius, J. and Hills, L.V. (1990) **Genera File of Fossil Spores. Supplement.** Cards 4585-4811. Special Publication. Department of Geology, University of Calgary, Canada.

Jaramillo, C., Dilcher, D.L. (2001) Middle Paleogene palynology of central Colombia, South America: a study of pollen and spores from tropical latitudes. **Palaeontographica Abteilung B**, 258: 87–213.

Jaramillo, C. (2002) Response of tropical vegetation to Paleogene warming. **Paleobiology**, 28: 222-243.

Jaramillo, C., Rueda, M., Mora, G. (2006) Cenozoic plant diversity in the Neotropics. **Science**, 311: 1893–96

Jaramillo, C., Bayona, G., Pardo-Trujillo, A., Rueda, M., Torres, V., Harrington, G., Mora, G. (2007) The palynology of the Cerrejón Formation (upper Paleocene) of northern Colombia. **Palynology**, 31: 153–189

Jaramillo, C. (2008) Five useful techniques for analysing palynological data. **The Palaeobotanist**, 57: 529-537.

Jaramillo, C., Hoorn, C., Silva, S. A.F., Leite, F., Herrera, F., Quiroz, L., Dino, R., Antonioli, L. (2010a) "The origin of the modern Amazon rainforest: implications of the palynolgical and palaeobotanical record" In Hoorn, C and Wesselingh, F.P. (eds.) **Amazonia: landscape and species evolution – a look into the past**. Oxford: Blackwell Publishing, pp. 317-334.

Jaramillo, C., Ochoa, D., Contreras, L., Pagani, M., Carvajal-Ortiz, H., Pratt, L.M., Krishnan, S., Cardona, A., Romero, M. Quiroz, L., Rodriguez, G., Rueda, M.J. de la Parra, F., Morón, S., Green, W., Bayona, G., Montes, C., Quintero, O., Ramirez, R., Mora, G., Schouten, S., Bermudez, H., Navarrete, R., Parra, F., Alvarán, M., Osorno, J., Croley, J.L. Valencia, V.,

Vervoort, J. (2010b) Effects of rapid global warming at the Paleocene-Eocene boundary on Neotropical vegetation. **Science**, 330: 957–61.

Jaramillo, C.A., Rueda, M., Vladimir, T. (2011) A palynological zonation for the Cenozoic of the Llanos and Llanos Foothills of Colombia. **Palynology**, 35, 46–84.

Jaramillo, C. and Cardenas, A. (2013) Global warming and Neotropical rainforests: a historical perspective. **Annual Review of Earth and Planetary Sciences**, 41:741–66

Jaramillo, C. and Rueda, M.J. (2013) **A Morphological Electronic Database of Cretaceous-Tertiary and Extant pollen and spores from Northern South America**, v. 2012/2013. Accessible at http://biogeodb.stri.si.edu/jaramillo/palynomorph/

Jaramillo, C., Moreno, E., Ramírez, V., Silva, S.A.F., Barrera, A., Barrera, A., Sánchez, C., Morón, S., Herrera, F., Escobar, J., Koll, R., Manchester, S.R., Hoyos, N. (2014) "Palynological record of the last 20 million years in Panama" In Stevens, W.D., Montiel, O.M., Raven, P. **Paleobotany and Biogeography: A Festschrift for Alan Graham in His 80th Year**, St. Louis: Missouri Botanical Garden Press.

Jardine, P.E., Harrington, G.J. (2008) The Red Hills Mine palynoflora: a diverse swamp assemblage from the Late Paleocene of Mississippi, U.S.A. **Palynology,** 32: 183-204.

Javaux, E.J., Scott, D.B. (2003) Illustration of modern benthic foraminifera from Bermuda and remarks on distribution in other subtropical/tropical areas. **Paleontologia Electronica**, 6 (1), 1–29.

Juggins, S. (2015) **rioja: Analysis of Quaternary Science Data**. R package version (0.9-5). (http://cran.r-project.org/package=rioja)

Junk, W.J., Piedade, M.T.F. (1997) "Plant Life in the Floodplain with Special Reference to Herbaceous Plants" In Junk, W. (ed.) **The Central Amazon Floodplain: Ecology of a Pulsating System. Ecological Studies, vol. 126**. Berlin: Springer Verlag. pp. 3-22.

Junk, W.J., Piedade, M.T.F., Schöngart, J., Cohn-Haft, M., Adeney, M., Wittmann, F. (2011) A classification of major naturally-occurring Amazonian lowland wetlands. **Wetlands**, 31: 623-640.

Kaandorp, R.J.G., Vonhof, H.B., Wesselingh, F.P., Romero Pittman, L., Kroon, D., Hinte, J.E. van. (2005) Seasonal Amazonian rainfall variation in the Miocene climate optimum. **Palaeogeography, Palaeoecology, Paleoclimatology**, 221: 1–6.

Kay, R.F. and Madden, R.H. (1997) "Paleogeography and paleoecology" In Kay, R.F., Madden, R.H., Cifelli, R.L., Flynn, J.J. (eds.) **Vertebrate Paleontology in the Neotropics: The Miocene Fauna of La Venta, Colombia**. Washington DC: Smithsonian Institution Press.

Kedves, M. (1995) **Upper Cretaceous spores from Egypt**. Hungary: Szeged, 87 p.

Kedves, M. and Solé de Porta, N. (1963) Comparacion de las esporas del género *Cicatricosisporites* R. Pot y Gell, 1933 de Hungria y Colombia. Algunos problemas referentes a su significado estratigráfico. **Boletin Geologico**, 12: 51-76.

Kelts, K. and Hsü, K.J. (1978) "Freshwater carbonate sedimentation" In **Lakes: chemistry, geology and physics** Lerman, A. (ed.). Berlin: Spring-Verlag, pp.295-323.

Kemple W.G., Sadler P.M., Strauss D.J. (1995) "Extending graphic correlation to many dimensions: stratigraphic correlation as constrained optimization" In Mann K.O., Lane H.R. (ed.) **Graphic correlation**. Tulsa (OK): SEPM (SEPM Special Publication No. 53), pp. 65–82.

Khan, A.M., and Martin, A.R.H. (1972) A note on genus Polypodiisporites R. Potonié. **Pollen et Spores**, 13: 475–480.

Klaus, W. (1960) Sporen der Karnischen Stufe der ostalpinen Trias. **Jahrbuch der Geologischen Bundesanstalt**, 5: 107-184.

Koch, A.K., Cardoso, A., L., R., Ilkiu-Borges, A., L. (2013) A new species of *Passiflora* subgenus series *Quadrangulares* (Passifloraceae) from the Brazilian Amazon. **Phytotaxa**, 104 (1): 43-48.

Komárek J. and Jankovská, V. (2001) **Review of the green algal genus *Pediastrum*: implication for pollen analytical research**. Bibliotheca Phycologica 108. Berlin: Cramer, pp. 1–127.

Konzalová, M. (1976) Micropalaeobotanical (palynogical) research of the Lower Miocene of Northern Bohemia. **Rozpravy Ceskoslovenské Akademie Ved**, 86 (12): 1–75.

Kouli, K., Brinkhuis, H., Dale, B. (2001) *Spiniferites cruciformis*: a freshwater dinoflagellate cyst. **Review of Palaeobotany and Palynology**, 133: 273– 286.

Krause, G., H., Winter, K., Krause, B., Jahns, P., García, M., Aranda, J., Virgo, A. (2010) High-temperature tolerance of a tropical tree, *Ficus insipida*: methodological reassessment and climate change considerations. **Functional Plant Biology**, 37: 890-900.

Kroonenberg, S. and Reeves, C.,V. (2011) "Geology and hydrocarbon potential Vaupés-Amazonas basin, Colombia" In **Petroleum geology of Colombia** Cediel, F (ed.). Bucaramanga: ANH, Fondo editorial Universidad Eafit, 16: pp. 17-102.

Krutzsch, W. (1959) Mikropaläontologische (sporenpaläontologische) Untersuchungen in der Braunkohle des Geiseltales-[Part] I, Die Sporen und die Sporenartigen sowie ehemals im Geiseltal zu Sporites gestellten Formeinheiten der Sporae dispersae der mitteleozänen Braunkohle des mittleren Geisel tales (Tagebau Neumark-West i.w.S.) unter Berücksichtigung und Revision weiterer Sporenformen aus der bisherigen Literatur. **Geologie**, 8 (21/22).

Krutzsch, W. (1967) **Atlas der mittel- und jungtertiaren dispersen Sporen- und Pollen-sowie der Mikroplanktonformen des nordlichen Mitteleuropas. Lieferung 4 und 5: Weitere azonotrilete (apiculate, murornate), monolete und alete Sporenformen**. Berlin: Veb Gustav Fischer Verlag Jena, 232 pp.

Kuhnt, W., Hall, R., Zuvela, M., Käse, R. (2004) "Neogene history of the Indonesian throughflow" In Clift, P., D., Wang, P., Kuhnt, W., Hall, R., Tada, R. (eds.) **Continent-Ocean interactions within ease Asian marginal seas**. American Geophysical Union, Geophysical Monograph Series 149, pp. 229-320.

Kürschner, W., M., Kvaček, Z., Dilcher, D. (2008) The impact of Miocene atmospheric carbon dioxide fluctuations on climate and the evolution of terrestrial ecosystems. **Proceedings of the National Academy of Sciences**, 105 (2): 449-453.

LaRiviere, J.P., Ravelo, A., C., Crimmins, A., Dekens, P.S., Ford, H., L., Lyle, M., Wara, M.W. (2012) Late Miocene decoupling of oceanic warmth and atmospheric carbon dioxide forcing. **Nature**, 489: 97-100.

Latrubesse, E.M., Bocquentin, J., Santos, J.C.R., Ramonell, C.G. (1997) Paleoenvironmental model for the Late Cenozoic of southwestern Amazonia: paleontology and geology: **Acta Amazonica**, 27: 103–118.

Latrubesse, E., Silva, S.F., Cozzuol, M., Absy, M.L. (2007) Late Miocene continental sedimentation in the southwestern Amazonia and its regional significance: Biotic and geological evidence. **Journal of South American Earth Science**, 23: 61–80.

Latrubesse, E.M., Cozzuol, M., Silva-Caminha, S.A.F., Rigsby, C.A., Absy, M.L., Jaramillo, C. (2010) The late Miocene paleogeography of the Amazon basin and the evolution of the Amazon River system. **Earth-Science Reviews**, 99: 99-124.

Legendre, P., and Legendre, L. (1998) **Numerical Ecology**. Amsterdam: Elsevier, p. 853.

Legoux, O. (1978) Quelques espéces de pollen caractéristiques du Néogène du Nigéria. **Bulletin des Centres de Recherche Exploration-Production Elf-Aquitaine**, 2: 265–317.

Leidelmeyer, P. (1966) The Paleogene and Lower Eocene pollen flora of Guyana. **Leidse geologische mededelingen**, 38: 49–70.

Lenoir, E.A. and Hart, G. (1988) Palynofacies of some Miocene sands from the Gulf of Mexico, offshore Louisiana, USA. **Palynology**, 12:151-165.

Linhares, A.P., Ramos, M.I.F., Gross, M., Piller, W.E. (2011) Evidence for marine influx during the Miocene in southwestern Amazonia, Brazil. **Geologia Colombiana**, 36: 91–104.

Lloyd, J., and Farquhar, G., D. (2008) Effects of rising temperatures and [CO_2] on the physiology of tropical forest trees. **Philosophical Transactions of the Royal Society B,** 363: 1811–1817.

Lorente, M.A. (1986) **Palynology and palynofacies of the Upper Tertiary in Venezuela.** Dissertatione Botanicae, Band 99. Berlin: Cramer, pp 222.

Louwye, S. and Laga, P. (2008) Dinoflagellate cyst stratigraphy and palaeoenvironment of the marginal marine Middle and Upper Miocene of the eastern Campine area, northern Belgium (southern North Sea Basin). **Geological Journal**, 43: 75-94.

Lovejoy, N.R., Bermingham, E., Martin, A.P. (1998) Marine incursion into South America. **Nature**, 396: 421–422.

Lovejoy, N.R., Albert, J.S., Crampton, W., G., R. (2006) Miocene marine incursions and marine/freshwater transitions: Evidence from Neotropical fishes. **Journal of South American Earth Sciences**, 21: 5-13.

Lundberg, J.G., Marshall, J.G., Guerrero, J., Horton, B., Malabarba, M.C.S.L., Wesslingh, F.P. (1998) "The stage for neotropical fish diversification: a history of tropical South American rivers" In Malabarba, L.R., Reis, R.E., Vari, R.P., Lucena, Z.M.S., Lucena, C.A.S. (eds.) **Phylogeny and Classification of Neotropical Fishes**. Porto Alegre: EDIPUCRS, pp. 13–48.

Lundberg, J.G., Sabaj Pérez, M.H., Dahdul, W.M., Aguilera, O.A. (2010) "The Amazonian Neogene fish fauna" In Hoorn, C., Wesseling, F.P. (eds.) **Amazonia: Landscape and Species Evolution: A Look into the Past**. Oxford: Wiley-Blackwell, pp. 281-301.

Maia, R.G., Godoy, H.K., Yamaguti, H.S., Moura, P.A., Costa, F.S., Holanda, M.A., Costa, J. (1977) **Projeto de carvão no Alto Solimões. Relatório Final**. Manaus: CPRM-DNPM, pp. 137.

Marret, F., Zonneveld, K.A.F. (2003) Atlas of modern organic walled dinoflagellate cyst distribution. **Review of Palaeobotany and Palynology**, 125: 1–200.

Marret, F., Leroy, S., Chalié, F., Gasse, F. (2004) New organic-walled dinoflagellate cysts from recent sediments of Central Asian seas. **Review of Palaeobotany and Palynology**, 129: 1– 20.

Martin-Gombojav, N., and Winkler, W. (2008) Recycling of Proterozoic crust in the Andean Amazon foreland of Ecuador: implications for orogenic development of the Northern Andes. **Terra Nova**, 20 (1): 22–31.

Martínez, C., Madriñán, S., Zavada, M., Jaramillo, C. (2013) Tracing the fossil record of *Hedyosmum* (Cloranthaceae), an old lineage with recent Neotropical diversification. Grana, 52 (3): 161-180.

Mathur, Y. K. (1966) On the microflora in the supratrappeans of western Kutch, India. **Quarterly Journal. The Geological, Mining and Metallurgical Society of India**, 38: 33–51

Mathur, Y. K. and Jain, A. K. (1980) Palynology and age of the Dras Volcanics near Shergol, Ladakh, Jammu and Kashmir, India. **Geoscience Journal**, 1: 55–74.

Matsuoka, K. (1983) Late Cenozoic dinoflagellates and acritarchs in the Niigata District, central Japan. **Palaeontographica B**, 187: 89-154.

Matsuoka, K. and Head, M.H. (1992) "Taxonomic revision of the Neogene marine palynomorphs *Cyclopsiella granosa* (Matsuoka) and *Batiacasphaera minuta* (Matsuoka), and a new species of *Pyxidinopsis* Habib (Dinophyceae) from the Miocene of the Labrador Sea" In **Neogene and**

Quaternary Dinoflagellate Cysts and Acritarchs Head, M.J. and Wrenn, J.H. (eds.). Utah: American Association of Stratigraphic Palynologists Foundation, pp. 165–180.

Mayle, F.E., Burbridge, R., Killeen, T,J. (2000) Millennial-Scale Dynamics of Southern Amazonian Rain Forests. **Science**, 290: 2291-2294.

Meerow, A.,W., Noblick, L., Borrone, J.,W. Couvreur, T.,L.,P., Mauro-Herrera, M., Hahn, W.,J., Kuhn, D.,N., Nakamura, K., Oleas, N., H., Schnell, R.,J. (2009) Phylogenetic Analysis of Seven WRKY Genes across the Palm Subtribe Attaleinae (Arecaceae) Identifies *Syagrus* as Sister Group of the Coconut. **PLOS ONE**, 4 (10): e7353.

Meyer, B.L. (1956) Mikrofloristische Untersuchungen an jungtertiaren Braunkohlen im ostlichen Bayern. **Geologica Bavarica**, 25: 100-128.

Miall, A. (1996) **The geology of fluvial deposits: Sedimentary facies, Basin analysis, and Petroleum Geology**. Berlin, Pringer-Verlag, 582 p.

Miller, K.G., Kominz, M.A., Browning, J. V., Wright, J.D., Mountain, G.S., Katz, M.E., Sugarman, P.J., Cramer, B. S., Christie-Blick, N., Pekas, S.F. (2005) The Phanerozoic record of global sea level change. **Science**, 310 (5752): 1293–1298.

Miura, K. (1972) Possibilidades petrolíferas da bacia do Acre. **Anais do 26 congresso brasileiro de geologia**, p. 15-20.

Molinares, C.E., Martinez, J.I., Fiorini, F., Escobar, J., Jaramillo, C. (2012) Paleoenvironmental reconstruction for the lower Pliocene Arroyo Piedras section (Tubará, Colombia): implications for the Magdalena River — paleodelta's dynamic. **Journal of South American Earth Sciences**, 39: 170–183.

Monsch, K.A. (1998) Miocene fish faunas from the northwestern Amazonia basin (Colombia, Peru, Brazil) with evidence of marine incursions. **Palaeogeography, Palaeoclimatology, Palaeoecology**, 143 (1): 31–50.

Montenegro, G., Barragán, M. (2011) "Caguán and Putumayo Basins" In **Petroleum geology of Colombia** Cediel, F. (ed.), ANH, Fondo editorial Universidad Eafit 4: 15-125.

Montes, C., Cardona, A., Jaramillo, C., Pardo, A., Silva, J.C., Valencia, V., Ayala, C., Pérez-Angel, L.C., Rodriguez-Parra, L.A., Ramirez, V., Niño, H. (2015) Middle Miocene closure of the Central American Seaway. **Science**, 348 (6231): 226-229.

Mora, A., Baby, P., Roddaz, M., Parra M., Brusset, S., Hermoza, W., Espurt, N. (2010) "Tectonic history of the Andes and sub-Andean zones: implications for the development of the Amazon drainage basin" In Hoorn, C., Wesselingh, F.P. (eds.) **Amazonia-Landscape and Species Evolution: a Look into the Past**. Oxford: Wiley-Blackwell, pp. 447.

Morales, K., and Vinicius, T. (2003) Amazon rainforest: biodiversity and biopiracy. **Student BMJ**, 13: 386-7

Morley R. J. (2000) **Origin and Evolution of Tropical Rain Forests**. New York: Wiley, pp. 362.

Mudie, P., J., Asku, A., E., Yasar, D. (2001) Late Quaternary dinoflagellate cysts from the Black, Marmara and Aegean seas: variations in assemblages, morphology and paleosaliity. **Marine micropaleontology**, 43: 155-178.

Muller, J., Giacomo, E., Van Erve, A.W. (1987) A palynological zonation for the Cretaceous, Tertiary and Quaternary of Northern South America. **American Association of Stratigraphic Palynologists, Contribution Series 19**, p. 7-76.

Müller, R.D., M. Sdrolias, C. Gaina, B. Steinberger, C. Heine. (2008) Long-term sea-level fluctuations driven by ocean basin dynamics. **Science**, 319 (5868): 1357–1362.

Nakoman, E. (1965) Description d'un noveau genre de for, *Corsinipollenites*. **Annales de la Societe Geologique du Nord**, 85: 155-158.

Nichols, D.J., Ames, H.T., Traverse, A. (1973) On *Arecipites* Wodehouse, *Monocolpopollenites* Thomson & Pflug, and the species "*Monocolpopollenites tranquillus*". **Taxon**, 22: 241-56.

Nogueira, A.C.R., Silveira, R.R., Guimarães, J.T.F. (2013) Neogene-Quaternary sedimentar and paleovegetation history of eastern Solimões Basin, central Amazon region. **Journal of South American Earth Sciences**, 46: 89-99.

Nores, M. (1999) An alternative hypothesis for the origin of Amazonian bird diversity. **Journal Biogeography**, 26: 475–485.

Nores, M. (2004) The implications of Tertiary and Quaternary sea level rise events for avian distribution patterns in the lowlands of northern South America. **Global Ecology and Biogeography**, 13: 149–161.

Norris, G. (1967) Spores and pollen from the Lower Colorado Group (Albian - ?Cenomanian) of Central Alberta. **Palaeontographica Abteilung B**, 120: 72-115.

Nuttall, C.P. (1990) A review of the Tertiary non-marine molluscan faunas of the Pebasian and other inland basins of north-western South America. **Bulletin of the British Museum (Natural History),** 45: 165 371.

Okay, A. I., Zattin, M., and Cavazza, W. (2010) Apatite fission-track data for the Miocene Arabia-Eurasia collision. **Geology**, 38: 35–38

Oksanen, J., Blanchet, F.G., Kindt, R., Legendre, P., Minchin, P.R., O'Hara, R.B., Simpson, G.L., Solymos, P., Stevens, M. H. H., Wagner, H. (2016) **vegan: Community Ecology Package**. R package version 2.3-3. https://CRAN.R-project.org/package=vegan

Ortiz, J., Moreno, C., Cardenas, A., and Jaramillo, C. (2015) **SDAR 1.0 a New Quantitative Toolkit for Analyze Stratigraphic Data**: Geophysical Research Abstracts 17, p. EGU2015-2790.

Palazzesi, L., Barreda, V.D., Cuitiño, J.I., Guler, M.V., Tellería, M.C., Santos, R.V. (2014) Fossil pollen records indicate that Patagonian desertification was not solely a consequence of Andean uplift. **Nature Communications**, 5: 3558.

Pant, D.D. (1954) Suggestions for the classification and nomenclature of fossil spores and pollen grains. **The Botanical Review,** 20: 33-60.

Pflanzl, G. (1956) Das Alter der Braunkohlen des Meißners, der Flöze 2 und 3 des Hirschberger und eines benachbarten Kohlenlagers bei Laudenbach. **Notizblatt des Hessischen Landesamtes für Amt Bodenforsch zu Wiesbaden**, 84: 232–244

Pflug, H.D. (1953) Zur Entstehung und Entwicklung des angiospermiden pollens in der Erdgeschichte. **Palaeontographica Abteilung B**, 95: 60-171.

Pierce, R.L. (1961) Lower Upper Cretaceous plant microfossils from Minnesota. **Minnesota Geological Survey Bulletin,** 42: 86 pp.

Pires, J.M. (1974) Tipos de Vegetação da Amazônia. **Brasil florestal**, 5: 17 pp.

Pires, J.M., and Prance, G.T. (1985) "The Vegetation Types of the Brazilian Amazon" In Prance, G.T. and Lovejoy, T.E. (eds) **Key Environments Amazonia**. Oxford: Pergamon Press, pp. 109-145.

Pires, J.M., Dobzhansky, T., Black, G.A. (1953) An estimate of the number of species of trees in an Amazonian forest community. **Botanical Gazette**, 114 (4): 467-477.

Pocknall, D.T., Crosbie, Y.M. (1982) Taxonomic revision of some Tertiary tricolporate and tricolpate pollen grains from New Zealand. **New Zealand Journal of Botany**, 20: 7-15.

Pocock, S.A.J. (1962) Microfloral analysis and age determinations of strata at the Jurassic Cretaceous boundary in the western Canada Plains. **Palaeontographica Abteilung B**, 111: 1095.

Potonié, R., and Venitz, A. (1934) Zur Mikrobotanik des miozanen Humodils der niederrheinischen Bucht. **Arbeiten aus dem Institut fur Palaobotanik und Petrographie der Brennsteine**, 5: 5-54.

Potonié, R. (1956) Synopsis der Gattungen der Sporae dispersae. I. Teil: Sporites. **Beihefte zum Geologischen Jahrbuch**, 23: pp. 103.

Potonié, R. and Gelletich, J. (1933) Uber Pteridophyten-sporen einer eozanen Braunkohle aus Dorog in Ungarn. **Sitzungsberichte der Gesellschaft naturforschender Freundes zu Berlin**, 33: 517-523.

Potonié, R. (1966) Synposis der Gattungen der Sporae dispersae. IV. Teil: Nachtrage zu allen Gruppen (Turmae). **Beihefte zum Geologischen Jahrbuch**, 72: pp. 244.

Potter, P.E., Szatmari, P., 2009. Global Miocene tectonics and the modern world. **Earth-Science Reviews**, 96: 279–295.

Poulsen, C.J., Ehlers, T.A., Insel, N. (2010) Onset of Convective Rainfall During Gradual Late Miocene Rise of the Central Andes. **Science**, 380: 490-793

Pound, M.J., Haywood, A.M., Salzmann, U., Riding, J.B. (2012) Global vegetation dynamics and latitudinal temperature gradients during the Mid to Late Miocene (15.97–5.33 Ma). **Earth Sciences Reviews**, 112: 1:22

Powell, C. and Conaghan, P.J. (1973) Plate Tectonics and the Himalayas. **Earth and Planetary Science Letters**, 20: 1-12

Prance, G. T. (1978) The Origin and Evolution of the Amazon Flora. **Interciência**, 3 (4): 207-22.

Punt, W., Hoen, P. P., Blackmore, S., Nilsson, S., Le-Thomas, A. (2007) Glossary of pollen and spore terminology. **Review of Paleobotany and Palynology**, 143: 1–81.

Punyasena, S.W., Dalling, J.W., Jaramillo, C., Turner, B.L. (2011) Comment on "The response of vegetation on the Andean flank in Western Amazonia to Pleistocene climate change". **Science**, 333: 1825a-b.

Quiroga, M. P., Mathiasen, P., Iglesias, A., Mill, R. R., Premoli, A. C. 2016. Molecular and fossil evidence disentangle the biogeographical history of Podocarpus, a key genus in plant geography. Journal of Biogeography 43: 372—383.

Raine, J.I. (1981) Palynological correlation of the Dunollie/Rewanui Member boundary in drillholes 621 and 622, Greymouth Coalfield. **New Zealand Geological Survey Report**, 47: pp. 11.

R Core Team (2015) **R: A language and environment for statistical computing. R Foundation for Statistical Computing**. Vienna, Austria. https://www.R-project.org/.

Ramanujam, C.G.K. (1966) Pteridophytic spores from the Miocene lignite of South Arcot District, Madras. Palynologycal Bulletin, 2-3: 29–40.

Räsänen, M., Linna, A.M., Santos, J.C.R., Negri, F.R. (1995) Late Miocene tidal deposits in the Amazonian foreland basin. **Science**, 269: 386–389.

Regali, M.S., Uesegui, N., Santos, A. (1974) **Palinologia dos sedimentos Meso–Cenozoicos do Brasil (I)**. Rio de Janeiro: Boletim Tecnico da Petrobras, 17: 263-362.

Retallack, G.J. 2009. Refining a pedogenic-carbonate CO^2 paleobarometer to quantify a middle Miocene greenhouse spike: **Palaeogeography, Palaeoclimatology, Palaeoecology**, 281: 57-65.

Ricklefs, R.E. and Renner, S.S. (2012) Global Correlations in Tropical Tree Species Richness and Abundance Reject Neutrality. **Science**, 335: 464-467.

Roddaz, M., Baby, P., Brusset, S., Hermoza, W., Darrozes, J.M. (2005) Forebulge dynamics and environmental control in western Amazonia: the case study of the Arch of Iquitos (Peru). **Tectonophysics**, 399: 87–108.

Rohde, K. (1992) Latitudinal gradients in species diversity - the search for the primary cause. **Oikos**, 65: 514–27

Roncal, J., Kahn, F., Millan, B., Couvreur, T.L.P., Pintaud, J.-C. (2013) Cenozoic colonization and diversification patterns of tropical American palms: evidence from Astrocaryum (Arecaceae). **Botanical Journal of the Linnean Society**, 171: 120–139.

Rosenzweig, M.L. (1995) **Species Diversity in Space and Time.** Cambridge: Cambridge University Press, 433 pp.

Rossignol, M. (1962) Analyse pollinique de sédiments marins quaternaires en Israël II. - Sédiments pleistocènes. **Pollen et Spores**, 4 (1): 121-148.

Roubik, D.W., Moreno, J. E. (1991) **Pollen and Spores of Barro Colorado Island**. St. Louis: Missouri Botanical Garden.

Rull, V. (2001) A quantitative palynological record from the early Miocene of western Venezuela, with emphasis on mangroves. **Palynology**, 25 (1): 109–126.

Rull, V., López-Sáez, J.A., Vegas-Vilarrúbia, T. (2008) Contribution of non-pollen palynomorphs to the paleolimnological study of a high-altitude Andean lake (Laguna Verde Alta, Venezuela). **Journal Paleolimnological**, 40: 399–411.

Saatchi, S.S., Houghton, R.A., Alvalá, R.C.S., Soares, J.V., Yu, Y. (2007) Distribution of aboveground live biomass in the Amazon basin. **Global Change Biology**, 13: 816-837.

Sacek, V. (2014) Drainage reversal of the Amazon River due to the coupling of surface and lithospheric processes. **Earth and Planetary Science Letters**, 401: 301–312.

Sah, S.C.D. (1967) Palynology of an Upper Neogene profile from Rusizi Valley (Burundi). **Annales du Musée Royal de l'Afrique Centrale. Tervuren. Series 8**. 57: pp. 173.

Sah, S.C.D., and Dutta, S.K. (1966) Palynostratigraphy of the sedimentary formations of Assam-1. Stratigraphical position of the Cherra Formation. **Palaeobotanist**, 15 (1-2): 72-86.

Salard-Cheboldaeff, M. (1974) Pollens tertiaries du Cameroun rapportés a la famille des Hippocratéacées. **Pollen et Spores**, 16 (4): 499-506.

Salas-Gismondi, R., Baby, P., Antoine, P.-O., Pujos, F., Benammi, M., Espurt, N., Brusset, S., Urbina, M., De Franceschi, D. (2006) Late middle Miocene vertebrates from the Peruvian Amazonian basin (Inuya and Mapuya Rivers, Ucayali): Fitzcarrald Expedition 2005. **XIII Congreso Peruano de Geología. SGP**, p. 643-646.

Salati, E. and Vose, P.B. (1984) Amazon basin: a system in equilibrium. **Science**, 225 (4658): 129-138.

Salgado-Labouriau, M.L. (1979) Pollen and spore rain in central Brazil. **Proceedings of the 1st International Conference in Aerobiology**. Berlin: Federal Environmental Agency, pp. 89–110.

Sanders, H.L. (1968) Marine Benthic Diversity: A Comparative Study. **The American Naturalist**, 102 (925): 243-282.

Sarmiento, G. (1992) Palinología de la Formación Guaduas – estratigrafía y sistemática. **Boletín Geológico**, 32: 45–126.

Sarmiento, F. (2011) "Llanos basin" In Cediel, F. and Ojeda, G.Y. (eds.) **Petroleum geology of Colombia,** ANH, Fondo editorial Universidad Eafit, 9: pp. 17-184.

Schemske, D.W., Mittelbach, G.G., Cornell, H.V., Sobel, J.M., Roy, K. (2009) Is there a latitudinal gradient in the importance of biotic interactions? Annual Review of Ecology, Evolution and Systematics, 40: 245–69

Schrank, E. (1994) Palynology of the Yesomma Formation in Northern Somalia: a Study of Pollen, Spores and Associated Phytoplankton from the Late Cretaceous Palmae Province. **Palaeontographica Abteilung B,** 231: 63-1 12.

Schreck, M., Matthiessen, J., Head, M.J. (2012) A magnetostratigraphic calibration of Middle Miocene through Pliocene dinoflagellate cyst and acritarch events in the Iceland Sea (Ocean Drilling Program Hole 907A). **Review of Palaeobotany and Palynology**, 187: 66-94.

Schubart, H.O.R. (2000) "Características Biológicas da Amazônia: Flora e Fauna" In Salati, E., Absy, M.L., Victoria, R.L, (eds.) **Amazônia: Um Ecossistema em Transformação**. Manaus: Editora INPA, pp. 269.

Scotese, C.R. (2009) "Late Proterozoic plate tectonics and palaeogeography: a tale of two supercontinents, Rodinia and Pannotia" In Craig, J., Thurow, J., Thusu, B., Whitham, A., Abutarruma, Y. (eds) **Global Neoproterozoic Petroleum Systems: The Emerging Potential in North Africa**. London: Geological Society Special Publications, 326: 67–83.

Secco, R. S., Campos, J., M., Hiura, A., L. (2014) Taxonomia atualizada de *Amazona* (Phyllanthaceae) no Brasil. **Acta Amazonica**, 44 (1): 25-44.

Selling, O.H. (1946) Studies in the Recent and fossil species of Schizaea, with particular reference to their spore characters. **Meddelanden fran Goteborgs Botaniska Tradgard**, 16: 1–112.

Sessa, J.A., Bralower, T.J., Patzkowsky, M.E., Handley, J.C., Ivany, L.C. (2012) Environmental and biological controls on the diversity and ecology of Late Cretaceous through early Paleogene marine ecosystems in the U.S. Gulf Coastal Plain. **Paleobiology**, 38: 218-239.

Shackelton, N., J. and Kennett, J.P. (1975) "Paleotemperature history of the Cenozoic and the initiation of Antarctic glaciations: Oxygen and carbon isotope analyses in DSDP sites 277, 279 and 281" In **Initial reports of the Deep Sea Drilling Project 29**, Washington D.C., pp. 39-55.

Shaw, A.B. (1964) **Time in stratigraphy**. New York: McGraw- Hill, 365 p.

Sherlock R. L. (1934) Notes on the Amazon. **Geological Magazine**, 71 (837): 112-116.

Silva-Caminha, S.A.F., Jaramillo, C., Absy, M.L. (2010) Neogene palynology of the Solimões Basin, Brazilian Amazonia. **Palaeontographica Abteilung B**, 283 (1-3): 1–67.

Simon, M.F., Grether, R., de Queiroz, L., Skema, C., Pennington, E.T., Hughes, C.E. (2009) Recent assembly of the Cerrado, a Neotropical plant diversity hotspot, by in situ evolution of adaptations to fire. **Proceedings of the National Academy of Sciences**, 106: 20359–64

Singh, C. (1971) Lower Cretaceous microflora of the Peace River area, northwestern Alberta. **Research Council of Alberta Bulletin,** 28: pp. 542.

Singh, C. (1983) Cenomanian microfloras of the Peace River area, northwestern Alberta. **Alberta Geological Survey Bulletin,** 44: pp. 322.

Soliman, A., Ćorić, S., Head, M.J., Piller, W. E., El-Beialy, S.Y. (2012) Lower and Middle Miocene biostratigraphy, Gulf of Suez, Egypt based on dinoflagellate cysts and calcareous nannofossils. **Palynology**, 36 (1): 1-42.

Sombroek, W. (2001) Spatial and temporal patterns of Amazon rainfall. **Ambio**, 30(7): 388-396.

Srivastava, S. K. (1971) Monolete spores from the Edmonton Formation (Maastrichian), Alberta, Canada. **Review of Palaeobotany and Palynology**, 11: 251–265.

Stebbins, G. L. (1974) **Flowering plants: evolution above the species level**. Cambridge: Harvard University Press, pp. 399.

Taiz, L. and Zeiger, E. (2015) **Plant Physiology and Development**. 6th ed. Sunderland: Sinauer Associates, Inc., pp. 761.

ter Steege, H, Pitman, N.C.A, Phillips, O.L, Chave, J, Sabatier, D, Duque, A, Molino, J.F, Prévost, M.F, Spichiger, R, Castellanos, H, von Hildebrand, H, Vásquez, R. (2006) Continental-Scale Patterns of Canopy Tree Composition and Function across Amazonia. **Nature**, 443: 444-447.

ter Steege, H. Pitman, N. C. A. Sabatier, D. Baraloto, C. Salomao, R. P. Guevara, J. E. Phillips, O. L. Castilho, C. V. Magnusson, W. E. Molino, J.-F. Monteagudo, A. Nunez Vargas, P. Montero, J. C. Feldpausch, T. R. Coronado, E. N. H. Killeen, T. J. Mostacedo, B. Vasquez, R. Assis, R. L. Terborgh, J. Wittmann, F. Andrade, A. Laurance, W. F. Laurance, S. G. W. Marimon, B. S., Marimon, B.-H. Guimarães Vieira, I. C. Amaral, I. L. Brienen, R. Castellanos, H. Cardenas Lopez, D. Duivenvoorden, J. F. Mogollon, H. F. Matos, F. D. D. A. Davila, N. Garcia-Villacorta, R. Stevenson Diaz, P. R. Costa, F. Costa, F. R. C. Emilio, T. Levis, C. Schietti, J. Souza, P. Alonso, A. Dallmeier, F. Montoya, A. J. D. Fernandez Piedade, M. T. Araujo-Murakami, A. Arroyo, L. Gribel, R. Fine, P. V. A. Peres, C. A. Toledo, M. Aymard C., G. A. Baker, T. R. Ceron, C. Engel, J. Henkel, T. W. Maas, P. Petronelli, P. Stropp, J. Aartman, C. E. Daly, D. Neill, D. Silveira, M. Paredes, M. R. Chave, J. Lima Filho, D. D. A. Jorgensen, P. M. Fuentes, A. Schongart, J. Cornejo Valverde, F. di Fiore, A. Jimenez, E. M. Penuela Mora, M. C. Phillips, J. F. Rivas, G. van Andel, T. R. von Hildebrand, P. Hoffman, B. Zent, E. L. Malhi, Y. Prieto, A. Rudas, A. Ruschell, A. R. Silva, N. Vos, V. Zent, S. Oliveira, A. A. Schutz, A. C. Gonzales, T. Trindade Nascimento, M. Ramirez-Angulo, H. Sierra, R. Tirado, M. Umana Medina, M. N. Van der Heijden, G. Vela, C. I. A. Vilanova Torre, E. Vriesendorp, C. Wang, O. Young, K. R. Baider, C. Balslev, H. Ferreira, C. Mesones, I. Torres-Lezama, A. Urrego Giraldo, L. E. Zagt, R. Alexiades, M. N. Hernandez, L. Huamantupa-Chuquimaco, I. Milliken, W. Palacios Cuenca, W. Pauletto, D. Valderrama Sandoval, E. Valenzuela Gamarra, L. Dexter, K. G. Feeley, K. Lopez-Gonzalez, G. Silman, M. R. 2013. Hyperdominance in the Amazonian Tree Flora. **Science,** 342: 1243092-1-1243092-9.

Takahashi, K. and Jux, U. (1989) Palynology of Middle Tertiary lacustrine deposits from the Jos Plateau, Nigeria. **Bulletin of the Faculty of Liberal Arts, Nagasaki University (Natural Science)**, 29(2): 181-367.

Ter Braak, C.J.F. (1986) Canonical Correspondence Analysis: A New Eigenvector Technique for Multivariate Direct Gradient Analysis. **Ecology**, 67 (5): 1167-1179.

Thiergart, F. (1938) Die Pollenflora der Niederlausitzer Braunkohle, besonders im Profil der Grube Marga bei Senftenberg. **Jahrbuch der Preussische geologischen Landesanstalt und Bergakademie zu Berlin**, 58: 282–356.

Thiergart, F. (1940) Die Mikropaläontologie als Pollenanalyse in Dienst der Braunkohlenforschung. **Brennstoff-Geologie**, 13: 1–82.

Thomson, P.W., Pflug, H. (1953) Pollen und Sporen des mitteleuropaischen Tertiars. **Palaeontographica Abteilung B**, 94: 1-138.

Traverse, A. (2007) **Paleopalynology,** 2nd ed. Dordrecht: Springer, pp. 813.

Uba, C., Strecker, M., Schmitt, A. (2007) Increased sediment accumulation rates and climatic forcing in the central Andes during the late Miocene. **Geology**, 979–982.

Uba, C.E., Hasler, C.-A., Buatois, L.A., Schmitt, A.K., Plessen, B. (2009) Isotopic, paleontologic, and ichnologic evidence for late Miocene pulses of marine incursions in the Central Andes. **Geology**, 37 (9): 827–830.

Vajda-Santivanez, V. (1999) Misopores from upper Cretaceous-Paleocene strata in Northwestern Bolivia. **Palynology**, 23: 181-196.

Van der Ent, R., Savenije, H.H.G., Schaefli, B., Steele-Dune, S.C. (2010) Origin and fate of atmospheric moisture over continents. **Water Resources Research**, (46): 1:12.

Van der Hammen, T. and Burger, D. (1966) Pollen flora and age of the Takutu Formation (Guyana). **Leidse Geologische Mededelingen**, 38: 173-180.

Van der Hammen, T. and Garcia, C. (1966) The Paleocene pollen flora of Colombia. **Leidse Geologische Mededelingen**, 35: 105-114.

Van der Hammen, T. amd Hooghiemstra, H. (2000) Neogene and Quaternary history of vegetation, climate, and plant diversity in Amazonia. **Quaternary Science Review**, 19: 725–742.

Van der Hammen, T., and Wymstra, T. A. (1964) A palynological study on the Tertiary and Upper Cretaceous of British Guayana. **Leidse Geologische Mededelingen**, 30: 183-241.

Van der Hammen, T. (1954) The development of Colombian flora throughout geologic periods: I, Maestrichtian to Lower Tertiary. **Boletín Geológico**, 2: 49–106.

Van der Hammen, T. (1956a) A Palynological Systematic Nomenclature. **Boletín Geológico**, 4: 63–101.

Van der Hammen, T. (1956b) Description of some genera and species of fossil pollen and spores. **Boletín Geológico**, 4: 103–109.

Van Hoeken-Klinkenberg, P.M.J. (1964) A palynological investigation of some Upper Cretaceous sediments in Nigeria. **Pollen et Spores**, 6: 209–231.

Van Hoeken-Klinkenberg, P.M.J. (1966) Maastrichtian Paleocene and Eocene pollen and spores from Nigeria. **Leidse Geologische Mededelingen**, 38: 37–48.

Vermeij, G.J. (2003) **Temperature, tectonics, and evolution. In Evolution on Planet Earth: The Impact of the Physical Environment**. Rothschild, L.J., Lister, A. (eds.). Amsterdam: Academic Press, pp. 209–32.

Vermeij, G.J. (2005) From phenomenology to first principles: toward a theory of diversity. **Proceedings of the California Academy of Sciences**, 56 (2): 12–23.

Vonhof, H.B., Wesselingh, F.P., Ganssen, G.M. (1998) Reconstruction of the Miocene western Amazonian aquatic system using molluscan isotopic signatures. **Palaeogeography, Palaeoclimatology, Palaeoecology**, 141, 85–93.

Vonhof, H.B., Wesselingh, F.P., Kaandorp, R.J.G., Davies, G.R., van Hinte, J.E., Guerrero, J., Räsänen, M., Romero-Pittman, L., Ranzi, A. (2003) Paleogeography of Miocene Western Amazonia: isotopic composition of molluscan shells constrains the influence of marine incursions. **Bulletin of the Geological Society of America**, 115: 983–993.

Wall, D. (1967) Fossil microplankton in deep-sea cores from the Caribbean Sea. **Palaeontology**, 10 (1): 95-123.

Wall, D. and Dale, B. (1973) Paleosalinity relationships of dinoflagellates in the Late Quaternary of the Black Sea: a summary. **Geoscience and Man**, 7: 95–102.

Wall, D., Dale, B., Lohman, G.P., Smith, W.K. (1977) The environmental and climatic distribution of dinoflagellate cysts in the North and South Atlantic Oceans and adjacent seas. **Marine Micropaleontology**, 2: 121–200.

Wallace A.R. (1878) Tropical Nature and Other Essays. New York: McMillan, pp. 377.

Wanderley-Filho, J.R., Eiras, J.F., Cunha, P.R.C., Van der Ven, P.H. (2010) "The Paleozoic Solimões and Amazonas basins and the Acre foreland basin of Brazil" In Hoorn, C., Wesselingh, F.P. (eds.) **Amazonia-Landscape and Species Evolution: a Look into the Past**. Oxford: Wiley-Blackwell, pp. 29-37.

Weiler, H. (1985) Grünalge *Pediastrum* Meyen in tertiären Sedimenten Südwestdeutchlands. **Meinzer geowissenschaftliche Mitteilungen**, 14: 307-43

Wesselingh, F.P., Räsänen, M.E., Irion, G., Vonhof, H.B., Kaandorp, R., Renema, W., Romero Pittman, L., Gingras, M. (2002) Lake Pebas: a palaeoecological reconstruction of a Miocene, long-lived lake complex in western Amazonia. **Cainozoic Research**, 1: 35–81.

Wesselingh, F.P. (2006) Molluscs from the Miocene Pebas Formation of Peruvian and Colombian Amazonia. **Scripta Geologica**, 133: 19–290.

Wesselingh, F.P. and Salo, J.A. (2006) A Miocene perspective on the evolution of the Amazonian biota. **Scripta Geologica**, 133: 439–458.

Wesselingh, F.P., Hoorn, C., Guerrero, J., Räsänen, M., Romero-Pitmann, L. (2006a) The stratigraphy and regional structure of Miocene deposits in western Amazonia (Peru, Colombia and Brazil), with implications for Late Neogene landscape evolution. **Scripta Geologica**, 133: 291–322.

Wesselingh, F.P., Guerrero, J., Räsänen, M., Romero-Pitmann, L., Vonhof, H. (2006b) Landscape evolution and depositional processes in the Miocene Amazonian Pebas lake/wetland system: evidence from exploratory boreholes in northeastern Peru. **Scripta Geologica**, 133: 323–356.

Wesselingh, F.P., Kaandorp, R.J.G., Vonhof, H.B., Räsänen, M.E., Renema, W., Gingras, M. (2006c) The nature of aquatic landscapes in the Miocene of western Amazonia: an integrated palaeontological and geochemical approach. **Scripta Geologica**, 133: 363–393.

Wesselingh, F.P. (2007) “Long-lived lake molluscs as island faunas: a bivalve perspective” In Renema, W. (ed.) **Biogeography, time and place: distributions, barriers and islands**. Dordrecht: Springer, pp. 275-314.

Wesselingh, F.P. (2008) Molluscan radiations and landscape evolution in Miocene Amazonia. **Annales Universitates Turkuensis. Biologica-Geographica-Geologica**, 232: 1-41.

Westaway, R. (2006) Late Cenozoic fluvial sequences in western Amazonia: fluvial or tidal? Deductions from the June 2003 IGCP 449 field trip. **Journal of South American Earth Sciences**, 21: 120–134.

Weyland, H., and Krieger, W. (1953) Die Sporen und Pollen der Aachener Kreide und ihre Bedeutung fur die Charakterisierung des Mittleren Senons. **Palaeontographica Abteilung B**, 95: 6-29.

White, H.J.R., Skopec, R.A., Ramirez, F.A., Rodas, J.,A., Guido, B. (1995) “Reservoir Characterization of the Hollin and Napo Formations, Western Oriente Basin, Ecuador: In Tankard, A.J., Soruco, R.S., Welsink, H.J. (eds.) **Petroleum basins of South America**, American Association of Petroleum Geologists Memoir 62: 573-596.

Whiteny, B.S. and Mayle, F.E. (2012) *Pediastrum* species as potential indicators of lake-level change in tropical South America. **Journal of Paleolimnology**, 47: 601-615.

Wing, S.L. (1998) “Late Paleocene–early Eocene floral and climatic change in the Bighorn Basin, Wyoming” In Berggren, W.A., Aubry, M.-P., Lucas, S. (eds.) **Late Paleocene–Early Eocene Biotic and Climatic Events**. New York: Columbia University Press, pp. 380–400.

Wing, S. L., Herrera, F., Jaramillo, C., Gómez-Navarro, C., Wilf, P., Labandeira, C.C. (2009) Late Paleocene fossils from the Cerrejón Formation, Colombia, are the earliest record of Neotropical rainforest. **Proceedings of the National Academy of Sciences**, 106 (44) 18627–18632.

Wittmann, F., Anhuf, D., Junk, W.J. (2002) Tree species distribution and community structure of Central Amazonian várzea forests by remote sensing techniques. **Journal of Tropical Ecology**, 18: 805-820.

Wittmann, F., Schöngart, J., De Brito, J.M., Wittmann, A.O., Piedade, M.T.F., Parolin, P., Junk, W.J., Guillaumet, J-L. (2010) **Manual de árvores de varzea da Amazônia Central: taxonomia,**

ecologia e uso = Manual of trees from Central Amazonian varzea floodplains: taxonomy, ecology and use. Manaus, Editora Inpa.

Wodehouse, R.P. (1933) The oil shales of the Eocene Green River Formation. **Bulletin of the Torrey Botanical Club**, 60: 479-535.

Wood, G.D., Gabriel, A.M., Lawson, J.C. (1996) "Palynological techniques e processing and microscopy" In Jansonius, J. and McGregor, D.C. (eds.) **Palynology: Principles and Applications, vol. 1**. Dallas: American of Stratigraphic Palynologists Foundation, pp. 29-50.

Woodward, H. (1871) The Tertiary shells of the Amazons Valley. **Bulletin de la Société Géologique de France**, 2 (25): 59-64.

Woodward, I.F. (1987) **Climate and Plant Distributions**. New York: Cambridge University press, pp. 188.

Wright, J.D. (1998) "The Role of the Greenland-Scotland Ridge in Cenozoic Climate Change" In Crowley, T.J. and Burke, K. (Eds.) **Tectonic Boundary Conditions for Climate Reconstructions**, Oxford: University Press, pp. 192-211.

Wright, J.D. and Miller, K.G. (1996) Control of North Atlantic deep water circulation by the Greenland-Scotland Ridge. **Paleoceanography**, 11: 157-170.

Wright, S., Keeling, J., Gillman, L. (2006) The road from Santa Rosalia: a faster tempo of evolution in tropical climates. **Proceedings of the National Academy of Sciences**, 103: 7718–22.

You, Y., Huber, M., Müller, R.D., Poulsen, C.J., Ribbe, J. (2009) Simulation of the Middle Miocene Climate Optimum. **Geophysical Research Letters**, 36: L04702.

Zachos, J., Pagani, M., Sloan, L., Thomas, E., Billups, K. (2001) Trends, rhythms, and aberrations in global climate 65 Ma to present. **Science**, 292: 686–693.

Zachos, J.C., Dickens, G.R., Zeebe, R.E. (2008) An early Cenozoic perspective on greenhouse warming and carbon-cycle dynamics. **Nature**, 451: 279-283.

Zhang, Y.G., Pagani, M., Liu, Z., Bohaty, S.M., DeConto, R. (2013) A 40-million-year history of atmospheric CO2. **Philosophical Transactions of the Royal Society A**, 371: 20130096.

Zonneveld, K. A. F., Bockelmann, F., Holzwarth, U. (2007) Selective preservation of organic-walled dinoflagellate cysts as a tool to quantify past net primary production and bottom water oxygen concentrations. **Marine Geology**, 237:109–26.

Zonneveld, K. A. F., Susek, E., Fischer, G. (2010) Seasonal variability of the organic-walled dinoflagellate cyst production in the coastal upwelling region off cape blanc (Mauritania): a five-year survey. **Journal of Phycology**, 46: 202–215.

Zonneveld, K.A.F., Marret, F., Versteegh, G.J.M., Bogus, K., Bonnet, S., Bouimetarhan, I., Crouch, E., de Vernal, A., Elshanawany, R., Edwards, L., Esper, O., Forke, S., Grøsfjeld, K., Henry, M., Holzwarth, U., Kielt, J.-F., Kim, S.-Y., Ladouceur, S., Ledu, D., Chen, L., Limoges, A., Londeix, L., Lu, S.-H., Mahmoud, M.S., Marino, G., Matsouka, K., Matthiessen, J., Mildenhal, D.C., Mudie, P., Neil, H.L., Pospelova, V., Qi, Y., Radi, T., Richerol, T., Rochon, A., Sangiorgi, F., Solignac, S., Turon, J.-L., Verleye, T., Wang, Y., Wang, Z., Young, M. (2013) Atlas of modern organic dinoflagellate cyst distribution based on 2405 data points. **Review of Palaeobotany and Palynology**, 191: 1–197.

Zuquim, G., Costa, F.R.C., Prado, J., Tuomisto, H. (2008) Guide to the ferns and lycophytes of REBIO Uatumã - Central Amazonia. Manaus: Attema Design Editorial, pp. 315.